Function of Cytoplasmic FMR1-interacting protein 2 (CYFIP2) in spinal motor neuron morphology during mouse embryonic development

Dissertation

zur

Erlangung des Doktorgrades (Dr. rer. Nat.)

der

Mathematisch-Naturwissenschaftlichen Fakultät

der

Rheinischen Friedrich-Wilhelms-Universität Bonn

vorgelegt von

Stefanie Carla Rosa Hauck

aus
Hamburg

Bonn 2021

Angefertigt mit Genehmigung der Mathematisch-Naturwissenschaftlichen Fakultät der
Rheinischen Friedrich-Wilhelms-Universität Bonn

1. Gutachter: Prof. Dr. Walter Witke
2. Gutachter: Prof. Dr. Dieter Fürst

Tag der Promotion: 02.05.2022

Erscheinungsjahr: 2022

Summary

The development of the nervous system is a tightly regulated spatio-temporal process that involves actin cytoskeletal dynamics. The remodelling of the neuronal cytoskeleton is important for dendritic and axonal guidance, neurite elongation, dendritic arborization and synapse assembly in both the central and peripheral nervous system. Cytoplasmic FMR1-interacting protein 2 (CYFIP2) is a component of the WAVE regulatory complex and essential in regulating ARP2/3-dependent branched actin networks. CYFIP2 is highly expressed in the mouse CNS and the complete deletion of CYFIP2 leads to a perinatal lethal phenotype. However, the exact cellular role of CYFIP2 in mouse embryonic development is still not fully understood.

We show in this study that CYFIP2 is a key component in peripheral nervous system development. The *Cyfip2*$^{-/-}$ mouse model fails to properly innervate the diaphragm leading to respiratory failure of newborn mice. CYFIP2 is essential for axonal growth properties that are needed for stereotyped phrenic motor neuron branching pattern. The formation of focal adhesion sites in the spinal motor neuron growth cone requires proper interaction between actin adaptor proteins (i.e., vinculin), scaffold proteins (i.e., FAK), and CYFIP2-mediated ARP2/3 actin polymerization. In addition, CYFIP2 modulation of tyrosine phosphorylation signaling might be required to stabilize focal adhesion sites mediated by the ECM-integrin adhesion pathway. The structural composition of the presynaptic neuromuscular junction is also highly dependent on CYFIP2.

The function of CYFIP2 in axonal elongation is cell autonomous in spinal motor neurons. However, A-to-I RNA editing of CYFIP2 in neurons (CYFIP2-K320E) could be a potential mechanism used to initiate neurite protrusion. Ultrastructural analysis demonstrated CYFIP2 is an important factor regulating the actin-microtubule crosstalk in spinal motor neuron growth cones and ensuring proper axonal outgrowth. Biochemical and histological assays showed CYFIP2 deletion did not alter the steady-state F-actin level in neurons but was mainly required for morphological properties. Furthermore, other actin nucleation/elongation factors, such as the CYFIP1-dependent WRC and MENA/VASP, did not compensate for the loss of CYFIP2. Proteomic analysis revealed novel CYFIP2 interaction partners which could help elucidate potential guidance signaling functions and cell adhesion mechanisms.

Table of Contents

List of Figures

List of Tables

List of Supplementary Figures

List of Supplementary Tables

List of Abbreviations

Abbreviation	Full name
°C	Degree Celsius
Ab	Antibody
ABI	Abelson-interacting protein
ABP	Actin binding protein
ACh	Acetylcholine
AChR	Acetylcholine receptor
ADP	Adenosine diphosphate
ANOVA	Analysis of variance
ANS	Autonomic nervous system
APS	Ammonium persulfate
ARP2/3	Actin related protein 2/3
ATP	Adenosine triphosphate
BDNF	Brain-derived neurotrophic factor
bp	Base pair
BSA	Bovine serum albumin
CB	Cytoskeleton buffer
ChAT	Choline acetyltransferase
CHT	Choline transporter
CNS	Central nervous system
CNTF	Ciliary neurotropic factor
Co-IP	Co-immunoprecipitation
CYFIP	Cytoplasmic FMR1-interacting protein
DAPI	4’,6-diamidino-2-phenylindole
DBE	Dibenzyl ether
DCM	dichloromethane
DIV	Days *in vitro*
DMSO	Dimethyl sulfoxide
DNA	Deoxyribonucleic acid
E	Embryonic day
ECL	Enhanced chemiluminescence
EDTA	Ethylenediaminetetraacetic acid
EGTA	Ethylene glycol-bis(2-aminoethylether)-N,N,N’,N’-tetraacetic acid
EtBr	Ethidium bromide
EtOH	Ethanol
F-actin	Filamentous actin
FCS	Fetal calf serum
flx	Floxed allele
FMR1	Fragile X mental retardation 1
FMRP	Fragile X mental retardation protein
FXS	Fragile X syndrome
G-actin	Globular actin

GA	Glutaraldehyde
GDNF	Glial-derived neurotrophic factor
h	Hour
HBSS	Hanks balanced salt solution
HEK293	Human embryonic kidney 293 cells
HS	Horse serum
HSPC300	Hematopoietic stem/progenitor cell protein 300
IF	Immunofluorescence
KCl	Potassium chloride
kDa	Kilodalton
KO	Knockout
KOH	Potassium hydroxide
LSM	Laser scanning microscope
MENA	Mammalian Enabled
MeOH	Methanol
MES	2-(*N*-morpholino)ethanesulfonic acid
mg	Milligram
$MgCl_2$	Magnesium chloride
min	Minute
ml	Milliliter
mM	Millimolar
MN	Motor neuron
$Na_2B_4O_7$	Sodium tetraborate (Borax)
$Na_4P_2O_7$	Sodium pyrophosphate
NaCl	Sodium chloride
NaOH	Sodium hydroxide
NAP1	Nck-associated protein 1
NF	Neurofilament
NGS	Normal goat serum
NH_4Cl	Ammonium chloride
nm	Nanometer
NMJ	Neuromuscular junction
NPF	Nucleation promoting factor
o/n	Overnight
P	Postnatal day
PAGE	Polyacrylamide gel electrophoresis
PBS	Phosphate buffered saline
PCR	Polymerase chain reaction
PDB	Protein data bank
PEG	Polyethylene glycol
PFA	Paraformaldehyde
PIPES	Piperazine-N,N’-bis(2-ethanesulfonic acid)
PMC	Phrenic motor column
PMN	Primary motor neuron
PNS	Peripheral nervous system

rpm	Rotations per minute
RT	Room temperature
s	Seconds
SDS	Sodium dodecyl sulfate
SNAP25	Synaptosome associated protein 25 kDa
TBS	Tris buffered saline
TBS-T	Tris buffered saline with Triton X-100
TEMED	Tetramethylethylenediamine
THF	Tetrahydrofuran
Tris	Tris(hydroxymethyl)aminomethane
Triton X-100	*t*-Octylphenoxypoly(ethoxy)$_9$-ethanol
Tween-20	Poly(oxyethylene)$_{20}$-sorbitan monolaurate
V	Volt
v/v	Volume per volume
VASP	Vasodilator-stimulated phosphoprotein
VCA	Verprolin-homology, cofilin, acidic domain
w/v	Weight per volume
WASP	Wiskott-Aldrich Syndrome protein
WAVE	WASP Verprolin homologous protein
WB	Western blot
WH	WASP homology
WRC	WAVE regulatory complex
WT	Wildtype
X-gal	5-bromo-4-chloro-3-indolyl-beta-D-galacto-pyranoside
α–BTX	Alpha Bungarotoxin
βIII-tubulin	Beta III-tubulin
µg	Microgram
µl	Microliter
µm	Micrometer

1. Introduction

1.1 The cytoskeleton

The cytoskeleton regulates several essential biological functions in eukaryotic cells. The three main polymers that provide structural and mechanical support for eukaryotic cells are actin filaments, microtubules, and intermediate filaments. These polymers coordinate different vital functions such as proliferation, motility, and migration (Fletcher & Mullins, 2010; Pollard & Cooper, 2009). The actin cytoskeleton is fundamental for regulating neuronal development in both the central nervous system (CNS) and the peripheral nervous system (PNS) (Coles & Bradke, 2015; Stiess & Bradke, 2011; Wang et al., 2018). One of the main goals in developmental neurobiology is understanding how specific nerve cells can reach their targets with precise spatio-temporal resolution. Several studies have shown that the remodeling of dynamic cytoskeletal proteins is pivotal for neuronal migration (Dent, Gupton, & Gertler 2011; Lowery & Vactor 2009; Yamada, Spooner, & Wessells, 1970).

1.1.1 Actin filaments

The actin cytoskeleton is highly conserved amongst eukaryotic cells, and the actin isoforms (α–, β– and γ-actin) have different cellular localization patterns (Herman, 1993; Perrin & Ervasti, 2010). α-actin is found in muscles, β-actin in non-muscle cells, while γ-actin is in both non-muscle and smooth muscle cells. Actin is found in two states as monomeric globular actin (G-actin) and filamentous actin (F-actin): G-actin monomer (42 kDa) can be polymerized to form F-actin, a helical double-stranded filament that is 7 nm in diameter (Holmes et al., 1990; Kabsch & Vandekerckhove 1992).
The actin filament is structurally polar as all actin monomers point towards the same direction. The actin monomers have adenosine triphosphate (ATP) binding clefts, which are directed towards the pointed (-) end, while the opposite end is termed the barbed (+) end. Electron microscopy experiments on actin filaments decorated with myosin revealed that filament elongation was faster at the barbed (+) end and slower at the pointed (-) end (Huxley, 1963).

The initial phase of nucleation requires adenosine triphosphate (ATP) loaded G-actin monomers to spontaneously form a stable G-actin trimer or actin nucleus. This actin nucleation process is the rate-limiting step in polymerization since spontaneous actin dimer intermediates and trimerization are kinetically unfavorable (Pollard & Cooper, 2009; Pollard & Craig, 1982). *In vitro,* the addition of ATP-loaded G-actin monomers is incorporation onto both sides of the

nucleus. Actin filament elongation occurs at the barbed end when the pool of available G-actin monomers is higher than the critical concentration (C_c). The C_c is defined as the concentration of free G-actin monomers at which the net rate of dissociation and association at one end of the filament is in equilibrium. However, the rate of polymerization differs at both ends: the barbed end is lower C_c (0.1 μM) compared to the pointed end (~10-fold higher) (Pollard, 1986). When the G-actin concentration is between the C_c of the barbed and the pointed end, there is a net monomer association at the barded end and net monomer dissociation at the pointed end. This process is also known as actin treadmilling (Figure 1.1). Once the ATP-bound G-actin assembles into the filament, the ATP is hydrolyzed into adenosine diphosphate (ADP) and a phosphate group (Pi). The ADP-bound G-actin is dissociated from the filament's pointed end, a process called depolymerization, and these monomers are recharged with ATP and recycled (Holmes et al., 1990; Pollard & Cooper, 2009). The elongation of the actin filament reaches an equilibrium (also known as steady-state) where polymerization and depolymerization occur at the same rate. As cellular actin nucleation is kinetically unfavorable, several regulatory proteins, known as actin-binding proteins (ABPs) (chapter 1.2), are used to facilitate and modulate the polymerization process (Pollard, 2016; Winder & Ayscough, 2005).

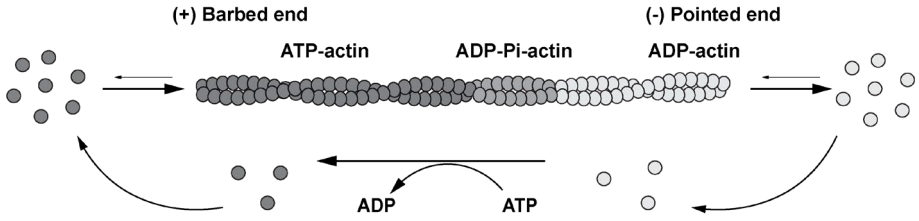

Figure 1.1. Actin treadmilling.
Scheme depicting actin treadmilling shows steady state of actin polymerization and depolymerization. The ATP-loaded G-actin monomers (dark grey) bind to the growing filament at the barbed (+) end. Over time the ATP is hydrolyzed to ADP and phosphate (Pi), eventually leaving only ADP-actin (light grey). The ADP-actin is depolymerized from the pointed (-) end. The ADP-actin monomers are replaced with ATP. These new ATP-actin monomers are recycled and incorporated back into the barded end.

1.1.2 Microtubules

The largest cytoskeletal polymers in eukaryotic cells are microtubules. Microtubules are important for maintaining cellular polarity during neurodevelopmental processes and provide scaffolds for molecular motor protein transport (Dent & Baas, 2014). Microtubules are comprised of α-and β- tubulin dimers that form cylindrical protofilaments or lattices, which are 25 nm in diameter (Amos & Klug, 1974; Desai & Mitchison, 1997). Microtubules are highly dynamic structures that undergo both polymerization (known as “rescue”) at the plus-end of

the filament and depolymerization (known as “catastrophe”) at the minus-end. This stochastic growth and shrinkage of the microtubules are known as dynamic instability. Several microtubule interacting proteins are used to regulate this dynamic process. At the microtubule filament plus-ends, filament stabilization or severing are regulated by plus-end tracking proteins (+TIPs) (Cammarata, Bearce, & Lowery, 2016). In comparison, the main body of microtubule filaments is regulated by microtubule-associated proteins (MAPs) (Coles & Bradke, 2015). In axons, the microtubules are orientated with the plus-ends directed distal or away from the cell body (plus-end-out), while the dendrites display mixed polarity orientations (Baas et al., 1988; Coles & Bradke, 2015). Microtubules also interact with actin filaments via molecular motor proteins, which are integral in the regulation of axonal stability (Ahmad et al., 2000; Dent & Baas, 2014). The migration of neuronal growth cones is a highly dynamic process dependent on actin-microtubule interactions (Coles & Bradke 2015; Dent, Gupton, & Gertler, 2011; Forscher & Smith, 1988; Kawabata, Galbraith & Kengaku, 2019).

1.1.3 Intermediate filaments and neurofilaments

Intermediate filaments interact with both microtubules and actin filaments, and this crosstalk is important for the overall integrity of cellular structures (Goldman et al., 1996; Hollenbeck et al., 1989; Svitkina, Verkhovsky, & Borisy, 1996). Intermediate filament polymers (10 nm in diameter) are not polar structures and do not undergo hydrolyzing activity or nucleoside triphosphate binding like microtubules or actin filaments (Chang & Goldman, 2004; Coulombe et al., 2000). There are five intermediate filament subgroups (I-V), and type IV is predominantly expressed in the CNS (Chang & Goldman, 2004). Type IV consists of neurofilaments (NF), nestin, α-internexin, and syncolin proteins (Chang & Goldman, 2004). This study will focus on NF as it is expressed in both the CNS and PNS at embryonic (E) stages in mice (Cochard & Paulin, 1984).

NFs are heteropolymers containing three subunits: NF light chain (NF-L), NF middle chain (NF-M), and NF heavy chain (NF-H), with apparent molecular masses of 70 kDa, 150 kDa, and 200 kDa, respectively (Yuan et al., 2012). The NF structure in CNS neurons consists of NF-L, NF-M, NF-H, and α-internexin. PNS sensory neurons consist of NF-L, NF-M, NF-H, and peripherin, a type III intermediate filament protein (Perrot & Eyer, 2009; Yuan et al., 2012). The NF structure consists of three domains 1) an N-terminal globular head, a central α-helical rod domain, and a C-terminal tail with variable length (Dale & Garcia, 2012; Yuan et al., 2012). The α-helical rod forms coiled-coil dimers, which then assemble to make antiparallel tetramers (Hohmann & Dehghani, 2019; Yuan et al., 2012). The assembly of eight tetramers forms

cylindrical rod-shaped structures called unit-length filaments, which are the basic building blocks used in NF elongation. In addition, NF is important in several aspects of neuronal maturation and can modulate microtubule assembly in axons (Bocquet et al., 2009; Hoffman, 1995; Miller et al., 2002). Developmental studies on *Xenopus laevis* (frog) showed NF-M facilitates axonal elongation (Lariviere & Julien, 2004). NF-M is predominantly found in large-myelinated axons. The serine-phosphorylation of specific lysine-serine-proline (KSP) repeat motifs in the C-terminal tail are essential for proper axonal caliber (Dale & Garcia, 2012; Hoffman et al., 1987; Miller et al., 2002). Impairment in NF function has been associated with neurodegenerative diseases such as Alzheimer's diseases (AD) and amyotrophic lateral sclerosis (ALS) (Lariviere & Julien, 2004; Perrot & Eyer, 2009; Szaro & Strong, 2010). While intermediate filaments are primarily abundant in the axon, there is evidence that NF (Chan et al., 2003) and nestin (Bott et al., 2019) can regulate growth cone migration.

1.2 Actin binding proteins and actin nucleators

Actin polymerization and depolymerization dynamics in eukaryotic cells are regulated by ABPs. There are a variety of ABPs used to either maintain the monomeric actin pool, nucleate actin into new filaments, promote filament elongation, cap the pointed or barbed ends, sever filaments or cross-link filaments (Figure 1.2) (Dominguez & Holmes, 2011; Pollard et al., 2017; Winder & Ayscough, 2005).

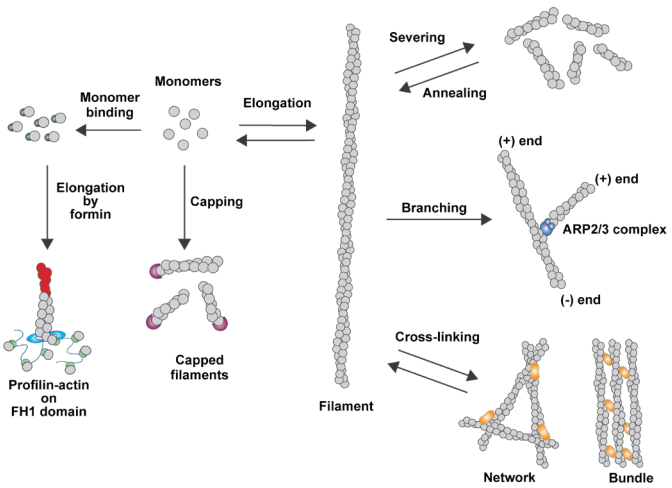

Figure 1.2. Diverse functions of actin-binding proteins.
Scheme depicting the various functions of actin-binding proteins (ABPs) modulating actin dynamics in the cell. The ABPs include monomer binding proteins (e.g., profilins and cofilins) along with filament nucleation factors (e.g., formins), capping proteins (e.g., CAPG, tropomodulin, and gelsolin), cross-linking proteins (e.g., α-actinin and filamin), severing proteins (e.g., ADF/cofilin and gelsolin) and branching proteins (e.g., the ARP2/3 complex). Reprinted and adapted from Pollard et al., (2017) with permission of Elsevier.

Since G-actin monomer nucleation is kinetically unfavorable, cells use specific actin nucleators to facilitate the formation of the actin nucleus from G-actin monomers and stimulate filament elongation at its barbed end (Chesarone & Goode, 2009; Winder & Ayscough, 2005). The actin nucleators are classified into three groups: Class 1) the actin-related protein 2/3 (ARP2/3) complex with its nucleation promoting factors (NPFs), Class 2) formins, and Class 3) tandem WH2 domain-containing nucleators (Figure 1.3). The Class 1 nucleator ARP2/3 complex is of particular interest for this study as it facilitates the polymerization of *de novo* branched actin networks located at the leading edge of several cellular subtypes. The functions of the ARP2/3 complex are discussed in chapter 1.2.2.

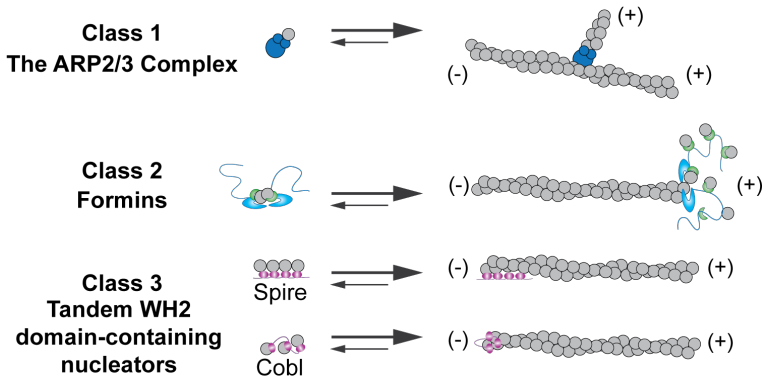

Figure 1.3. The different classes of actin nucleators in the cell.
Scheme depicting the three classes of actin nucleators and their distinct modes of actin nucleation. The class 1 ARP2/3 complex is activated by nucleation promoting factors (not depicted) and serves to mimic an actin trimer and initiate polymerization of *de novo* branched actin filaments. The class 2 formins are linear actin elongators, and after initial actin, monomer nucleation will remain attached to the barbed (+) end of the linear filament. The class 3 tandem WH2 domain-containing nucleators, e.g., Spire, Cobl, or Lmod (not shown), contain various actin monomer binding WH2 repeats separated by various linker sequences. Class 3 nucleators remain associated with the pointed (-) end, and elongation continues at the filament's barbed end. The actin nucleus has different properties, but the actin nucleation mechanism is similar. Reprinted and adapted from Chesarone & Goode (2009) with permission of Elsevier.

Class 2 nucleators (formins) can nucleate actin monomers and function as polymerization factors that remain bound to the filament's barded end and prevent capping proteins from attaching to the actin filament (Faix & Grosse, 2006; Kovar, 2006). This results in the fast elongation of linear actin filaments (Figure 1.3). Formins contain the formin homology domain 1 and 2 (FH1 and FH2), of which the latter is used to initiate and stabilize the actin nucleus required for polymerization (Chhabra & Higgs, 2007; Faix & Grosse, 2006; Kovar, 2006). However, several studies have shown that formins display a diverse spectrum of regulatory properties, including nucleation, bundling, and severing (Kawabata Galbraith & Kengaku, 2019). Class 3, or WH2 domain-binding actin nucleators, consist of Spire, Cordon-bleu (Cobl),

and Leiomodin (Lmod) that share tandem WASP homology 2 (WH2) domains which bind to G-actin monomers (Firat-Karalar & Welch, 2011) (Figure 1.3). Spire, Coble, and Lmod (not shown) are multifunctional adapters and have four, three, and two WH2 domains, respectively (Campellone & Welch, 2010; Qualmann & Kessels, 2009). They form an actin nucleus, each with distinct properties. Spire remains associated with the pointed end of the actin nucleus allowing elongation to continue at the barded end (Qualmann & Kessels, 2009). Spire was also shown to bind to the barbed end of the actin filament and block profilin-mediated actin binding (Bosch et al., 2007). Cobl has three actin-binding WH2-domains, and its nucleation mechanism is similar to Spire's. However, Cobl has longer linkers between the WH2 domains, which seem to be critical for efficient actin nucleation (Campellone & Welch, 2010).

1.2.1 The ENA/VASP family

The elongation of actin filaments also uses a variety of ABPs that prevent the capping proteins from binding to the barded end and actively participate in the actin monomer addition. One elongation factor is the Enabled (ENA)/Vasodilator-stimulated phosphoprotein (VASP) protein family. The ENA/VASP family consists of Ena, mammalian ENA (MENA), VASP and ENA/VASP-like protein (EVL) (Bear & Gertler, 2009; Gertler et al., 1996). The ENA/VASP proteins form tetramers which bind to the barbed end of actin filaments and accelerate actin polymerization, and in addition, prevent capping proteins from binding to the filament (Bear et al., 2002; Krause et al., 2003). The N-terminal ENA/VASP homology domain 1 (EVH1) can bind to focal adhesion sites (Holt, Critchley, & Brindle, 1998; Lanier et al., 1999; Reinhard et al., 1992). Both MENA and VASP proteins have been found located near focal contact site and in close proximity to the focal adhesion markers vinculin and zyxin (Gertler et al., 1996b; Reinhard et al., 1992; Reinhard et al., 1996). Whereas the C-terminal EVH2 domain is the F-actin binding site (Bachmann et al., 1999; Breitsprecher et al., 2008). ENA/VASP-driven actin elongation creates filopodia which are thin actin-rich protrusions at the leading edge of the cell. Several studies showed that ENA, MENA, and VASP are also essential for leading-edge cell migration and for proper axonal extension (Bear & Gertler, 2009; Gertler et al., 1996; Lanier et al., 1999; Rottner et al., 1999). Studies in *Caenorhabditis elegans* (nematode) and *Drosophila melanogaster* (fly) showed ENA/VASP also interacts with the ARP2/3 complex via the WAVE complex to promote cell migration (Chen et al. 2014; Havrylenko et al., 2015; Norris, Dyer, & Lundquist, 2009). Recent studies showed the deletion of ENA/VASP using CRISPR/Cas9 on mouse melanoma cells resulted in reduced ARP2/3 complex levels at the lamellipodium and slower protrusion dynamics (Damiano-Guercio et al., 2020).

1.2.2 The ARP2/3 complex

The ARP2/3 complex regulates branched actin polymerization at the leading ledge or in lamellipodia of neuronal and non-neuronal cells during cell protrusion and migration (Falet et al., 2002; Machesky et al., 1997; Vinzenz et al., 2012; Wu et al., 2012). The ARP2/3 complex (~220 kDa) was first identified as a profilin-binding ligand in *Acanthamoeba* (amoeba) (Machesky et al. 1994) and consists of seven subunits ARP2, ARP3, ARPC1 (p40), ARPC2 (p34), ARPC3 (p21), ARPC4 (p20) and ARPC5 (p16) (Goley & Welch, 2006; Machesky et al., 1994). It is well known that the ARP2/3 complex initiates *de novo* branched actin filament polymerization (Pollard, Blanchoin, & Mullins, 2000; Rotty, Wu, & Bear, 2013). The complex by itself weakly binds to actin monomers and is therefore inhibited. In the presence of NPFs, the ARP2/3 complex undergoes a conformational change allowing the complex to bind to a mother actin filament and bring closer the ARP2 and ARP3 subunits to mimic an actin dimer, while the NPF provides the third G-actin monomer to form an actin nucleus that will produce a daughter filament (Goley & Welch, 2006; Robinson et al., 2001; Rouiller et al., 2008). Subsequently, the ARP2/3 complex caps the pointed end of the daughter actin filament, and polymerization continues at the barded end of the filament (Mullins et al., 1998). These *de novo* branched filaments have a stereotypical morphology as they are branched with a 70° angle (Korobova & Svitkina, 2008; Mullins et al., 1998). NPFs add to the diverse repertoire of regulatory mechanisms required for branched actin polymerization.

1.2.3 Nucleation promoting factors

There are two main classes of NPFs which differ in their mode of ARP2/3 activation and subsequent branching properties (Campellone & Welch, 2010; Goley & Welch, 2006). Class, I NPFs are the Wiskott-Aldrich syndrome protein (WASP) and the WASP Verprolin homologous protein (WAVE) family (Derry, Ochs, & Francke, 1994; Eden et al., 2002; Machesky & Insall, 1998; Miki, Suetsugu, & Takenawa, 1998). The diversity of the Class 1 NPFs has increased over the years and now includes neuronal-WASP (N-WASP), WASP and SCAR homolog (WASH), WASP homolog associated with actin membranes and microtubules (WHAMM), junction-mediating regulatory protein (JMY), and WAVE homolog in membrane protrusions (WHIMP) (Goley & Welch, 2006; Kabrawala et al., 2020; Rottner et al., 2010; Rotty et al., 2013; Stradal et al., 2004). In this study, we will focus on the role of the WAVE complex and how it regulates ARP2/3-dependent actin polymerization.

All Class 1 NPFs have a similar C-terminal binding domain called the VCA domain (verprolin homology (known as WH2) domain, the cofilin homology domain (C), and the acidic domain (A) (Stradal et al., 2004). The cofilin/acidic (CA) region of the VCA binds to the ARP2/3 complex while one actin monomer binds to the V region (Boczkowska et al., 2008; Marchand et al., 2001; Miki, Suetsugu, et al., 1998). When the NPF is absent, the ARP2 and ARP3 subunits of the ARP2/3 complex are splayed apart (Nolen & Pollard, 2007; Robinson et al., 2001). In the presence of the NPF, the ARP2/3 complex binds to an existing actin filament and mimics an actin dimer that trimerizes with the actin subunit provided by the V domain of the NPF. This creates an actin nucleus from which a daughter actin filament can extend. At the N-terminus, WASP and N-WASP have the WASP homology 1 (WH1) domain that binds to proline-rich sequences and the autoinhibitory domain (AI). WAVE has neither a WH1 nor an AI but instead has the WAVE homology domain (WHD, also known as SCAR homology domain SHD) (Kurisu & Takenawa, 2009). This domain is involved in the formation of the WAVE regulatory complex (WRC) and functions as an inhibitory mechanism for WAVE. Both WASP and N-WASP are activated by the small GTPase CDC42 via the GTPase binding domain (GBD, also known as the CDC42/RAC-interactive binding (CRIB) domain), which regulates filopodia formation (Miki, Sasaki et al., 1998). However, the WRC is activated upon RAC1 binding to the WRC subunit, CYFIP, which induces conformational changes that release the WAVE VCA region (Z. Chen et al., 2010; Goley & Welch, 2006). Class II NPFs consist of actin-binding protein 1 (ABP1), PAN1, and cortactin. However, these class II NPFs lack the complete VCA domain and are unable to bind a G-actin monomer and are therefore less effective ARP2/3 activators (Goley & Welch, 2006).

1.2.4 The WAVE regulatory complex

The WAVE regulatory complex (WRC) (Figure 1.4) is a hetero-pentameric protein (~400 kDa) and consists of WAVE itself, cytoplasmic FMR1-interacting protein (CYFIP), NCK-associated protein 1 (NAP1), Abelson-interacting protein (ABI), and hematopoietic stem progenitor cell 300 (HSPC300) (Chen et al., 2010; Gautreau et al., 2004; Takenawa & Suetsugu, 2007). WAVE-ABI-HSPC300 form a heterotrimer while CYFIP-NAP1 form a heterodimer.

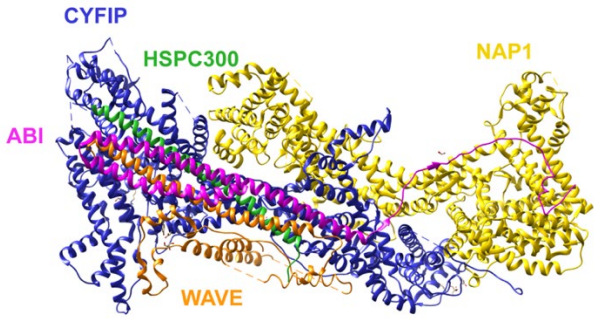

Figure 1.4. Structure of the WAVE regulatory complex.
Model of the WAVE regulatory complex (WRC) crystal structure with CYFIP1 (blue), NAP1 (yellow), ABI1 (magenta), WAVE2 (orange), and HSPC300 (green) subunits. CYFIP1 and NAP1 form a heterodimer complex while ABI1, WAVE2, and HSCPC300 establish a heterotrimer complex. Adapted crystal structure of PDB 3P8C from Chen et al., (2010).

The WRC can exist in different subunit compositions as WAVE, ABI, and CYFIP have different isoforms (Eden et al., 2002; Takenawa & Suetsugu, 2007). WAVE has three isoforms: WAVE1 and WAVE3 are primarily expressed in the CNS, and WAVE2 is ubiquitously expressed except in skeletal tissue (Suetsugu et al., 1999). In neuroblastoma cells, overexpression of WAVE1-GFP was located along the leading edge, while WAVE2-GFP and WAVE3-GFP were at filopodium initiation points in the lamellipodium (Nozumi et al., 2003). ABI has three isoforms (ABI1, ABI2, and ABI3/NESH) that can all bind to the WRC, but ABI3 has a different regulatory signaling pathway compared to ABI1 and ABI2 (Hirao et al., 2006). ABI2 and ABI3 are expressed in the brain and ABI1 and ABI3 are located at the leading edge of the lamellipodium (Eden et al., 2002; Hirao et al., 2006). During development, *Abi1* mRNA is expressed at postnatal stages while *Abi2* mRNA is found already in early embryonic stages (Courtney et al., 2000). During development, NAP1 regulates neuronal differentiation in the cortical plate (Yokota et al., 2007). In *Drosophila*, HSPC300 is highly expressed in axons in both the CNS and PNS (Qurashi et al., 2007). There are two CYFIP isoforms, CYFIP1 and CYFIP2 (Schenck et al., 2001), and their functions will be discussed in section 1.2.5.

WAVE in the WRC is in a trans-inhibited conformation, while WASP and N-WASP are autoinhibited (Rotty et al., 2013). The WRC is intrinsically inactive, as the VCA domain of WAVE is sequestered by the CYFIP/NAP1 subcomplex but is activated by the binding of the small RHO GTPase RAC1 to CYFIP (Ismail et al., 2009; Miki, Suetsugu, & Takenawa, 1998; Steffen et al., 2004; Tahirovic et al., 2010). There are some conflicting views on the role of RAC1-mediated WRC regulation. One study showed that the WRC is constitutively active, and RAC1 does not affect WRC activity (Innocenti et al., 2004). However, more studies showed the inactive WRC is recruited to the membrane upon RAC1 activation or other extracellular

signaling cues, such as phosphatidylinositol (3,4,5)-triphosphate (PIP_3) (Derivery et al., 2009; Ismail et al., 2009; Lebensohn & Kirschner, 2009; Padrick et al., 2008). The regulation of WRC activation has also been linked to the Abelson tyrosine kinases (ABL) and scaffolding proteins, e.g., insulin receptor substrate p53 (IRSp53) (Chen et al., 2014; Derivery & Gautreau, 2010). Recently, transmembrane receptors involved in adhesion, ion channels, G-protein coupled receptors, and scaffolding proteins were shown to interact with the WRC via a WRC interacting receptor sequence (WIRS) (Chen et al., 2014).

Studies investigating the regulation of the WRC have focused on CYFIP, as it is the main subunit that mechanistically initiates WRC activation (Chen et al., 2010). When CYFIP binds to RAC1-GTP (Kobayashi et al., 1998), the CYFIP/NAP1 subcomplex undergoes a conformation change and releases the sequestered VCA domain of WAVE (Chen et al., 2010; Eden et al., 2002). The free WAVE-VCA domain can bind to the ARP2/3 complex and recruit actin monomers to start branched actin polymerization (Figure 1.5). Several studies have highlighted the importance of CYFIP-dependent WRC activation for proper lamellipodium morphology (Schaks et al., 2018, 2020; Steffen et al., 2004).

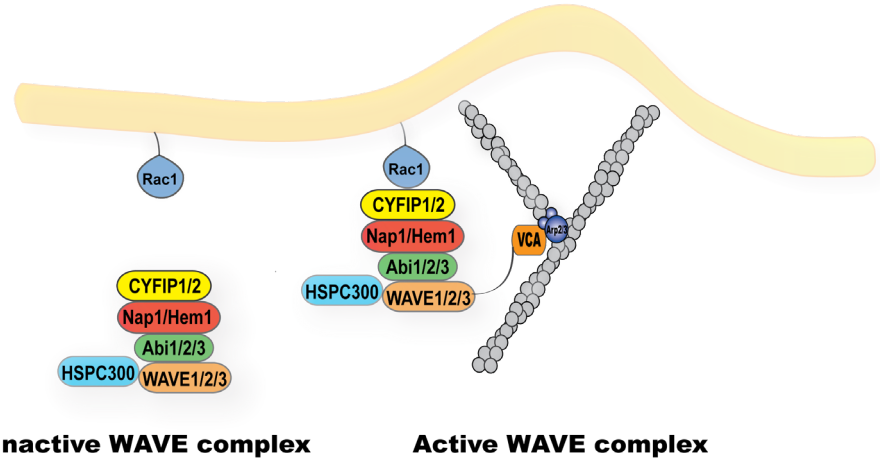

Figure 1.5. WRC activation relayed to the ARP2/3 complex.
The WRC is initially inactive as the VCA domain of WAVE is sequestered by binding to CYFIP. Upon an extracellular stimulus, RAC1 binds to CYFIP, and the VCA domain undergoes a conformational change of the complex. The VCA then binds to the ARP2/3 complex bringing along a G-actin monomer to allow actin nucleation. This process starts the polymerization of *de novo* branched actin filaments at the leading edge/lamellipodium of the cell and results in membrane protrusion. Reprinted and adapted from Stradal et al., (2004) with permission of Elsevier.

1.2.5 Cytoplasmic FMR1-interacting protein (CYFIP)

CYFIP is an evolutionarily conserved gene with two known paralogues in higher eukaryotes: CYFIP1 and CYFIP2 (Schenck et al., 2001). Both CYFIPs has 31 exons which encode a protein

of 1253 amino acids with a molecular weight of ~145 kDa. Mouse CYFIP1 and CYFIP2 share 88 % sequence identity, while human CYFIP1 and CYFIP2 share 98 % and 99 % sequence identity with the mouse orthologues, respectively (Schenck et al., 2001). Several seminal studies on CYFIP identified it as an interaction partner of various proteins. The interaction between CYFIP1 and RAC1, an RHO family GTPase, gave rise to its alternative name, specifically RAC1-associated protein 1 (SRA1) (Kobayashi et al., 1998). In the literature, CYFIP is also known as partner of profilin (POP) as it binds to profilin 2 (Witke et al., 1998). The nomenclature p53-inducible RNA, 121F-specific (PIR121), was appointed after increased CYFIP2 mRNA was found in cell lines expressing 121F p53 variant, resulting in p53-dependent apoptosis (Saller et al., 1999). The current nomenclature, CYFIP, is now widely used as both CYFIP1 and CYFIP2 were identified as an interaction partner of the Fragile X mental retardation protein (FMRP) and the FMRP-related proteins 1 and 2 (FXR1P and FXR2P) (Schenck et al. 2001). The FMRP is encoded by the Fragile X mental retardation 1 (*FMR1*) gene, and mutations of this gene causes a commonly inherited form of mental retardation called Fragile X syndrome (FXS) (Abekhoukh & Bardoni, 2014). During various developmental stages, FMRP, FXR1P, and FXR2P are expressed in the CNS (Bonaccorso et al., 2015). However, only the reduction of FMRP leads to FXS (Bagni et al., 2012).

Studies showed CYFIP1 forms a complex with the eukaryotic translation initiation factor 4E (eIF4E) and FMRP and inhibits mRNA translation in neuronal synapses (Napoli et al., 2008; De Rubeis et al., 2013). It was proposed the upstream signaling of the brain-derived neurotrophic factor (BDNF) activated RAC1-GTP to shuttle CYFIP1 from the CYFIP1-elF4E-FMRP complex to the CYFIP1-WRC complex (De Rubeis et al., 2013). This shift activated the translation of synaptic proteins and the remodeling of the actin cytoskeleton, which are both required for spine morphology. CYFIP1 is also associated with autism spectrum disorder (ASD) (Abekhoukh & Bardoni, 2014). Both the duplication of 15q11-13 in the genome, resulting in increased CYFIP1 expression, and *Cyfip1* haploinsufficiency due to loss of chromosomal material between break points (BP) 1 and 2 in the Angelman and Prader-Willi syndromes correlated with increased ASD risk (Abekhoukh & Bardoni, 2014; Doornbos et al., 2009; Nishimura et al., 2007; van der Zwaag et al., 2009). Patients diagnosed with ASD also had increased levels of both *Cyfip1* and *Cyfip2* mRNA (Noroozi et al., 2018). Morphological abnormalities in axonal myelination are also associated with ASD (Domínguez-Iturza et al., 2019). Recent murine studies on *Cyfip1* haploinsufficiency showed aberrant myelination in the corpus callosum (Domínguez-Iturza et al., 2019; Fricano-Kugler et al., 2019; Silva et al., 2019). Surprisingly, *Cyfip2* haploinsufficiency had no effect on global FMRP protein expression in

the CNS, despite dendritic spine abnormalities and behaviors associated with FXS (Han et al., 2015). However, the behavioral correlation between CYFIP, FMRP, and ASD is still unclear.

The cellular localization of CYFIP1 and CYFIP2 differs despite high amino acid sequence identity. Mouse developmental studies showed the complete deletion of *Cyfip1* leads to early embryonic lethality at E8.5 due to gastrulation defects and improper mesoderm induction (Massimi, 2008; Pathania et al., 2014; Stöcker, 2015). The complete deletion of *Cyfip2* leads to perinatal lethality shortly after birth (Kumar et al., 2013; Zhang et al., 2019). Previous work in our lab showed that both CYFIPs have distinct expression profiles in peripheral organs (Beuck, 2018). In adult mice, CNS tissue CYFIP1 is expressed in both neurons and astrocytes, while CYFIP2 expression is exclusively neuronal (Zhang, Kang, & Han, 2019). *In vitro* assays showed that CYFIP2 is localized in both excitatory and inhibitory synapses, and overexpression of CYFIP2 results in increased dendritic branching (Davenport et al., 2019; Pathania et al., 2014). These studies indicate that in hippocampal cells, the role of CYFIP2 is highly localized to synaptic compartments. Recent studies using a *Cyfip2* haploinsufficiency mouse model showed CYFIP2 was only reduced in neurons located in layer 5 of the medial prefrontal cortex (mPFC) (Lee et al., 2020). This group also showed *Cyfip2*$^{+/-}$ mice made multiple axonal contacts to dendrites and had reduced docked vesicle in layer 5 presynaptic terminals compared to controls. In a conditional mouse model where *Cyfip2* was specifically deleted in the pyramidal neurons, there was a reduction of CYFIP2 in cortical layer 2/3 and layer 5 (Zhang et al., 2020). However, CYFIP2 expression is not exclusively neuronal. Patients with multiple sclerosis (MS) had increased CYFIP2 protein expression in their $CD4^+$ T-cells along with increased fibronectin-mediated adhesion (Mayne et al., 2004). CYFIP2 is also implicated in other disease physiology. *Cyfip2*$^{+/-}$ mice had increased levels of proteins associated with Alzheimer's diseases (AD), e.g., BACE1 and amyloid $\beta_{1–42}$ in cortical, hippocampal, and thalamic regions (Ghosh et al., 2020; Tiwari et al., 2016). We showed the conditional deletion of *Cyfip2* in the forebrain only upregulated amyloid precursor protein (APP) in hippocampal neurons (Özer, 2019). CYFIP2 has also been associated with binge eating, cocaine sensitization, schizophrenia, and epilepsy (Babbs et al., 2019; Föcking et al., 2015; Kirkpatrick et al., 2017; Kumar et al., 2013; Nakashima et al., 2018).

Studies are emerging on the role of CYFIP2 and posttranscriptional gene regulation. RNA editing usually occurs in noncoding regions, but *Cyfip2* was identified as a coding gene that undergoes post-transcriptional RNA editing known as A-to-I RNA editing (Levanon et al., 2005). The result is an amino acid exchange at position 320 (on exon 9), resulting in the

production of glutamic acid (E) instead of lysine (K) (Levanon et al., 2004, 2005). The CYFIP2 K/E editing occurs in mammalian brain tissue and spinal MNs and is catalyzed by the enzyme adenosine deaminase acting on RNA 2 (ADAR2) (Hideyama & Kwak, 2011; Levanon et al., 2004; Nishimoto et al., 2008; Riedmann et al., 2008). CYFIP2 K/E editing occurs in both embryonic and postnatal development stages in mouse and human: mice showed an increase in CYFIP2 K/E editing from 4 % at E15 to 75 % at P21 (Shtrichman et al., 2012; Wahlstedt et al., 2009). To date, the exact mechanism regulating CYFIP2 K/E editing is unclear. Recently, CYFIP2 circular RNA (circRNA), termed circCYFIP2 was identified as a marker upregulated in gastric cancer cells, which increased proliferation and metastasis in mouse xenografts (Lin et al. 2020). It was proposed circCYFIP2 inhibited the microRNA miR-1205, thus disrupting its function in translational inhibition (Lin et al., 2020).

1.3 Development of the mammalian spinal cord

The nervous system consists of both the CNS and the PNS. While the CNS is the brain and spinal cord, the PNS is comprised of the cranial nerves and spinal nerves that control both sensory and motor outputs (Purves et al., 2018). Both the CNS and PNS use highly specialized neurons and glia cells to communicate and undergo various physiological functions. The typical structure of a neuron consists of a cell body, multiple dendrites, and an axon. Communication amongst these neurons happens at sites called synapses consisting of the presynaptic terminal, the synaptic cleft, and the postsynaptic target. The axons have presynaptic compartments called boutons and can release neurotransmitters into the synaptic cleft, and postsynaptic terminals can integrate the incoming presynaptic inputs. Neuronal communication is performed by either 1) electrical synapses that use gap junctions to allow ions to travel from the pre- to the postsynapse or 2) chemical synapses that release neurotransmitters loaded in vesicles into the synaptic cleft after an action potential depolarizes the axonal bouton (Purves et al., 2018).

The spinal cord is part of the CNS and is used to communicate between the brain and peripheral organs. The spinal cord is located caudal to the forebrain and consists of the central canal, the grey matter, and the white matter, which contains the myelinated axonal tracts. The grey matter consists of neuronal cell bodies, interneurons, astroglia cells, and unmyelinated axons and synapses. The glia in the spinal cord consists of astrocytes and oligodendrocytes, which are important for the myelination of axons to enable proper signaling. The human spinal cord is divided into 31 segments that are grouped into cervical (C1-8), thoracic (T1-12), lumbar (L1-5), sacral (S1-5), and coccygeal (Co1) segments. The murine spinal cord is also divided into

five subgroups with different segmentation: cervical (C1-8), thoracic (T1-13), lumbar (L1-6), sacral (S1-4), and coccygeal (Co1-3). Other nomenclature used is cervical (neck), brachial (forelimbs), thoracic (trunk), lumbar (hindlimb), and sacral (tail) (Sengul & Watson, 2012).

Spinal cord development, known as neurulation, starts when the neural plate folds to form the neural tube using several signaling pathways, e.g., bone morphogenetic proteins (BMP), Wnt signaling, and Sonic hedgehog (Shh) (Ashwell, 2009; Frisén et al., 1998; Jessell, 2000). The spinal cord is organized into dorsal and ventral regions. The dorsal spinal cord has commissural and association neurons; the ventral spinal cord contains ventral interneurons and motor neurons (MNs) (Goulding et al., 2002). The spinal cord has over 23 different neuronal subtypes, and several transcription factors distinguish the diverse populations in the dorsal-ventral axis patterning (Alaynick, Jessell, & Pfaff, 2011; Jessell 2000; Lu, Niu, & Alaynick, 2015). MNs arise from Olig2-positive progenitor cells, and these neurons innervate different muscles in the body (Davis-Dusenbery et al., 2014). The MNs are the most diverse group of cells, and they express specific transcription factors, e.g., Islet1/2, homeobox gene 9 (HB9), Ngn2, Nkx6.1, and MNR2 (Lu, Niu, & Alaynick, 2015; Shirasaki & Pfaff, 2002). MNs can be classified into two main groups: 1) upper MNs, which project between the cerebral cortex and the spinal cord, and 2) lower MNs that innervate muscle targets belonging to the PNS (Davis-Dusenbery et al., 2014; Stifani, 2014). Upper MNs use glutamate as their main neurotransmitter, while lower MNs use acetylcholine (Stifani, 2014). The coordination of muscle movements integrates signals from the brain that are relayed to upper MNs followed by lower MNs to execute a motor movement.

MNs are organized into motor columns, which have distinct rostro-caudal anatomical placement along the spinal cord, express specific transcription profiles and target specific muscle targets. The main motor columns are the spinal accessory column (SAC), the phrenic motor column (PMC), the medial motor column (MMC), the preganglionic column (PGC), the hypaxial motor column (HMC), and the lateral motor column (LMC) (Francius & Clotman, 2014; Stifani, 2014). The MMC innervates axial muscles, the HMC innervates the body wall, the PGC innervates the sympathetic ganglia, and the LMC innervates the limb muscles. This study will focus on the PMC located in the cervical segments (C3-C5) and its MNs, which innervate the diaphragm to regulate respiration.

1.3.1 The neuromuscular junction

The process of muscle movement requires the coordination of spinal MNs (clustered into specific spinal nuclei called MN pools), which innervates its respective skeletal muscle target. The neuromuscular junction (NMJ) is a chemical synapse located in the PNS and consists of a spinal MN (presynaptic compartment), a muscle fiber (postsynaptic compartment), and perisynaptic (terminal) Schwann cells (Figure 1.6) (Sanes & Lichtman, 2001; Witzemann, 2006).

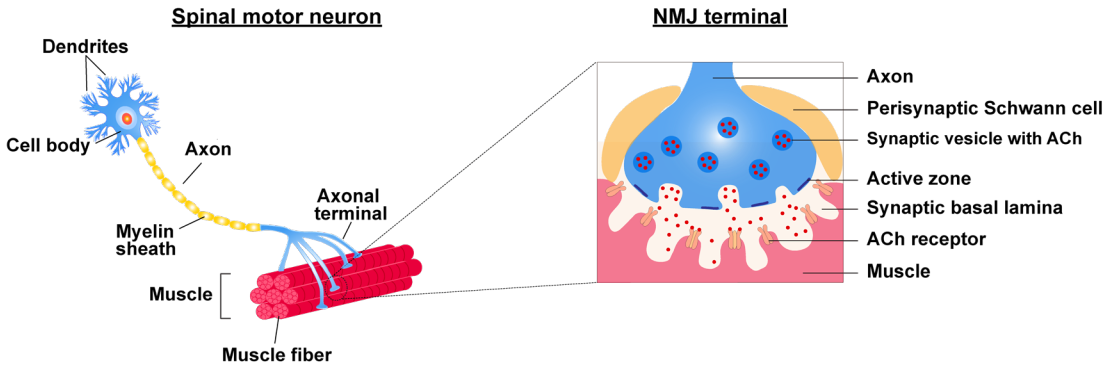

Figure 1.6. The spinal motor neuron and the neuromuscular junction.
A spinal motor neuron (MN) is a cell that forms connections with skeletal and smooth muscle in the peripheral nervous system (PNS). The spinal MN cell body is located in the spinal cord, and its axon branches at the axonal terminal onto the muscle. Schwann cells produce myelin sheaths which wrap around the axon and promote rapid transmission along the axon to the muscle. The neuromuscular junction (NMJ) is the chemical synapse between a MN, a muscle fiber, and a terminal Schwann cell. The action potential travels along the axon and releases the neurotransmitter acetylcholine (ACh), which will travel through the synaptic cleft and bind to the nicotinic acetylcholine receptors (AChR) to depolarize the muscle fiber and start the signaling cascade to innervate the muscle. One individual muscle fiber is innervated by one NMJ. Reprinted and adapted from Shi, Fu, & Ip, (2012) with permission of Elsevier.

All spinal MNs in the PNS have myelin sheaths along the axon, which are produced by glial Schwann cells. These cells are different from the non-myelinating perisynaptic Schwann cells at the nerve terminal. The muscle itself consists of individual muscle fibers, and these fibers are innervated by only one spinal MN. There is only one NMJ associated with a single muscle fiber. However, a single MN is able to innervate several muscle fibers, and this is called the motor unit (Mantilla & Sieck, 2008). In various organisms, the NMJ has been used to study synaptic properties due to its large size and easy accessibility.

The main NMJ neurotransmitter in vertebrates is acetylcholine (ACh), and several nicotinic acetylcholine receptors (AChR) are located in the muscle along with voltage-gated sodium voltage-gated calcium, and voltage-gated calcium potassium channels (Sanes & Lichtman,

1999; Tintignac, Brenner, & Rüegg ,2015). ACh is synthesized by the enzyme choline acetyltransferase (ChAT) from choline and acetyl-CoA. The ACh is stored in secretory vesicles located in the nerve terminal until it is released upon an action potential. ACh can then bind and open the nicotinic AChR clusters located on the postsynaptic terminal on the muscle end plate. The open AChR receptors also allow an influx of sodium ions and will cause a local depolarization of the motor end plate called an end-plate potential. This depolarization event will cause voltage-gated sodium channels to open and initiate an action potential along the muscle fiber. Subsequently, this triggers calcium (Ca^{2+}) release from the sarcoplasmic reticulum, which innervates the muscle to contract. After neurotransmitter release in the synaptic cleft (space between the MN and muscle), ACh is hydrolyzed by acetylcholinesterases, and the choline byproduct is taken up and recycled by choline transporters (CHT) in the axonal bouton. The choline reuptake via CHT is the rate-limiting step in ACh synthesis in the PNS. Mouse models of *Chat* and *Cht* deletion are perinatal lethal due to impaired cholinergic signaling (Brandon et al., 2003; Ferguson et al., 2004; Misgeld et al., 2002).

During development, the AChR are composed of α, β, γ, and δ subunits, and in postnatal development, the δ is replaced with the ε subunit for enhanced Ca^{2+} conductance (Mishina et al., 1986). At embryonic stages, the AChR clusters from a rudimentary oval shape which later develops into a more perforated branched morphology (Sanes & Lichtman, 1999; Shi, Fu, & Ip, 2012). In a process known as 'prepatterning,' AChR clusters form along the muscle before the arrival of MN axons (Sanes & Lichtman, 1999; Shi, Fu, & Ip, 2012). The most well-known regulation of AChR clustering is by agrin, a proteoglycan secreted by MNs and muscle cells (Magill-Solc & McMahan, 1988; Samuel et al., 2012). The MN-derived agrin isoform is z-agrin, and it activates muscle-specific kinase (MuSK), a receptor-like tyrosine kinase (RTK) via the co-receptor low density lipoprotein receptor-related protein 4 (LRP4) to initiates AChR aggregation (Burden et al., 2013; DeChiara et al., 1996)**.** MuSK regulates both agrin-dependent and agrin-independent AChR clustering (Gautam et al., 1999). The muscle fiber is surrounded by the basal lamina, or extracellular matrix (ECM), which also secretes laminin into the synaptic cleft to induce AChR clustering (Hunter et al., 1989; Rogers & Nishimune, 2017). Studies using muscle cell cultures showed that AChR cluster formation induced by either laminin or agrin was dependent on RAC1 and CDC42 signaling activation via the c-Jun amino terminal kinase (JNK) pathway (Weston et al., 2000; Weston et al., 2007). Studies on *Agrin* knockout mice showed aberrant MN axon branching patterns that extended over the entire diaphragm, and these mice were perinatal lethal (Gautam et al., 1996).

Histological studies on *Xenopus* muscle cells showed the presence of the ARP2/3 complex subunits Arp2 and p34arc at sites of AChR clusters (Madhavan et al., 2009). Several studies on *Drosophila* showed impaired NMJ morphology for the knockout of WRC subunits, *d*Cyfip (Bogdan et al., 2004; Schenck et al., 2003; Zhao et al., 2013), *d*Abi (Lin et al. 2009), *d*HSPC300 (Qurashi et al., 2007), *d*WAVE/SCAR (Schenck et al., 2004) and *d*Nap1/Kette (Schenck et al., 2004). However, the role of the WRC on actin polymerization in the murine NMJ is still not fully understood.

1.3.2 The synaptic vesicle cycle in presynaptic boutons

As previously mentioned, the integration of signals via chemical synapses uses neurotransmitters stored in synaptic vesicles located at the presynaptic bouton of an axon. Neurotransmitter release occurs when an action potential depolarizes the bouton, thus inducing the opening of voltage-gated Ca^{2+} channels and the influx of Ca^{2+} that triggers vesicle exocytosis. Three main pools of vesicles are found in the presynaptic bouton: 1) the readily releasable pool (RRP), 2) the recycling pool, and 3) the reserve pool (Denker & Rizzoli, 2010). The RRP describes vesicles that are docked at the active zone of the bouton and primed for release upon Ca^{2+} signaling. After depletion of the RRP vesicles, the recycling pool vesicles (which are located behind the RRP vesicles) are recruited to the active zone. The recycling pool of vesicles release their neurotransmitters under moderate stimulation, but this pool can be refilled by newly recycled vesicles. The reserve pool vesicles make up ~80-90 % of the total vesicle pool and are located furthest away from the active zone. The reserve pool vesicles are only released during high-frequency stimulation and after depletion of the recycling pool (Denker & Rizzoli, 2010). Ultrastructural analysis of the presynaptic boutons in the CNS has shown that actin, along with synapsins, tethers and thus sequesters the RRP of vesicles at the active zone (Cingolani & Goda, 2008; Pilo Boyl et al., 2007; Rizzoli & Betz, 2005). However, histological and electrophysiological analysis of the frog NMJ showed that F-actin was localized in non-release sites and was not used to tether vesicles (Dunaevsky & Connor, 2000; Richards et al., 2004). The machinery used for docking neuronal synaptic vesicles requires SNARE (soluble *N*-ethylmaleimide-sensitive factor attachment protein receptor) proteins. The SNARE complex consists of SNAP25 (25 kDa synaptosome-associated protein), syntaxin, and synaptobrevin (also referenced as VAMP) (Jahn & Scheller, 2006; Südhof, 2012; Yoon & Munson, 2018). The docking of the vesicles occurs when synaptobrevin located on the vesicle membrane binds to syntaxin and SNAP25 at the plasma membrane. Studies showed that

SNARE proteins mediate MN axonal growth cone guidance and innervation in *Drosophila,* chick, and mouse models (Barrecheguren et al., 2017; Islamov et al., 2015).

1.3.3 The ARP2/3 complex in growth cone dynamics and axonal elongation

In 1890 Ramon y Cajal discovered the growth cone, which is crucial for regulating the development of neuronal processes. Growth cones are dynamic structures located at the tips of dendrites or axons that respond to extracellular cues and either extend or retract during pathfinding (Campbell & Holt, 2001; Gomez & Letourneau, 2014; Lowery & Vactor, 2009). Growth cone migration uses both actin and microtubule dynamics to navigate through the environment (Bradke & Dotti, 1999; Letourneau, 1996; Lowery & Vactor, 2009). The growth cones have three distinct compartments: the peripheral (P) domain, the transition (T) zone, and the central (C) domain (Figure 1.7).

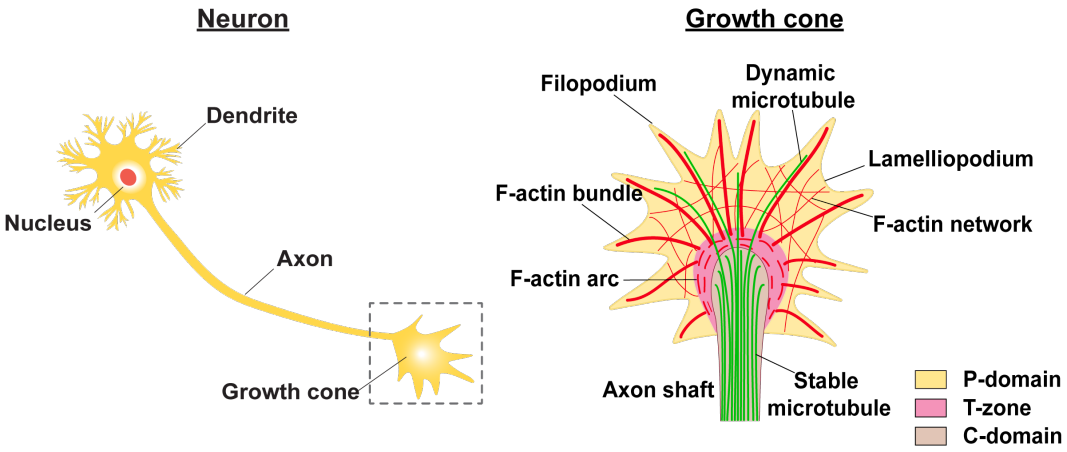

Figure 1.7. Assembly of the axonal growth cone.
The neuron uses its growth cone to navigate through the environment and reach target cells. The growth cone (box) is located at the tip of the axon and has three main domains: 1) the central (C)-domain, 2) the transition (T)-zone, and 3) the peripheral (P)-domain. The P-domain contains actin-based structures that consist of both lamellipodia and filopodia. Branched actin networks are located in the lamellipodium, while the filopodium has F-actin bundles. F-actin arcs are located in the T-zone, the thin region between the C and the P-domain. The C-domain contains microtubules supporting the axonal shaft end and is rich in transported organelles and vesicles. Single microtubules also enter the P-domain due to a phenomenon called dynamic instability. Adapted by permission from Springer Nature: Nature publishing group, Nature Reviews Molecular Cell Biology, "The trip of the tip: understanding the growth cone machinery." Lowery and Van Vactor © (2009).

The P-domain is composed of actin-based lamellipodia and filopodia structures. Branched actin networks are localized in the lamellipodium, while the filopodium has F-actin bundles. The C-domain is located at the neck of the growth cone and in the axonal shaft. Most microtubules end in the C-domain, but there are single microtubules that grow transiently (a process called dynamic instability) into the P-domain and interact with the actin network (Vitriol & Zheng,

2012). The T-zone is a thin region between the P and C-domain. Both the P-domain and the T-zone undergo constant actin dynamic turned over (Lowery & Vactor, 2009). The C-domain has more stable actin ring structures that are formed by adducin and spectrin (Xu et al., 2013).
ABPs are known to regulate both filopodia and lamellipodia dynamics at the leading edge of the growth cones (Dent & Gertler, 2003; Pollard & Borisy, 2003; Theriot & Mitchison, 1991; Wear, Schafer, & Cooper, 2000). However, the role of the ARP2/3 complex in growth cone guidance is still not fully understood. In addition, ARP2/3-dependent branched networks were also detected in filopodia sites at the leading edge in hippocampal neurons (Korobova & Svitkina, 2008). In contrast, ARP2/3 was localized to the C-domain and not in the P-domain in hippocampal neurons (Strasser et al., 2004). The literature on ARP2/3 seems to have some contradicting views on the role in axonal outgrowth. Inhibition of the ARP2/3 complex using *Arp3* RNAi and dominant-negative GFP-CA constructs (binds to and prevents ARP2/3 complex activation *in vitro*) showed an increase in axonal elongation in hippocampal neurons (Pinyol et al., 2007; Strasser et al., 2004). Studies on *Drosophila* mushroom body neurons where WAVE/SCAR was deleted did not show any defects in axonal outgrowth (Ng & Luo, 2004). However, another study showed that WAVE/SCAR deletion reduced both commissural and longitudinal axon bundles in *Drosophila* embryos (Zallen et al., 2002). In *C. elegans,* the ARP2/3 complex was also shown to act in parallel with ENA in regulating actin polymerization essential for axonal guidance (Norris et al., 2009). ARP2/3 inhibition reduced filopodia formation in chick sensory neuron growth cones grown on both laminin (ECM substrate) and L1 (cell adhesion molecule) (San Ruiz-Miguel & Letourneau, 2014). This group did observe differences in actin retrograde flow and growth cone guidance and motility, which were substrate dependent.

Axons are the longest extensions of the neuronal cell body and can extend over 1 meter. Axonal outgrowth requires the coordination of several spatio-temporal events that include biophysical forces and cytoskeletal reorganization (Suter & Miller, 2011). The coordinated interactions between actin and microtubules are essential for proper axonal elongation, which occurs at the growth cone (Bradke & Dotti, 1999; Lewis, Courchet, & Polleux, 2013; Tanaka, Ho, & Kirschner, 1995). It was shown that stable microtubules are essential for axonal elongation (Dent & Gertler, 2003; Lowery & Vactor, 2009). The main events of axonal outgrowth were first described in *Aplysia californica* (marine snail) neurons, and these main stages are protrusion, engorgement, and consolidation (Goldberg & Burmeister, 1986; Lowery & Vactor, 2009). During protrusion, the growth cones attach to the substratum, and retrograde actin polymerization occurs at the leading edge, from the P- towards the C-domain. The engorgement

phase occurs when microtubule polymerization starts to enter the protrusion site bringing in new organelles and membranous vesicles, which are released at the tip of the C-domain. In consolidation, the microtubules form stable bundles, and the axonal shaft is elongated as F-actin depolymerizes at the neck of the growth cone (Dent & Gertler, 2003; Lowery & Vactor, 2009). Axonal elongation is regulated by various factors, including ECM ligands, receptor protein tyrosine kinase receptors, cell adhesion molecules, chemoattractive and chemorepulsive cues (Tessier-Lavigne & Goodman, 1996). The regulation of MN axon outgrowth from the motor column is highly dependent on repulsive cues secrete from the spinal cord floor plate and attractive cues to guide MNs to the appropriate exit points (Bonanomi & Pfaff, 2010).

The role of RHO GTPases, RAC1, CDC42, and RHOA, has been studied in depth in order to understand how upstream signals affect growth cone cytoskeletal dynamics (Gomez & Letourneau, 2014; Kozma et al., 1997; Lowery & Vactor, 2009). Both RAC1 and CDC42 signaling promoted axonal elongation and are associated with chemoattractive growth cues (Lundquist, 2003; Meyer & Feldman, 2002). Studies on CNS axons showed that RHOA signaling inhibited axonal elongation and was associated with chemorepulsive cues (Fujita & Yamashita, 2014; Lowery & Vactor, 2009; Robles et al., 2005; Tahirovic et al., 2010). Recent studies on hippocampal neurons showed that RHOA inhibited neurite extension by blocking microtubule extension via the formation of a myosin II-mediated actin arc in the C-domain (Dupraz et al., 2019).

1.3.4 The ARP2/3 complex in axonal branching

The function of axonal branching and arborization allows neurons to increase the network connectivity at postsynaptic target sites (Kalil & Dent, 2014). Axons branch and connect with their targets using different modes, either by 1) growth cone bifurcation/splitting or 2) axon collateral/interstitial branching (Gallo, 2011; Luo, 2002). The initial stages of branching occur when filamentous actin concentrates at the axonal membrane to form actin patches, sites where actin nucleators (e.g., the ARP2/3 complex) initiate polymerization to produce branched actin networks (Kalil & Dent, 2014). Actin elongation factors, such as ENA/VASP, are also located at actin patches to inhibit capping proteins. Actin patches serve as precursors for filopodia formation; however, only a subset will become collateral branches, and the exact regulation is still unclear (Gallo, 2011; Kalil & Dent, 2014).

Several studies have shown that the RHO-family of GTPases, RAC1, CDC42, and RHOA are upstream signaling pathways that regulate axonal branching (Spillane & Gallo, 2014).

However, the majority of these studies were performed on spinal commissural sensory neurons, which have different molecular profiles compared to spinal MNs. In sensory axons, the actin patches are initiated by phosphoinositide-3 kinase (PI3K) signaling via the nerve growth factor (NGF)-PI3K signaling (Ketschek & Gallo, 2010; Spillane et al., 2012). The signaling of ECM protein laminin to β1-integrins also induced actin patches (Ketschek & Gallo, 2010). Studies on embryonic chick sensory neurons showed the ARP2/3 complex was located at actin patch sites, and inhibiting it with a CA peptide resulted in reduced branching (Spillane et al., 2011).

1.3.5 The ECM-integrin-actin connection links mechanisms of focal adhesion and membrane protrusion

During embryonic development, cells migrate using focal adhesion complexes, which provide a physical link between the ECM and the actin cytoskeleton (Figure 1.8). There are a variety of ECM proteins (e.g., laminin and fibronectin) that regulate neurite outgrowth across various neuronal subtypes, e.g., MNs and dorsal root ganglia (DRG) neurons (Myers et al., 2011). Focal adhesions are formed when the ECM ligands bind to the transmembrane integrin receptors, which dimerize and start the signaling cascade to recruit several focal adhesion proteins to form focal contacts. Integrin receptors are ubiquitously expressed in neurons with dense expression in the growth cones (Wu & Reddy, 2012). Integrins undergo bi-directional signaling, as external environmental cues can alter chemical signaling within the cell, and intracellular changes affect the affinity for extracellular ligand binding (Harburger & Calderwood, 2009). These signaling cascades regulate the turnover of focal adhesion formation and disassembly. However, integrin receptors do not have an actin binding site and use adaptor proteins to link the actin cytoskeleton to the ECM.

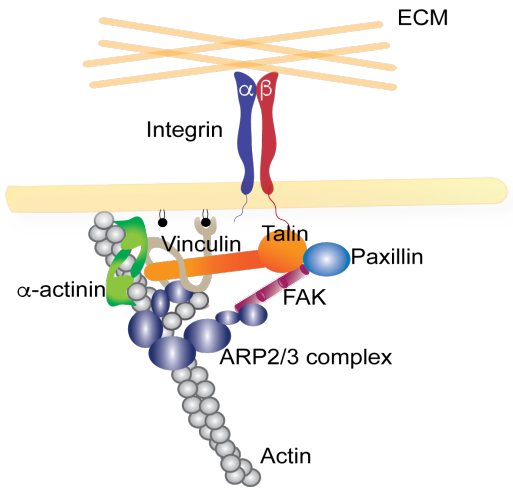

Figure 1.8. Scheme of ECM-integrin-F-actin interaction mediated by the ARP2/3 complex. The actin cytoskeleton is connected to the extracellular matrix (ECM) by various adaptor proteins. The adapter protein talin binds to the β-subunit of the transmembrane protein integrin and links F-actin to the ECM. The ARP2/3 complex can bind to vinculin and focal adhesion kinase (FAK) and is required for stable, mature adhesion formation. PIP_2 modulates the activity of both vinculin and α-actinin, which can bind to actin. Paxillin can regulate the activity of the RHO GTPases RAC1 and RHO. Phosphorylation of FAK and paxillin regulates the assembly of adhesion complexes. Reprinted and adapted from Vicente-Manzanares, Choi, & Horwitz (2009) with permission of Journal of Cell Biology.

The adaptor protein talin binds to the integrin β-subunit upon ECM signaling. Talin then recruits the integrin-associated proteins, vinculin and α-actinin, which all can bind directly to the actin cytoskeleton (Humphries et al., 2007; Vicente-Manzanares, Choi, et al., 2009). Vinculin interacts with several proteins, including the scaffold protein paxillin, the ARP2/3 complex, and VASP, and is important for both nascent and mature focal contacts (Bays & DeMali, 2017; Burridge & Chrzanowska-Wodnicka, 1996; Turner, 2000; Ziegler et al., 2006). The focal adhesion kinase (FAK) also interacts with the ARP2/3 complex and paxillin (Parsons, 2003; Vicente-Manzanares, Choi, et al., 2009). Studies showed FAK tyrosine autophosphorylation (Y397) induced SRC signaling and created new focal contacts (Calalb et al., 1995; Mitra et al., 2005). SRC belongs to the family of non-receptor tyrosine kinases and is highly expressed in the CNS during development (Yagi, 1994). FAK signaling also regulates neurogenesis, axonal outgrowth, axonal guidance, and arborization (Chacón et al., 2012; Navarro & Rico, 2014; Ren et al., 2004).

The extension of growth cones at their leading edge occurs through a model known as the 'molecular clutch' hypothesis, a process that is driven by actin dynamics coupled to adhesion (Lowery & Vactor, 2009; Mitchison & Kirschner, 1988; Nichol et al., 2016). In order for protrusion to occur, there must be a) rapid actin polymerization at the leading edge, b) actin filament attachment to a substratum (the 'clutch'), and c) traction forces on the ECM to drive protrusion away from the adhesion site (Figure 1.9).

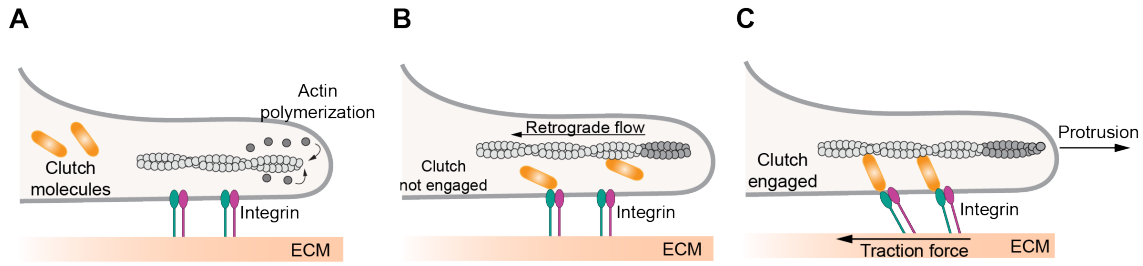

Figure 1.9. The 'molecular clutch' model applied to growth cone protrusion.
(**A**) G-actin is incorporated into the barded end of F-actin located at the leading edge of the lamellipodium. Integrin receptors are bound to the extracellular matrix (ECM). (**B**) When the clutch (orange) is not engaged, actin is not tethered to the ECM, and actin polymerization occurs in a rapid retrograde fashion that drives actin treadmilling. There is no traction force and no protrusion at the leading edge. (**C**) When the clutch is engaged, the filament produces forces that are transmitted to the ECM, and retrograde flow is slowed down. This allows for protrusion of the membrane at the leading edge. Adapted by permission from Springer Nature: Nature publishing group, Nature Cell Biology, "Integration of actin dynamics and cell adhesion by a three-dimensional, mechanosensitive molecular clutch." Case and Waterman © (2015).

When the clutch is not engaged (i.e., adhesion is weak), there is a balance between actin polymerization at the leading edge and retrograde cytoskeletal flow towards the C-domain: this

results in no net filament movement. Myosin II contractility also aids in the retrograde flow of actin filaments (Medeiros et al., 2006). When the clutch is engaged, the filament is linked to the substratum at an adhesion site, traction is created, and protrusion occurs. Actin filaments at the leading edge can attach to the substratum, e.g., the ECM or adjacent cells, through integrin receptors or cadherins (Hynes, 1987, 2002). RAC1 signaling regulates the binding of the ARP2/3 complex to vinculin (DeMali et al., 2002; Swaminathan et al., 2016). FAK-SRC signaling can promote RAC1-dependent membrane protrusion (Hsia et al., 2003; Huveneers & Danen, 2009). In this study, we will focus on the focal adhesion proteins vinculin, FAK, and paxillin based on their interaction with the ARP2/3 complex and their recruitment to form focal adhesion sites in the growth cone for axon protrusion.

1.4 Role of CYFIP2 in axonal morphology

Increasing evidence is emerging of the importance of CYFIP2 in axonal morphology. In *Drosophila*, *d*Cyfip was identified as an important regulator for presynaptic terminal formation and endocytosis in the NMJ (Bogdan et al., 2004; Schenck et al,. 2003; Zhao et al., 2013). *d*Cyfip was expressed in MN axons and was essential for invertebrate axonal outgrowth and branching: *d*Cyfip deletion led to lethality in the larval stages (Schenck et al., 2003). The deletion of *d*Cyfip also impaired F-actin formation during bristle development (Bogdan et al., 2004).

A cell-autonomous function of CYFIP2 was described in *Danio rerio* (zebrafish) retinal ganglion cell (RGC). *Nevermind* (*nev*), the ortholog of CYFIP2, selectively regulated RGC axon guidance and sorting, despite its ubiquitous expression in the CNS (Cioni et al., 2018; Pittman et al., 2010). While CYFIP2 is used in RGC axonal sorting, CYFIP1 was mainly required for axonal elongation (Cioni et al., 2018). In *Xenopus* embryos, retinal axon-axon interactions stimulated CYFIP2-FMRP complex to translocate along the axonal shaft to the growth cone where CYFIP2 was recruited/shuffled to form CYFIP2-WRC complexes (Cioni et al., 2018). However, CYFIP2 in zebrafish also regulated axonal regrowth (Bremer et al., 2019) and the auditory innate startle circuit in reticulospinal Mauthner cells (Marsden et al., 2018). Therefore, these findings suggest CYFIP2 is important in axonal morphogenesis in a variety of motor neuron circuits across different species. To date, the role of CYFIP2 in murine axonal function/morphogenesis has not been clearly established.

1.5 Diaphragm development - a model to study respiratory mechanisms

The mammalian diaphragm is a sheet-like skeletal muscle required for proper respiration function as well as a barrier between the thoracic and abdominal cavities (Merrell & Kardon, 2013; Perry et al., 2010). The contractions initiated by the diaphragm expand the thoracic cavity and start the inspiration phase of respiration, enabling air to flow into the lungs (Campbell, Agostoni, & Davis, 1970). The diaphragm is dome-shaped and is composed of the costal and crural muscle domains, which are connected together by the central tendon connective tissue (Merrell & Kardon, 2013). The costal muscle consists of two muscle halves with myofibers located in both the ventral and the dorsal axis. The crural muscle is located dorsally near the spinal cord. The diaphragm is innervated by phrenic MNs clustered in the phrenic motor column (PMC) originating from the cervical spinal cord segments C3-C6 (Goshgarian & Rafols, 1981; Merrell & Kardon, 2013). Phrenic motor neurons can be distinguished from other MN pools by their transcriptional expression profile.

The development of the mouse diaphragm (Figure 1.10), along with NMJ synaptogenesis, occurs in a stereotyped fashion that starts at E11.5 and continues until postnatal (P) day 20 (Merrell & Kardon, 2013; Witzemann, 2006). The diaphragm develops from specific structures called the pleuroperitoneal folds (PPFs), two transient pyramidal-shaped structures located between the thoracic (pleural) and abdominal (peritoneal) cavities (Merrell et al., 2015; Sefton et al., 2018). The septum transversum is the initial barrier between the thoracic and abdominal cavities. Both muscle progenitor cells in the somites and phrenic nerve axons travel to the PPFs and form the diaphragm (Babiuk et al., 2003; Merrell et al., 2015). Once the muscle progenitor cells reach the PPFs, they will differentiate into myofibers between E11.5 and E15.5. The phrenic nerve is essential for the innervation of the diaphragm muscle and reaches the primordial diaphragm by E13.5, where it splits into three (trifurcate) branches: dorsocostal, sternocostal and crural branches (Allan & Greer, 1997; Laskowski, Norton, & Berger, 1991; Merrell & Kardon, 2013). Each phrenic nerve can arborize to form higher-order branches and form NMJs along the central band of the costal muscle (Babiuk et al., 2003; Laskowski, Norton, & Berger, 1991; Lin et al., 2001). The right and left hemidiaphragm display asymmetrical phrenic branching patterns, as the right hemidiaphragm covers a larger area compared to the left hemidiaphragm (Laskowski et al., 1991). Mouse studies showed that the SLIT-ROBO guidance signaling is essential to establish the left-right hemidiaphragm asymmetry (Charoy et al., 2017). Developmental studies on rat diaphragms showed that both low-affinity nerve growth factor (p75) receptor and neural cell adhesion molecule (NCAM) expressing cells created a migratory track for phrenic MN

axons (Allan & Greer, 1997). Guidance molecules ligands, e.g., netrin receptor UNC5C have also been shown to be important for phrenic nerve migration (Burgess, Jucius & Ackerman, 2006).

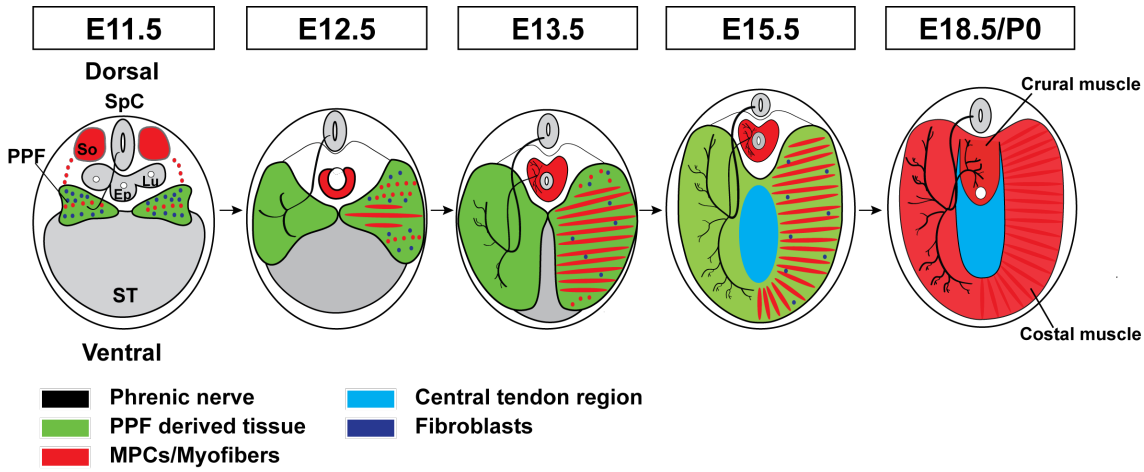

Figure 1.10. Overview of embryonic murine diaphragm development.
The diaphragm develops from multiple embryonic sources. The septum transversum (ST) is the initial structure that separates the thoracic and abdominal cavities. The somites (So) are the main source of muscle cells, and the pleuroperitoneal folds (PPFs) give rise to non-myogenic connective tissue and the central tendon. Muscle progenitor cells (MPCs) migrate from the somites reaching the PPFs by E11.5. The phrenic nerves migrate out of the spinal cord and also reaches the PPFs around E11.5. The innervation of the phrenic nerve starts at E12.5 and continues when the first NMJs are formed at E13.5. Complete phrenic nerve branching occurs by E15.5. At birth (P0), the myofibers are fully developed, forming the costal and crural muscles. The phrenic nerve can then innervate the diaphragm muscle, which is essential for proper breathing. Ep: esophagus, Lu: lung, SpC: spinal cord. Adapted by permission from Springer Nature: Nature publishing group, Nature Genetics, "Muscle connective tissue controls development of the diaphragm and is a source of congenital diaphragmatic hernias.", Merrell, Ellis, Fox, Lawson, Weiss, and Kardon © (2015).

Breathing is an essential physiological function where oxygen is acquired for metabolic processes that use adenosine triphosphate (ATP). Respiratory movements are generated by rhythmic motor circuits located in the brainstem and spinal cord. The neural networks that generate these semi-autonomous functions are called central pattern generators (CPGs) and are located in the brainstem (Smith et al., 2013). CPGs consist of various excitatory neurons and inhibitory interneurons that generate rhythmic outputs independent of any sensory input or feedback (Smith et al., 2013). In the brain stem, controlled rhythmic breathing movements are generated by respiratory neurons located in the pre-Bötzinger complex (pre-BötzC) (Smith et al., 1991). The pre-BötzC is located in the ventral respiratory column (VRC) of the lower brainstem (Feldman, Del Negro, & Gray, 2013; Smith et al., 1991). The output of the VRC premotor circuits regulates spinal MNs of the phrenic nerve, which innervates the diaphragm and abdominal muscles (Smith et al., 2013). Disruption of this circuitry can lead to impaired respiratory function and potential lethality.

1.6 Aim of the Study

CYFIP2 is predominantly expressed in both the brain and spinal cord where the CYFIP2-WRC regulates ARP2/3-dependent branched actin polymerization. Studies on the function of CYFIP2 during mouse embryonic development discovered the perinatal lethal phenotype of the conventional *Cyfip2* knockout model and focused primarily on the anatomy of the brain (Zhang, Kang, Lee, et al., 2019). In the adult CNS the role of CYFIP2 might function to maintain proper dendritic morphology required for synaptic transmission. However, evidence is emerging on the role of CYFIP2 in axonal outgrowth and pathfinding in motor neurons and sensory neurons in various model organisms (e.g., *Drosophila* and zebrafish). Yet, the mechanisms that regulate CYFIP2 axonal morphogenesis in both the CNS and PNS are still under debate, and to date there is no study that has investigated the function of CYFIP2 in mouse PNS motor neuron development.

The aim of this study was to characterize the role of CYFIP2 during embryonic development with the focus on motor neurons and NMJ development to explain the perinatal lethal phenotype. We used various transgenic *Cyfip2* mouse models (e.g., $Cyfip2^{LacZ/wt}$ and $Cyfip2^{-/-}$) to elucidate the localization of CYFIP2 in the spinal cord and in peripheral projections. We also studied the function of CYFIP2 in growth cones and for axonal outgrowth properties using *in vivo* and *in vitro* approaches.

We also used biochemical assays to elucidate the CYFIP2-WRC composition in comparison to the more well studied CYFIP1-WRC. Since CYFIP1 is known to take part in both the WRC and the eIF4E-FMRP complex, we asked if CYFIP2 could be involved in other interactions, presenting evidence that it might be linked to adhesion signaling pathways. Finally, we analyzed if other actin nucleators could compensate for the loss of CYFIP2 in regulating ARP2/3 branched actin polymerization.

2. Results

CYFIP2 is expressed in vertebrates and previous studies have focused on identifying its function in neuronal development in the CNS. Thus far the role of CYFIP2 in axonogenesis and synaptic morphology in select neuronal cell types i.e. hippocampal neurons and RGCs, have been investigated (Cioni et al., 2018; Davenport et al., 2019; Lee et al., 2017; Zhang, Kang, & Han, 2019; Zhang, Kang, Lee, et al., 2019). There is also evidence from our group showing the importance of CYFIP2 for neuronal presynaptic structural integrity in adult mice (Özer, 2019). However, the exact physiological role of CYFIP2 in embryonic development and the cause of immediate lethality after birth (known as perinatal lethality) was still unclear.

2.1 CYFIP2 expression during embryonic development in the PNS

Cyfip2$^{-/-}$ homozygous knockout mice are perinatal lethal, but are present in normal Mendelian ratios at E18.5, the last day of mouse embryonic development (Kumar et al., 2013; Zhang, Kang, & Han, 2019). This indicated that CYFIP2 is important for organ development essential for survival such as respiratory organs (e.g., lungs and/or diaphragm) or skin barrier function.

Based on these observations, we used a *Cyfip2-LacZ* reporter mouse model (Supplementary Figure. 8.1) to investigate the expression profile of CYFIP2 in the CNS and PNS at various embryonic developmental stages. Whole-mount X-gal staining of E13.5 *Cyfip2*$^{LacZ/wt}$ embryos showed prominent CYFIP2/β-Galactosidase (CYFIP2/β-Gal) expression in the brain, spinal cord and dorsal root ganglia (DRG) (Figure 2.1 A, black arrowheads). At E18.5, CYFIP2/β-Gal was still prominently expressed in these regions on both transverse and sagittal sections (Figure 2.1 B, C). The expression of CYFIP2/β-Gal in the spinal cord was confined to the dorsal and ventral grey matter, which is comprised of pools of interneurons, sensory neurons and motor neurons (MNs) (Goulding, 2009) with diffuse expression in the ventral median fissure (Figure 2.1 B). The expression of CYFIP2/β-Gal in the DRGs which are highly enriched in sensory neurons is also in line with other studies that CYFIP2 in sensory neurons in zebrafish (Cioni et al., 2018; Pittman et al., 2010).

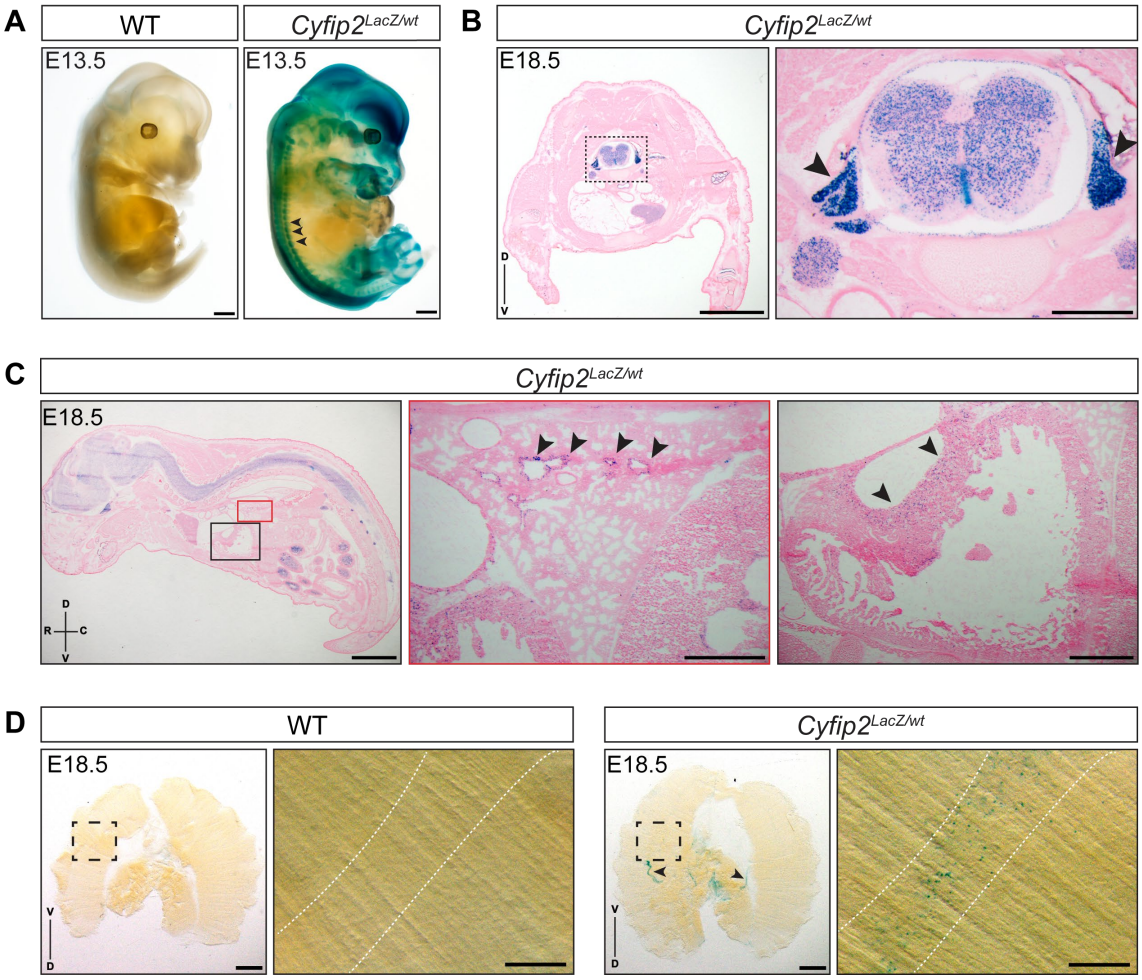

Figure 2.1. *Cyfip2-LacZ* expression in the CNS and PNS during murine development.
(**A**) Whole-mount X-gal staining of E13.5 WT and *Cyfip2*$^{LacZ/wt}$ mouse embryos shows CYFIP2 expression in the brain, spinal cord and DRGs (black arrowheads) Scale bar: 2 mm. (**B**) E18.5 *Cyfip2*$^{LacZ/wt}$ mouse transverse body section shows *Cyfip2-LacZ* expression in the thoracic spinal cord region. Boxed region is magnified and shows the spinal cord with prominent CYFIP2/β-Gal expression in the grey matter and in the dorsal root ganglia (arrowheads). Scale bar: 5 mm; 1 mm in magnification. (**C**) E18.5 *Cyfip2*$^{LacZ/wt}$ mouse sagittal body section shows prominent CYFIP2/β-Gal expression in the CNS, including the spinal cord. Red boxed region is magnified in the middle panel and shows CYFIP2/β-Gal expression in the lung bronchioles (black arrowheads). The black boxed region is magnified in the right panel and shows CYFIP2/β-Gal expression in the wall of the heart ventricle muscle (black arrowheads). Scale bar: 5 mm; 1 mm in magnification. (**D**) Whole- mount X-gal staining of dissected diaphragms from E18.5 WT (left panel) and *Cyfip2*$^{LacZ/wt}$ embryos (right panel). CYFIP2/β-Gal expression is visible in the phrenic nerve and along the costal and crural muscle (black arrowheads). Boxed regions are magnified to show the costal muscle surface with puncta-like CYFIP2/β-Gal expression in the central band region where neuromuscular junctions (NMJs) are formed. Scale bar: 2 mm in overview panels; 500 µm in magnification. C: caudal; D: dorsal; R: rostral; V: ventral.

We noticed faint CYFIP2/β-Gal expression in regions adjacent to the thoracic spinal cord where the heart and lungs are located at E13.5. Sagittal E18.5 *Cyfip2*$^{LacZ/wt}$ sections showed CYFIP2/β-Gal expression in the lungs and heart (Figure 2.1 C, magnification panels). MNs of the thoracic

segments of the spinal cord innervate the heart and lungs (Francius & Clotman, 2014). We also investigated if CYFIP2 is located in the diaphragm, which is part of the respiratory system. Whole-mount X-gal analysis of E18.5 diaphragms from *Cyfip2*$^{LacZ/wt}$ embryos showed CYFIP2/β-Gal expression in the phrenic nerve and in the central band region of the costal muscle (Figure 2.1 D). The phrenic nerve consists of axons that innervate the diaphragm and is vital for proper respiration. However, CYFIP2 protein expression was not detected in E13.5 diaphragm lysates compared to other muscle lysates and brain tissue (Supplementary Figure. 8.3). Overall, these results are the first report of murine CYFIP2 expression in the PNS and specifically in the phrenic nerve of the murine diaphragm.

2.2 CYFIP2 is required for proper respiration: role in murine diaphragm

The prominent expression of CYFIP2 in the phrenic nerve and the central band (location of the NMJs) of the diaphragm pointed to a possible function of the protein in the respiratory system. One typical cause of perinatal lethality is caused by respiratory failure (Turgeon & Meloche 2009). Therefore, we investigated the function of the lungs, an important organ in respiration in P0 *Cyfip2*$^{-/-}$ mice.

We performed a lung inflation test on dissected lungs of newborn *Cyfip2*$^{-/-}$ and WT mice 20 min after birth. The lungs were submerged in water and the lungs of *Cyfip2*$^{-/-}$ mice sank to the bottom, indicating that they were not properly aerated (Figure 2.2). This finding indicated that respiratory failure was the main cause of perinatal lethality. To exclude joint causes, we also checked the skin barrier hydration properties, which when impaired is another common cause of perinatal lethality. We performed a Toluidine blue staining assay on E18.5 *Cyfip2*$^{-/-}$ and WT mice to exclude epidermal abnormalities. The Toluidine blue assay showed no irregularities in skin barrier permeability properties (Supplementary Figure 8.4). The lung failure together with our previous observation of CYFIP2/β-Gal expression in the phrenic nerve and NMJs on the diaphragm muscle (Figure 2.1 D) prompted us to investigate the development of the phrenic nerve in *Cyfip2*$^{-/-}$ mice.

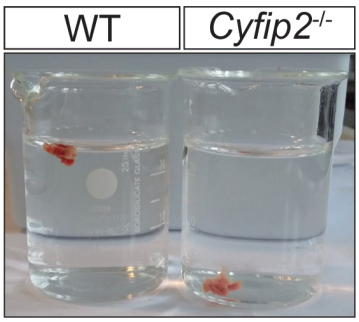

Figure 2.2. The lungs of *Cyfip2*$^{-/-}$ newborn mice are not properly aerated.
P0 *Cyfip2*$^{-/-}$ mouse lungs (right) are not aerated and sink when immersed in water while WT lungs float (left). This indicates *Cyfip2*$^{-/-}$ mice have problems with the global respiratory machinery.

2.2.1 CYFIP2 is essential for phrenic nerve development

We performed whole-mount immunohistochemistry on E18.5 *Cyfip2*$^{-/-}$ diaphragms with anti-neurofilament-200 antibody (Ab), a well-established axonal marker, and α-bungarotoxin (α-BTX), a snake derived toxin that irreversibly binds to AChR clusters in the motor endplate (Lee, Tseng, & Chiu, 1967). The stainings showed that E18.5 *Cyfip2*$^{-/-}$ diaphragms did not have the stereotyped phrenic nerve morphology seen in the control embryos and the sternocostal (ventral) branch was never formed (Figure 2.3). Interestingly, the E18.5 *Cyfip2*$^{-/-}$ diaphragms had AChR clusters in the dorsal costal muscle aligned along the innervating dorsocostal phrenic nerve branch. In WT E18.5 diaphragms the phrenic nerve displayed higher order branching patterns that made synaptic contacts with the AChR clusters (Figure 2.3 C'). Instead, the *Cyfip2*$^{-/-}$ phrenic nerve showed signs of reduced higher order branching (Figure 2.3 F') which is an indication of impaired defasciculation. The thinner nerve fiber in the *Cyfip2*$^{-/-}$ mouse could have two causes: 1) motor neuron cell death; or 2) a fundamental problem with axon growth and/or guidance.

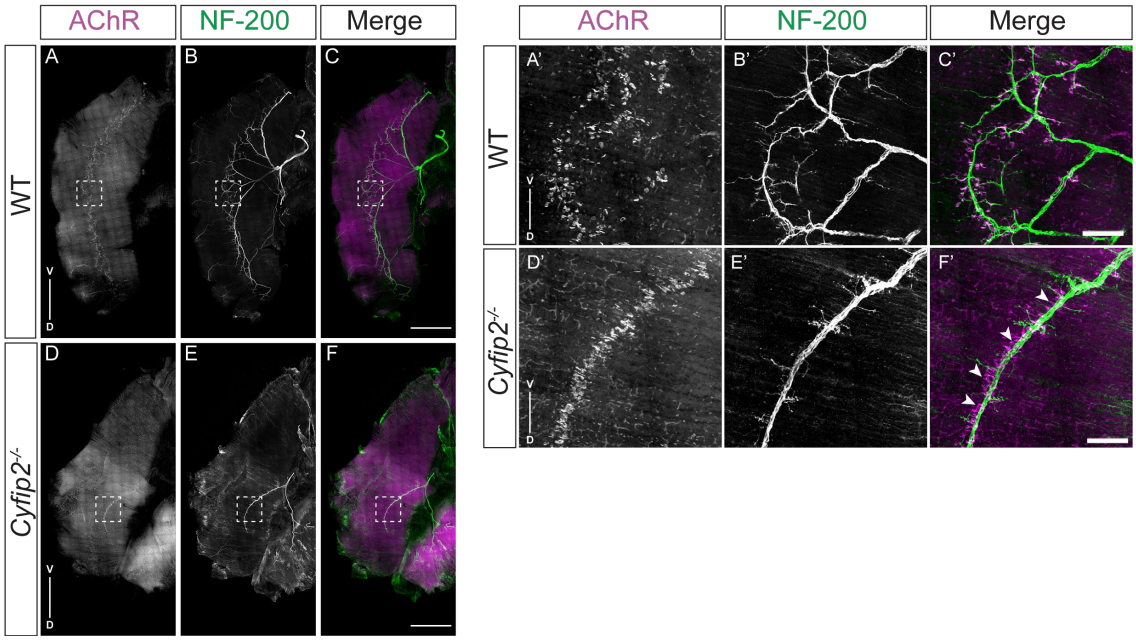

Figure 2.3. CYFIP2 is required for phrenic nerve development.
Whole-mount E18.5 diaphragms labelled with Alexa 555-conjugated α-BTX (A,D,A',D', and C,F,C',F' magenta) and anti-neurofilamnent-200 (NF-200) Ab (B,E,B',E', and C,F,C',F' green). α-BTX labels the AChR clusters and anti-NF-200 labels the motor axons in the phrenic nerve. White boxed region is shown magnified on the right. *Cyfip2*$^{-/-}$ diaphragms lack the stereotyped phrenic nerve branching (D-F) seen in the WT controls (A-C). *Cyfip2*$^{-/-}$ phrenic nerve also lacks higher order branching and shows AChR clusters aligned along the primary phrenic branch (D'-F', arrowheads) compared to WT controls (A'-C'). Scale bar: 1 mm in A-F; 100 μm in A'-F'. D: dorsal; V: ventral.

At E13.5 the phrenic nerve reaches the diaphragm and trifurcates into the sternocostal (ventral), dorsocostal (dorsal) and crural branches, and by E15.5 the stereotyped higher order branching pattern of the phrenic nerve is complete (Allan & Greer 1997; Merrell & Kardon 2013). Therefore, we immunolabeled E13.5 diaphragms and observed the phrenic nerve in *Cyfip2*$^{-/-}$ embryos did not bilaterally trifurcate as seen in the WT control (Supplementary Figure 8.5). The E15.5 *Cyfip2*$^{-/-}$ diaphragms displayed similar branching properties as seen at E18.5 (Figure 2.4 A). The sternocostal branch was missing and the dorsocostal branches were much shorter. This indicated that axonal elongation and/or guidance is at least in part responsible for the defective phenotype. Next, we quantified the phrenic nerve diameter of E15.5 and E18.5 *Cyfip2*$^{-/-}$ diaphragms and observed a significant decrease in diameter when compared to WT controls (E15.5: ~40 % decrease, $p = 0.003$, and E18.5: ~50 % decrease, $p < 0.001$) (Figure 2.4 B). In order to analyze axonal outgrowth properties, we also analyzed the length of the phrenic nerve length at E15.5 (Figure 2.4 C) and E18.5 (Figure 2.4 E). At both ages the *Cyfip2*$^{-/-}$ mice had shorter axons in all dorsal and ventral quadrants compared to WT. This indicated CYFIP2 is required for proper spinal MN axonal outgrowth in the diaphragm. In addition, we wanted to know if CYFIP2 was required for axonal guidance as we observed E13.5 *Cyfip2*$^{-/-}$ diaphragms lacked proper phrenic nerve trifurcation and branching morphology. We quantified the number of higher order secondary branches at E15.5 and *Cyfip2*$^{-/-}$ mice did not have secondary branched in the dorsal hemidiaphragms (Figure 2.4 D). Some secondary branches in the dorsal quadrants were observed in E18.5 *Cyfip2*$^{-/-}$ diaphragms, but still fewer when compared to controls (Figure 2.4 F). Thus, arguing that CYFIP2 is also required for proper spinal MN axon guidance in the diaphragm.

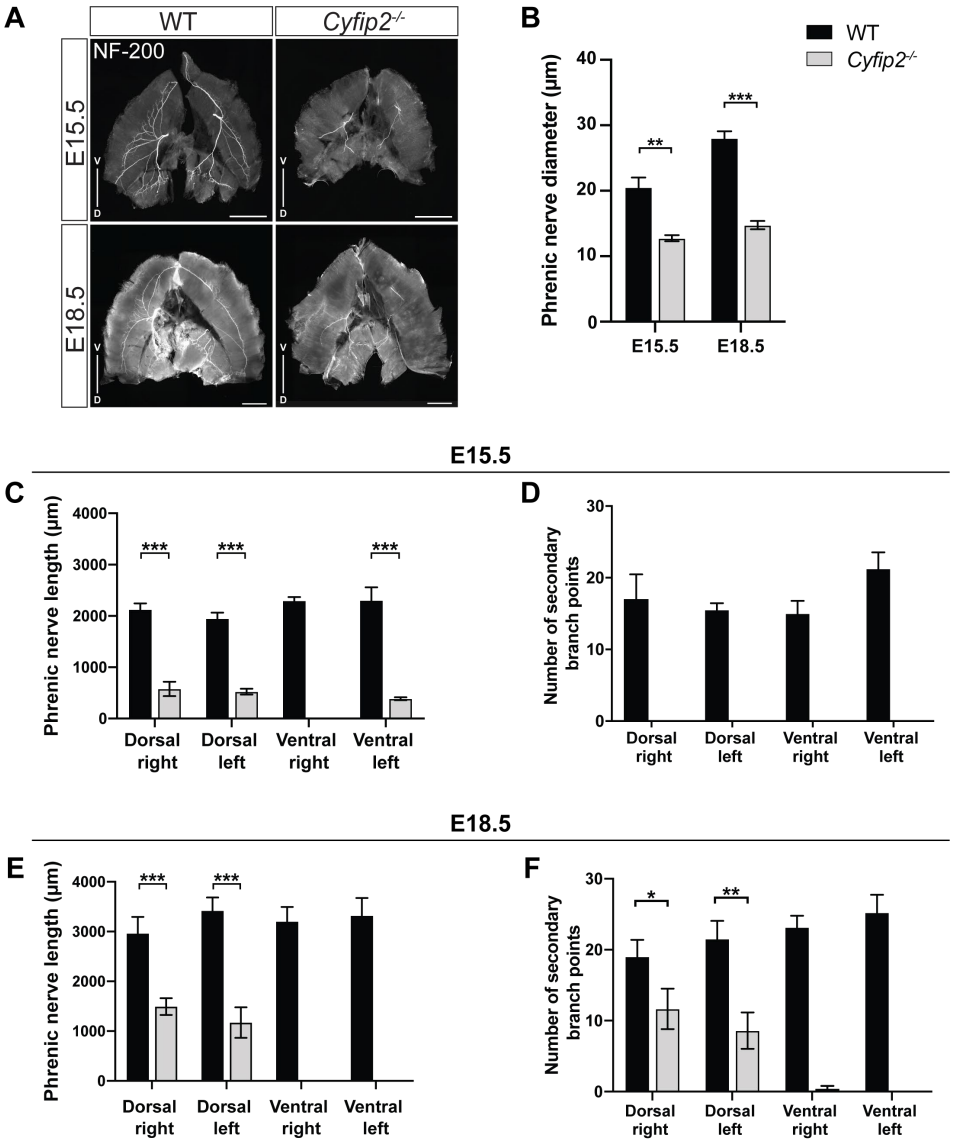

Figure 2.4. CYFIP2 is essential for spinal motor axon outgrowth and branching.
(**A**) Whole-mount immunolabelled E15.5 and E18.5 diaphragms with anti-neurofilament-200 Ab (NF-200) shows higher-order phrenic nerve branching properties are reduced in *Cyfip2*$^{-/-}$ mice compared to WT. (**B**) Phrenic nerve diameter in E15.5 and E18.5 is significantly reduced by ~40 % ($p = 0.003$) and ~50 % ($p < 0.001$), respectively in *Cyfip2*$^{-/-}$ mice. (WT: n = 4, *Cyfip2*$^{-/-}$: n = 4). (**C**) Reduced length of dorsocostal (dorsal) and sternocostal (ventral) phrenic nerve branches in E15.5 *Cyfip2*$^{-/-}$ diaphragms in the dorsal right (~80 % reduction, $p < 0.001$,), dorsal left (~73 % reduction, $p < 0.001$,), ventral right (100 % reduction, $p < 0.001$,) and ventral left (~92 % reduction, $p < 0.001$) quadrants. (WT: n = 4, *Cyfip2*$^{-/-}$: n = 4). (**D**) Reduced secondary branching of *Cyfip2*$^{-/-}$ phrenic nerve in E15.5 diaphragms shows no visible secondary branches in the dorsal and ventral hemidiaphragms. (**E**) Reduced length of dorsal and ventral phrenic nerve branches in E18.5 *Cyfip2*$^{-/-}$ diaphragms in the dorsal right (~50 % reduction, $p = 0.005$,), dorsal left (~66 % reduction, $p < 0.001$,), ventral right (100 % reduction, $p < 0.001$,) and ventral left (~100 % reduction, $p < 0.001$) quadrants (WT: n = 6, *Cyfip2*$^{-/-}$: n = 5). (**F**) Reduced number of secondary branches in E18.5 diaphragm in the dorsal right (~54 % reduction, $p = 0.04$), dorsal left (~60 % reduction, $p = 0.006$), ventral right (~98 % reduction, $p < 0.001$) and ventral left (100 % reduction, $p < 0.001$) (WT: n = 6, *Cyfip2*$^{-/-}$: n = 5). Unpaired two-tailed *t*-test. *$p < 0.05$, **$p < 0.01$, ***$p < 0.001$. Data are mean ± S.E.M. Scale bar: 1 mm. D: dorsal; V: ventral.

Interestingly, we also observed axonal swellings along the phrenic nerve in P0 *Cyfip2*$^{-/-}$ diaphragms (Figure 2.5) along with reduced phrenic nerve diameter when compared to WT controls. This was comparable to observations from E15.5 and E18.5 *Cyfip2*$^{-/-}$ shown in Figure 2.4.

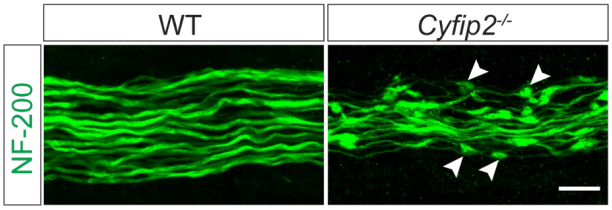

Figure 2.5. Axonal swelling in *Cyfip2*$^{-/-}$ phrenic nerve.
Phrenic nerve immunolabeling with anti-neurofilament-200 Ab (NF-200, green) shows accumulation of NF along the single motor neuron axons (white arrowheads) in P0 *Cyfip2*$^{-/-}$ diaphragms. Scale bar: 5 µm.

This could be caused by an accumulation of neurofilament or organelles, such as mitochondria, similarly to what was described in a mouse model of spinal muscular atrophy (McGovern et al., 2008). Overall, these results indicated that the signaling mechanism required for proper axonal elongation, axonal guidance and axonal branching was severely impaired and delayed. The phrenic nerve of *Cyfip2*$^{-/-}$ mice lack the properties required for physiological diaphragm innervation and as a result this leads to perinatal lethality.

2.2.2 CYFIP2 and the postsynaptic NMJ- effects on AChR cluster morphology

The diaphragm undergoes 'prepatterning' where AChR clusters localize along the central band after the formation of the muscle fibers, but before innervation by MNs (Witzemann, 2006; Yang et al., 2001). Previous studies showed CYFIP2 was localized in postsynaptic compartments in rat hippocampal neurons (Lee et al. 2017; Pathania et al. 2014). Therefore, we wanted to investigate if CYFIP2 is required for proper postsynaptic NMJ development and positioning.

α-BTX immunolabelling of E18.5 diaphragms showed AChR clusters only in the dorsal quadrant of the costal muscle in *Cyfip2*$^{-/-}$mice, were aligned to form a central band (Figure 2.6 A). Interestingly, the ventral hemidiaphragms, which lacked the phrenic sternocostal branch (Figure 2.6 E), contained AChR clusters broadly spread out across the entire surface of the muscle (Figure 2.6 A, white boxes). In WT control diaphragms these ventral AChR clusters were tightly aligned along the central band in the entire costal muscle. We measured the length of the AChR clusters located along the dorsocostal (dorsal) phrenic nerve branch (Figure 2.6 B). The AChR cluster length in E18.5 *Cyfip2*$^{-/-}$ diaphragms were similar to WT controls (Figure 2.6 C). Since endplate clusters were present in mutant mice this indicated that CYFIP2 loss per

se does not inhibit the initial AChR cluster formation in the muscle. However, CYFIP2 deletion did lead to aberrant AChR cluster localization, likely due to altered nerve-muscle crosstalk and refinement of AChR cluster patterning.

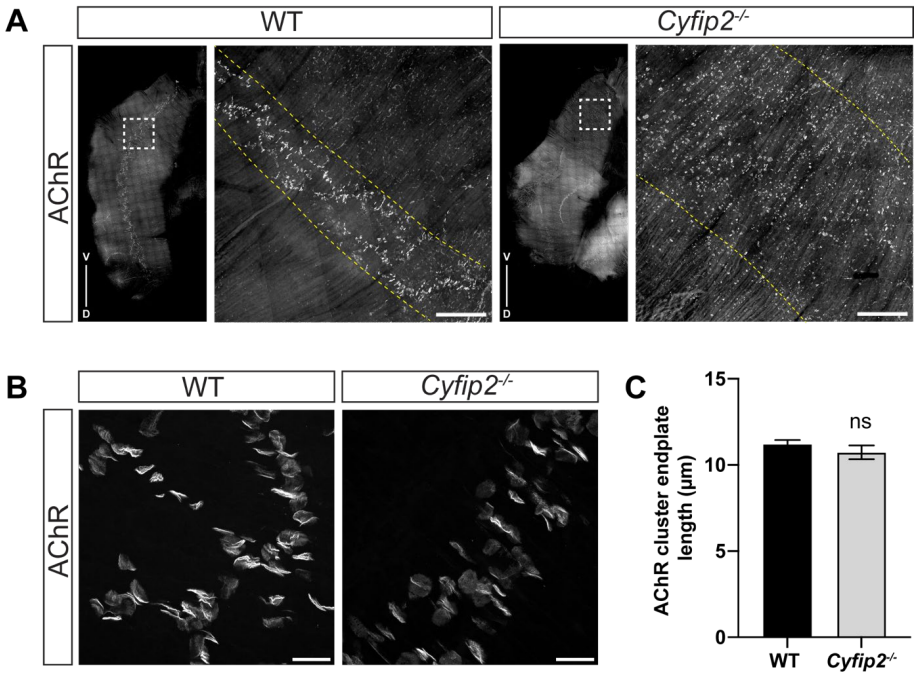

Figure 2.6. CYFIP2 deletion affects endplate cluster morphology in the diaphragm.
(**A**) Hemidiaphragms of WT and *Cyfip2*$^{-/-}$ E18.5 embryos labelled with Alexa 555-conjugated α-BTX to label AChR clusters. White boxed areas in the ventral costal quadrant are enlarged on the right side and shows abnormal AChR cluster formation in *Cyfip2*$^{-/-}$ mice. (**B**) Representative images of the dorsal costal region of E18.5 diaphragms labeled with Alexa 555-conjugated α-BTX to measure the endplate cluster width in the presence of the phrenic nerve. (**C**) AChR cluster length in *Cyfip2*$^{-/-}$ mice is comparable to WT controls. WT: n = 220 clusters/4 animals, *Cyfip2*$^{-/-}$: n = 220 clusters/4 animals from at least three independent experiments. Unpaired two-tailed *t*-test. Data are mean ± S.E.M. Scale bar: 200 µm in **A**, 20 µm in **B**. D: dorsal; V: ventral.

2.2.3 SNARE dysfunction due to CYFIP2 loss

The physiology of the diaphragm NMJ is based on synaptic vesicle exocytosis primarily regulated by the SNARE complex (Jones et al. 2017; Liu et al. 2019; Liu, Sugiura, & Lin 2011). The SNARE proteins along with other active zone protein complexes in the presynapse are integral for neurotransmitter release (Südhof, 2012). The presynaptic membrane in the NMJ contains the SNARE proteins SNAP25 and syntaxin 1 (SYN1), which have been extensively characterized in various model systems (Jones et al. 2017; Sanes & Lichtman 1999; Südhof 2012; Washbourne et al. 2002). The two membrane SNARE proteins join in a complex with one vesicular SNARE protein, synaptobrevin 2 (VAMP2), tethering the vesicles to the membrane in what is known to be the docking/priming process. These tethered vesicles have a

chance to be exocytosed, releasing the neurotransmitter (Südhof, 2012) which in the case of spinal MNs is acetylcholine (ACh). Since we did not perform electrophysiological experiments to test whether the NMJ were functional we used SNARE complexes and vesicles markers to check if the NMJ was present. This morphological data would be a good indication of a possible functional synapse in the diaphragm required for respiration. Therefore, we investigated if CYFIP2 loss in MNs affected the level of SNARE proteins and vesicles in the presynaptic terminals of the diaphragm NMJ.

We performed whole-mount immunolabelling on E18.5 diaphragms using anti-SNAP25 Abs to label SNARE complexes on presynaptic membranes. As previously mentioned, axons were labelled with anti-neurofilament-200 Abs and the AChR clusters in the endplates with α-BTX. The results showed that E18.5 *Cyfip2*$^{-/-}$ mutants had reduced SNAP25 labelling indicating reduced functional axonal terminals compared to WT controls (Figure 2.7 A). In E18.5 *Cyfip2*$^{-/-}$ diaphragms, contact sites between SNAP25-labeled membranes and AChR clusters were also reduced. We constructed surface rendered images (using Imaris) of Z-stack maximum projections to obtain higher resolution spatial information. The 2D surface rendered images confirmed that E18.5 *Cyfip2*$^{-/-}$ diaphragms had reduced synaptic contacts needed for proper muscle innervation (Figure 2.7 B). 3D surface rendered videos highlighting the NMJ organization in WT and *Cyfip2*$^{-/-}$ diaphragms can be seen using the QR codes in Figure 2.7 C, D. We also carried on a complementary approach to study the functionality of presynaptic terminals in *Cyfip2*$^{-/-}$ diaphragms, immunolabeling vesicles through synaptophysin, a protein involved in regulating synaptic vesicle exocytosis. Studies showed that synaptophysin-positive synaptic vesicles are present in both axons and presynaptic terminals in embryonic diaphragm NMJs (Brandon et al., 2003; Heredia et al., 2018; Liu et al., 2008). Whole-mount immunostaining of E18.5 diaphragms using anti-synaptophysin and anti-neurofilament-200 Abs showed the absence of synaptophysin-positive presynaptic terminals near the endplates in *Cyfip2*$^{-/-}$ mice (Figure 2.7 E). These results indicate that CYFIP2 has an essential role during development in the establishment of complete presynaptic terminals.

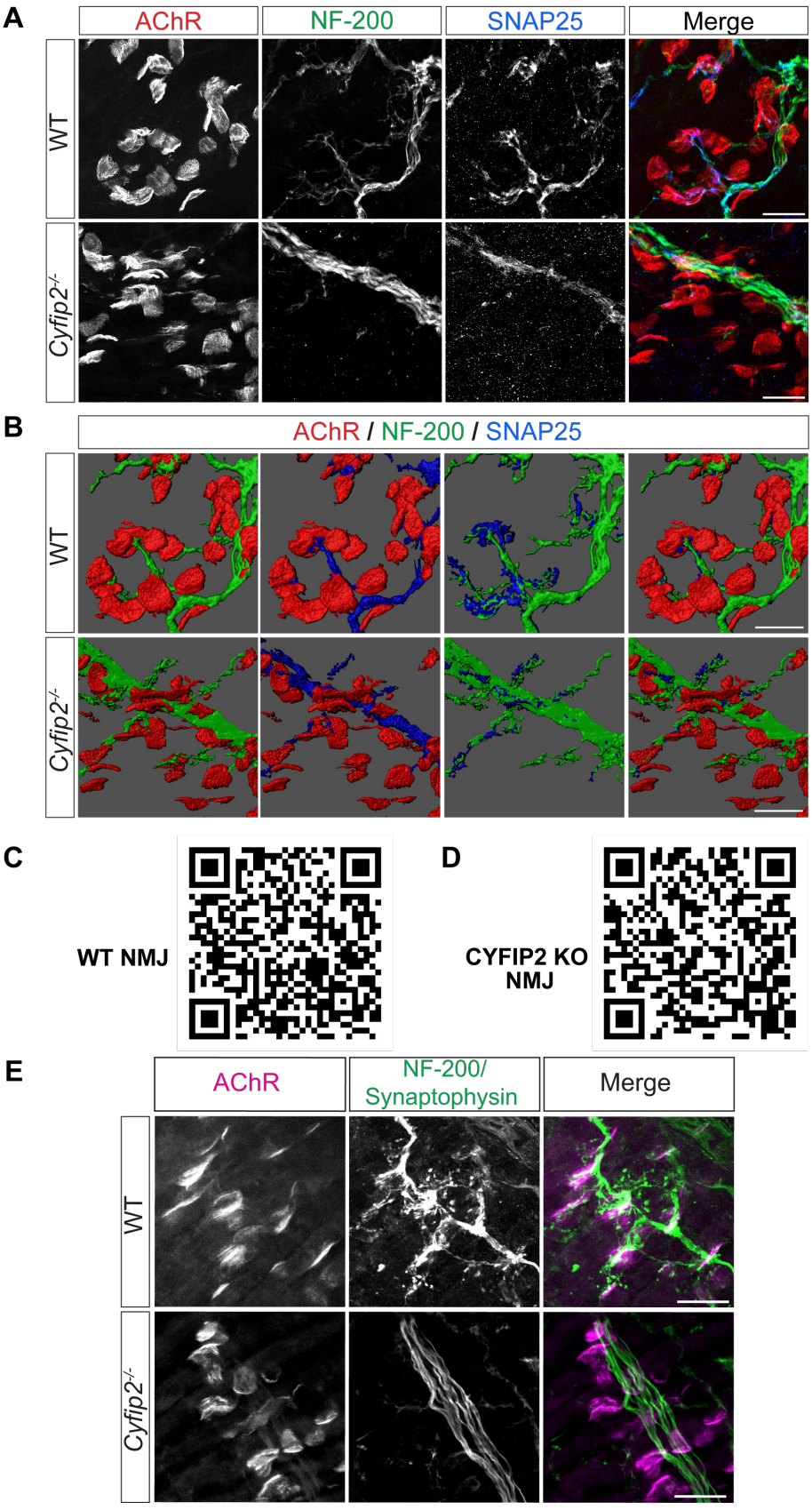
A
AChR
NF-200
SNAP25
Merge
WT
Cyfip2-/-
B
AChR / NF-200 / SNAP25
WT
Cyfip2-/-
C
WT NMJ
D
CYFIP2 KO NMJ
E
AChR
NF-200/ Synaptophysin
Merge
WT
Cyfip2-/-

Figure 2.7. CYFIP2 is required for the formation of NMJ presynaptic terminals.
(**A**) Whole-mount labelling of E18.5 diaphragms with Alexa 555-conjugated α-BTX (red) to label AChR clusters, anti-neurofilament-200 (NF-200) Ab (green) and anti-SNAP25 Ab (blue) shows that the *Cyfip2*$^{-/-}$ phrenic nerve lacks proper presynaptic terminals compared to WT controls. (**B**) Surface rendered images of **A** shows dramatic reduction in contact surface between SNAP25 and the AChR clusters in *Cyfip2*$^{-/-}$ diaphragms. (**C**) QR code for WT and (**D**) *Cyfip2*$^{-/-}$ (CYFIP2 KO) videos of 3D surface rendered diaphragm NMJ. (**E**) Whole-mount immunolabelling of E18.5 diaphragms with α-BTX (magenta) and anti-NF-200 together with anti-synaptophysin Abs (green) shows that *Cyfip2*$^{-/-}$ phrenic nerve terminals have extremely reduced presynaptic vesicle content compared to WT controls. Scale bar: 20 μm.

2.2.4 CYFIP2 is required for proper localization of choline transporters

The main neurotransmitter used by MNs is ACh which is cleaved into choline and acetate in the synaptic cleft by acetylcholinesterase (Hughes, Kusner, & Kaminski 2006; Sanes & Lichtman 1999). The presynaptic membrane recycles choline for further ACh production, and the reuptake of choline is carried out by the choline transporter (CHT). The supply of choline and its reuptake is the rate limiting step in ACh neurotransmitter production in the presynaptic terminal (Abreu-Villaça, Filgueiras, & Manhães 2011; Ferguson et al. 2003, 2004). Complete deletion of *Cht* in mice also resulted in perinatal lethality, implying that a functional presynaptic terminal requires the expression of the CHT (Ferguson et al., 2003, 2004). We previously showed *Cyfip2* deletion impaired the development of SNAREs in the phrenic nerve presynaptic terminals (Figure 2.7) Therefore wanted to test if choline reuptake machinery might also be impaired in the absence of CYFIP2. Whole-mount immunolabelling of E18.5 diaphragms with anti-CHT Abs showed reduced CHT-positive clusters contacting motor endplates in *Cyfip2*$^{-/-}$ mice compared to WT controls (Figure 2.8). The reduced CHT expression in *Cyfip2* mutants implies inefficient reuptake of choline needed for ACh synthesis. Altogether these *in vivo* results showed that CYFIP2 is a requisite for the correct presynaptic terminal development, neurotransmitter vesicle localization and membrane docking and the recycling of choline.

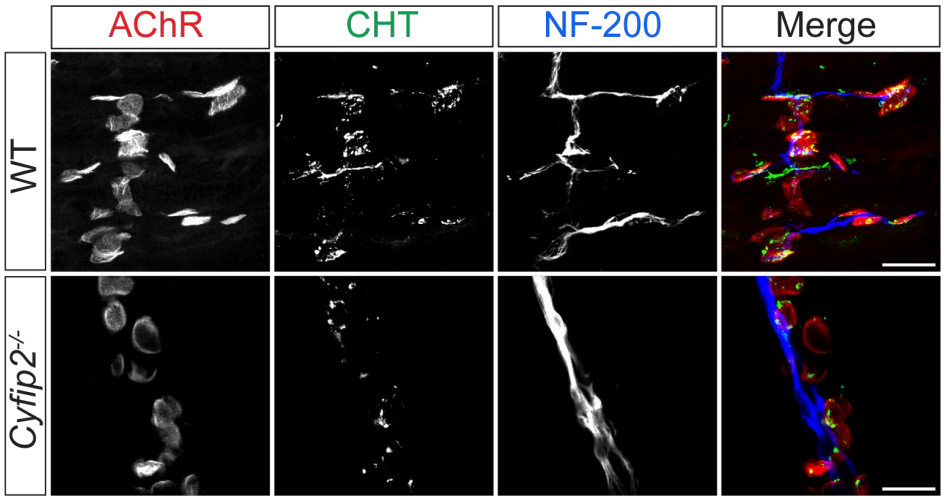

Figure 2.8. CYFIP2 deletion causes loss of choline transporter in the NMJ.
Whole-mount labelling of E18.5 diaphragms with Alexa 555-conjugated α-BTX (red) to label AChR clusters, anti-choline transporter (CHT) Ab (green) and anti-neurofilament-200 (NF-200) Ab (blue) shows reduced choline transporters localization with motor endplates in *Cyfip2*$^{-/-}$ mice compared to WT controls. Scale bar: 20 μm.

2.2.5 CYFIP1 does not compensate for CYFIP2 loss

Our *in vivo* data indicated that CYFIP2 is essential for NMJ presynaptic terminal formation, however what about the role of CYFIP1 in the NMJ? To date, the presence of CYFIP1/SRA1 in the murine NMJ has not been reported. Therefore, we used immunohistological assays to check if CYFIP1/SRA1 is expressed in the NMJ. E18.5 diaphragms were immunolabeled with the CYFIP1/2-5C9 antibody that recognizes both CYFIP isoforms. Since previous biochemical assays in our lab have established CYFIP2 is 3 to 5 times more abundant than CYFIP1 in neurons, we assumed that most of the signal in WT diaphragm corresponded to CYFIP2 protein. CYFIP2 signal in WT tissue was localized in axon terminal endings that made contacts with the AChR clusters (Figure 2.9). As E18.5 *Cyfip2*$^{-/-}$ diaphragms are completed devoid of CYFIP2, any positive signal is attributed to CYFIP1 protein. We observed consistently fewer CYFIP1-positive puncta along the AChR clusters in E18.5 *Cyfip2*$^{-/-}$ diaphragms (Figure 2.9) which did not colocalize with the neurofilament staining labelling the axons. It is therefore possible that the CYFIP1 staining is mainly in the postsynaptic compartment of the NMJ and in the muscle fibers.

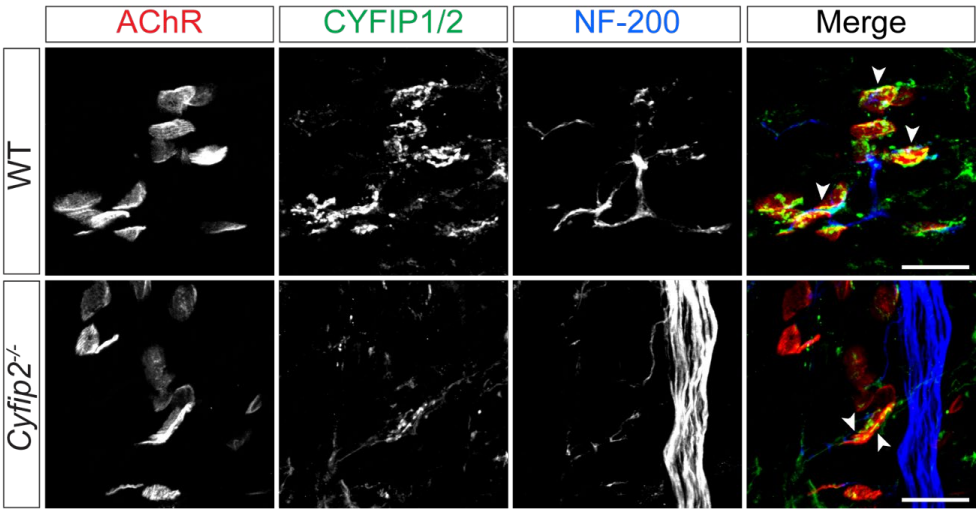

Figure 2.9. CYFIP1 does not compensate for the loss of CYFIP2.
Whole-mount labelling of E18.5 diaphragms with Alexa 555-conjugated α-BTX (red) to label AChR clusters, anti-CYFIP1/2-5C9 Ab (green) and anti-neurofilament-200 (NF-200) Ab (blue) shows the prominent fluorescence signal in presynaptic terminals in contact with endplates, attributable to CYFIP2. In *Cyfip2*$^{-/-}$ diaphragms CYFIP1-positive puncta are absent from the axon. Low levels of CYFIP1-positive are detected and colocalize with the motor endplates (arrowheads) and muscle fibers indicating a possible muscle expression of this isoform. Scale bar: 20 μm.

2.2.6 The actin binding proteins MENA/VASP levels are not affected by the loss of CYFIP2

Since *Cyfip2* mutants removes the WRC nucleation activity, likely reducing ARP2/3 activity, we asked whether other actin nucleators/elongation factors could be affected by the absence of CYFIP2. As previously mentioned CYFIP1-dependent ARP2/3 actin nucleation does not compensate for the loss of CYFIP2. Since the actin elongation protein profilin 2 is an interaction partner of CYFIP2 we checked biochemically if it was upregulated in the absence of CYFIP2. Biochemical assays using spinal cord protein lysates showed there were no differences in Pfn2 protein levels (Supplementary Figure. 8.6). We focused on MENA/VASP family proteins that are localized in lamellipodium and filopodium (Rottner et al., 1999; Svitkina et al., 2003). MENA is also important for axonal projection outgrowth in the brain (Lanier et al., 1999) and is also localized to focal adhesion sites (Gertler et al., 1996). There is evidence both *in vitro* and *in vivo* that the ARP2/3 complex initiates filopodia formation (Korobova & Svitkina, 2008; Vignjevic et al., 2003). Since we observed both VASP and CYFIP2 proteins are localized in similar filopodia-like structures (Supplementary Figure. 8.7) we asked if the loss of CYFIP2 might lead to a shift towards MENA/VASP-dependent linear actin polymerization.

MENA and VASP protein levels were measured in E18.5 brain and spinal cord protein lysates. The Western blot analysis showed no significant difference in both MENA isoforms (140 kDa and 80 kDa) and total VASP (46 kDa) protein levels in the brain (Figure 2.10 A, B) and in spinal cord (Figure 2.10 C, D) when *Cyfip2* was deleted. Interestingly, phosphorylated VASP (VASP-P, 50 kDa) appeared reduced in E18.5 *Cyfip2*$^{-/-}$ spinal cord extracts (Figure 2.10 D). The ratio of phosphorylated VASP to total VASP was substantially decreased in both *Cyfip2*$^{+/-}$ and *Cyfip2*$^{-/-}$ spinal cord extract (~50 %), but the difference was not significant (Figure 2.10 E). In *Drosophila, in vitro* assays showed the direct interaction between GST-EVH1 domain of Mena and *d*Cyfip (Chen et al. 2014). We therefore asked if in the mouse MENA and/or VASP are interaction partners of CYFIP2. Co-IP of CYFIP2 from E18.5 brain lysates showed that neither MENA nor VASP directly interacted with CYFIP2 (Figure 2.10 F). The protein band at 55 kDa visible on the VASP blot is the IgG heavy chain from the antibody used in the IP. The findings demonstrated that MENA/VASP protein levels are not altered by loss of CYFIP2 in the CNS, although VASP phosphorylation seems to be reduced.

In summary these results are the first report of murine CYFIP2 and CYFIP1 in the diaphragm NMJ. CYFIP2 has been shown to be essential for the stereotyped MN axon elongation and branching pattern. The disruption of this process affected proper AChR clusters alignment with the phrenic nerve, causing a complete loss of innervation of the ventral diaphragm and a partial loss in the dorsal costal and crural muscles. In the innervated areas, presynaptic terminal development was heavily affected in the absence of CYFIP2, with little or no neurotransmitter vesicles present and strongly reduced CHT expression. On the other hand, CYFIP1 appeared to be localized in the postsynaptic compartment of the NMJ. However, CYFIP1 was clearly unable to compensate for the loss of CYFIP2 during embryonic development, considering the strong developmental defects summarized above and the perinatal lethality of *Cyfip2*$^{-/-}$ mice. This is a strong indication that in the mouse CYFIP2 and CYFIP1 have divergent roles in neurodevelopment.

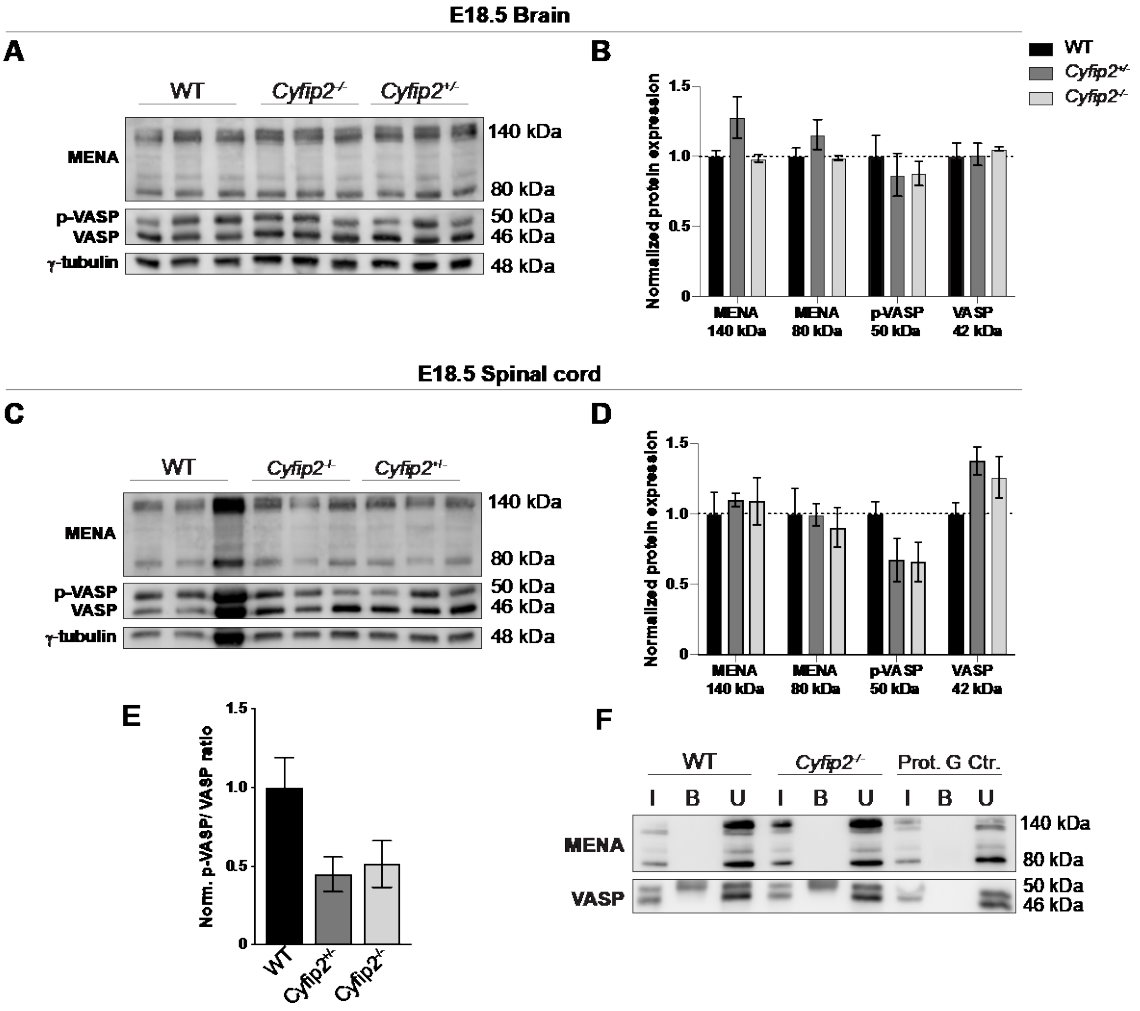

Figure 2.10. MENA and VASP levels are not altered loss of CYFIP2 in the CNS.
(**A**) Western blots and (**B**) quantitation of E18.5 *Cyfip2*$^{+/-}$ and *Cyfip2*$^{-/-}$ total brain lysates show no significant differences of both MENA isoforms (140 kDa and 80 kDa), total VASP (46 kDa) and phosphorylated VASP (p-VASP, 50 kDa) protein levels compared to WT controls. (**C**) Western blots and (**D**) quantitation of E18.5 *Cyfip2*$^{+/-}$and *Cyfip2*$^{-/-}$ total spinal cord lysates also show no differences in both MENA isoforms (140 kDa and 80 kDa). There is no significant difference between total VASP (46 kDa) and p-VASP (50 kDa). (**E**) Ratio of p-VASP to total VASP shows a tendency to reduce in *Cyfip2*$^{+/-}$ and *Cyfip2*$^{-/-}$ but it is not significance compared to WT controls ($F(2,6) = 3.9$, $p = 0.82$). WT: *Cyfip2*$^{+/-}$, $p = 0.1$; WT: *Cyfip2*$^{-/-}$, $p = 0.14$). (**F**) Co-IP of CYFIP2 from E18.5 brain lysate shows that neither MENA nor VASP interact with CYFIP2. B: bound fraction, I: input fraction. WT: n = 3-5, *Cyfip2*$^{+/-}$: n = 3-4, *Cyfip2*$^{-/-}$: n = 3-5. One-way ANOVA with Tukey's post-hoc test. Data are mean ± S.E.M.

2.3 CYFIP2 is essential for spinal MN axonal morphology

We have shown that CYFIP2 is essential for phrenic nerve development in the mouse. To address the molecular aspects of CYFIP2 depletion that might be responsible for the phenotype we used cultured spinal MNs. We performed immunocytochemical analysis on spinal MNs at

different *in vitro* developmental stages labelling F-actin with phalloidin and analyzing various morphological parameters (Figure 2.11 A).

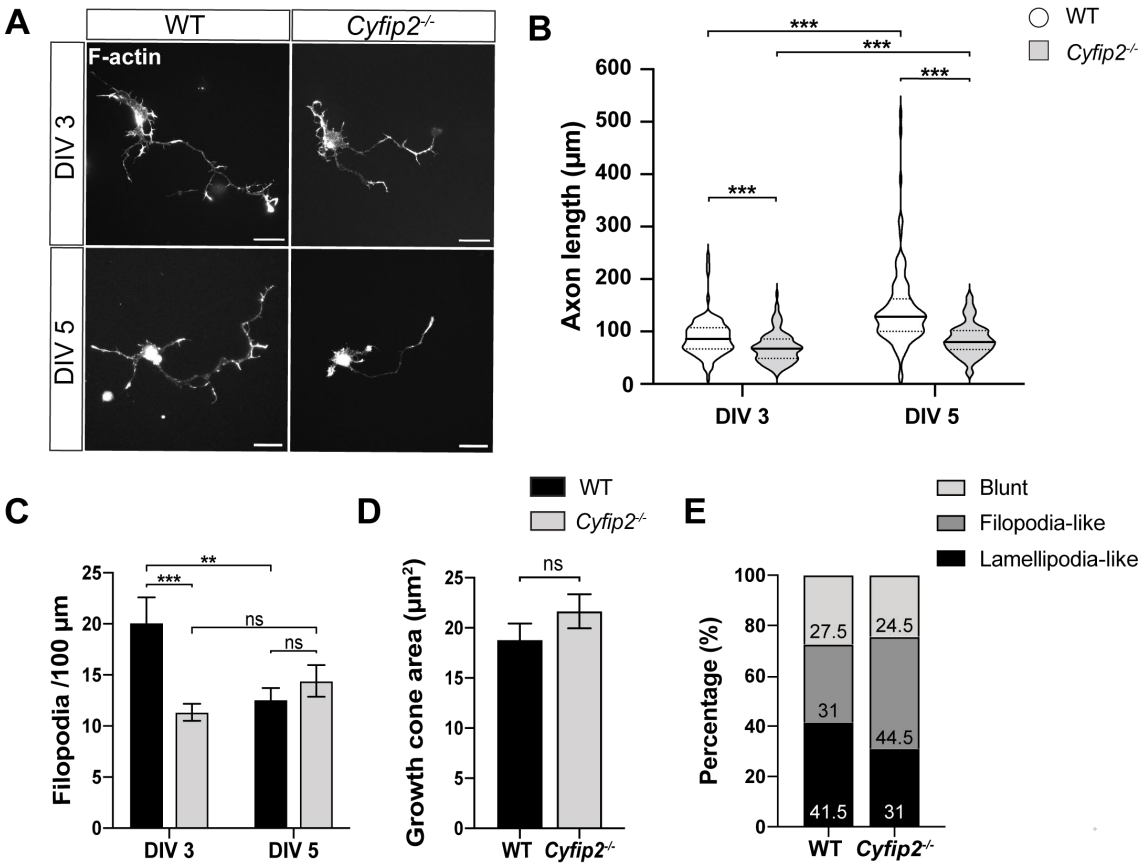

Figure 2.11. CYFIP2 affects axonal growth in spinal motor neurons *in vitro*.
(**A**) Representative images of days in vitro (DIV) 3 and DIV 5 WT and *Cyfip2*$^{-/-}$ spinal MNs grown on laminin labeled with Alexa 488-conjugated phalloidin to visualize F-actin and to analyze axonal morphological properties. (**B**) At DIV 3 *Cyfip2*$^{-/-}$ MNs have ~20 % shorter axons compared to WT ($p < 0.001$). At DIV 5 *Cyfip2*$^{-/-}$ MNs have ~40 % shorter axons compared to WT ($p < 0.001$). Two-tailed Mann Whitney unpaired test. Both WT and *Cyfip2*$^{-/-}$ DIV 5 axons are longer compared to DIV 3 ($p < 0.001$, paired Wilcoxon test). Violin plot shows the 25th to 75th percentile range (dashed line) and the median (solid line). (**C**) DIV 3 *Cyfip2*$^{-/-}$ MNs have less filopodia along the axonal shaft ($p < 0.001$). At DIV 5 *Cyfip2*$^{-/-}$ MNs have comparable number of filopodia to WT controls ($p = 0.34$). WT: DIV 3 n = 102, DIV 5 n = 110; *Cyfip2*$^{-/-}$: DIV 3 n = 110, DIV 5 n = 100 from at least three independent experiments. (**D**) CYFIP2 deletion in MNs at DIV 3 has no significant effect on growth cone area ($p = 0.23$; WT: n = 135, *Cyfip2*$^{-/-}$: n = 125 from three independent experiments). (**E**) Distribution of lamellipodia-like, filopodia-like and blunt growth cones in DIV 3 MNs. CYFIP2 deletion leads to ~14 % increase in filopodia-like growth cones compared to controls (WT: n = 200, *Cyfip2*$^{-/-}$: n = 200 from three independent cultures). Unpaired two tailed *t*-test. ns: not significant, $^{**}p < 0.01$, $^{***}p < 0.001$. Data in **C**, **D** and **E** are mean ± S.E.M. Scale bar: 20 µm.

At both days in vitro (DIV) 3 and DIV 5, *Cyfip2*$^{-/-}$ MN axons were significantly shorter compared to WT controls (~20 % and ~40 % length reduction, respectively) (Figure 2.11 B). We calculated the number of filopodia along the axonal shaft, as these structures are the

potential precursors of collateral axonal branches (Gallo, 2011). At DIV 3, *Cyfip2*$^{-/-}$ spinal MNs had significantly fewer filopodia compared to WT controls (Figure 2.11 C). Surprisingly, at DIV 5 fewer filopodia structures were observed compared to DIV 3 in both genotypes, without significant difference. We also analyzed growth cone morphological properties which might influence axonal outgrowth. While the DIV 3 *Cyfip2*$^{-/-}$ MNs growth cones were not significantly larger than WT controls (Figure 2.11 D) they did display an increased proportion of filopodia-like growth cones (Figure 2.11 E).

Next, we examined if *Cyfip2*$^{-/-}$ MNs could synthesize ACh, the main neurotransmitter in spinal MNs, by studying the expression of the cellular choline acetyltransferase (ChAT), the enzyme required for the final step of ACh synthesis. Immunolabelling of DIV 3 MNs with anti-ChAT Ab showed that *Cyfip2*$^{-/-}$ MNs had less ChAT-positive signal in the growth cone (but not in the axon shaft) compared to controls (Figure 2.12 A, B). These findings correlate with the previous results of reduced choline transporter expression in the presynaptic terminals of the motor neurons in *Cyfip2*$^{-/-}$ diaphragms (Figure 2.8).

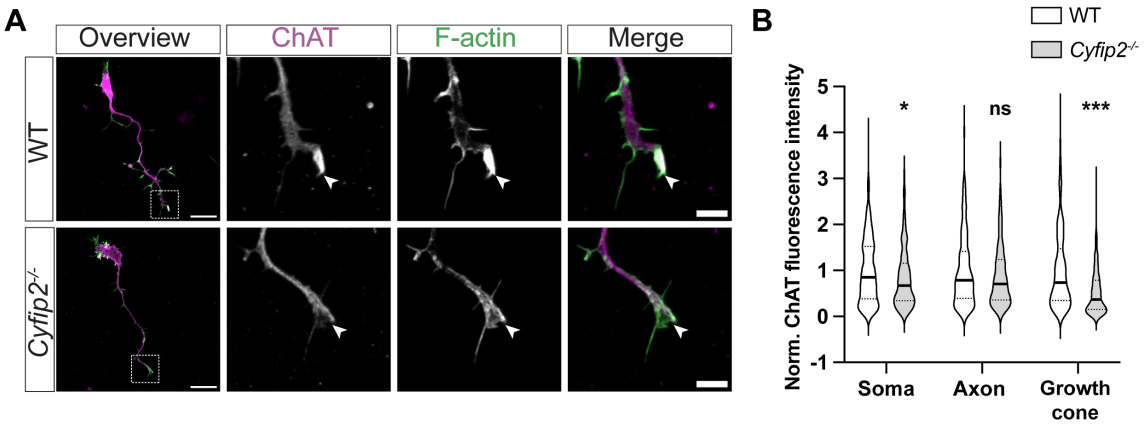

Figure 2.12. CYFIP2 affects the expression of ChAT in MNs.
(**A**) Representative images of DIV 3 MNs and magnification of their growth cone (arrowhead) immunolabelled with anti-ChAT Ab (magenta), and Alexa 488-conjugated phalloidin (green) shows reduced ChAT levels in *Cyfip2*$^{-/-}$ MNs. (**B**) Normalized ChAT fluorescence intensity graph shows a decrease in the growth cone ($p < 0.001$), but not in the soma nor axonal shaft in *Cyfip2*$^{-/-}$ MNs. WT: n = 266-269, *Cyfip2*$^{-/-}$: n = 244 from at least three independent experiments. Two-tailed Mann-Whitney unpaired test. ns: not significant, *$p < 0.05$, ***$p < 0.001$. Violin plot shows the 25th to 75th percentile range (dashed line) and the median (solid line). Scale bar: 20 µm in overview, 5 µm in magnification panels.

In order to test the role of CYFIP2 in a more physiological context we used organotypic spinal cord explants from E13.5 mice. All explants were plated on laminin coated surfaces (similar to the cultured spinal MNs) for 72 h to promote MN neurite growth. We labelled the explants with

anti-neurofilament-200 Ab, anti-ChAT Ab (to confirm the analyzed neurites were from MNs) and phalloidin. Binary images were used to quantify neurite outgrowth parameters using the NeuriteJ analysis software (Figure 2.13 A).

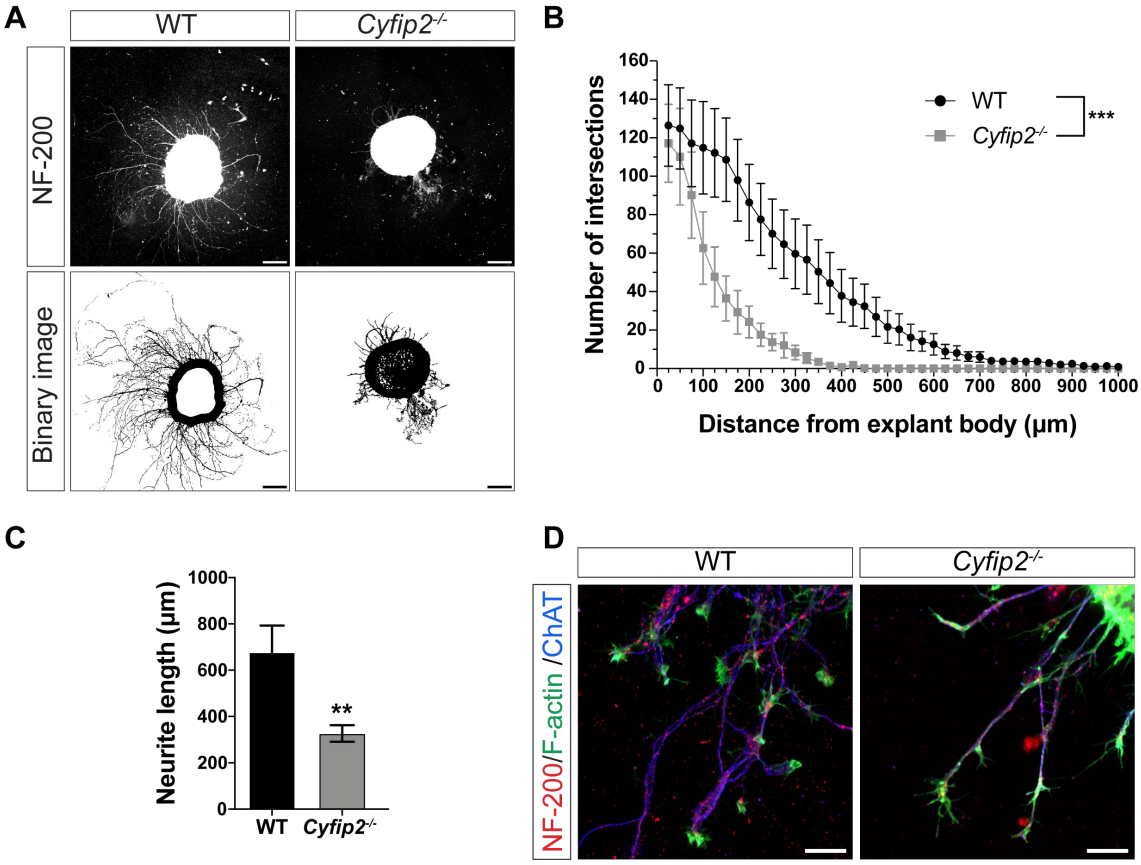

Figure 2.13. Neurite outgrowth and branching is strongly reduced in *Cyfip2*$^{-/-}$ spinal cord explants.
(**A**) Representative images of spinal cord explants plated on laminin for 72 h and immunolabeled with anti-neurofilament-200 (NF-200) Ab. *Cyfip2*$^{-/-}$ explants show reduced neurite outgrowth and complexity compared to WT controls. Binary images (lower panel) were used for Neurite-J analysis of axonal parameters. (**B**) Organotypic quantification using Neurite-J software in (**A**) shows *Cyfip2*$^{-/-}$ explants have significantly reduced ($p < 0.001$) neurite outgrowth and branching complexity, as indicated by the number of intersections, compared to WT controls. WT: n = 18, *Cyfip2*$^{-/-}$: n = 16 from at least three independent experiments. Two-tailed Mann-Whitney unpaired test, ***$p < 0.001$. (**C**) *Cyfip2*$^{-/-}$ neurites are shorter ($p = 0.01$) compared to WT. (**D**) WT and *Cyfip2*$^{-/-}$ sample explants immunolabelled with anti-NF-200 Ab (red), Alexa 488-conjugated phalloidin (green) and anti-ChAT Ab (blue) shows the analyzed neurites are MNs. Scale bar: 200 µm in **A**, 20 µm in **D**. **$p < 0.01$. Data are mean ± S.E.M.

The *Cyfip2*$^{-/-}$ explants had significantly reduced neurite outgrowth and branching complexity (Figure 2.13 B) along with substantially shorter neurites (Figure 2.13 C) compared to controls. As this system specifically selects the growth of MNs (Figure 2.13 D) we concluded that CYFIP2 regulates neurite development in a cell autonomous fashion in MNs. These results

confirmed the role of CYFIP2 as an essential molecular regulator of axonal development. CYFIP2 deletion affected axonal outgrowth, elongation, and branching as well as filopodia formation along the axonal shaft and in the growth cone.

2.4 Ultrastructural analysis of *Cyfip2*$^{-/-}$ MNs growth cones revealed decreased microtubule content in the central domain

Actin filaments are 7 nm in diameter and the analysis of actin cytoskeletal structures using conventional confocal laser scanning microscopy is a challenge. The smallest structures that could be clearly resolved are around 250 nm due to diffraction limits (Abbe, 1873). One way to circumvent this problem is to use a scanning electron microscope which uses irradiates electrons instead of light to observe the topography of the MN surface. Several studies have used this approach to illustrate how ARP2/3-dependent branched actin networks are important for both fibroblasts and hippocampal growth cone morphology (Korobova & Svitkina, 2008; Svitkina & Borisy, 1999). Therefore, we asked if CYFIP2 deletion would affect branched actin networks in spinal MNs *in vitro*. To date there are no ultrastructural analyses investigating the role of CYFIPs, WAVE or ARP2/3 in murine spinal MNs growth cones.

We performed ultrastructural analysis by scanning electron microscopy on DIV 3 WT and *Cyfip2*$^{-/-}$ spinal MN. We looked at both non-extracted and membrane extracted samples (prepared applying Triton X-100 detergent prior to cell fixation). When we analyzed the *Cyfip2*$^{-/-}$ non-extracted MNs growth cone morphology, no apparent differences were observed compared to WT growth cones (Figure 2.14 A). The growth cones analysis of membrane extracted MN was difficult to perform. We were unable to identify intact branched actin structures in most growth cone samples in both WT and *Cyfip2*$^{-/-}$ MNs, as only remnants of the actin cytoskeleton were detected along the growth cones (Figure 2.14 B). Interestingly, *Cyfip2*$^{-/-}$ growth cones had fewer microtubules and reduced microtubule complexity in the central region compared to WT growth cones (Figure 2.14 B). These results suggested that CYFIP2 might be an important component in the regulation of actin-microtubule crosstalk needed for growth cone migration.

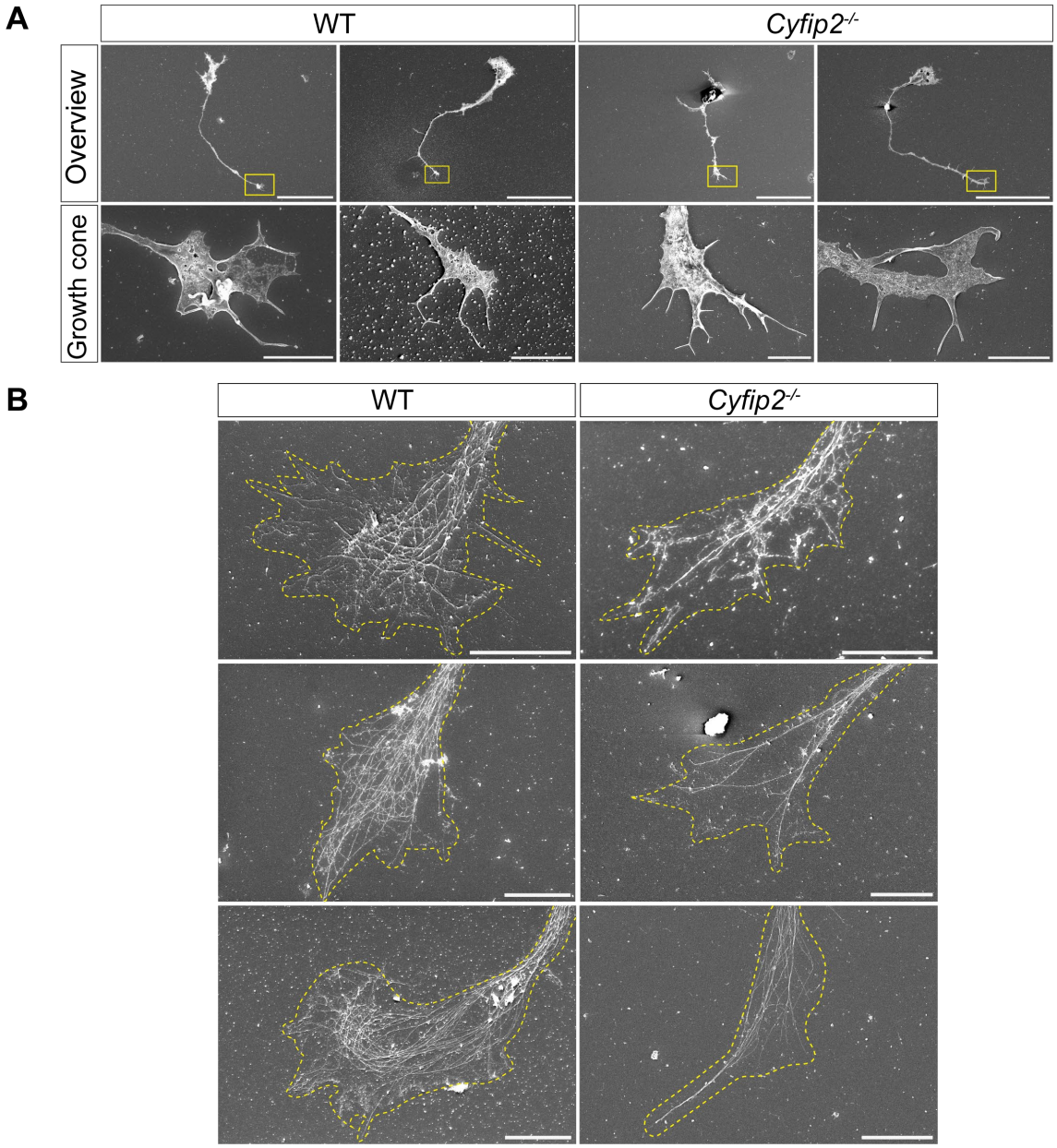

Figure 2.14. Ultrastructural analysis of *Cyfip2*$^{-/-}$ spinal MN growth cones show reduced microtubules in the C-domain.

(**A**) Representative overview scanning electron micrographs of non-extracted DIV 3 WT and *Cyfip2*$^{-/-}$ MNs show no apparent morphological abnormalities in filopodia or lamellipodia structures in the growth cones. Yellow boxed areas show the magnified growth cone micrograph (bottom panel). (**B**) Scanning electron micrographs of membrane extracted DIV 3 WT and *Cyfip2*$^{-/-}$ MN growth cones (outlined in yellow). Branched actin filaments in lamellipodia of both WT and *Cyfip2*$^{-/-}$ MNs are not clearly detected. Fewer microtubules extend into the growth cones of *Cyfip2*$^{-/-}$ MNs with less microtubule cytoskeletal network complexity in the central domain compared to WT MNs. Scale bar: 50 µm in **A** (top panel), 5 µm in **A** (bottom panel), **B**.

2.5 CYFIP2 loss affects the level of focal adhesion proteins in spinal MN growth cones

Our previous results showed that lack of CYFIP2 alters growth cone structure and morphology and affects its migration efficiency. Since growth cone migration is mostly based on cell-cell and cell-ECM adhesion interactions (Lowery & Vactor, 2009), we reasoned that CYFIP2 might be important for integrin-dependent focal adhesion formation in spinal MNs growth cones. The ARP2/3 complex in the growth cone has been shown to interact with focal adhesion adaptor proteins that link integrin signaling with the actin cytoskeleton (Vicente-Manzanares, Choi, et al., 2009). The link between the adhesion site and the actin filaments, or 'molecular clutches', is required to anchor the cytoskeleton so that actin polymerization can protrude the membrane forward at the leading edge of the growth cone. Several ECM proteins are also important for proper vertebrate NMJ development (Singhal & Martin, 2011). Therefore, we investigated if CYFIP2 regulated focal adhesion molecules.

Western blot analysis on E18.5 *Cyfip2*$^{-/-}$ spinal cord lysates showed no differences in vinculin and paxillin protein levels compared to controls (Supplementary Figure. 8.8 A, B). However, focal adhesion kinase (FAK) was substantially reduced in mutant spinal cords. This indicated that the actin-integrin complex was impaired. However, MNs in the spinal cord only account for 2-3 % of the cell population and these results could be attributed to other cell types. Therefore, we immunolabelled DIV 3 spinal MNs to analyze vinculin and FAK levels in their compartments: soma, axon and growth cone. The results showed that both vinculin (Figure 2.15 A, B) and FAK (Figure 2.15 C, D) were only significantly reduced in *Cyfip2*$^{-/-}$ growth cones compared to controls.

Next, we investigated if CYFIP2 loss could affect the upstream signals that regulate the establishment of focal adhesion contact sites. Since FAK is regulated by tyrosine phosphorylation we initially checked if *Cyfip2*$^{-/-}$ spinal cord lysates were deficient in this process. Biochemically the *Cyfip2*$^{-/-}$ spinal cords lysates only had a tendential reduction of tyrosine phosphorylation (Figure 2.16 A, B). As previously mentioned, we could not definitively conclude that this biochemical result was solely caused by spinal MNs as the spinal cord protein lysate consisted of a heterogenous cell population. Histological analysis on cultured MNs showed that *Cyfip2* deletion caused an increase in tyrosine phosphorylation together with myosin II in growth cones (Figure 2.16 C). This finding was unexpected and not in agreement with the reduction of vinculin and FAK expression we have previously observed in MN growth cones (Figure 2.15). This might indicate that CYFIP2 is a checkpoint or switch

for multiple signaling pathways as previously proposed by Schenck et al. 2004. However, the cause of this increased tyrosine phosphorylation expression has yet to be fully elucidated.

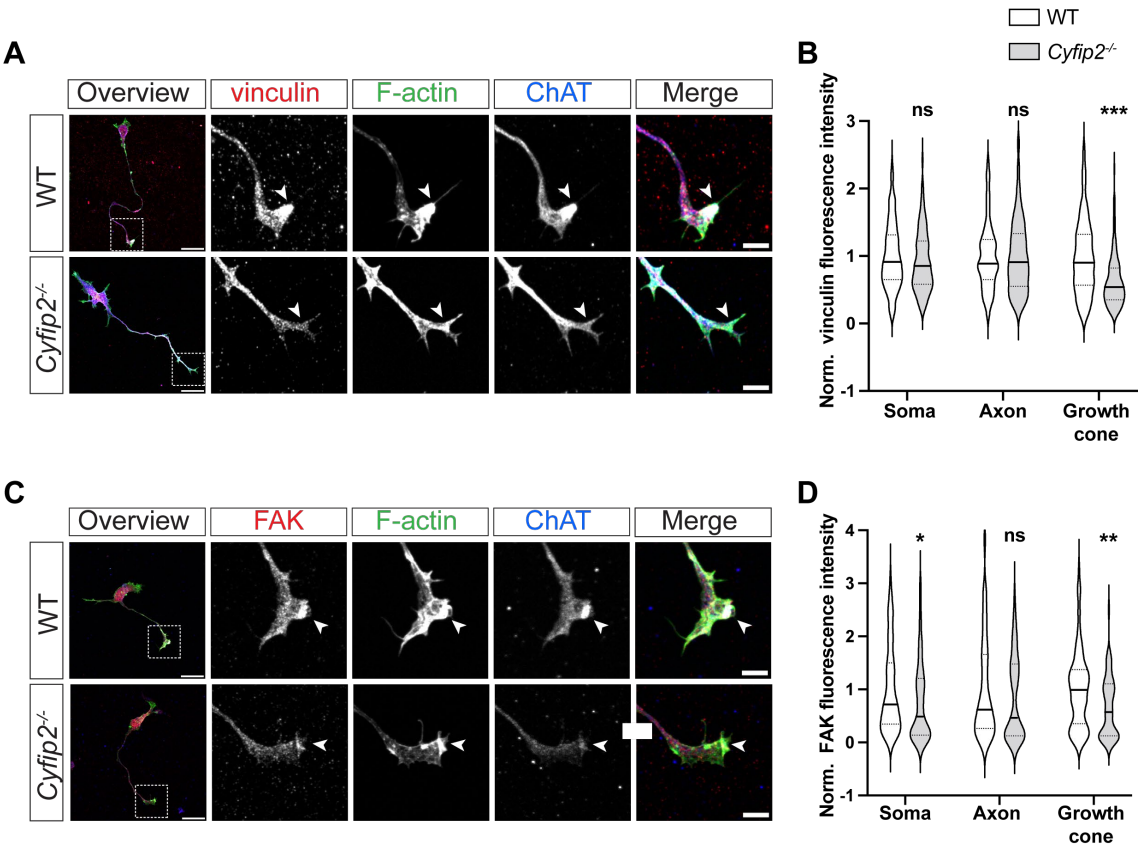

Figure 2.15. ***Cyfip2*** **deletion causes loss of focal adhesion proteins in the motor neuron growth cone.**

(**A**) Immunolabeling of DIV 3 MNs with anti-vinculin Ab (red), Alexa 488-conjugated phalloidin (green) and anti-ChAT Ab (blue) shows that vinculin colocalizes with F-actin in the growth cone. *Cyfip2*$^{-/-}$ MNs have reduced vinculin-positive signal in this region. White boxed regions in Overview are shown magnified in the four panels on the right to enlarge the growth cone. (**B**) Normalized vinculin fluorescence intensity quantification shows no difference in soma ($p = 0.18$) and axons ($p = 0.98$), but strongly reduced vinculin levels in growth cones ($p < 0.001$) of *Cyfip2*$^{-/-}$ MNs compared to WT shows. (**C**) Immunolabeling of DIV 3 MNs with anti-FAK Ab (red), Alexa 488-conjugated phalloidin (green) and anti-ChAT Ab (blue) shows reduced FAK colocalization with F-actin in *Cyfip2*$^{-/-}$ growth cones. White boxed regions in Overview are shown magnified in the four panels on the right to enlarge the growth cone. (**D**) Normalized FAK fluorescence intensity quantification shows a FAK decrease in the soma ($p = 0.02$) and in growth cones ($p = 0.002$) of *Cyfip2*$^{-/-}$ MNs compared to WT. WT: $n = 90$, *Cyfip2*$^{-/-}$: $n = 62$ from three independent experiments. Mann-Whitney unpaired test. ns: not significant, *$p < 0.05$, **$p < 0.01$, ***$p < 0.001$. Violin plot shows the 25th to 75th percentile range (dashed line) and the median (solid line). Scale bar: 20 µm in Overview, 5 µm in magnification images.

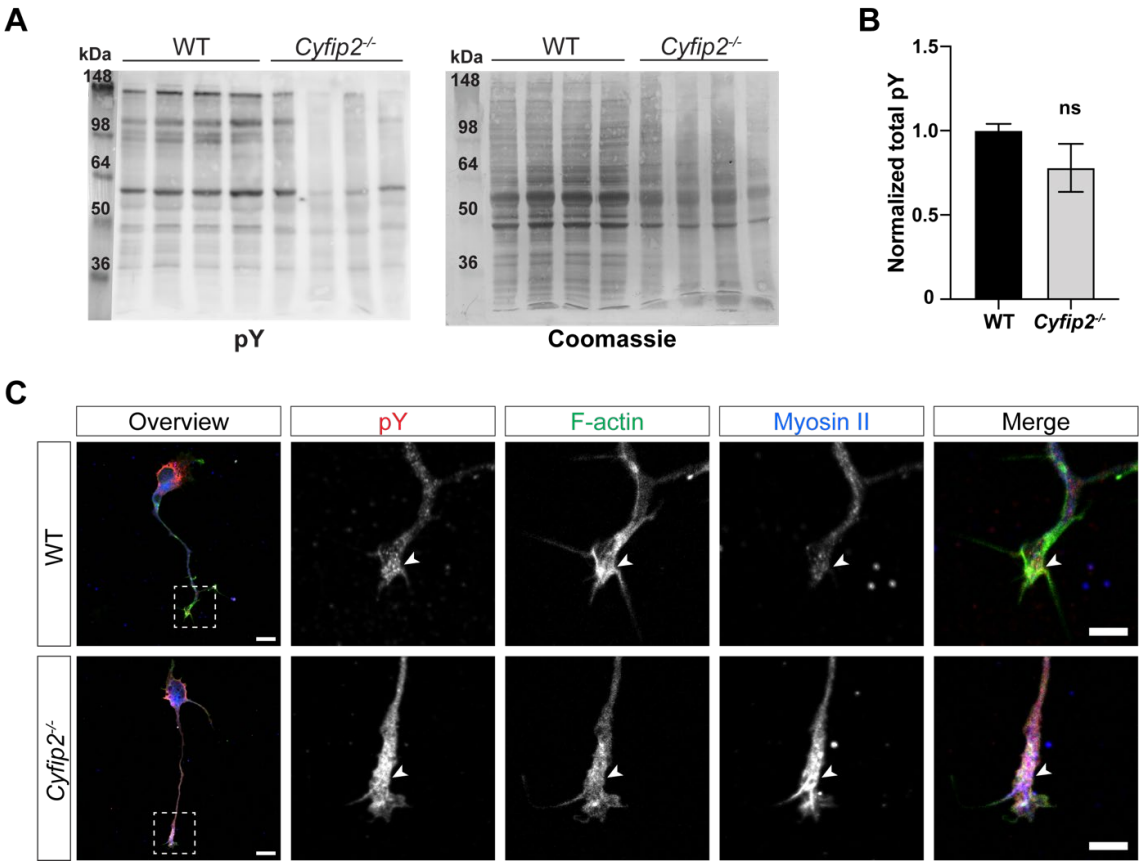

Figure 2.16. Increased tyrosine phosphorylation in *Cyfip2*$^{-/-}$ MN growth cones.
(**A**) Western blot shows tyrosine phosphorylation (pY) pattern in E18.5 spinal cord total protein lysates. (**B**) Normalized total pY quantification shows a tendential reduction (p = 0.185) in *Cyfip2*$^{-/-}$ spinal cord compared to WT. WT: n = 4, *Cyfip2*$^{-/-}$: n=4. (**C**) Immunolabelling of DIV 3 MNs with anti-pY Ab (red), Alexa 488-conjugated phalloidin (green) and anti-myosin II Ab (blue) shows increased pY and myosin II levels in *Cyfip2*$^{-/-}$ growth cones compared to WT. White boxed regions in Overview are shown magnified in the four panels on the right to enlarge the growth cone. Unpaired two-tailed t-test. ns: not significant. Data are mean ± S.E.M. Scale bar: 10 µm overview, 5 µm in magnification.

2.6 Role of CYFIP2 in hippocampal neurons

The role of actin cytoskeletal dynamics in determining neuronal cell polarity has been extensively studied (Bradke & Dotti 1997; Tahirovic et al. 2010; Yogev & Shen 2017). Previous studies using DIV 4 *Cyfip2*$^{-/-}$ hippocampal neurons showed that axonal elongation was not impaired (Zhang, Kang, Lee, et al., 2019). These results differed from our data on cultured spinal MNs indicating possible cell type specific functions of CYFIP2. We also analyzed *Cyfip2*$^{-/-}$ hippocampal neurons at an earlier stage as cell polarity mechanisms are time-dependent (Dotti, Sullivan, & Banker 1988).

We immunolabeled βIII-tubulin (neuronal microtubule marker) and F-actin in DIV 3 hippocampal neurons (Figure 2.17 A) to analyze various morphological parameters: filopodia and lamellipodia-like growth cones, neurite length, number of neurites and number of branched neurites (Figure 2.17 B, D, E, F). Taken together, these results indicated that CYFIP2 deletion had a minimal effect on hippocampal neuron morphology: only the total number of growth cones was reduced (Figure 2.17 C). Our data confirm the findings described by Zhang et al. 2019 and suggest that CYFIP2 has specific cell type functions during embryonic development.

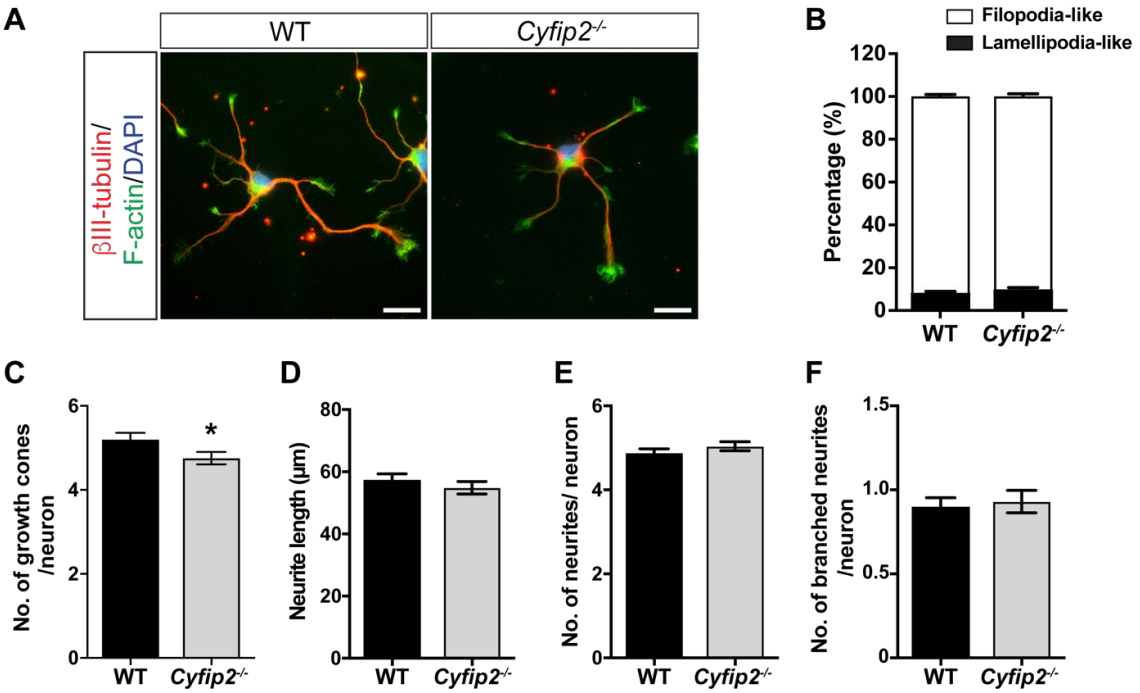

Figure 2.17. CYFIP2 deletion leads to mild hippocampal morphological defects.
(**A**) Representative images used for morphological analysis of DIV 3 hippocampal neurons immunolabelled with anti-βIII-tubulin Ab (labels neuronal microtubules, red), Alexa 488-conjugated phalloidin to label F-actin (green) and DAPI (blue). (**B**) Percent distribution of filopodia-like or lamellipodia-like growth cones is similar in *Cyfip2*$^{-/-}$ compared to WT neurons. (**C**) Average number of growth cones per neuron is reduced in *Cyfip2*$^{-/-}$ hippocampal neurons compared to WT ($p = 0.037$). However, there is no significant difference in (**D**) average neurite length ($p = 0.38$), (**E**) the average total number of neurites per neuron ($p = 0.28$) and (**F**) the average number of branched neurites per neuron ($p = 0.72$) between *Cyfip2*$^{-/-}$ and WT hippocampal neurons. WT: n = 200, *Cyfip2*$^{-/-}$: n = 200 for at least three independent experiments). Unpaired two-tailed *t*-test. *$p < 0.05$. Data are mean ± S.E.M. Scale bar: 10 µm.

2.7 A-to-I editing of *Cyfip2* RNA– a possible role in neurite formation

CYFIP2 exists in two variants because of A-to-I mRNA editing that changes the lysine at amino acid position 320 to glutamate. The editing occurs during embryonic development specifically

in the brain (Bonini et al., 2015; Levanon et al., 2004; Wahlstedt et al., 2009). However, the specific molecular functions of the edited CYFIP2-320E variant are still unclear.

We used an *in vitro* system to study the functions of the two CYFIP2 variants, the unmodified 320K and the RNA-edited 320E. We overexpressed the two variants fused to a C-terminal fluorescent tag (CYFIP2-320K-mCherry and CYFIP2-320E-mCherry) in HEK293 cells. We stained the fixed cells with phalloidin to investigate the cellular location of these variants and the actin cytoskeletal organization. Both CYFIP2-320K-mCherry and CYFIP2-320E-mCherry were localized throughout the cytoplasm and along the protrusions, especially in the filopodial tips (Figure 2.18 A). Morphologically, cells transfected with the edited CYFIP2-320E-mCherry did not differ from CYFIP2-320K-mCherry transfected cells after 24 h transfection. After 96 h only cells transfected with the CYFIP2-320E variant had significantly more protrusion-like structures (reminiscent of neurite extensions) compared to 24 h (Figure 2.18 B). The cells transfected with the CYFIP2-320K variant had similar morphological properties as the as mock transfected cells. Interestingly overexpression of NAP1, an essential interactor of CYFIP in the WRC, induces a similar phenotype as the overexpression of CYFIP2-320E (Figure 2.18 B).

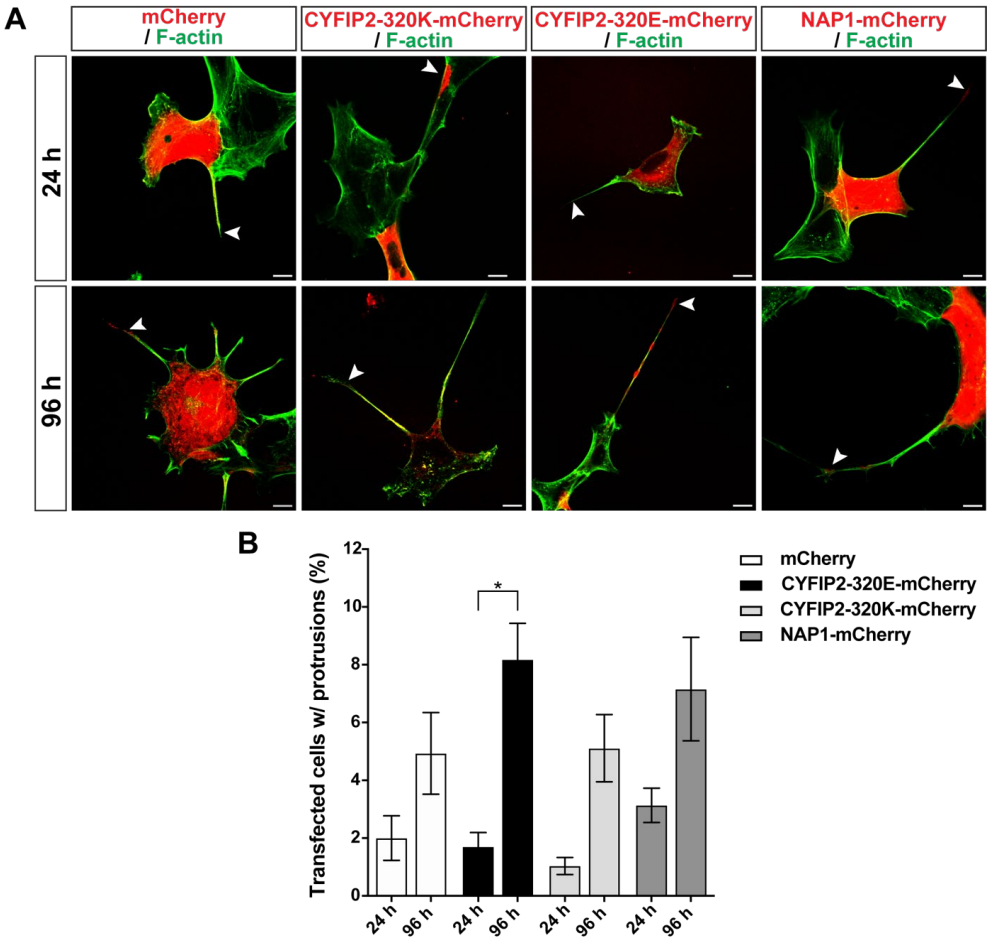

Figure 2.18. Overexpression of the edited CYFIP2-320E isoform induces neurite-like protrusions in HEK293 cells.
(**A**) Representative images of HEK293 cells expressing mCherry, CYFIP2-320K-mCherry, CYFIP2-320E-mCherry, and NAP1-mCherry (red) along with phalloidin (green) after 24 h (top panels) and 96 h (bottom panels). Neurite-like structures observed in the transfected cells are marked with white arrowheads. (**B**) Quantification of transfected cells displaying neurite-like structures (in %) in **A** shows that cells overexpressing CYFIP2-320E-mCherry produce significantly more neurite-like structures ($p = 0.015$) at 96 h compared to 24 h. (CYFIP2-320K-mCherry: 24 h n = 750, 96 h n = 1000; CYFIP2-320E-mCherry: 24 h n = 750, 96 h n = 1000; NAP1-mCherry: 24 h, 96 h n = 800; pmCherry-N1: 24 h n = 400, 96 h n = 1000, from three independent experiments). Paired two-tailed *t*-test. *$p < 0.05$. Data are mean ± S.E.M. Scale bar: 10 µm.

2.8 CYFIP2 role in the canonical WRC

Studies from our lab showed that the *Cyfip1*$^{-/-}$ embryonic stem cells (ESC) had reduced NAP1, WAVE1, WAVE2, ABI1 and ABI2 protein levels (Stöcker, 2015). In several systems the removal of one component of the WRC is accompanied by reduction of several other components of the WRC (Abekhoukh et al., 2017; Dubielecka et al., 2011; Qurashi et al., 2007). However, in native tissues it is still unclear how the different isoforms of the WRC components

assemble. Here we report for the first time the CYFIP2-dependent WRC composition in the murine CNS.

2.8.1 CYFIP2-dependent WRC co-regulated components in the brain and spinal cord

Western blot analysis was performed on WT and *Cyfip2*$^{-/-}$ total spinal cord and brain protein lysates to quantify the relative levels of several isoforms of the WRC components.
In the *Cyfip2*$^{-/-}$ spinal cord lysates NAP1, WAVE1 and WAVE3 were significantly reduced (Figure 2.19 A, B). Interestingly, in the *Cyfip2*$^{-/-}$ spinal cord lysates CYFIP1 and ABI1 proteins levels were tendentially increased compared to WT. In the E18.5 *Cyfip2*$^{-/-}$ brain lysates the NAP1, WAVE1, WAVE3, and ABI2 subunits were significantly reduced compared to WT controls (Figure 2.19 C, D). In contrast, both CYFIP1 and ABI1 protein levels were similar to controls. Overall, the data showed that CYFIP2 deletion also results in reduced WAVE1, WAVE3 and ABI2 levels during embryonic development: a strong indication that these isoforms take part in the same complex. The WRC subunits CYFIP1 and WAVE2 are also not part of the CYFIP2-dependent WRC.

2.8.2 The CYFIP2-WRCs in the mouse brain

To determine the protein interaction partners of CYFIP2 we performed a co-IP using a specific anti-CYFIP2 monoclonal antibody (CYFIP2-1C4, Supplementary Figure. 8.2). We used E18.5 total brain lysates to determine the CYFIP2-dependent WRC subunit composition. CYFIP2 co-immunoprecipitated NAP1, WAVE1, WAVE3 and ABI1 subunits (Figure 2.19 E). Interestingly, *Cyfip2* deletion did not alter ABI1 protein levels in both brain and spinal cord, but all other binding partners were downregulated. We also observed (using a specific anti-CYFIP1 antibody) that the CYFIP1 and CYFIP2 isoforms do no co-exist in the same WRC. This is in agreement with previous work that showed the WRC contains only one isoform of each of the five components (Gautreau et al., 2004). Furthermore, WAVE2 and ABI2 were the only subunits that did not interact with CYFIP2.

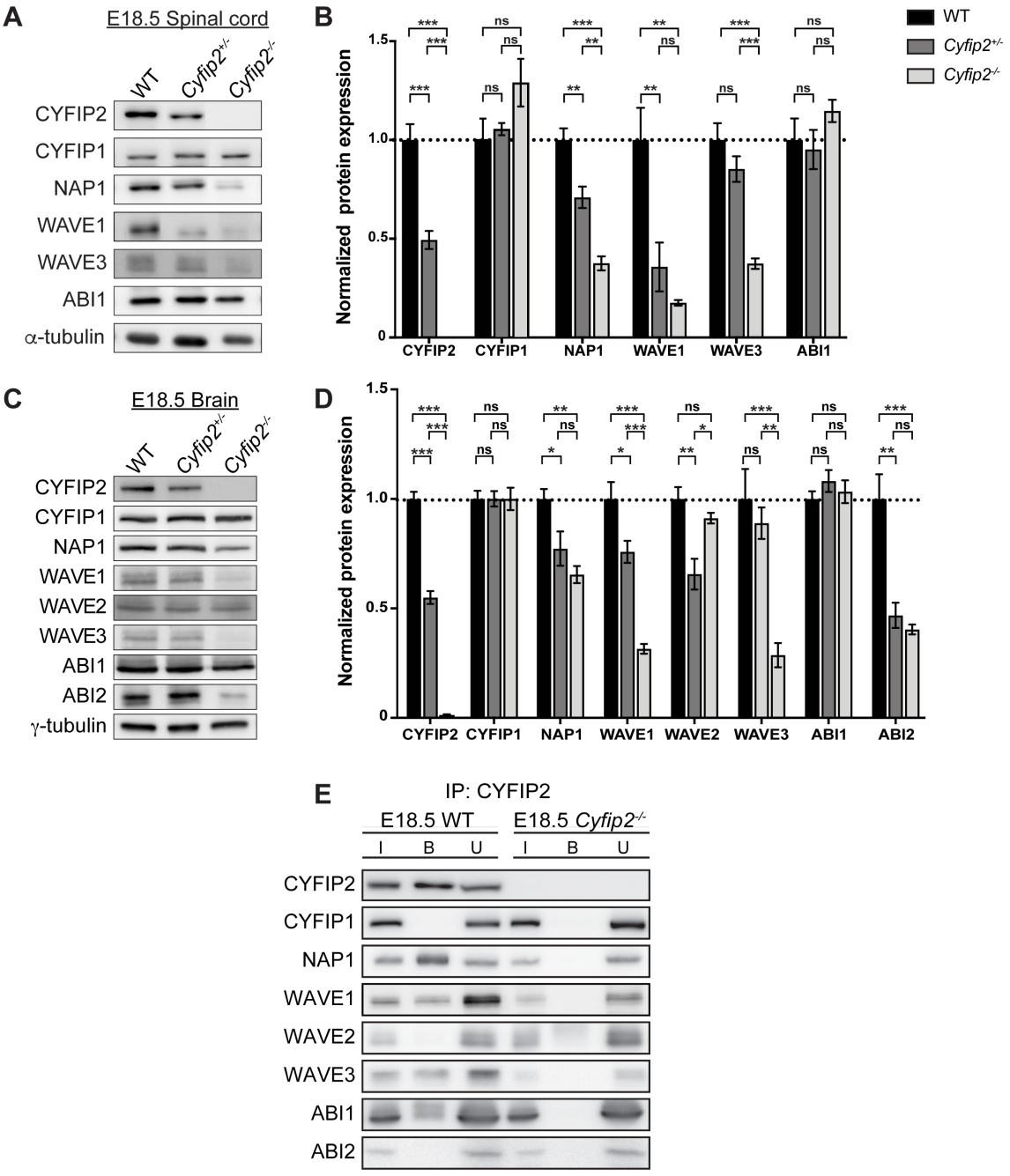
A
E18.5 Spinal cord
WT
Cyfip2+/-
Cyfip2-/-
CYFIP2
CYFIP1
NAP1
WAVE1
WAVE3
ABI1
α-tubulin
B
Normalized protein expression
WT
Cyfip2+/-
Cyfip2-/-
CYFIP2
CYFIP1
NAP1
WAVE1
WAVE3
ABI1
C
E18.5 Brain
WAVE2
ABI2
γ-tubulin
D
E
IP: CYFIP2
E18.5 WT
E18.5 Cyfip2-/-
I
B
U

Figure 2.19. CYFIP2-dependent WRC composition in the brain and spinal cord.
(**A**) Representative Western blots show reduced CYFIP2, NAP1, WAVE1 and WAVE3 protein levels in E18.5 *Cyfip2*$^{+/-}$ and *Cyfip2*$^{-/-}$ spinal cord lysates compared to WT controls. (**B**) Quantification of the WRC subunits levels in *Cyfip2*$^{+/-}$ and *Cyfip2*$^{-/-}$ spinal cord lysates. There is a significant reduction only in CYFIP2, NAP1, WAVE1 and WAVE3 protein levels in *Cyfip2*$^{-/-}$ spinal cords compared to WTs. (CYFIP2 $F(2,6) = 88.95$, $p < 0.001$; NAP1 $F(2,11) = 41.06$, $p < 0.001$; WAVE1 $F(2,11) = 14.21$, $p < 0.001$; WAVE3 $F(2,11) = 27.63$, $p < 0.001$). (**C**) Representative Western blots show reduced NAP1, WAVE1, WAVE3 and ABI2 protein levels in E18.5 *Cyfip2*$^{+/-}$ and *Cyfip2*$^{-/-}$ total brain lysates compared to WT controls. (**D**) Quantification of the WRC subunits levels in *Cyfip2*$^{+/-}$ and *Cyfip2*$^{-/-}$ brain lysates. There is a significant reduction only in CYFIP2, NAP1, WAVE1, WAVE3 and ABI2 protein levels in *Cyfip2*$^{-/-}$ spinal cords compared to WTs (CYFIP2 $F(2,17) = 376.1$, $p < 0.001$; NAP1 $F(2,11) = 11.61$, $p = 0.002$; WAVE1 $F(2,11) = 41.29$, $p < 0.001$; WAVE3 $F(2,11) = 16.0{,}1$ $p < 0.001$; ABI2 $F(2,11) = 18.80$, $p < 0.001$. (**E**) Western blot of CYFIP2 and WRC subunits in the co-IP using the CYFIP2-1C4 antibody to determine CYFIP2-dependent WRC composition in E18.5 brain extracts. CYFIP2 forms a complex with NAP1, WAVE1/3, and ABI1. *Cyfip2*$^{-/-}$ brain lysate was used as a negative control. I: input fraction, B: bound fraction, U: unbound fraction. WT: n = 3-5, *Cyfip2*$^{+/-}$: n = 4, *Cyfip2*$^{-/-}$: n = 5-6. One-way ANOVA with Bonferroni post-hoc test. ns: not significant, *$p < 0.05$, **$p < 0.01$, ***$p < 0.001$. Data are mean ± S.E.M.

2.8.3 Steady-state F-actin levels are not altered by the loss of CYFIP2

As previously stated, CYFIP2 is the predominant isoform in neurons, and we showed biochemically that CYFIP2 deletion removes most of the WRC in the CNS. Therefore, we wanted to know if the loss of CYFIP2 could also affect the F-actin levels in the CNS. We prepared insoluble F-actin and soluble G-actin fractions from E18.5 *Cyfip2*$^{-/-}$, *Cyfip2*$^{+/-}$ and WT brains and compared the F/G-actin ratio in each genotype. No significant differences in the F/G-actin ratio were found (Figure 2.20 A, B). This indicated that removal of CYFIP2 and its ARP2/3 activating function does not affect the total steady state F-actin levels. These finding were similar to those in *Cyfip1*$^{-/-}$ embryonic stem cells (ESCs) (Stöcker, 2015). Since CYFIP2 function has been previously shown to be essential in MNs we also specifically checked if the F-actin content was altered in *Cyfip2*$^{-/-}$ spinal MNs. Surprisingly, immunofluorescence staining of F-actin (using labelled phalloidin) showed unaltered F-actin levels in *Cyfip2*$^{-/-}$ MN soma, axon and growth cones (Figure 2.20 C).

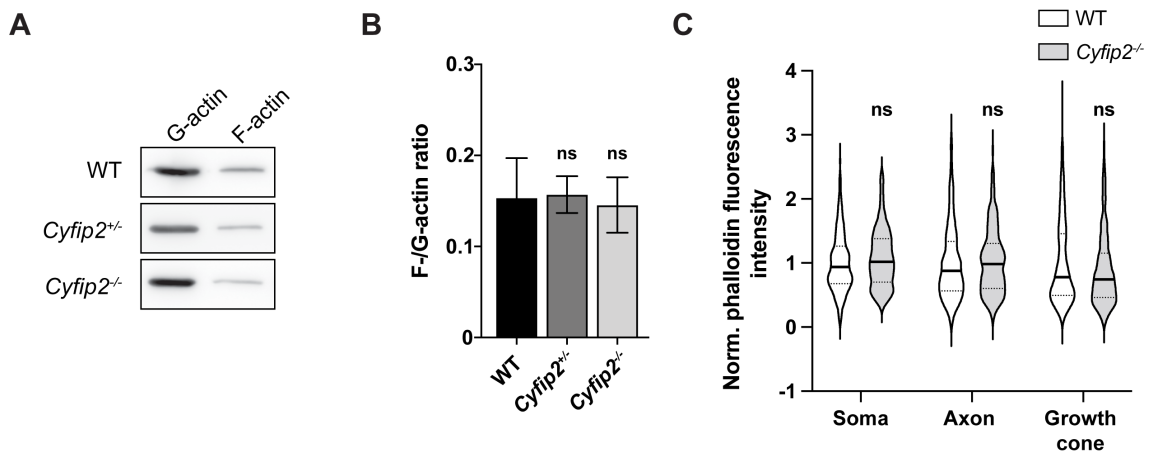

Figure 2.20. Steady state F-actin levels are unaltered in the CNS of *Cyfip2*$^{-/-}$ mice.
(**A**) Representative Western blots shows F-actin and G-actin protein levels in fractionated WT, *Cyfip2*$^{+/-}$ and *Cyfip2*$^{-/-}$ E18.5 total brain lysates. (**B**) F-/G-actin ratios shows no significant difference between *Cyfip2*$^{+/-}$, *Cyfip2*$^{-/-}$ and WT mice ($F(2,15) = 0.04$, $p = 0.97$). One-way ANOVA with Tukey's post-hoc test (WT: n = 5, *Cyfip2*$^{+/-}$: n = 5, *Cyfip2*$^{-/-}$**:** n = 8). Data are mean ± SEM. **(C)** Immunolabelling of *Cyfip2*$^{-/-}$ MNs with Alexa 488-conjugated phalloidin and quantification of the fluorescence intensity shows unaltered F-actin content in the soma ($p = 0.055$), axon ($p = 0.247$) and growth cone ($p = 0.134$) (Mann Whitney unpaired test. WT: n = 266, *Cyfip2*$^{-/-}$: n = 243 from at least three independent experiments). ns = no significant difference. Violin plot shows the 25th to 75th percentile range (dashed line) and the median (solid line).

2.9 Novel interaction partners of CYFIP2

*d*Cyfip was identified as a novel interaction partner of *d*Fmrp and its related proteins Fxr1/2 (Schenck et al. 2001). Other studies showed that CYFIP1/SRA1 interacts with elF4E, the cap binding factor used in mRNA translation (Napoli et al., 2008). Recent RNA-sequencing studies showed that genes involved in the ECM and focal adhesion were altered in *Cyfip2*$^{-/-}$ CNS tissue (Zhang, Kang, Lee, et al., 2019). We performed a proteomic approach with immunoprecipitation followed by mass spectrometry analysis, using the monoclonal CYFIP2-1C4 antibody we generated, on adult brain tissue lysates to identify novel CYFIP2 interaction partners. The genes that were highly enriched (2.5-fold) in the CYFIP2 IP where grouped into general biological function categories based on preliminary literature search (Supplementary Table 8.1-Supplementary Table 8.4). We also performed a GO enrichment analysis using PANTHER for the classification of biological process (describes the general physiological role) and cellular component (where the gene is located) of the enriched genes.

The results showed that the CYFIP2 interaction partners are in involved in a range of biological processes. Some of the most enriched pathways were synapse organization, neuron projection development, synaptic signaling and cytoskeleton organization (Figure 2.21 A). The cellular

component analysis showed that these genes were associated with the presynapse, synaptic membrane, axon, lamellipodium and NMJ to name a few (Figure 2.21 B). The proteomic analysis confirmed that CYFIP2 interacted with WAVE1/3, NAP1, ABI1, ABI2 and HSPC300 which is in line with our previous biochemical data (Figure 2.19). The GO term analysis also supported our findings of CYFIP2 interacting with proteins involved in axonal morphology and presynaptic terminal development in the NMJ.

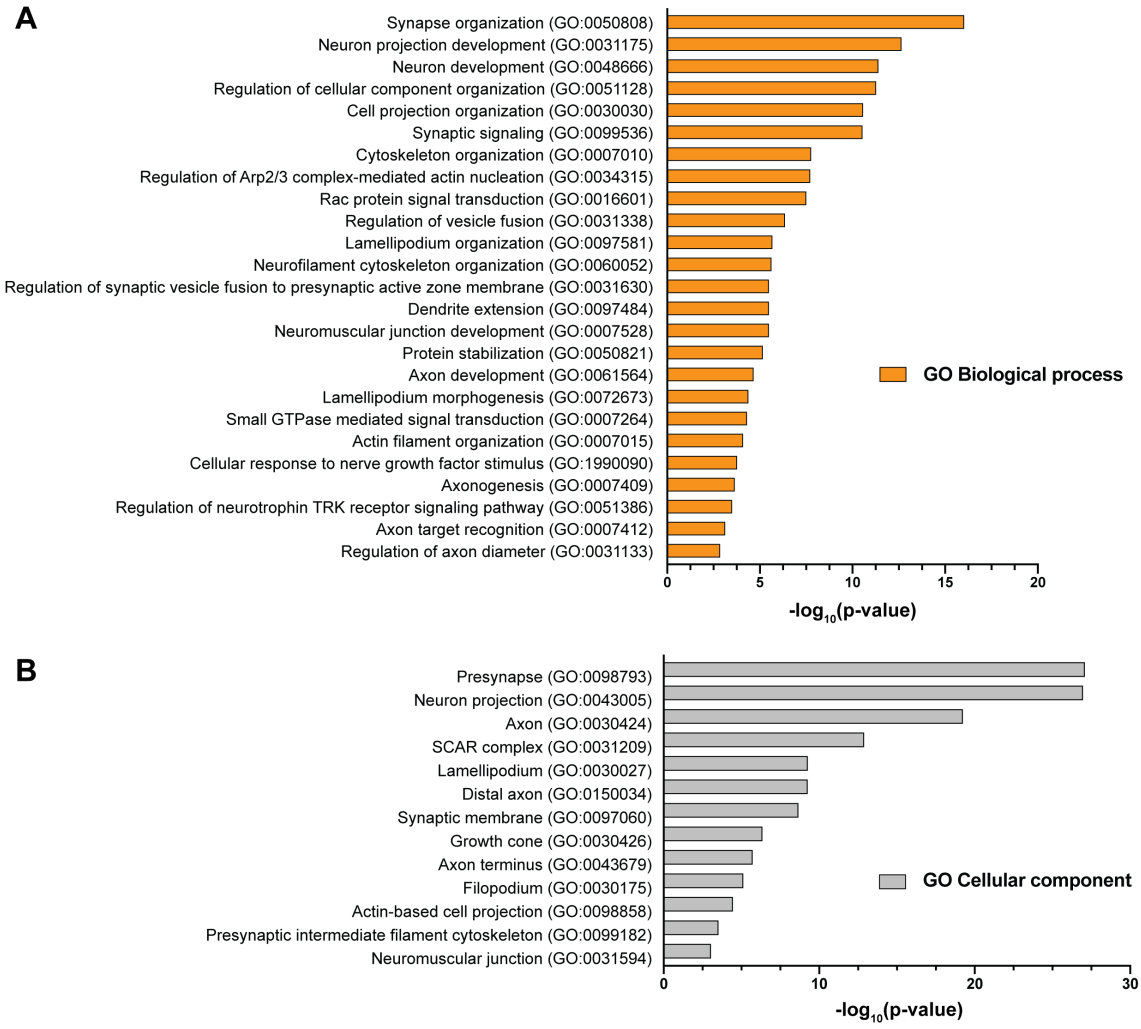

Figure 2.21. GO enrichment analysis of CYFIP2 interaction partners in *Mus musculus*.
Gene ontology (GO) enrichment analysis of (**A**) biological processes and (**B**) cellular component of enriched genes that interact with CYFIP2. All GO terms shown for each category were statistically significant ($p < 0.05$).

3. Discussion

3.1 The role of CYFIP2 in spinal MN axon development in the murine diaphragm

The role of CYFIP2 during murine development has been difficult to assess due to the perinatal lethal phenotype caused by the complete deletion of CYFIP2 (Han et al., 2015; Kumar et al., 2013; Zhang et al., 2019). A common cause for murine perinatal lethality is respiratory dysfunction and, in this study using a reporter mouse model, we show for the first time that CYFIP2 is expressed in spinal MNs that control the diaphragm. We also show that CYFIP2 in the spinal MNs is required for the proper axonal growth during embryonic development (Figure 2.3 & Figure 2.4). Our *in vivo* morphological studies show that axonal elongation was impaired in *Cyfip2*$^{-/-}$ mice, as indicated by shorter dorsocostal phrenic nerves and the absence of the sternocostal nerve. In addition, axonal branching was also impaired, as *Cyfip2*$^{-/-}$ diaphragms have fewer high order branch points which are misaligned with the postsynaptic AChR endplates. CYFIP2 could also be important for axonal guidance, as spinal MNs axons did not migrate from the spinal column towards what should become the sternocostal phrenic nerve. The *Cyfip2*$^{-/-}$ phrenic nerve did not display the stereotyped trifurcation patterns at the known developmental stages which implies impaired axonal guidance. In addition, the reduced phrenic nerve diameter indicates that fewer spinal MN axons migrate from the phrenic motor column (in the spinal cord) towards the designated targets in the diaphragm. We observed the same aberrant axonal morphological properties when we selectively promoted spinal MN outgrowth in both our *in vitro* and *ex vivo* assays (Figure 2.11 & Figure 2.13). This indicates that CYFIP2 has a cell autonomous role in spinal MN axonal elongation, branching and guidance which is not influenced by other spinal interneurons or Schwann cells.

Studies in sensory neurons using RNAi-mediated knockdown of *Wave*, a nucleation promoting factor that regulates actin dynamics by activating the ARP2/3 complex, showed reduced higher order branching points in *D. Melanogaster* larva (Sturner et al., 2019) and aberrant axonal guidance in *C. elegans* larva (Shakir et al., 2008). Previous studies using *Drosophila* larvae indicated that *d*Cyfip had an essential role in proper axonal and synaptic development in the NMJ (Bogdan et al. 2004; Schenck et al. 2003). In addition CYFIP2 was expressed in zebrafish Mauthner cells, neurons that are used for escaping reflexes and have sensory inputs and motor output connections (Cioni et al., 2018; Pittman et al., 2010). The consequence of CYFIP2 deletion during murine embryonic development causes improper formation of the NMJ in the diaphragm and respiratory dysfunction shortly after birth.

3.2 Molecular signaling in the axonal development of spinal MNs requires proper CYFIP2 regulation

There are several complex and diverse biological processes that govern axonal outgrowth and guidance at the growth cone. As we observed impaired spatio-temporal axonal guidance in our histological analysis of the mouse tissue, we hypothesized that chemoattractive and/or chemorepulsive signaling cues might be impaired in the absence of CYFIP2. Studies have shown that chemoattractive and/or chemorepulsive signals are major regulators of axonal guidance that function both locally or over long distances (McCormick & Gupton, 2020; Tessier-Lavigne & Goodman, 1996). The main known guidance cues are netrins, ephrins, semaphorins and SLITS, which can have chemoattractive, chemorepulsive or dual functions (Nakamoto et al., 2004; Tessier-Lavigne & Goodman, 1996). Cioni et al., showed that CYFIP2 in RGCs axons require topographic cues for long-range projections to extend. They speculated that repulsion cues might regulate long-range axonal sorting in RGC cells in a CYFIP2-dependent fashion, but they did not mention specific guidance ligands containing the WRC interacting receptor sequence (WIRS) binding motif. Given the phenotype of *Cyfip2*$^{-/-}$ mice, it is plausible that spinal MNs outgrowth is also regulated by signaling cues specific for long-range projections.

Based on literature we postulated that that netrin signaling might be impaired in *Cyfip2*$^{-/-}$ spinal MNs. The netrin receptor, uncoordinated locomotion 5c (UNC5C), has been shown to be essential for phrenic MN axonal outgrowth and guidance, since the *Unc5c* knockout mouse model (Burgess, Jucius, and Ackerman 2006) phenocopies the phrenic nerve defects we observed in the *Cyfip2*$^{-/-}$ diaphragms. Interestingly, the deletion of the other netrin 1 signaling receptors, deleted in colorectal cancer (DCC) and neogenin, did not display any aberrant phrenic nerve morphology probably due to their reciprocal functional redundancy. The UNC5C receptor can dimerize with DCC in the presence of netrin 1, which is used for long-range repulsion (Boyer & Gupton, 2018), while UNC5C and Down syndrome cell adhesion molecule (DSCAM) can form heterodimers used for short-range repulsion cues (Boyer & Gupton, 2018). Our mass spectrometry analysis of CYFIP2 pull-down complexes from brain protein lysates showed an interaction of CYFIP2 with srGAP3, an RHO GTPase activating protein downstream of the SLIT-ROBO signaling, which is also a repulsive guidance cue. Additional mass spectrometry analysis of CYFIP2 complexes in spinal cord lysates would be required to validate if netrin, SLIT-ROBO or other guidance molecules interact with CYFIP2. It is plausible that the absence of CYFIP2 in MN growth cones causes an imbalance in receptor

dimerization signaling or membrane receptor levels required for proper long-range (UNC5C:DCC) and/or short-range (UNC5C:DSCAM) repulsion cues.

Immunohistochemical assays on cultured spinal MNs, staining for the different netrin receptors, could help elucidating the role of CYFIP2 in long-range and/or short-range guidance and if it is solely specific to repulsive cues or might also affect attractive cues. It might be a combination of several repulsive guidance cues (i.e., netrin/UNC5C and SLIT-ROBO) that are altered in the absence of CYFIP2 leading to reduced and/or abnormal dorso-ventral topographic axonal projections outgrowth and guidance.

3.3 CYFIP2 is required for ECM-integrin mediated focal contact formation

Another mechanism used for localized axonal outgrowth and guidance occurs when receptors on the surface of the growth cone use ECM proteins (e.g., laminin) and initiate contact adhesion to navigate to the target destination. The ECM glycoprotein laminin interacts with integrin receptors and stimulates axonal outgrowth via focal adhesion (Bixby et al., 1987; Myers et al., 2011; Short et al., 2016). The ARP2/3 complex interacts with focal adhesion adaptor proteins (e.g., vinculin, FAK and paxillin) (Chorev et al., 2014; Parsons et al., 2010; Vicente-Manzanares, Choi, et al., 2009). The interaction between the ARP2/3 complex and vinculin is mediated by PI3K and RAC1 signaling (DeMali et al., 2002). The role of cell adhesion molecules e.g., neural cell adhesion molecule 1 (NCAM1) in the ECM also influences axonal migration. It was previously shown that the first phrenic axons (known as pioneering axons) used NCAM expressing cells to reach the diaphragm at E13.5 (Allan & Greer, 1997).

In this study we show a specific function of CYFIP2 in mediating the ECM-integrin-actin cytoskeleton link. We show that CYFIP2 has a role in the establishment of focal adhesion sites in spinal MN growth cones (Figure 2.15). Immunolabeling assays show that the actin adaptor proteins, vinculin and FAK, are reduced in *Cyfip2*$^{-/-}$ MN growth cones. The deletion of *Cyfip2* significantly reduced the FAK protein also in the spinal cord of the mutant mice and both vinculin and paxillin appeared tendentially reduced (Supplementary Figure. 8.8 A, B). In addition, we show that CYFIP2 is not a direct binding partner of vinculin, FAK nor paxillin, therefore its effect on focal adhesion formation is indirect. Indeed, our proteomic data show that CYFIP2 interacts with the adhesion molecules NCAM, catenin and contactin (Figure 2.21, Supplementary Table 8.2).

Studies where neuronal PC12 cells were cultured on laminin had shorter neurites when vinculin was deleted with a siRNA (Varnum-Finney & Reichardt, 1994), which is also in line with our findings. The localization of vinculin and FAK positive signal in the growth cones is similar to

localization in rat DRG growth cones (Renaudin et al., 1999). The work of Cioni et al., also showed that axon-axon contacts are required for CYFIP2 to translocate from the axonal shaft to the periphery of the growth cone, further supporting a function of CYFIP2 in focal contact formation. Our findings are also in line with previous studies that showed altered expression of ECM-and focal adhesion-related genes in *Cyfip2*$^{-/-}$ embryonic brains using RNA sequencing (Zhang et al. 2019). Furthermore, transmembrane receptors involved in adhesion, G-protein coupled receptors and scaffolding proteins can bind to the WRC via a WRC interacting receptor sequence (WIRS) (Chen et al. 2014). The modulation of CYFIP2-dependent ARP2/3 actin networks through adhesion is not only specific to neuronal cells. CYFIP2 was also found to facilitate fibronectin-mediated adhesion of T-cells from multiple sclerosis (MS) patients (Mayne et al., 2004). Altogether, these findings indicate the importance of CYFIP2-WRC in mediating adhesion across various cell types.

There are some contradictory views on the role of the ARP2/3 complex in the formation of focal adhesions. The deletion of the ARP2/3 complex or the WRC reduced FAK-positive and paxillin-positive focal contact sites in cortical neurons (Gupton & Gertler, 2010; Swaminathan et al., 2016). The deletion of the ARP2/3 complex in 2xKD cells cultured on fibronectin resulted in increased focal contacts (Wu et al. 2012). The deletion of the WRC in human carcinoma cells using shCyfip1/Sra1 and shNap1 resulted in increased FAK expression (Tang et al., 2013). The deletion of ARP2/3 using *Arp3* siRNAs resulted in reduced vinculin-positive focal contacts in HeLa cells (DeMali et al., 2002). However deletion of the ARP2/3 complex using *p34-Arc* siRNAs showed increased vinculin focal sites in B35 differentiated neuroblastoma cells (Korobova & Svitkina, 2008). Biochemical assays showed that GST-vinculin fusion proteins are able to bind to the p34 ARP2/3 complex subunit and colocalization assays on mouse embryonic fibroblasts show this is a transient interaction occurring only at nascent focal sites at the leading edge (DeMali et al., 2002). It was recently proposed that neuronal migration may not even depend on adhesion. Recent studies on hippocampal neurons grown in 3D collagen matrices showed that axonal elongation was independent of integrin mediated adhesion (Santos et al., 2020). Therefore, the function of focal adhesions both depends on the experimental approach and is cell type specific. The findings that are contradictory to what we observed in mouse spinal MNs could be attributed to either the experimental approaches and/or the cell lines that were used. We believe our findings on *Cyfip2*$^{-/-}$ spinal MNs reflect a more physiological scenario to understand the role of focal contact formation in mouse motor neurons during embryonic development.

3.3.1 Tyrosine kinase phosphorylation: the key to CYFIP2-mediated focal adhesion establishment?

The recruitment of FAK and paxillin to the nascent focal contacts is regulated by tyrosine phosphorylation. SRC kinases mediate FAK tyrosine phosphorylation, as has been previously described in various cell types (Mitra et al., 2005; Parsons, 2003; Playford & Schaller, 2004). Tyrosine phosphorylation of FAK in the growth cones is as well regulated by SRC-family tyrosine kinases, such as FYN or YES (Desai, Sun, and Zinn 1997). Paxillin, another focal adhesion protein, can also undergo tyrosine phosphorylation and along with FAK regulate both RAC1 and RHOA-mediated actin dynamics (Deakin & Turner, 2008; Leventhal & Feldman, 1996; López-Colomé et al., 2017).

We showed that CYFIP2 is required for proper focal adhesion formation in the spinal MNs growth cones, therefore we studied if upstream signaling was also affected by the loss of CYFIP2. Immunolabeling assays showed an increase in phosphotyrosine-positive signal in *Cyfip2*$^{-/-}$ spinal MN growth cones (Figure 2.16). Why would *Cyfip2*$^{-/-}$ spinal MNs have increased phosphotyrosine-signaling in their growth cones? One possible reason could be the activity of other tyrosine kinases compensating for the loss of CYFIP2-dependent FAK mediated focal contacts. The *Cyfip2*$^{-/-}$ spinal MNs had similar myosin II-positive and phosphotyrosine-positive localization patterns in the growth cones. Myosin II is activated by the RHOA kinase (ROCK) signaling pathway. In the absence of RAC1-CYFIP2-mediated actin dynamics there might be a shift towards RHOA-mediated actin dynamics in the spinal cord (Witke, personal communication). In addition RAC1 could potentially negatively regulate myosin II by inhibiting the myosin light chain kinase PAK (Luo, 2000). RHOA can activate mDIA, a member of the formin actin nucleators family (Ridley, 2006). Thus, mDIA-dependent actin polymerization might compensate for the loss of CYFIP2-WRC-ARP2/3-dependent branched actin networks. Myosin II only has serine or threonine phosphorylation sites, therefore the increase in phosphotyrosine signaling is not from myosin II hyperactivation (Vicente-Manzanares, Ma, et al., 2009). It must be noted that we were not able to discriminate between the specific tyrosine phosphorylation sites that are known to regulate FAK focal adhesion sites (Calalb et al., 1995).

It is possible that CYFIP2 also works as a ‘switch’ between cell adhesion (i.e., laminin-integrin)-dependent and receptor tyrosine kinase (RTK)-dependent SRC activation. We propose that CYFIP2 is a negative regulator of RTK-SRC-dependent phosphorylation thus

favoring laminin-integrin based tyrosine phosphorylation. This would favor the signaling cues that promote anchoring of actin to focal adhesion contacts and allow cell membrane protrusion. When focal adhesion contacts are disrupted, other cytoskeletal proteins e.g., microtubules, are unable to attach to stabilized F-actin filaments, thereby delaying the migration of axons. Taken together our data show that in the MN growth cones the tethering of actin filaments to focal adhesion sites is essential for outgrowth. Future morphological analysis on spinal MNs using specific antibodies for different tyrosine phosphorylation sites and live-cell imaging would help elucidate how CYFIP2 might regulate the upstream signaling of the focal contacts.

3.4 Role of the neuron-specific *Cyfip2* mRNA A-to-I editing in protrusion formation

Cyfip2 mRNA undergoes editing in the brain and spinal cord at position 320, where the amino acid K is changed into E (Hideyama & Kwak, 2011; Levanon et al., 2005). Given our previous findings on the role of CYFIP2 in axonal outgrowth in the MNs, we speculated that the CYFIP2-320E isoform expressed in neurons following mRNA editing might have a specialized function to initiate and promote neurite extension.

We performed gain-of-function experiments in an exogenous cell system and showed that transiently expressed CYFIP2-320K and CYFIP2-320E were localized in neurite-like extensions in HEK293 cells (Supplementary Figure. 8.9). However, the percentage of cells with longer neurite-like extensions was higher in cells overexpressing the CYFIP2-320E isoform compared to those expressing CYFIP2-320K, particularly at later time-points after transfection (Figure 2.18). We could speculate that the specific neuronal RNA editing of *Cyfip2* might have evolved as a mechanism for axonal outgrowth and to enable long-range projections required to reach target cells. Previous studies using fibroblasts showed that the CYFIP2 RAC1 binding sites (A site and D site) have different function: the RAC1 A site is used for WRC activation whereby the RAC1 D site is important for maintaining the morphological formation of lamellipodia (Schaks et al., 2018). Since the CYFIP2-320 amino acid is located closer to the RAC-A binding site, it is not unlikely that this neuronal editing affects the RAC1 interaction to exclusively initiate WRC-dependent actin polymerization in growth cones.

Interestingly, recent *in vivo* studies on zebrafish RGCs showed that the CYFIP2 point mutation K727E rescued topographic axonal missorting caused by *Cyfip2* deletion (Cioni et al., 2018). The CYFIP2-727E variant was expressed along the axon and growth cone periphery, which was similar to the CYFIP2-320E expression pattern in transfected HEK293 cells. Therefore, CYFIP2-320E-dependent WRC actin polymerization could be essential for axon growth and

guidance to allow axons to migrate in bundles and reach their designated targets. As previously mentioned, axonal migration is highly dependent on a variety of ECM ligands or guidance molecules to reach target cells. In our experiments, the HEK293 cells overexpressing the two variants CYFIP2-320K/E were not cultured on any ECM substrate, which might be critical for the functions of CYFIP2-320E required for neurite outgrowth. Finally, the neuronal CYFIP2-320E editing might exclusively affect the interaction of CYFIP2 with RAC,1 but not with the elF4E (as seen with the K727E mutation in RGCs), favoring actin cytoskeleton regulation versus mRNA translation. Further experiments would be needed to prove this hypothesis.

3.5 CYFIP1-dependent WRC and MENA/VASP do not compensate for the loss of CYFIP2

The absence of CYFIP2 results in severe defects in axonal elongation, branching and guidance in mouse spinal MN both *in vivo* and *in vitro*. However, other actin nucleators must be used to drive actin polymerization and form the rudimentary phrenic nerve observed in the *Cyfip2*$^{-/-}$ diaphragms. Studies showed that *Cyfip1* haploinsufficiency causes reduced corpus callosum projections indicating that CYFIP1 might contribute to the proper formation of cortical axonal projections in the mouse and the rat (Domínguez-Iturza et al., 2019; A. I. Silva et al., 2019). CYFIP1 also functions in regulating axonal elongation in zebrafish RGCs (Cioni et al., 2018).

It would be feasible that CYFIP1-dependent WRC actin nucleation could compensate for the loss of CYFIP2, since both CYFIP paralogues share 88 % amino acid identity. Our biochemical data on *Cyfip2*$^{-/-}$ spinal cord lysates showed a tendential upregulation of CYFIP1 at E18.5. However, our immunolabeling analysis on *Cyfip2*$^{-/-}$ diaphragms showed that CYFIP1 is localized in the postsynaptic compartments (AChR-positive motor endplates) and not in presynaptic compartments (i.e., axons and synaptic boutons). This indicated CYFIP1 is unable to compensate for the loss of CYFIP2 in murine embryonic development. Our findings coincide with the expression pattern in hippocampal neurons, where CYFIP1 was primarily found in postsynaptic compartments (Davenport et al., 2019; Napoli et al., 2008; Pathania et al., 2014). The discrepancy between biochemical and morphological data can be accounted for due to the heterogenous cell population in the spinal cord where MNs only account for 2-3 % of the total cell population. The observed tendency of CYFIP1 protein upregulation could come from any other non-MN neuronal subtype in the spinal cord e.g., sensory neurons and interneurons.
Another potential candidate actin nucleator is MENA/VASP, as it regulates focal adhesion formation and is also localized at the lamellipodium (Bear & Gertler, 2009; Damiano-Guercio

et al., 2020; Krause et al., 2003; Rottner et al., 1999). We showed that both CYFIP2 and VASP are localized in close proximity in filopodia structures in HEK293 cells (Supplementary Figure. 8.7), similar to what is described in various cell lines (Gertler et al. 1996; Reinhard et al. 1992). Biochemical results showed that neither MENA nor VASP were upregulated in brain and spinal cord lysates in the absence of CYFIP2 (Figure 2.10), but VASP phosphorylation appeared tendentially reduced compared to controls. VASP has several known phosphorylation sites that can regulate focal adhesion binding, SRC binding and F-actin binding (Döppler & Storz, 2013). Previous studies in both non-neuronal and neuronal cells showed that MENA/VASP and ARP2/3 cooperate to facilitate actin polymerization (Chen et al. 2014; Goldberg et al. 2000; Havrylenko et al. 2015; Laurent et al. 1999; Norris, Dyer, and Lundquist 2009). Our results suggest that the MENA/VASP family alone is not able to rescue focal adhesion formation in *Cyfip2*$^{-/-}$ mice. The deletion of *Mena* in the mouse did not affect spinal motor neurons, which is also in line with our findings (Lanier et al., 1999).

There are a plethora of actin nucleators to consider as potential compensatory candidates. N-WASP-dependent ARP2/3 actin polymerization could compensate for the loss of CYFIP2. N-WASP was shown to modulate integrin-adhesion signaling which could potentially compensate for CYFIP2 dysregulation (Brunton et al., 2004). The most recent NPF regulating the ARP2/3 complex, WHIMP, which is highly expressed in peripheral autonomous nervous organs (i.e. heart, kidney and liver), was shown to be regulated by SRC-mediated tyrosine phosphorylation (Kabrawala et al., 2020). Immunolabeling assays on NIH3T3 fibroblasts showed that WHIMP, WAVE and N-WASP are all in close proximity to each other. Overall, our findings suggest that the actin nucleators partially compensating for the loss of CYFIP2-WRC could be either other Class I NFPs (e.g., N-WASP or WHIMP), class II NPFs or other elongation factors (excluding MENA/VASP). The ABP profilin 2 also interacts with CYFIP2 and is important for actin polymerization (Witke et al., 1998). *Profilin 2* mutant mice did have impaired motor coordination, however the mechanism by which PFN2 regulates NMJ function are still not fully understood (Pilo Boyl, personal communication).

3.6 The role of CYFIP2 in the canonical WAVE regulatory complex

The majority of WRC subunit composition studies are based on CYFIP1/SRA1 and tagged-CYFIP2 proteins that might not reflect the real physiological scenario of CNS development (Chen et al. 2014; Chen et al. 2010; Kumar et al. 2013; Steffen et al. 2004). Therefore, we created and validated a monoclonal anti-CYFIP2 antibody to circumvent potential false-positive readouts.

Our immunoprecipitation show that during embryonic development the CYFIP2-WRC complex consists of NAP1, WAVE1, WAVE3 and ABI1 (Figure 2.19). These findings are in line with results from Zhang et al. and Eden et al. In contrast, immunoprecipitation studies on Cos-7 and HeLa cells showed that CFYIP2/PIR121 made a complex with NAP1, ABI1, and WAVE2 that was RAC1-dependent and CDC42-independent (Innocenti et al., 2004). In CYFIP2 stably transfected HEK293 cells, CYFIP2 made a complex with NAP1, WAVE1, ABI2 and HSPC300 (Kumar et al., 2013). Pull-down assays using profilin 2, a protein that efficiently binds to CYFIP1/2, showed a CYFIP1/2-NAP1-ABI1-WAVE2 complex in the lungs (Stöcker, 2015). This supports the idea that different CYFIP2-dependent WRC compositions are both tissue and cell-type specific.

In our *Cyfip2*$^{-/-}$ mouse model, the complete deletion of CYFIP2 led to the reduction of NAP1, WAVE1, WAVE3 and ABI2 proteins in Western blots. This is in line with similar studies that showed that the integrity of the WRC is affected when one subunit is removed (Grove et al., 2004; Hsiao et al., 2016; Kumar et al., 2013; Rakeman & Anderson, 2006; Yan et al., 2003). Our findings were also in line with the CYFIP2-dependent WRC in adult brain (Özer, 2019). Despite CYFIP1 and CYFIP2 sharing 88 % amino acid sequence identity the *Cyfip1/Sra1* knockout model is embryonic lethal at E8.5 (Pathania et al., 2014; Stöcker, 2015) while *Cyfip2*$^{-/-}$ mice die at birth. Our lab showed that during gastrulation CYFIP1 is an essential component for endodermal cell proliferation and mesendoderm differentiation, which is regulated by the BMP/SMAD signaling pathway (Stöcker, 2015). *Nap1* knockout mice showed aberrant developmental morphology with improper neural tube formation at E9 (Rakeman & Anderson, 2006). Similar neural tube defects were seen in *Abi1* knockout mice along with cardiac failure, and these mice were only viable until E12.5 (Dubielecka et al., 2011). *WAVE2* knockout mice were also only viable until E12.5 and displayed gross CNS abnormalities, but peripheral organs were normal compared to controls (Yan et al., 2003). *Abi2* knockout mice only showed morphological defects in the cortex, hippocampus and eye lens yet were viable and fertile (Grove et al., 2004). *WAVE1* knockout mice were viable until P21-26 and reduced cortical thickness and projection fibers in the corpus callosum were correlated to lethality (Dahl et al., 2003). To date, *WAVE3* and *HSPC300* knockout mouse models have not been described in the literature. This finding highlights the difference in both CYFIP1-dependent and CYFIP2-dependent WRC composition and the divergent temporal roles of each WRC subunit during embryonic development.

3.6.1 The role of CYFIP2 in actin dynamics during embryonic development

We assumed that actin dynamics would be altered as a consequence of decreased WRC-ARP2/3 complex signaling in the absence of CYFIP2. However, fluorescence labeling of F-actin in cultured motor neurons showed that CYFIP2 deletion does not alter F-actin localization in spinal MN growth cones. In addition, our biochemical data showed no alteration of the F-/G-actin ratio in the brain of the mutant mice, where CYFIP2 is predominantly expressed in pyramidal neurons (Figure 2.20). These results are similar to those obtained in *Cyfip1* knockout embryonic stem cells (Stöcker, 2015). The fact that the overall F-actin content was not altered in the absence of CYFIP2 can be explained by the presence of many other actin nucleators in cells, which might compensate for the loss of the CYFIP2-WRC. *In vitro* assays on cortical neurons transfected with *Cyfip1* shRNA have reported reduced F-actin in spines (De Rubeis et al., 2013). In contrast, the conditional deletion of *Cyfip2* in the adult brain and *Cyfip1* haploinsufficiency in the hippocampus were reported to increase the F-/G-actin ratio (Hsiao et al., 2016; Özer, 2019). Fluorescence recovery after photobleaching (FRAP) analysis on *d*Cyfip mutants also exhibited enhanced F-actin in the fly NMJ presynaptic terminals (Zhao et al., 2013). In recent studies, F-actin levels were shown to be increased also in layer 5 cortical neurons of *Cyfip2* conditional knockout mice (Zhang et al. 2020). The enhanced F-actin levels were attributed to CYFIP1 or other NPFs/NFs compensatory mechanisms for the loss of CYFIP2.

3.6.2 Loss of CYFIP2 affects the microtubule cytoskeleton in the axon and growth cones

Since conventional confocal microscopy is not an ideal method to detect fine actin cytoskeletal changes, due to its resolution limit too low for structures in the nanometer range, we opted to use an ultrastructural approach. Electron micrographs of cultured *Cyfip2*$^{-/-}$ MNs showed that axonal shafts and growth cones had fewer microtubules compared to controls (Figure 2.14). We observed reduced stable microtubules in the C-domain as well as dynamic microtubules in the P-domain. *Cyfip2*$^{-/-}$ MNs also did not display microtubule looping, splaying or bundling features, which have previously been described in *Xenopus* spinal cord explants and cortical neurons (Dent and Kalil 2001; Tanaka and Kirschner 1991). These microtubule morphological properties are prominent features seen during axonal elongation and branching.

It is well established that the actin cytoskeleton interacts with microtubules and this crosstalk influences axon outgrowth and growth cone dynamics (Cammarata et al., 2016; Dent et al.,

2011; Dent & Gertler, 2003; Tanaka et al., 1995). As previously discussed, the loss of CYFIP2 reduced the ECM-integrin-actin coupling at both nascent focal contacts at the leading edge and mature focal adhesions in the growth one lamella. This destabilizes the 'molecular clutch' that is needed for the retrograde flow of actin to protrude the leading edge. As a consequence, traction forces transmitted to the ECM when the 'motor clutch' is activated are weakened or disrupted. Fewer dynamic microtubules can migrate into the P-domain of the growth cone. If growth cone migration is impaired, the formation of stable microtubule bundles in the C-domain is also reduced, as observed in *Cyfip2*$^{-/-}$ MNs.

The visualization of branched actin networks in spinal MN growth cones was technically challenging as MNs lack large flat lamella as observed in both hippocampal and sensory neurons (Korobova & Svitkina, 2008; Letourneau, 1983; Svitkina & Borisy, 1999). Even with stringent glutaraldehyde fixation we only detected remnants of actin filaments at the leading edge of the growth cones. We assumed that MN growth cones contain only smaller F-actin filaments and networks that are easily lost during the membrane extraction procedure. The stabilization of smaller F-actin filaments using phalloidin might circumvent this loss for any future ultrastructural analysis.

3.7 Physiological markers required for proper NMJ morphology are altered in the absence of CYFIP2

The murine diaphragm has a stereotyped pattern during development (section 1.5), allowing the detection of morphological changes in either the presynaptic or the postsynaptic compartment of the NMJs in mutant mice. Since diaphragm innervation was impaired in the absence of CYFIP2, this strongly suggested that cholinergic neurotransmitter release and/or reuptake could also be dysregulated. In fact, we show that CYFIP2 is essential for the establishment of the machinery that drives acetylcholine neurotransmission in the NMJ. The cellular localization of SNAP25, synaptophysin, CHT and ChAT was severely altered in both *Cyfip2*$^{-/-}$ mice and cultured spinal MNs systems (Figure 2.7, Figure 2.8 & Figure 2.12). This indicates that CYFIP2 is also essential for proper formation of presynaptic compartments in the diaphragm NMJ.

SNAP25 is required for the fusion of synaptic vesicles to the plasma membrane during exocytosis (Han, Pluhackova, and Böckmann 2017) and labels the entire membrane of the presynaptic compartment. Almost no staining was detected in *Cyfip2*$^{-/-}$ diaphragms, indicating that the compartment is missing. The very reduced synaptophysin staining suggests that CFYIP2 might participate in the transport of the synaptic ACh vesicles to the active zone where

they are docked and primed for exocytosis. Our proteomics analysis showed CYFIP2 interacts with proteins associated with presynaptic vesicle docking (e.g., the t-SNARE protein syntaxin 1B) and fusion (e.g., synaptotagmin and Rab3a), further supporting a role of CYFIP2 in synaptic vesicle docking and fusion, which is necessary for ACh neurotransmitter release in the diaphragm muscle. Interestingly, *Chat*, *Cht*, and vesicular ACh transporter (*Vacht*) knockout mouse models all exhibited a lethal phenotype at birth along with aberrant NMJ morphology (Brandon et al., 2003; de Castro et al., 2009; Ferguson et al., 2004).

SNARE proteins are also used in regulating axonal and growth cone outgrowth. Plasma membrane components are located in plasmalemmal precursor vesicles (PPVs) or growth cone particles (GCPs) which fuse into the membrane upon SNARE-mediated exocytosis (Osen-Sand et al., 1996; Tojima & Kamiguchi, 2015). However, the role of SNARE mediated axonal outgrowth is under debate. In both *Drosophila* and chick models the SNARE complex was important in MN axon guidance (Barrecheguren et al., 2017). Specifically, the downregulation of t-SNARE proteins SNAP25 and STX1 resulted in axonal defects. SNAP25 deletion reduced axonal extensions in rat primary hippocampal cells and growth cone extensions in DRG cells (Morihara et al., 1999; Osen-Sand et al., 1993, 1996). In contrast, deletion of the v-SNARE protein VAMP2 had no effect on axonal outgrowth (Osen-Sand et al., 1996). Additionally, *in vitro* studies on PC12 cells (tumor cell line) showed that SNAP25 initiated neurite sprouting, while VAMP2 was required for neurite elongation (Shirasu et al., 2000). *Snap25* and synaptobrevin 1 (*Syb1*)/vesicle-associated membrane protein 2 (*Vamp2*) knockout mouse models exhibited impaired synaptic plasticity, yet no structural deficits in the NMJ (Liu, Sugiura, and Lin 2011; Washbourne et al. 2002). This shows the complexity of SNARE regulation in axonal outgrowth process in various biological systems. While we did see a reduction of SNAP25 in *Cyfip2*$^{-/-}$ diaphragm NMJs, we were unable to verify if SNARE proteins regulated axonal outgrowth, as some studies suggested. We would need to perform further analyses to see if other SNARE complex proteins such as VAMP2 or Sytaxin 1A, which are required for MN axon guidance in fly and chick models (Barrecheguren et al., 2017), are altered in *Cyfip2*$^{-/-}$ diaphragms. We also did not address the physiological properties of the *Cyfip2*$^{-/-}$ diaphragms as these animals only survived for 20 minutes after birth, making it technically difficult to assess motor end-plate potentials. In summary we have provided evidence that CYFIP2 deletion affects the formation of presynaptic terminals, the correct localization of acetylcholine vesicles and possibly the reuptake of choline into the NMJ

presynaptic terminal. The proper formation of the presynaptic compartments in the diaphragm NMJ are essential for the physiological process of respiration.

3.7.1 CYFIP2, a biomarker for peripheral neuropathies?

CYFIP2 has been associated with Alzheimer's disease (Ghosh et al., 2020; Tiwari et al., 2016), schizophrenia (Föcking et al., 2015) and epilepsy (Nakashima et al., 2018; Zweier et al., 2019). A specific amino acid mutation (S968F) in CYFIP2 has also been implicated in cocaine response (Kumar et al., 2013). Human clinical studies showed that CYFIP2 expression was upregulated in patients with Fragile X syndrome (FXS) and autism spectrum disorder (ASD) (Hoeffer et al., 2012; Noroozi et al., 2018). Since we showed the important role of CYFIP2 in spinal MN developmental processes, could CYFIP2 be a potential biomarker for peripheral neurodegenerative diseases with axonal pathophysiology?

Studies showed that CYFIP2 is upregulated in amyotrophic lateral sclerosis (ALS) (Lilo et al., 2013; Nachmany et al., 2012) and multiple sclerosis (MS) patients (Mayne et al., 2004). The main pathophysiology of MS, a fatal autoimmune disease, is axonal loss and demyelination (Mayne et al., 2004). ALS is a neurodegenerative disorder that affects both upper and lower MNs and the cause of death is respiratory failure (Kiernan et al., 2011). The actin cytoskeleton and guidance cues play an important role in ALS, but many mechanisms are still unclear (Moloney et al., 2014). In addition the majority of research on ALS and MS have focused on the ABPs profilin 1 and profilin 2 (Hensel & Claus, 2018). As previously mentioned, CYFIP2 interacts with profilin 2, which is mainly expressed in the CNS down to the NMJs and interacts with the RHOA kinase ROCK (Witke et al., 1998). It was also shown in hippocampal neurons that the phosphorylation of profilin 2 via the RHOA/ROCK pathway inhibited neurite formation by favoring more stable F-actin dynamics (Da Silva et al., 2003). It was recently shown that the RHOA/ROCK pathway interacts with myosin II to inhibit axonal elongation by restricting the microtubules (Dupraz et al., 2019). Our immunocytochemical stainings in MN growth cones showed an increase in myosin II-positive signal and microtubule morphology (from ultrastructural analysis) was aberrant. It is possible the absence of CYFIP2 leads to a shift towards the GTPase RHOA signaling and ROCK activation as observed in axonal growth in pyramidal neurons (Dupraz et al., 2019). However, we would also need to verify if the GTPase CDC42 was also affected by the loss of CYFIP2 in spinal MNs. CYFIP2 could be a new biomarker and future model to study the function of ARP2/3-dependent actin nucleation in motor neurodegenerative diseases.

4. Conclusion and Outlook

This study presented a novel function for CYFIP2, a component of the WRC, in mouse embryonic PNS development. Various mouse models (*Cyfip2-LacZ* and *Cyfip2*$^{-/-}$) showed CYFIP2 is localized in peripheral tissue and required for proper diaphragm NMJ innervation and respiration. CYFIP2-WRC signaling is required for both spinal MN axonal elongation and branching *in vivo*, *in vitro* and *ex vivo.* The structural components needed for cholinergic neurotransmission (i.e., CHT and ChAT) and exocytosis (i.e., SNAP25, synaptophysin) in the diaphragm NMJ were also CYFIP2-dependent. The formation of proper dorsal-ventral patterned postsynaptic synaptic terminals (AChR) are CYFIP2-independent. However, the modulation of the AChR cluster stability is CYFIP2-dependent and essential for diaphragm innervation. This provides new insight into how CYFIP2-WRC regulates ARP2/3 actin polymerization in motor circuits in the PNS.

Our proteomic mass spectrometry analysis showed CYFIP2 also interacted with gene involved in neurite extension, adhesion and presynaptic regulation in the adult CNS. Histological analysis on cultured spinal MNs showed CYFIP2 regulated ECM-integrin mediated focal adhesions contact sites. The focal adhesion actin adaptor proteins, vinculin, FAK and paxillin required CYFIP2 to properly tether the actin filament to integrin-mediated focal contacts. Tyrosine phosphorylation signaling regulates recruitment of branched actin networks to the focal adhesion sites. Ultrastructural analysis on spinal MNs growth cones showed that actin-microtubule crosstalk is CYFIP2-dependent. The regulation of CYFIP2 in axonal outgrowth is cell autonomous to spinal MNs. The function of CYFIP2 in CNS neurons is still not fully understood. Collateral branching in the CNS could be regulated by the A-to-I RNA edited CYFIP2-320E variant. HEK293 cells transfected with CYFIP2-320E had longer neurite protrusions compared to the non-edited CYFIP2-320K variant.

We elucidated the composition of the mouse embryonic CYFIP2-dependent WRC in the CNS, which differs from the adult CYFIP2-WRC and the CYFIP1-WRC. Biochemical and histological assays showed that despite high amino acid sequence identity CYFIP1 did not compensate for the loss of CYFIP2. The MENA/VASP family (nucleators for linear actin filaments) which is known to interact with Arp2/3 complex, also did not compensate for the loss of CYFIP2-WRC branched actin polymerization. In addition, F-actin dynamics were not disrupted in the absence of CYFIP2. These findings add to the repertoire of CYFIP2 function besides the canonical CYFIP2-WRC and CYFIP2-FMRP-elF4E complexes.

There are some open questions that arise from this study. Is CYFIP2-dependent branched actin required for the formation of nascent focal contact, mature stable focal contacts, or both? Additional histological assays would be required to differentiate focal adhesions proteins for nascent contacts (e.g., talin and α-actinin) and mature focal adhesions (e.g., zyxin and tensin). The role of CYFIP2 and microtubules dynamics would be investigated using markers for dynamic microtubules (e.g., +TIPS) and mature microtubules (e.g., MAPS). This would give more insight into how CYFIP2-dependent actin-microtubule crosstalk is regulated. Further biochemical and histological assays are needed to determine which NFPs compensates for the loss of CYFIP2 in spinal MNs. In addition, we do not know which guidance cues are used to modulate CYFIP2-dependent axonal outgrowth. Live-cell imaging experiments on *Cyfip2*$^{-/-}$ spinal cord explants would elucidate how MN axons respond to various chemoattractive and chemorepulsive cues (e.g., netrin-1, SLIT-ROBO). Could the A-to-I RNA edited CYFIP2-320E rescue aberrant *Cyfip2*$^{-/-}$ spinal MN axonal phenotypes? Microinjection of CYFIP2-320K and CYFIP2-320E plasmid DNA into spinal cord explants, or transduction into cultured spinal MNs would help elucidate the function of CYFIP2 RNA editing in axon morphogenesis. Most likely several actin polymerization processes are working simultaneously to regulate axonal outgrowth and branching processes. It is possible other Class I NPFs such as N-WASP compensate for the loss of CYFIP2. Furthermore, CYFIP2 could be a potential biomarker to help understand how MN neurodegenerative and/or respiratory diseases function.

5. Methods

5.1 Transgenic mouse lines

Cyfip2 homozygous knockout (*Cyfip2*$^{-/-}$) embryos were generated by breeding heterozygous (*Cyfip2*$^{+/-}$) males and females. *Cyfip2*$^{lacZ/wt}$ embryos were generated by breading *Cyfip2*$^{lacZ/wt}$ with C57 WT breeders. The *Cyfip2-LacZ* line was generated using the *Cyfip2*$^{tm1a(EUCOMM)Wtsi}$ transgenic mouse line created by the EUCOMM consortium (Supplementary Figure. 8.1). All mice were kept in IVC cages in a controlled environment with 55 % humidity and 22°C following a 12h light/ dark cycle. To obtain embryos at the correct stage, single caged males were mated on the evening with 1-2 females. The following morning females were weighed and checked for a vaginal plug and separated into new cages if a plug was visible. The time point when the vaginal plug was seen was considered embryonic (E) developmental stage 0.5 (E0.5). All experiments were in accordance with the German Animal Protection Law and the State Agency for Nature, Environment and Consumer Protection (LANUV) of North Rhine-Westphalia, Germany.

5.2 Molecular Biology

5.2.1 Genomic DNA extraction from mouse biopsy

Tail biopsies (~2 mm) from E15.5-E18.5 embryos were used to extract the genomic DNA to determine the genotypes. Biopsies were put into 1.5 ml Eppendorf tubes containing 200 µl of genomic DNA Extraction Buffer (section 6.5.1) and 0.25 mg/ml Proteinase K solution and digested o/n at 55 °C. The salting-out method was used to isolate the DNA. This method uses high salt concentrations to precipitate the proteins leaving the DNA in solution, which is then precipitated with 70 % ethanol solution and rehydrated with water. Briefly, 100 µl saturated NaCl (>6 M) was added to the digested biopsy samples, shaking vigorously (1-2 min) then spun at 14,000 rpm for 15 min at RT. 220 µl of the supernatant was added to ~2.5 volumes (500 µl) of absolute EtOH and inverted several times to allow DNA flocculation. The DNA was spun down at 14,000 rpm for 1 min at RT; the EtOH was removed, and the DNA pellet was left to air dry. The DNA was resuspended in 200 µl of MilliQ H_2O and stored at 4°C until further use.

5.2.2 Fast Genomic DNA extraction using the KAPA Express Extraction Kit

The DNA extraction to genotype embryos used for *in vitro* studies was done according to instructions provided by the KAPA Express Extract Kit (Roche). Briefly, the DNA was digested and extracted from biopsies using the reaction setup and thermocycler program in Table 1. The DNA was used for the polymerase chain reaction (PCR) using the AptaTaq Fast PCR kit (Roche) in Table 3.

Table 1. KAPA Express Extract Kit mix and protocol for fast DNA extraction.

Reaction mix	
KAPA Express Extract Kit	**Volume (µl)**
Buffer 10x	5
Enzyme (1 U/µl)	1
ddH_2O	44

DNA Lysis program		
Temperature (°C)	**Time (min)**	**Cycles**
75	15	1
95	5	1
15	2	1

5.2.3 Polymerase chain reaction

Polymerase chain reaction (PCR) is a highly sensitive method used to amplify specific DNA fragments from a range of DNA sources. The method is based on three consecutive steps, DNA template denaturation, primer annealing and primer elongation (Garibyan & Avashia, 2013). These steps are repeated to allow DNA fragment amplification, which then can be visualized on an agarose gel. PCR was used to determine the genotypes of the embryos used in this study. The following PCR mixes and PCR programs were used to amplify the alleles of the *Cyfip2-del* mouse line (Table 2 and Table 3) and the *Cyfip2-LacZ* mouse line (Table 4). The expected amplicon size for the WT allele, the *Cyfip2-del* allele and the *Cyfip2-LacZ* allele was 220 bp, 516 bp, and 416 bp, respectively.

Table 2. *Cyfip2-del* PCR reaction mix and PCR program.

PCR reaction mix	
PCR Reagent	**Volume (µl)**
MilliQ ddH_2O	12.4
3Buffer 5x	4
$MgCl_2$ (25 mM)	1.2
dNTPs (10 mM)	0.4
Primer: C2EULoxP3-for/ C2EULoxP3-rev2 (20 µM)	0.5
Primer: C2EULoxP2-for/ C2EULoxP3-rev2 (20 µM)	0.2
Taq Polymerase (5 U/µl)	0.3
DNA	1
Total	20

PCR cycle program		
Temperature (°C)	**Time (min:sec)**	**Cycles**
98	2:00	1
96	0:30	
56	1:00	35x
72	0:30	
72	5:00	1
25	∞	

Table 3. *Cyfip2-del* AptaTaq Fast PCR reaction mix and PCR program.

PCR reaction mix	
PCR Reagent	**Volume (µl)**
MilliQ ddH_2O	14.25
Buffer 5x	4
Primer: C2EULoxP3-for/ C2EULoxP3-rev2 (20 µM)	0.5
Primer: C2EULoxP2-for/ C2EULoxP3-rev2 (20 µM)	0.25
KAPA extracted genomic DNA	1
Total	20

PCR cycle program		
Temperature (°C)	**Time (s)**	**Cycles**
96	30	1
96	5	
60	12	35x
15	120	1

Table 4. *Cyfip2-LacZ* PCR reaction mix and PCR program.

PCR reaction mix	
PCR Reagent	**Volume (µl)**
MilliQ ddH_2O	11.8
Buffer 5x	4
$MgCl_2$ (25 mM)	1.2
dNTPs (10 mM)	0.4
Primer: C2EULoxP3-for/ C2EULoxP3-rev (20 µM)	0.4
Primer: *Cyfip-LacZ*-for/ C2EULoxP3-rev (20 µM)	1
Taq Polymerase (5 U/µl)	0.2
DNA	1
Total	20

PCR cycle program		
Temperature (°C)	**Time (min:sec)**	**Cycles**
98	2:00	1
96	0:30	
58	1:00	35x
72	0:30	
72	5:00	1
25	∞	

5.2.4 Gel Electrophoresis

The amplified DNA fragments can be visualized by gel electrophoresis on agarose gels. The DNA is labeled with ethidium bromide that intercalates into the DNA and can be seen under UV light. The PCR reactions were run on 1.5 % agarose gels made in 1x TAE buffer (5 µl EtBr stock (10 mg/ml) in 100 ml agarose in TAE). 5 µl 6x DNA loading buffer was added to the PCR products from the fast-genomic DNA extraction kit before being loaded onto the agarose gels. The gels ran at 90 V for 15-20 min and were documented using the Bio-Rad Gel Doc™ EZ imager.

5.3 Biochemistry

5.3.1 Tissue preparation

All tissues of interest were dissected on ice with cold 1x PBS. Tissues were then immediately lysed for protein lysates or were shock frozen in liquid nitrogen (N_2(l)) and stored at -80°C until further use.

5.3.2 Total protein organ lysate

Mouse organs were lysed in 2x sodium dodecyl sulfate (SDS) loading buffer (section 6.5.2) in glass/Teflon homogenizer either manually or electrically on ice. The manual homogenization was used for organs that were lysed in volumes of 500 µl or less (e.g., hippocampus and spinal cord). All other tissues were electrically homogenized at 600 revolutions per minute (rpm) until dissociated. The homogenized tissue was transferred into a new 1.5 ml Eppendorf tube and denatured at 99°C for 10 min and vortexed every 2-3 minutes to shear genomic DNA. Samples were then cooled 2-3 min on ice and spun down at 14,000 rpm for 5 min. The lysates were quantified with the Bradford assay and protein dilutions of 1 µg/µl were prepared with 2x SDS for Western blot analysis. All SDS-treated protein samples were stored at -20°C.

5.3.3 Cytoplasmic protein lysates

Organs (fresh or frozen) were homogenized in a glass/Teflon homogenizer in cold Triton X-100 lysis buffer (section 6.5.2) at 600 rpm. Afterwards the homogenates were transferred into new 1.5 ml Eppendorf tubes and kept on ice for 10 min for complete lysis of the tissue. Samples were centrifuged at 14,000 rpm at 10 min at 4 °C to remove nuclei and cell debris. Subsequently the supernatant was transferred to a new 1.5 ml Eppendorf tube and the protein concentration was determined using the Bradford assay. Stocks of 1 µg/µl protein lysates were prepared in 1x SDS protein loading buffer and denatured at 99°C for 10 min, cooled on ice, spun down and stored at -20°C. Surplus cytoplasmic lysates were shock frozen in N_2(l) and stored at -80°C until further use.

5.3.4 Protein Quantification by Bradford assay

The Bradford assay was used to determine the protein concentration of all organ protein lysates. This method uses the Coomassie Brilliant Blue dye, which is a red/brown color in unbound acidic conditions. When the dye binds to proteins the solution turns blue as the dye undergoes

a spectral shift (Laemmli, 1970). One can read the absorbance maximum shift from 465 nm (red, unstable state) to 595 nm (blue, stable state) when the protein-dye complex is made using a spectrophotometer.

The BSA calibration curve was made using defined sets of protein amounts (0.5-16 µg BSA in 1x SDS protein loading buffer diluted 10 times in water) and the absorption of each protein amount was read at 595 nm. The cytoplasmic protein lysates were prepared by adding 1 µl 5x SDS loading buffer to 4 µl of lysate, denatured at 99°C for 2-3 min, cooled on ice and spun down. The blank sample was prepared in the same way using lysis buffer instead of a sample. The total protein lysates were prepared using 5 µl of each sample and the blank was 5 µl of the 2x SDS loading buffer. All total and cytoplasmic protein samples were diluted 10-fold with 45 µl water. Then 10 µl of the total or 12.5 µl of the cytoplasmic protein lysate was added to 1 ml of 1x Bradford solution in cuvettes. The cuvettes were inverted several times to ensure proper protein mixing and the absorbance at 595 nm was taken with the spectrophotometer. The absorbance of the protein samples was divided by the slope of the calibration curve to determine the protein concentration in µg/µl.

5.3.5 SDS-polyacrylamide gel electrophoresis (SDS-PAGE)

In order to assess the presence of specific proteins of interest SDS-polyacrylamide gel electrophoresis (SDS-PAGE) is used to separate proteins in one-dimensional based on molecular mass alone (Laemmli, 1970). SDS-PAGE gels can be used to determine homogeneity of protein samples. Proteins will migrate through a gel in response to an electric field towards the anode depending on the proteins shape, charge and size (Gallagher, 2006). SDS is an anionic detergent and used to denature proteins into a linear structure and add uniformly negative charge density to the proteins. Whereas β-mercaptoethanol (a reducing agent) is used to reduce disulfide bonds. The SDS-PAGE system uses a discontinuous buffer system that uses different buffer ions and pH in the gel and electrode reservoir (Gallagher, 2006). In polyacrylamide gels the pore size decreases with higher acrylamide concentrations. Proteins are loaded into a stacking gel that has a larger pore size and this overlays the resolving gels with has a smaller pore size. The stacking gel has lower porosity and a lower acidic buffer pH (pH 6.8) and concentrates the proteins samples into a ‘stack’ before they reach the resolving gel which has a higher basic buffer pH (pH 8.8). The resolving gel has a higher buffer pH proteins and smaller pore size.

The polyacrylamide gels were cast using homemade chambers (10 x10.5 cm) with 4 % stacking gels and 6 %, 8 % or 10 % resolving gel. These acrylamide percentages of the resolving gels were used based on the proteins of interest which had molecular weights ranging from 150 kDa-45 kDa. The denatured protein samples (10 µg unless otherwise stated) were loaded onto the gels and run at 80 V until the proteins were stacked and reached the resolving gels. Standard molecular markers were used for the correct orientation of proteins of interest. The proteins were then run at 130 V until the blue running front ran out of the gels.

5.3.6 Western blotting

After the SDS-PAGE the protein samples were transferred to polyvinylidene difluoride (PVDF) membrane. Proteins will bind to the PVDF through hydrophobic interaction and PVDF has higher protein binding capacity and higher sensitivity enabling the detection of low expressed proteins (Bass et al., 2017). PVDF membranes are more robust compared to nitrocellulose making them useful for multiple rounds of antibody labelling and detection. However, one disadvantage is the potential for higher background signal to noise ratio.

The SDS-PAGE gels were transferred onto PVDF membranes by the submerged/ wet blot transfer method. Firstly, the PVDF membranes were activated with MeOH before being placed in the 'transfer sandwich' (sponge-2x Whatman filter paper-resolving gel-PVDF memebrane-2x- Whatman paper-sponge). The SDS-PAGE resolving gel was carefully placed to the PVDF making sure air bubbles were removed. The transfer sandwich was placed into the transfer tank with the gel side faced the cathode (-) side and the PVDF membrane side faced the anode (+) side. The transfer chamber was filled cold Towbin transfer buffer (section 6.5.2) and an ice pack. The transfer blot was run at 20 V o/n at RT.

5.3.7 Enhanced chemiluminescent Western blot analysis

After the wet blot transfer the PVDF membranes were removed and washed in 1x NCP (section 6.5.2) then blocked in 5 % non-fat milk powder/ 1x NCP for 1 h at RT prevent any non-specific antibody binding. The membranes were then cut into half along the respective marker length to avoid reprobing the membrane too many times. The membranes were incubated with the respective antibodies (made in 5 % milk/ 1x NCP unless otherwise stated) o/n at 4°C on a shaker. Then the membranes were washed three times for 15 min with 1x NCP then incubated in horseradish peroxidase (HRP)-conjugated secondary antibody for 1 h at RT on a shaker. Afterwards the membranes were washed three times for 10 min at RT. All proteins signals were

detected using enhanced chemiluminescence (ECL). The ECL solution consists of a 1:1 ratio of Luminol (3-aminophthalhydrazide) and H_2O_2. The reaction between luminol and H_2O_2 is catalyzed by the HRP and light is released as a byproduct. The light signal was detected using a digital imager with a CCD-camera (LAS 4000 Mini, GE Healthcare). The software Multi Gauge V3.0 (Fujifilm Life Science) was used to quantify all antibody signals on all lanes and gels analyzed. Housekeeping genes (e.g., γ-tubulin) were used as controls to normalize the detected protein levels.

5.3.8 Coomassie staining

This method is used to stain proteins and estimate the quality and concentration of the proteins. The proteins on the SDS-PAGE gels or PVDF membranes were fixed with 40 % MeOH/ 10 % acetic acid for 20 min. The gels were then incubated in Coomassie Brilliant Blue solution for 30-60 min at RT on a shaker. The gels were then destained twice for 15 min in 40 % MeOH/ 10 % acetic acid and then 20 min in 20 % MeOH/ 10 % acetic acid. PVDF membranes were stained in 40 % MeOH/ 10 % acetic acid for 10-15 min. The gels/membranes were rinsed in distilled water then left to air dry. All membranes were scanned and analyzed using Multi Gauge software.

5.3.9 F-/G-actin ratio analysis

The F-/G-actin content in the tissue can be separated using centrifugation processes, G-actin is localized in the supernatant and F-actin is in the pellet (McRobbie & Newell, 1983). Fresh brain tissue was homogenized ten times at 600 rpm with ice cold 1x PHEM buffer (section 6.5.2) with 1 % Triton X-100. The samples were centrifuged at 14,000 rpm for 10 min at 4°C.Then 80 % of the supernatant (G-actin fraction) was removed and denatured with 5 x SDS loading buffer at 99°C for 10 min then cooled on ice. The remaining supernatant was carefully removed from the pellet (F-actin fraction). The pellet was resuspended in 1x SDS loading buffer (1.25 volume) and denatured at 99°C for 10 min then cooled on ice. Equal volumes of the F-actin and G-actin samples were loaded onto 10 % SDS-PAGE gels and transferred as previously described (sections 5.3.5-5.3.6). The membranes were blotted with anti-β-actin antibody to analyze and quantify the F-/G-actin ratio.

5.3.10 Co-immunoprecipitation of CYFIP2

Proteins rarely act singularly in nature but interact with several other proteins. A tool used to identify these protein-protein interaction partners is co-immunoprecipitation (co-IP). A specific antibody (or bait) binds to the solid substrate (e.g. Protein G) and can pull down other proteins that bind/interact with the antibody of interest (Markham et al., 2007).

The embryonic brains were lysed in 1 ml RIPA buffer (section 6.5.3) and placed on ice for 10 min and spun down at 14,000 rpm for 10 min at 4°C. The supernatant was transferred to a new 1.5 ml Eppendorf tube and used for co-IP analysis or stored at -80°C. 100 µl Protein G beads (stored as a 1:1 slurry in 20 % EtOH) were washed twice with 1 ml cold 1x PBS and then incubated with 0.1 % BSA/ 1x PBS for 1 hour at 4°C on a rotating wheel. The beads when spun down at 1,500 rpm for 1 min at 4 °C and washed twice with 1 ml RIPA buffer with phosphatase inhibitors. Then 1 ml of the undiluted CYFIP2-1C4 hybridoma supernatant was added to the Protein G bead slurry and incubated o/n at 4°C on a rotating wheel. Control protein G beads were incubated with only 1 ml RIPA buffer. The beads were then washed three times with ice cold 1ml RIPA buffer. Afterwards 1 mg of E18.5 embryonic total brain lysate was added to the bead slurry o/n at 4°C. An input IP fraction (1µg/ml) was prepared by denaturing the brain protein lysate with 5x SDS at 99°C for 10 min then stored at -20°C.

The supernatant was collected (unbound IP fraction) and denatured with 5x SDS loading buffer at 99°C for 10 min and stored. The beads were washed three times with 1 ml RIPA wash buffer by inverting the beads, placing them on ice for 5 min and spun down at 1,500 rpm for 1 min at 4°C. Any excess buffer was removed with a Kimwipe after the last wash. The bound proteins were eluted with 100 µl 2x SDS at 99°C for 10 min, placed on ice for 2-3 min; then spun down at 14,00 rpm for 1 min at RT. The supernatant was transferred into a new 1.5 ml Eppendorf tube and stored at -20°C until further use for Western blot analysis. The samples were loaded onto 6-8 % SDS-PAGE gels for Western blot analysis. The CYFIP2 co-IP experiments on adult brain protein were kindly performed by Carina Beuck.

5.3.11 MALDI-TOF mass spectrometry analysis

Mass spectrometry (MS) is an analytical tool used to identify various biomolecules such as DNA, RNA and proteins based on their mass-to-charge (*m/z*) ratio in various biological system. In order to study larger biomolecules a soft ionization method called matrix-assisted-laser-desorption ionization time-of-flight mass spectrometry (MALDI-TOF MS) was developed (Karas & Hillenkamp, 1988; K. Tanaka et al., 1988). MALDI-TOF MS is routinely used for

large scale proteomic analysis and generates protein spectral fingerprints that are compared to an online databased with reference proteins spectra. We used MALDI-TORF MS to identify novel protein interaction partners of CYFIP2.

Co-IP was performed as mentioned in section 5.3.10 with a few modifications. Adult total brain was lysed in 4 ml Triton lysis buffer, pH 8. A 12 % SDS-PAGE gel was used to run the samples for a 2 cm run. The gels was stained by Coomassie Brilliant blue and gel bands (2 mm x 4 mm) were cut and digested according to (Shevchenko et al. 2007). The gels were washed and incubated in ddH_2O followed by 50 % ACN, and 100 % ACN (section 6.5.5) for 10 min. Gels were then covered by DTT and incubated for 30 min. Then the gels bands were incubated in NH_4HCO_3 for 1 h, the solution was removed, and acrylamide was added to the samples. Washes with dH_2O, 50 % ACN and 100 % ACN occurred before the samples were vacuum dried for 15 min at 30°C at 1000 rpm. The o/n enzymatic digestion using trypsin occurred at 37°C. Peptides were extracted from the supernatant and washed in ddH_2O, 50 % ACN and 100 % ACN. All samples were vacuum air dried and stored at -20°C until MALDI-TOF mass spectrometry was performed.

All MALDI-TOF MS analysis was performed by Carina Beuck, Dr. Marc Sylvester and Bernd Gehrig at the Institute for Molecular Biology and Biochemistry, University of Bonn. Anti-L-protein, Sendai was used as a control. All MS sequences data was aligned to the UniProt protein database (UniSwiss). Protein abundance scores were calculated as percentages and proteins that were at least 2.5-fold enriched were used for further analysis. All genes that fit this criteria were further classified using Gene Ontology (GO) Enrichment Analysis and Protein Analysis Through Evolutionary Relationships (PANTHER) for genes involved in both biological and cellular processes using the website http://geneontology.org (Ashburner et al., 2000; Mi et al., 2019).

5.4 Cell Biology

5.4.1 Monoclonal CYFIP2 antibody production.

C57/BL6N mice were immunized with a CYFIP2-375 peptide (coupled to keyhole limpet) with TiterMax- Gold-Adjuvant (Sigma) intraperitoneally. After two weeks the mice were boosted with the same peptide and blood samples were taken via cheek bleeding in accordance with animal laws. The blood was allowed to coagulate o/n at 4°C. Next, the blood samples were spun at 14,000 rpm at for 15 min at 4°C and the serum was collected without any blood platelets. The serum was screened for antibody production using E18.5 WT and *Cyfip2*$^{-/-}$ total brain

protein lysates of on 8 % SDS-PAGE gels. The mice received a total of four peptide boosts in two-week intervals before the fusion assay. A final immunization boost was performed 24 h before the spleen B cells were harvested for the hybridoma fusion assay.

Myeloma P3 cells (ATCC) were grown in T-175cm^2 tissue culture flasks with RPMI/ 10 % FCS (section 5.4.1) medium until 80-90 % confluent. The myeloma cells were counted using a Neubauer chamber and 5x10^7 cells were seeded used for the fusion protocol. The spleen of the mouse was removed and mechanically disrupted between sterile frosted glass slides in RPMI medium and put into a 50 ml Falcon tube. The spleen B cells (lymphocyte) clumps were left to settled (4-5 min) then were spun down at 1500 rpm for 5 min at RT. The supernatant was collected, and B cells were counted to have a total of 1x10^8 cells. These cells were then resuspended in fresh RPMI medium. The cells were centrifuged down at 1000 rpm for 5 min and washed two times with RMPI medium. The myeloma and B-cells were mixed in a 1:3 ratio, respectively in 20 ml RPMI medium. The cells were spun at 1000 rpm for 10 min, the supernatant was carefully aspirated and 0.8 ml of PEG-1500 (prewarmed to 37°C) was gently added to the pellet. The cells were incubated for 1 min at 37°C then 1 min at RT. Then RPMI medium was added dropwise as follows: 1 ml/ 1 min, 3 ml/ 1 min then 10 ml/ 3 min then 6 ml/ 1 min.

After the cells were left on ice for 10 min and then spun down at 700 rpm for 5 min. Briefly, the pellet was resuspended in 125 ml fresh RPMI-fusion medium. Then 1ml of the cell suspension was plated out on 24-well plates and incubated at 37°C/ 5 % CO_2. After 24 h 500 µl RPMI/ 2x HAT medium was added to the cells. Two weeks later the medium was changed with RPMI/ 1x HAT medium. The cells were slowly weaned off the HAT medium and changing only to RMPI/ 5 % FCS / 100 % Hybridoma supplement medium. Once the supernatant was yellow (indication of antibody production), 1ml was collected to test on ELISA, Western blot and/or Dot blot analysis. Once positive clones were detected, these cells were expanded for single clone limited serial dilution and seeded at 0.7 cell/ml in RMPI medium in 96-well plates. The supernatant of the single clones was retested for antibody production and then expanded into 6-well plates followed by T-25 cm^2 flasks. All antibody producing clone stocks were harvested with pre-chilled RPMI medium containing 50 % glycerol and stored in N_2(l) storage tanks.

5.4.2 Monoclonal antibody purification

The amount of ammonium sulfate needed for 60 % saturation to precipitate the CYFIP2 calculated. The hybridoma supernatant (600 mL) was brought to 60 % saturation with

ammonium sulfate by slowing adding 234 g ammonium sulfate to the supernatant on ice while continuously stirring. Then the antibody was precipitated o/n at 4°C. The antibody was transferred to 250 ml beakers and centrifuged for 30 min at 8000 x g at 4°C. The pellet was resuspended in 20 ml 1x PBS and then dialyzed twice with cold 1x PBS solution o/n at 4°C. The antibody was purified over a Protein G column (5 ml column volume) using the Äkta FPLC (GE Healthcare). The Protein G was washed with sterile water and equilibrated in 10 column volumes binding buffer (section 0). The protein was loaded into a Superloop and passed over the Protein G column at a rate of 0.1 ml/min. The column was then washed 2-3 times with the column volume. The elution buffer was injected into the column and 10-12x 500 µl fractions were collected into 1.5 ml Eppendorf tubes containing 100 µl 1M Tris-HCl, pH 9.0. The fractions were places on ice and quantified using the Bradford assay. The samples were run on a 15 % SDS-PAGE gel at 130 V. The gels were stained with Coomassie Brilliant B to check for heavy and light chain IgG bands at 55 kDa and 25 kDa, respectively. The fractions with the highest antibody concentration were pooled together. These samples were dialyzed twice with cold 1x PBS solution o/n at 4°C and then with 50 % glycerol/1x PBS o/n at 4°C. l All antibody aliquots were stored at -80°C. The purified CFYIP2 antibody was isotyped using the IsoStrip™ Mouse Monoclonal Antibody Isotyping kit (Roche) following manufacturer instructions.

5.4.3 Calcium phosphate transfection of HEK293 cells

Calcium phosphate ($Ca_3(PO_4)_2$) transfection is a method used to introduce foreign DNA into cells. The calcium phosphate-DNA coprecipitates attach to the cells and are taken up via endocytosis. The calcium phosphate transfection is ideal for primary cell lines as they have lower cellular toxicity. In order to optimize this transfection protocols for potential neuronal cells we performed preliminary tests using HEK293. However, one disadvantage is that calcium phosphate transfection efficiency is on the lower range (approx. 10 %). Briefly, HEK293 cells were expanded and grown in 10 ml DMEM medium supplemented with 10 % FCS in a T-75 flask at 37°C/ 5 % CO_2. The cells were grown to 70-90 % confluency and 1.5x 10^4 cells were seeded onto 19 mm coverslips in 24-well plates containing 1.5 ml DMEM. The calcium phosphate solution (section 6.8.3) was added dropwise onto the cells and left to incubated o/n at 37°C/ 5 % CO_2. After 16 h fresh DMEM medium added and the cells were fixed with 4 % PFA after 24 h and 96 h. Tagged CYFIP2-320K and CYFIP2-320E plasmid constructs used for the transfections were kindly designed and provided by Dr. Michael Reinke (section 6.3).

5.5 Histology

5.5.1 Cryostat sectioning of mouse tissue

E18.5 embryos were fixed in 4 % PFA/ 1x PBS o/n at 4°C and then washed in 1x PBS. The embryos were embedded in Tissue Tek OCT mounting medium in cryo-molds and then frozen on dry ice. The sections were cut on a Cryostat with the setting chamber temperature (-19°C) and object temperature (-18°C). These temperatures could vary depending on the quality of the cryofixation. Sagittal or transverse sections were cut (12-16 µm) and placed onto Superfrost slide objective and left to air dry until stored at -80°C until further use.

5.5.2 X-Gal staining on cryosections

To detect the expression of the β-galactosidase transgene in the *Cyfip2-LacZ* reporter mouse model, X-gal staining of frozen sections (cryosections) was performed. All microscope slides with crysectioned tissues were fixed in LacZ fixation solution (section 6.7.1) for 5 min at RT. The slides were washed three times for 5 min in LacZ wash solution. then incubated in LacZ substrate solution o/n at 37°C and cover in foil (light sensitive solution). The slides were washed twice for 5 min with LacZ wash solution then once for 5 min with tap water. The slides were counterstained in 0.01 % Eosin for 1 min. The slides were rinsed with tap water, air dried and cover slipped with Entellan embedding medium.

5.5.3 Whole-mount X-gal staining

E13.5 embryos were fixed in 4 % PFA/ 1x PBS o/n at 4°C. The embryos were rinsed in 1x PBS three time for 5 min then transferred into 15 ml falcons and then incubated in LacZ substrate solution (section 6.7.1) o/n at 37°C. The embryos were then washed three times for 5 min with LacZ wash solution then once for 5 min in tap water. The embryos were then cleared in 20 % Glycerol/ 1 % KOH for 48 h.

5.5.4 Whole-mount immunofluorescence staining of diaphragms

The embryos were removed and places in cold 1x PBS and the diaphragms were carefully dissected, and residual connective tissue was removed without damaging the muscle. The diaphragms were fixed in 4 % PFA/ 1x PBS o/n at 4°C. The diaphragms were then rinsed quickly in 1x PBS then quenched in 0.1 M glycine/ 1x PBS for 1 h at RT. The diaphragms were washed 3x 5 min in 1x TBS then incubated in permeabilization buffer 0.5 % Triton X-100/ 1x

TBS o/n at 4°C with strong agitation. The following day the tissue was rinsed 3x for 15 min in 1x TBS followed by an autofluorescence quenching treatment: 1 h in 100 mM NH_4Cl, then 0.1 % sodium borohydride/ 1x TBS for 5 min. Between each quenching treatment the tissue was rinsed with 3 x 5 min with 1x TBS. The diaphragm was incubated in blocking buffer (section 6.7.2) o/n at 4°C on an orbital. The tissue was then incubated in primary antibody in blocking buffer for 48 h at 4°C on an orbital shaker. The diaphragms were washed 3x 1 h followed by secondary antibody incubation for 48 h at 4°C. NMJ endplates were labeled with Alexa Fluor 555-conjugated α-Bungarotoxin for 48 h along with any other secondary antibody. The tissue was washed 2x 1 h at RT with 1x TBST-0.1% Triton X-100, then 1 h with TBS. Afterwards the diaphragms were quickly rinsed in ddH_2O and mounted onto a microscope slide and embedded with 300 µl Mowiol/NGP per diaphragm. The slide was air dried, sealed with clear nail varnish around the edges to prevent any oxidation and stored at 4°C.

5.5.5 Preparation of coverslips

Coverslips (13 mm diameter and 0.17 mm thickness) were placed in a porcelain staining rack and incubated in HNO_3 ($\geq$ 69 %) covered with aluminum under a fume hood o/n at RT. The coverslips were then washed 4-5 times for 20 min with MilliQ H_2O and then sterilized for 6 h at 220°C. The coverslips were stored at RT until further use. Sterile coverslips used for hippocampal cultures had three paraffin dots applied with a Pasteur pipette. 200 µl poly-L-lysine in borate solution was applied to each coverslip in a humid chamber 48 h before planned hippocampal dissections. These coverslips were washed three times with sterile H_2O before MEM-HS was added. All coverslips were equilibrated at 37°C.

5.5.6 Coverslip coating for motor neuron culture

The sterile coverslips were coated in 200 µl Poly-DL-ornithine hydrobromide (PLO)/ 0.15 M borate buffer pH 8.35 o/n at 4°C. The coverslips were then washed three times with sterile ddMilliQ water and then left to air day. Afterwards the coverslips were coated with 300 µl laminin (2.5 µg/ml in 1x HBSS) for 2 h at RT. The laminin was removed and rinsed with 1x HBSS shortly before cell plating. The 6-well dishes were coated with lectin solution (section 6.8.1) for 30 min at RT and then washed four times with 2 ml 1x HBSS and stored in 1ml HBSS directly before the motor neuron dissection.

5.5.7 Primary spinal motor neuron culture

E13.5 embryos were dissected and placed in sterile petri dishes containing ice cold 1x HBSS. The embryos tail tips were taken for genotyping and the spinal cord was carefully dissected out. The spinal cords were carefully transferred to 1.5 ml Eppendorf tubes containing ice cold 1 ml HBSS and the meninges and dorsal root ganglion were removed. Then 700 µl HBSS was removed and 7.5 µl trypsin (1 % trypsin/ HBSS) was added and mixed by carefully inverting the tubes. The spinal cords were trypsinized for 7 min at 37°C then inactivated by adding 30 µl trypsin inhibitor. The spinal cord cells were physically dissociated by carefully pipetting up and down 10-15 times with a 1000 µl pipette then 200 µl pipette until no cell aggregates were visible.

The cells with then transferred dropwise into the 6-well lectin coated plated and incubated at RT for 1 h on a vibration free surface. Afterwards the HBSS was removed and the plates were gently washed with 4 x 2 ml pre-warmed (37°C) 1x HBSS to remove cell fragments. Then the cells were incubated with 500 µl depolarization solution (30 mM KCl/ 0.8 % NaCl) for 1 min. The plate was gently tapped to help the motor neurons detach from the lectin p75 receptor. The cells were collected in 2 ml pre-warmed motor neuron medium (section 6.8.1) and transferred to a 15 ml falcon tube. Then cells were counted with a Neubauer chamber and 3.0 x 10^3 cells were plated on the PLO/ laminin coated 24-well plate with 1ml motor neurons medium and incubated at 37°C/ 5 % CO_2. Half the medium was replaced after 24 h and then every other day.

5.5.8 Spinal cord explant preparation

Spinal cords were dissected as previously described prepared in an open book preparation. Briefly, the spinal cords were cut along the midline and then cut in 250 µm pieces with a McIlwain Tissue Chopper. The spinal cord explants with placed into a new petri dish with 1 ml HBSS. Then using a 200 ml pipette the pieces were carefully transferred to a 24-well plate containing 13 mm PLO/ laminin coated coverslips (section 6.8). Then 150 µl MN medium was added to the spinal cord explants and incubated at 35°C/ 5 % CO_2. After 2 h an additional 100 µl MN medium was added. The explants were fixed after 72 h with 4 % PFA/ CB overnight then washed with 1x PBS and then stored at 4°C.

5.5.9 Fixation of cultured cells and explants

Hippocampal neurons coverslips in the 6 cm dishes were flipped (paraffin facing up) and the medium was removed. The cells were fixed with 4 % PFA/ 2 % sucrose in 1x PBS for 20 min. Afterwards the cells were briefly washed with 2x 2.5 ml PBS then stored at 4°C. The spinal motor neurons and explants were washed once with prewarmed 1x HBSS then fixed with prewarmed 4 % PFA/ CB (section 6.8) for 15 min (1 h for the explants) to preserve the cytoskeletal structures. The coverslips were washed in 1x PBS then stored at 4°C until further use.

5.5.10 Astrocyte culture

Astrocytes for the hippocampal co-cultures were prepared using P0 cortices. After the cortex was dissected the meninges were removed from the cortices and the cells were dissociated in 10 ml MEM-HS and plated on a T-75cm^2 flask. The cortex was dissected using a stereomicroscope and transferred to sterile 6 cm^2 Petri dishes with 5 ml HBSS/ HEPES buffer. The meninges were removed and the cortex were transferred to a 15 ml Eppendorf tube with 4 ml HBSS/ HEPES. The HBSS was removed and trypsin (0.05 %) was added to dissociate the individual cells in a water bath at 37°C for 15 min. After trypsin removal the cortices were washed 3x with HBSS/ HEPES. The cortices were dissociated with a glass Pasteur pipettes coated in 5 % BSA/ 1x PBS and then were plated into T-75cm^2 and incubated at 37°C/ 5 % CO_2 until 80-90 % confluent. The cells were seeded into 6 cm^2 dishes prepared with coverslips for hippocampal co-culture and medium was changed every 2-3 days.

5.5.11 Hippocampal neuron culture

The hippocampi from E16.5 embryos were dissected using a stereomicroscope and transferred to sterile 6 cm^2 Petri dishes with 5 ml HBSS /HEPES. The meninges were removed, and the hippocampi were transferred to a 1.5 ml Eppendorf tube with 1 ml HBSS/ HEPES buffer. The HBSS was removed and trypsin (0.05 %) was added to dissociate the individual cells in a water bath at 37°C for 15 min. After trypsin removal and the hippocampi were washed 3x with 1 ml HBSS/ HEPES. The hippocampi cells were physically dissociated using a P1000 Pipette (10-15x) followed by a P200 Pipette (10-15x). The cell density was calculated, and cells were seeded at 1.5 x 10^5 in 6 cm dishes containing 8 x 13 mm coverslips that were prepared with astrocyte co-cultures with MEM-FCS (section 6.8.2). The medium was changed after 24 h and the coverslips were filled over to enable the hippocampus astrocyte co-culture. The medium

was changed ever 48 h and cells were fixed at DIV 1, 3 and 5 with 4 % PFA/ 2 % sucrose in 1x PBS.

5.5.12 Immunofluorescence staining of cultured cells

All immunofluorescence staining was done in a humid chamber that was protected from light. The coverslips were stained with the cells facing upwards. The cells were washed 3x for 5 min with 150 µl TBS. The solution was carefully removed with a pipette from once area of the coverslip. The cells were quenched with 100 µl NH_4Cl for 10 min at RT. The coverslips were then washed 3x with TBS. The cells were incubated in blocking buffer (section 6.7.2) o/n at 4°C to block unspecific binding sites. The cells were incubated in 120 µl primary antibody o/n at RT or 4°C. Stainings with Alexa 488-conjugated phalloidin were added with the primary antibodies. The coverslips were washed 3x for 10 min at RT. The cells were then incubated in secondary antibody for 2 h at RT then washed 4x with TBS for 10 min at RT. The coverslips were then dipped in MilliQ H_2O and then mounted with 12 µl Mowiol/ NPG and left o/n to airdry. The coverslips were sealed with clear nail varnish and then stored at 4°C.

5.5.13 Scanning electron microscope preparation of MN cultures

The scanning electron microscope is a tool used to analyze ultrastructural details using electrons instead of light. The cytoskeletal polymers of interest are in the range of 7-25 nm which is below the resolution of conventional confocal microscopy: We used scanning electron microscopy approach, which scans electron beans over a surface to resolve topographic images and structures in the range of 5-10 nm (Erdman et al., 2019).

Spinal MNs prepared as described in section 5.5.7 were rinsed briefly in prewarmed CB followed by 500 µl prewarmed extraction buffer for 5 min. Afterwards the cells were rinsed in CB and fixed in CB/ 4 % glutaraldehyde (section 6.9). The coverslips were placed in metal racks and dehydrated in 10 %, 30 %, 50 %, 70 % 90 %, 100 % EtOH followed by 100 % EtOH dried over molecular sieves (2Å) for 5 min each. The coverslips were transferred into the critical point drier chamber (Bal-Tec CPD 030) filled with dried 100 % EtOH. The CO_2 critical drying point method was performed to reduce the surface tension of the motor neurons before ultrastructural microscopy. Briefly eight exchanged of liquid CO_2 at 10°C were performed to remove excess EtOH. Then the chamber was heated to 40°C to obtain the critical point gas phase. Then the CO_2 gas was slowly released with controlled pressure to ensure no condensation of the coverslips. The coverslips were then placed on scanning electron

micrograph grids and sealed with Acheson 1415 silver polish (Plano G3692) and left to air dry. The coverslips were coated with a 2 μm platinum/rubidium (Rb) layer. All scanning electron micrographs were taken using the Everhart-Thornley detector (ETD) or 'through-lens' detector (TLD) with an accelerating voltage of 10-15 kV.

5.6 Image analysis

All acquired images were taken in 16-bit format and saved as TIF files. Maximum-intensity projections of Z-stack images were obtained for whole mount diaphragms when required. Z-stack image post processing was performed using ImageJ and Adobe Photoshop software. All spinal cord explant analysis was performed using the NeuriteJ Plugin for ImageJ. All surface render images and videos were processed with Imaris (Bitmap).

5.7 Statistical Analysis

Parametric data is represented as mean ± standard error of the mean (SEM). Nonparametric data is represented as a violin plot showing the median and 25^{th} and 75^{th} quartiles. All data was analyzed with GraphPad Prism version 8.4.1. Data sets with only two groups were analyzed using paired or unpaired Student's t-test. Data that was not normality distributed were analyzed with Mann Whitney unpaired test. Data sets with more than two groups were analyzed using one-way ANOVA (one independent variable) with Bonferroni post-hoc tests were used when appropriate. All detailed results (F ratio and p-value) for effects are listed in the figure legend. Statistical significance was accepted at $p < 0.05$ and asterisks represent the following p-values: * $p < 0.05$; ** $p < 0.01$, *** $p < 0.001$ on the graphs.

6. Materials

6.1 Animal Lines

Line	Reference
Cyfip2$^{LacZ/wt}$	AG Witke
Cyfip2$^{+/-}$	AG Witke
Cyfip2$^{-/-}$	AG Witke
WT C57 Bl6/6N	Charles River

6.2 Oligonucleotides

Oligonucleotides were produced by Eurofins MWG Operon.

Oligo	Sequence (5'-3' direction)
C2EULoxP3-for	5'- AGG AAG GCA TTT CCG AG -3'
C2EULoxP3-rev2	5'- GGG GAG AGC TGG TAA GAG -3'
C2EULoxP2-for	5'- AGG GCC TTT GCA GGA TGG -3'
Cyfip2-LacZ for	5'- GCT ACC ATT ACC AGT TGG -3'

6.3 Plasmids

Plasmid	Source
pMcy-CYFIP2-320K-mCherry-N1	AG Witke (M. Reinke), Bonn
pNckap1 (Nap1)-mCherry-N1	AG Witke (N. Blank), Bonn
pMcy-CYFIP2-320E-mCherry-N1	AG Witke (M. Reinke), Bonn
pMcy-CYFIP2-320K-EGFP-N1	AG Witke (M. Reinke), Bonn

6.4 Antibodies

6.4.1 Primary Antibodies

Epitope	Species	Type	Dilution	Company
ABI1	rb	pc	1:1000	Sigma A5106
ABI2	rb	pc	1:1000	Abcam ab133593
CHT	ms	mc	1:250	SySy Synaptic System
ChAT	rb	pc	1:200	Abcam ab6168
CYFIP1/2 -5C9	ms	mc	WB 1:2 IF 1:200	AG Witke
CYFIP2-1C4	ms	mc	WB 1:1000 IF 1:200	Stefanie Hauck/Walter Witke
FAK	ms	mc	1:200	BD Biosciences 610088
MAP2	rb	pc	1:500	Merck AB5622
MENA	rb	pc	IF 1:200; WB 1:500	AG Witke
Myosin IIA	rb	py	1:500	Merck M8064
NAP1	rb	pc	1:1000	Proteogenix
Neurofilament-200	rb	pc	1:250-500	Sigma N4142
Neurofilament-200	ms	mc	1:100	Cell Signaling Technology 2836

Paxillin	ms	mc	1:200	BD Biosciences 610051
Phosphotyrosine (4G10)	ms	mc	1:100	Millipore
SNAP25	rb	pc	1:250	Sigma S9684
CYFIP1/SRA1	rb	pc	WB 1:1000	Merck 07-531
Synaptophysin	ms	mc	1:250	Sigma S5768
VASP	rb	pc	IF 1:200	AG Witke
Vinculin	ms	mc	1:200	Sigma V9131
WAVE2	rb	mc	1:1000	Cell Signaling Technology 3659
WAVE/SCAR	rb	pc	1:1000	Merck 07-037
WAVE3	rb	pc	1:1000	Merck 09-145
α-tubulin	ms	mc	1:1000	Sigma T9026
β-actin (C4)	ms	mc	1:5000	MP Biomedical 08-691002
β-III tubulin	ms	mc	1:5000	Promega G7121
γ–tubulin	ms	mc	1:5000	Sigma T6557

6.4.2 Secondary Antibodies

Antibody	Species	Dilution	Company
Anti-mouse Alexa 488	gt	1:500	Molecular Probes
Anti-mouse Alexa 555	gt	1:500-750	Molecular Probes
Anti-rabbit Alexa 488	gt	1:500	Molecular Probes
Anti-mouse CF 633	ck	1:500	Biotium
Anti-rabbit CF 633	ck	1:500	Biotium
Anti- mouse HRP	gt	1:5000	Jackson ImmunoResearch
Anti- rabbit HRP	gt	1:5000	Jackson ImmunoResearch

6.4.3 Dyes and Staining Conjugates

Dye	Conjugate	Dilution	Company
DAPI		1:2000	Sigma
Draq5		1:2000	Biostatus
Phalloidin	Alexa 488	1:50	Life Technologies
Phalloidin	Alexa 555	1:100	Life Technologies
Phalloidin	Alexa 680	1:100	Life Technologies
α-Bungarotoxin	Alexa 555	1:250	Molecular Probes

6.5 General Stock Solutions and Buffers

6.5.1 Solutions for nucleic acid analysis

Name	Reagent	Concentration
50x TAE buffer, pH 8.3 (1L)	Tris base	2 M
	Glacial acetic acid	57.1 ml
	EDTA, pH 8.0	50 mM
Proteinase K (stock in H_2O)	Proteinase K	10 µg/ml
TE buffer, pH 8.3 (1L)	Tris-HCl, pH 8.0	100 mM
	EDTA, pH 8.0	1 mM

DNA extraction buffer	Tris-HCl, pH7.4	50 mM
	NaCl	100 mM
	SDS (20 %)	1 % (w/v)
	EDTA, pH 8.0	5 mM
	Proteinase K	0.25 µg/µl
DNA loading buffer (100 ml)	Sucrose	40 %
	SDS	0.5 %
	Bromophenol blue	0.25 %
	TE buffer	add to 100 ml

6.5.2 Solutions for biochemical analysis

Name	Reagent	Concentration
Coomassie staining Solution	Methanol	50 %
	Acetic acid	10 %
	Coomassie Brilliant B	0.1 %
Coomassie fixation and destain	Methanol	40 %
Solution	Acetic acid	10 %
Coomassie destain Solution	Methanol	20 %
	Acetic acid	10 %
Enhanced chemiluminescent	Tris-HCl, pH 8.6	0.1 M
(ECL) solution A (200 ml)	Luminol stock	4 ml
	p-hydroxy-coumarin stock	0.1 ml
Enhanced chemiluminescent	Tris-HCl, pH 8.6	0.1 M
(ECL) solution B (200 ml)	H_2O_2 (30 %)	0.2 ml
Luminol stock solution (10ml)	Luminol	0.44 g
		Dissolved in DMSO
NCP 10x, pH 8.0-8.2	NaCl	1.47 M
	Tris base	0.4 M
	Tween-20	0.5 %
	HCl 6M	Approx. 40-45 ml
p-hydroxy-coumarin stock	p-hydroxy-coumarin	150 ml
		Dissolved in DMSO
Polyacrylamide resolving gel 6 %	ddH_2O	30 ml
(50 ml of 7 gels)	Acrylamide (30 %)	10 ml
	Tris-HCl 2 M, pH 8.8	9.4 ml
	SDS (20 %)	250 µl
	APS (10 %)	240 µl
	TEMED	45 µl
Polyacrylamide resolving gel 8 %	ddH_2O	26.7 ml
(50 ml of 7 gels)	Acrylamide (30 %)	13.3 ml
	Tris-HCl 2 M, pH 8.8	9.5 ml
	SDS (20 %)	250 µl
	APS (10 %)	320 µl
	TEMED	45 µl
Polyacrylamide resolving gel 15	ddH_2O	15 ml
% (50 ml of 7 gels)	Acrylamide (30 %)	25 ml
	Tris-HCl 2 M, pH 8.8	9.5 ml

	SDS (20 %)	250 µl
	APS (10 %)	320 µl
	TEMED	45 µl
SDS running buffer 10x	Tris base	0.25 M
	Glycine	1.92 M
	SDS (20 %)	1 %
Polyacrylamide stacking gel 4 % (30 ml of 7 gels)	ddH_2O	18.3 ml
	Acrylamide (30 %)	3.9 ml
	Tris-HCl 0.5 M, pH 6.8	7.5 ml
	SDS (20 %)	150 µl
	APS (10 %)	180 µl
	TEMED	14 µl
SDS loading buffer 5x	Tris-HCl, pH 6.8	110 mM
SDS sample buffer 5x	Glycerol	20 %
	SDS (20 %)	3.8 %
	β-mercaptoethanol	8 %
	Bromophenol blue	ad libitum
Triton lysis buffer (TLB)	Tris-HCl. pH 8.0	50 mM
	KCl	150 mM
	TritonX-100	1 %
	NaF	50 mM
	Na_3VO_4	1 mM
	$Na_4P_2O_7$	10 mM
	Complete protease inhibitor, EDTA free, Roche	
Towbin transfer buffer 1x	Tris base	25 mM
	Glycine	192 mM
	MeOH	20 %
PHEM buffer (10x), pH 7	PIPES	600 mM
	HEPES	200 mM
	EGTA	100 mM
	$MgCl_2$	20 mM

6.5.3 Solution for co-immunoprecipitation

Name	Reagent	Concentration
RIPA Lysis Buffer	Tris-HCl, pH 8.0	50 mM
	NaCl	150 mM
	NP40	1 %
	Na deoxycholate	0.1 %
	SDS	0.1 %
	NaF	50 mM
	Na_3VO_4	1 mM
	$Na_4P_2O_7$	10 mM
	Protease inhibitor tablet	Roche

6.5.4 FPLC Solutions

Name	Reagent	Concentration
Binding Buffer ($NaPO_4$), pH 7.0	NaH_2PO_4	100 mM
	$Na_2H\ PO_4$	100 mM
		pH with NaH_2PO_4 solution
		Dilute to 20 mM
		Sterile filter
Elution Buffer, pH 2.7 (250 ml)	Glycine	100 mM
		pH with HCl solution to reach 2.7
		Sterile filter
Neutralizing Buffer, pH 9.0 (100 ml)	Tris	1 M
		pH with HCl solution to reach 9.0
		Sterile filter

6.5.5 Solution for MALDI-TOF MS

Reagent	Concentration
Acetic Acid (AcOH)	100 %
Acetonitrile (ACN)	50 %, 100 %
Acrylamide 9 mol/L (40 %)	40 mM
Ammonium bicarbonate (NH_4HCO_3)	50 mM
Dithiothreitol (DTT)	20 mM in NH_4HCO_3
Ethanol (EtOH)	98 %
Trypsin (Promega)	250 ng/gel piece

6.6 Solutions for monoclonal antibody generation

Name	Reagent	Concentration
RPMI- medium	RPMI (1x)	
RPMI-fusion medium +10% FCS (500 ml)	RPMI (1x)	415.5 ml
	FCS	50 ml
	Glutamine (100x)	6 ml
	Penn/Strep	5 ml
	MEM essential amino acids (50x)	10 ml
	MEM non-essential amino acids (100x)	2.5 ml
	β-mercaptoethanol (5 µl/75 µl) Made fresh for every use made	6 ml
	Hybridoma supplement	5 ml
		Sterile filter
RPMI- medium + 5 % FCS (500 ml)	RPMI (1x)	440.5 ml
	FCS	25 ml

	Glutamine 100x	6 ml
	Penn/Strep	5 ml
	MEM essential amino acids (50x)	10 ml
	MEM non-essential amino acids (100x)	2.5 ml
	β-mercaptoethanol (5 µl/75 µl) Made fresh for every use made	6 ml
	Hybridoma supplement	5 ml Sterile filter
RPMI-medium+10 % FCS + 2x HAT (125 ml)	RPMI (1x)	98.9 ml
	50x HAT	5 ml
	FCS	12.5 ml
	Glutamine 100x	1.5 ml
	Penn/Strep	1.25 ml
	MEM essential amino acids (50x)	2.5 ml
	MEM non-essential amino acids (100x)	625 µl
	β-mercaptoethanol (5 µl/75 µl) Made fresh for every use made	1.5 ml
	Hybridoma supplement	1.25 ml Sterile filter
RPMI-medium+10 % FCS + 1x HAT (500 ml)	RPMI (1x)	405.5 ml
	50x HAT	10 ml
	FCS	50 ml
	Glutamine 100x	6 ml
	Penn/Strep	5 ml
	MEM essential amino acids (50x)	10 ml
	MEM non-essential amino acids (100x)	2.5 ml
	β-mercaptoethanol (5 µl/75 µl) Made fresh for every use made	6 ml
	Hybridoma supplement	5 ml Sterile filter

6.7 Solutions for Histology

6.7.1 Solutions for X-Gal staining

Name	Reagent	Concentration
Sodium phosphate buffer ($NaPO_4$) pH7.4	NaH_2PO_4	0.5 M
	Na_2HPO_4	0.5 M
		Add 140 ml $Na_2H\ PO_4$ and pH with NaH_2PO_4 solution
		Add Elix water to make 500 ml
LacZ base solution (1 L)	$NaPO_4$ pH 7.4	200 mM
	$MgCl_2$	50 mM
	EGTA pH 8.0	100 mM
		Add Elix H_2O to 1 L
LacZ fixation solution	LacZ base solution	100 mM
	Glutaraldehyde (25 %)	0.2 % (v/v)
LacZ wash solution (1 L)	$NaPO_4$ pH 7.4	200 mM
	$MgCl_2$	50 mM
	EGTA pH 8.0	100 mM
	Na-Deoxycholate (10 %)	0.01 % (v/v)
	Nonidet P40 (100 %)	0.02 % (v/v)
		Add Elix H_2O to 1 L
LacZ substrate solution (50 ml)	LacZ washing solution	48 ml
	($K_3[Fe(CN_6)]$)	5 mM
	($K_4[Fe(CN_6)]$)	5 mM
	X-Gal (4%)	1 mg/ml

6.7.2 Solutions for immunofluorescence

Name	Reagent	Concentration
Tris Buffered Saline (TBS) (10X)	NaCl	1.5 M
	Tris-HCl, pH 8	0.25 M
Phosphate buffered Saline (10X) pH 7.4	NaCl	1.5 M
	Na_2HPO_4	162 mM
	NaH_2PO_4	38 mM
Cytoskeleton fixation buffer (CB)	PIPES	10 mM
	NaCl	100 mM
	$MgCl_2$	3 mM
	EDTA	1 mM
	Sucrose	10 mM
	PFA	4 %
TBS-T 0.1 %	TBS	1x
	Triton X-100	1 ml
		Adjust volume to 1L
TBS-T 0.5 %	TBS	1x
	Triton X-100	5 ml
		Adjust volume to 1L
Quenching Solution (NH_4Cl)	NH_4Cl	50 mM

Quenching Sodium borohydride	$NaBH_4$	0.1 % w/v Dissolved in TBS
PFA solution for tissue fixation	PFA	4 % (w/v) Dissolved in 1x PBS
PFA solution for *in vitro* fixation	PFA	4 % (w/v) Dissolved in CB buffer
Blocking Solution (Motor neurons)	FCS BSA Cold Fish skin gelatin	2 % (w/v) 2 % (w/v) 0.2 % (v/v) Diluted in 1x TBS
Blocking Solution	NGS Triton X-100	5 % (v/v) 0.1 % (v/v) Diluted in 1x TBS
	FCS BSA Fish gelatin	2 % (w/v) 2 % (w/v) 0.2 % (v/v) Diluted in 1x TBS
Antibody blocking solution	NGS BSA	5 % (w/v) 2 % (w/v) Diluted in 1x TBS-T
Mowiol mounting medium	Mowiol Tris-HCl, pH 8.5 n-propyl-gallate (NPG)	20 % (w/v) 40 mM 5 %

6.8 Solution and buffers for cell culture

6.8.1 Solutions for primary spinal MN culture

Name	Reagent	Concentration
Borate buffer (0.15 M), pH 8.35	$Na_2B_4O_7$ (Borax) H_3BO_3 (Boric acid)	0.2 M 0.2 M Add boric acid to borax solution until pH 8.35 is reached Dilute to 0.15M with cell culture grade water
Bovine serum albumin (BSA)	BSA	0.1 % (w/v) Dissolved in cell culture grade water
Depolarization solution (50 ml)	KCl NaCl	30 mM 0.8 % (w/v)
Tris-HCl pH, 9.5 (50 ml)	Tris-base	0.0 61 g Dissolve in cell culture grade water, adjust pH to 9.5
Lectin coating solution	Tris-HCl, pH 9.5 Lectin (1 mg/ml) BDNF	10 mM 10 µg/ml 10 µg/ml

Brain-derived neurotrophic factor (BDNF)		Dissolved in 0.1% BSA
Ciliary neurotrophic factor (CNTF)	CNTF	10 µg/ml Dissolved in 0.1% BSA
Glial cell-derived neurotrophic factor (GDNF)	GDNF	10 µg/ml Dissolved in 0.1% BSA
Motor neuron Medium	Neurobasal	46 ml
	Heat inactivated horse serum	5 % (w/v) 2.5 ml
	B-27 Supplement (50x)	1 ml
	Glutamax (100x)	0.5 ml
	Penicillin-streptomyosin (10 U/ml)	0.5 ml
	Amphotercin B (250 mg/ml)	125 µl
	BNDF	10 ng/ml
	CNTF	10 ng/ml
	GDNF	10 ng/ml
Poly-DL-ornithine (PLO) coating solution	Borate buffer, pH 8.35	0.15 M
	Poly-DL-ornithine (50 mg/ml)	0.5 mg/ml
Laminin coating buffer	HBSS	1x
	Laminin (1mg/ml)	2.5 µg/ml Dissolved in HBSS and sterile filtered
Trypsin (1 %)	Trypsin	1 mg/ml Dissolved in 1x HBSS

6.8.2 Solution for hippocampal neuronal culture

Name	Reagent	Concentration
N2- Medium	MEM (10x)	50 ml
	Neuropan2	5 ml
	Pyruvic acid	5 ml
	Glucose (20 %)	15 ml
	$NaHCO_3$ (5.5 %)	20 ml
	H_2O	Adjust to 400 m, adjust pH to 7.3 fill to 500 ml then sterile filter
MEM-HS/FCS	MEM (10x)	50 ml
MEM-HS for astrocytes	Horse serum/fetal calf serum	50 ml
MEM-FCS for hippocampus	heat inactivated	
	Glucose (20 % w/v)	15 ml
	$NaHCO_3$ (5.5 %)	20 ml
	L-glutamine (200 mM)	5 ml
	MEM essential amino acids (50x)	10 ml
	MEM non-essential amino acids (100x)	10 ml

	ddH_2O (cell culture grade)	Adjust pH to 7.3 with 1M NaOH, then filled to 500 ml, sterile filtered
HBSS/HEPES	HBSS	500 ml
	HEPES 1 M, pH 7.25	3.5 ml
Trypsin	Trypsin/EDTA (0.05 %)	100 ml
	HEPES 1 M, pH 7.25	700 µl
Borate buffer	Boric acid	1.24 g
	Borax	1.9 g
	H_2O	Adjust to 400 ml, adjust pH to 8.5
Poly-L-lysine	Poly-L-lysine hydrobromide	100 mg
	Borate buffer	100 ml

6.8.3 Calcium phosphate transfection solution

Name	Reagent	Concentration
$Ca_3(P0_4)_2$ Solution	$CaCl_2$ (2.5 M)	7.5 µl
	Plasmid DNA	1 µg/µl
	2x HBSS, pH 7.05	75 µl
	MilliQ H_2O	63.5 µl

6.9 Solutions for scanning electron microscopy

Name	Reagent	Concentration
Cytoskeleton buffer (CB)	MES, pH 6.1	10 mM
	KCl	138 mM
	$MgCl_2$	3 mM
	EGTA	2 mM
Extraction buffer pH 7.2	PIPES	10 mM
	EDTA	50 mM
	KOH	10 mM
	KCl	27 mM
	TritonX-100	0.1 % (w/v)
	Polyethylene glycol (MW 6000)	4 % (v/v)
	Glycerol	10 % (v/v)
Fixation solution (50 ml)	Cytoskeleton buffer (CB)	42 ml
	Glutaraldehyde EM Grade (25 %)	4 % (v/v)

6.10 Commercial Solutions

6.10.1 Commercial solutions for nucleic acid analysis

Name	Manufacturer
dNTPs (100 µm)	Promega

$MgCl_2$ (25 mM)	Promega
PCR-flexi-buffer (5x)	Promega
Go-*taq*-polymerase (5 U/µl)	Promega

6.10.2 Commercial solutions for tissue culture

Name	Manufacturer
HBSS	Gibco
Neurobasal (1x)	Gibco
L-Glutamine (100x)	Gibco
Laminin	Invitrogen Cat# 23017-015
FCS	PAA
Non-essential amino-acids (100x)	Gibco
Go-*taq*-polymerase (5 U/µl)	Promega

6.10.3 Commercial solutions for protein analysis

Name	Manufacturer
Bradford reagent (5x)	Bio-Rad
Broad Range marker	Bio-Rad
SeeBlue Plus2 Prestained marker	Invitrogen

6.10.4 Commercial chemicals and reagents

Liquid chemicals

Reagent	Manufacturer
Acidic acid glacial	Merck
Acrylamide (30 %)	Bio-Rad
Dimethylsulfoxide (DMSO)	Merck
Eosin	Merck
Ethanol, absolute	VWR
Ethanol (technical)	VWR
Ethidiumbromide (1 %)	Bio-Rad
Glacial acetic acid	Merck
Glutaraldehyde (25 %)	Sigma
Glycerol	Sigma
HCl (37 %)	Merck
Hydrogen peroxide (30 %)	Merck
Isopropanol	Merck
β-Mercaptoethanol	Merck
Nitric acid	Merck
Methanol	VWR
TEMED	Sigma
Triton X-100	Roche
Tween 20	Sigma

Kits

Reagent	Manufacturer
Roche KAPPA Genomic extraction Kit	Roche/Merck

IsoStrip™ Mouse Monoclonal Antibody Isoyping Kit	Roche/Merck

Solid Chemicals

Name	Manufacturer
Agar	AppliChem
APS	Fischer Scientific
Bromophenol blue	Bio-Rad
BSA	Merck
Coomassie Brilliant Blue	Bio-Rad
EDTA	Sigma
Glucose	Merck
Glycine	Grüssing
Luminol	Sigma
$MgCl_2$	Sigma
Milk Powder (non-fat)	Roth
Na_2HPO_4	Sigma
NaH_2PO_4	Sigma
NaOH pellets	Sigma
P-hydroxy-coumain	Sigma
Protease inhibitor cocktail tablet, Complete EDTA free	Roche
Proteinase K	Sigma
SDS	Merck
Sodium chloride	Merck
Tris base Ultra	Roch

6.11 Technical equipment and software

6.11.1 General technical equipment

Description	Manufacturer
Agarose gel electrophoresis running chamber	European Molecular Biology Laboratory
Binocular MS 5 +	Leica
Centrifuge 5415 D	Eppendorf
Centrifuge 5417 R	Eppendorf
Cryostat CM 3050S	Leica
ImageQuant LAS4000 Mini	GE Healthcare
Binocular MS 5	Leica
Light source KL 1500 LCD	Leica
Äkta FPLC	Ge Healthcare
Freezer (-80°C)	Thermo Scientific
Glass Teflon tissue grinders	Kimbel Kontes
Heating block	Grant/QBT
Homogenizer	Bosch
Incubator for tissue culture	Heraeus
Light source 1500 LCD	Leica
Magnetic stirring plate	Heidolph
McIlwain Tissue Chopper	Campden Instruments Ltd.
Microscope slides	VWR

PCR machine PTC-200 Peltier thermal cycler	MJ Researcher
pH-meter	InoLab
Pipette Controller Accu-jet	Brand
PCR machine PTC-200 PTC	MJ Research
Pipettes	Gilson
Polyacrylamide gel electrophoresis running chamber	Hoefer
Power supply PowerPAC 200/300	Bio-Rad
Scale	Sartorius
Scale (analytic)	Kern & Sohn
SDS-PAGE apparatus	Pharmacia Biotech
Spectrophotometer UV-DU 640	Beckmann
UV gel documentation machine	Bio-Rad
Vibratome VT 1200S	Leica
Vortex	Scientific Industries
Water purification system	Millipore
Western blotting apparatus	Bio-Rad

6.11.2 Microscopes

Name	Manufacturer
Keyence BZ-9000 (Epifluorescence)	Keyence
FEI (Scanning electron microscope)	Thermo Fischer Scientific Inc.
Leica MZ95 (Stereo microscope)	Leica
Olympus SZX16 (Stereo microscope)	Olympus
Zeiss LSM 510 (Confocal)	Carl Zeiss
Zeiss LSM 710 (Confocal)	Carl Zeiss
Zeiss LSM 880 Airyscan (Confocal)	Carl Zeiss

6.11.3 Software

Name	Manufacturer
Adobe Illustrator 2019	Adobe
Adobe Photoshop 2019	Adobe
BZ-II Analyzer ver. 1.42	Keyence
GraphPad Prism ver. 8.41	GraphPad Software
Gene Ontology (GO) Resource/PANTHER	The Gene Ontology Consortium (NIH)
ImageJ/Fiji	National Institutes of Health (NIH)
Imaris	Bitplane, Oxford Instruments
Microsoft Excel	Microsoft
Multi Gauge ver. 3.0	FujiFilm
Olympus CellSens Dimension ver. 1.6	Olympus
Zen 2.3 SP1	Carl Zeiss

7. References

Abbe, E. (1873). Beiträge zur Theorie des Mikroskops und der mikroskopischen Wahrnehmung. *Archiv Für Mikroskopische Anatomie*, *9*(1), 413–468. https://doi.org/10.1007/BF02956173

Abekhoukh, S., & Bardoni, B. (2014). CYFIP family proteins between autism and intellectual disability: links with Fragile X syndrome. *Frontiers in Cellular Neuroscience*, *8*(MAR). https://doi.org/10.3389/fncel.2014.00081

Abekhoukh, S., Sahin, H. B., Grossi, M., Zongaro, S., Maurin, T., Madrigal, I., Kazue-Sugioka, D., Raas-Rothschild, A., Doulazmi, M., Carrera, P., Stachon, A., Scherer, S., Drula Do Nascimento, M. R., Trembleau, A., Arroyo, I., Szatmari, P., Smith, I. M., Milà, M., Smith, A. C., … Bardoni, B. (2017). New insights into the regulatory function of CYFIP1 in the context of WAVE- and FMRP-containing complexes. *Disease Models & Mechanisms*, *10*(4), 463–474. https://doi.org/10.1242/dmm.025809

Abreu-Villaça, Y., Filgueiras, C. C., & Manhães, A. C. (2011). Developmental aspects of the cholinergic system. *Behavioural Brain Research*, *221*(2), 367–378. https://doi.org/10.1016/j.bbr.2009.12.049

Actin and Actin-Binding Proteins. (2017). In *Cell Biology* (pp. 575–591). Elsevier. https://doi.org/10.1016/B978-0-323-34126-4.00033-5

Ahmad, F. J., Hughey, J., Wittmann, T., Hyman, A., Greaser, M., & Baas, P. W. (2000). Motore protiens regulate force interactions between microtubules and microfilaments in the axon. *Nature Cell Biology*, *2*(5), 276–280. https://doi.org/10.1038/35010544

Alaynick, W. A., Jessell, T. M., & Pfaff, S. L. (2011). SnapShot: Spinal Cord Development. *Cell*, *146*(1), 178-178.e1. https://doi.org/10.1016/j.cell.2011.06.038

Allan, D. W., & Greer, J. J. (1997). Embryogenesis of the phrenic nerve and diaphragm in the fetal rat. *The Journal of Comparative Neurology*, *382*(4), 459–468. https://doi.org/10.1002/(SICI)1096-9861(19970616)382:4<459::AID-CNE3>3.0.CO;2-1

Amos, L. A., & Klug, A. (1974). Arrangement of subunits in flagellar microtubules. *Journal of Cell Science*, *14*(3), 523–549.

Ashburner, M., Ball, C. A., Blake, J. A., Botstein, D., Butler, H., Cherry, J. M., Davis, A. P., Dolinski, K., Dwight, S. S., Eppig, J. T., Harris, M. A., Hill, D. P., Issel-Tarver, L., Kasarskis, A., Lewis, S., Matese, J. C., Richardson, J. E., Ringwald, M., Rubin, G. M., & Sherlock, G. (2000). Gene Ontology: tool for the unification of biology. *Nature Genetics*, *25*(1), 25–29. https://doi.org/10.1038/75556

Ashwell, K. W. S. (2009). Development of the Spinal Cord. In *The Spinal Cord*. Elsevier Ltd. https://doi.org/10.1016/B978-0-12-374247-6.50006-7

Baas, P. W., Deitch, J. S., Black, M. M., & Banker, G. A. (1988). Polarity orientation of microtubules in hippocampal neurons: uniformity in the axon and nonuniformity in the dendrite. *Proceedings of the National Academy of Sciences of the United States of America*, *85*(21), 8335–8339. https://doi.org/10.1073/pnas.85.21.8335

Babbs, R. K., Beierle, J. A., Ruan, Q. T., Kelliher, J. C., Chen, M. M., Feng, A. X., Kirkpatrick, S. L., Benitez, F. A., Rodriguez, F. A., Pierre, J. J., Anandakumar, J., Kumar, V., Mulligan, M. K., & Bryant, C. D. (2019). Cyfip1 Haploinsufficiency Increases Compulsive-Like Behavior and Modulates Palatable Food Intake in Mice: Dependence on Cyfip2 Genetic Background, Parent-of Origin, and Sex. *G3 (Bethesda, Md.)*, *9*(9), 3009–3022. https://doi.org/10.1534/g3.119.400470

Babiuk, R. P., Zhang, W., Clugston, R., Allan, D. W., & Greer, J. J. (2003). Embryological origins and development of the rat diaphragm. *The Journal of Comparative Neurology*, *455*(4), 477–487. https://doi.org/10.1002/cne.10503

Bachmann, C., Fischer, L., Walter, U., & Reinhard, M. (1999). The EVH2 domain of the vasodilator-stimulated phosphoprotein mediates tetramerization, F-actin binding, and actin bundle formation. *Journal of Biological Chemistry*, *274*(33), 23549–23557. https://doi.org/10.1074/jbc.274.33.23549

Bagni, C., Tassone, F., Neri, G., & Hagerman, R. (2012). Fragile X syndrome: Causes, diagnosis, mechanisms, and therapeutics. In *Journal of Clinical Investigation* (Vol. 122, Issue 12, pp. 4314–4322). American Society for Clinical Investigation. https://doi.org/10.1172/JCI63141

Barrecheguren, P. J., Ros, O., Cotrufo, T., Kunz, B., Soriano, E., Ulloa, F., Stoeckli, E. T., & Araújo, S. J. (2017). SNARE proteins play a role in motor axon guidance in vertebrates and invertebrates. *Developmental Neurobiology*, *77*(8), 963–974. https://doi.org/10.1002/dneu.22481

Bass, J. J., Wilkinson, D. J., Rankin, D., Phillips, B. E., Szewczyk, N. J., Smith, K., & Atherton, P. J. (2017). An overview of technical considerations for Western blotting applications to physiological research. In *Scandinavian Journal of Medicine and Science in Sports* (Vol. 27, Issue 1, pp. 4–25). Blackwell Munksgaard. https://doi.org/10.1111/sms.12702

Bays, J. L., & DeMali, K. A. (2017). Vinculin in cell–cell and cell–matrix adhesions. *Cellular and Molecular Life Sciences*, *74*(16), 2999–3009. https://doi.org/10.1007/s00018-017-2511-3

Bear, J. E., & Gertler, F. B. (2009). Ena/VASP: towards resolving a pointed controversy at the barbed end. *Journal of Cell Science*, *122*(12), 1947–1953. https://doi.org/10.1242/jcs.038125

Bear, J. E., Svitkina, T. M., Krause, M., Schafer, D. A., Loureiro, J. J., Strasser, G. A., Maly, I. V., Chaga, O. Y., Cooper, J. A., Borisy, G. G., & Gertler, F. B. (2002). Antagonism between Ena/VASP Proteins and Actin Filament Capping Regulates Fibroblast Motility. *Cell*, *109*(4), 509–521. https://doi.org/10.1016/S0092-8674(02)00731-6

Beuck, C. (2018). *A proteomic approach to identify specific interaction partners of CyFIP1 and CyFIP2 in the mouse brain*. Rheinische Friedrich-Wilhems-Universität Bonn.

Bixby, J. L., Pratt, R. S., Lilien, J., & Reichardt, L. F. (1987). Neurite outgrowth on muscle cell surfaces involves extracellular matrix receptors as well as Ca2+-dependent and -indpendent cell adhesion molecules. *Proceedings of the National Academy of Sciences of the United States of America*, *84*(8), 2555–2559. https://doi.org/10.1073/pnas.84.8.2555

Bocquet, A., Berges, R., Frank, R., Robert, P., Peterson, A. C., & Eyer, J. (2009). Neurofilaments bind tubulin and modulate its polymerization. *Journal of Neuroscience*, *29*(35), 11043–11054. https://doi.org/10.1523/JNEUROSCI.1924-09.2009

Boczkowska, M., Rebowski, G., Petoukhov, M. V., Hayes, D. B., Svergun, D. I., & Dominguez, R. (2008). X-Ray Scattering Study of Activated Arp2/3 Complex with Bound Actin-WCA. *Structure*, *16*(5), 695–704. https://doi.org/10.1016/j.str.2008.02.013

Bogdan, S., Grewe, O., Strunk, M., Mertens, A., & Klämbt, C. (2004). Sra-1 interacts with Kette and Wasp and is required for neuronal and bristle development in Drosophila. *Development*, *131*(16), 3981–3989. https://doi.org/10.1242/dev.01274

Bonaccorso, C. M., Spatuzza, M., Di Marco, B., Gloria, A., Barrancotto, G., Cupo, A., Musumeci, S. A., D'Antoni, S., Bardoni, B., & Catania, M. V. (2015). Fragile X mental retardation protein (FMRP) interacting proteins exhibit different expression patterns during development. *International Journal of Developmental Neuroscience*, *42*(1), 15–23. https://doi.org/10.1016/j.ijdevneu.2015.02.004

Bonanomi, D., & Pfaff, S. L. (2010). Motor axon pathfinding. *Cold Spring Harbor Perspectives in Biology*, *2*(3), 1–19. https://doi.org/10.1101/cshperspect.a001735

Bonini, D., Filippini, A., La Via, L., Fiorentini, C., Fumagalli, F., Colombi, M., & Barbon, A. (2015). Chronic glutamate treatment selectively modulates AMPA RNA editing and ADAR expression and activity in primary cortical neurons. *RNA Biology*, *12*(1), 43–53. https://doi.org/10.1080/15476286.2015.1008365

Bosch, M., Le, K. H. D., Bugyi, B., Correia, J. J., Renault, L., & Carlier, M.-F. (2007). Analysis of the Function of Spire in Actin Assembly and Its Synergy with Formin and Profilin. *Molecular Cell*, *28*(4), 555–568. https://doi.org/10.1016/j.molcel.2007.09.018

Bott, C. J., Johnson, C. G., Yap, C. C., Dwyer, N. D., Litwa, K. A., & Winckler, B. (2019). Nestin in immature embryonic neurons affects axon growth cone morphology and Semaphorin3a sensitivity. *Molecular Biology of the Cell*, *30*(10), 1214–1229. https://doi.org/10.1091/mbc.E18-06-0361

Boyer, N. P., & Gupton, S. L. (2018). Revisiting Netrin-1: One Who Guides (Axons). *Frontiers in Cellular Neuroscience*, *12*, 221. https://doi.org/10.3389/fncel.2018.00221

Bradke, F., & Dotti, C. G. (1997). Neuronal Polarity: Vectorial Cytoplasmic Flow Precedes Axon Formation. *Neuron*, *19*(6), 1175–1186. https://doi.org/10.1016/S0896-6273(00)80410-9

Bradke, F., & Dotti, C. G. (1999). The Role of Local Actin Instability in Axon Formation. *Science*, *283*(5409), 1931–1934. https://doi.org/10.1126/science.283.5409.1931

Brandon, E. P., Lin, W., D'Amour, K. A., Pizzo, D. P., Dominguez, B., Sugiura, Y., Thode, S., Ko, C.-P., Thal, L. J., Gage, F. H., & Lee, K.-F. (2003). Aberrant patterning of neuromuscular synapses in choline acetyltransferase-deficient mice. *The Journal of Neuroscience : The Official Journal of the Society for Neuroscience*, *23*(2), 539–549. https://doi.org/10.1523/JNEUROSCI.23-02-00539.2003

Breitsprecher, D., Kiesewetter, A. K., Linkner, J., Urbanke, C., Resch, G. P., Small, J. V., & Faix, J.

(2008). Clustering of VASP actively drives processive, WH2 domain-mediated actin filament elongation. *EMBO Journal*, *27*(22), 2943–2954. https://doi.org/10.1038/emboj.2008.211

Bremer, J., Marsden, K. C., Miller, A., & Granato, M. (2019). The ubiquitin ligase PHR promotes directional regrowth of spinal zebrafish axons. *Communications Biology*, *2*(1), 195. https://doi.org/10.1038/s42003-019-0434-2

Brunton, V. ., MacPherson, I. R. ., & Frame, M. . (2004). Cell adhesion receptors, tyrosine kinases and actin modulators: a complex three-way circuitry. *Biochimica et Biophysica Acta (BBA) - Molecular Cell Research*, *1692*(2–3), 121–144. https://doi.org/10.1016/j.bbamcr.2004.04.010

Burden, S. J., Yumoto, N., & Zhang, W. (2013). The role of MuSK in synapse formation and neuromuscular disease. *Cold Spring Harbor Perspectives in Biology*, *5*(5), a009167. https://doi.org/10.1101/cshperspect.a009167

Burgess, R. W. (2006). Motor Axon Guidance of the Mammalian Trochlear and Phrenic Nerves: Dependence on the Netrin Receptor Unc5c and Modifier Loci. *Journal of Neuroscience*, *26*(21), 5756–5766. https://doi.org/10.1523/JNEUROSCI.0736-06.2006

Burgess, Robert W., Jucius, T. J., & Ackerman, S. L. (2006). Motor Axon Guidance of the Mammalian Trochlear and Phrenic Nerves: Dependence on the Netrin Receptor Unc5c and Modifier Loci. *Journal of Neuroscience*, *26*(21), 5756–5766. https://doi.org/10.1523/JNEUROSCI.0736-06.2006

Burridge, K., & Chrzanowska-Wodnicka, M. (1996). FOCAL ADHESIONS, CONTRACTILITY, AND SIGNALING. *Annual Review of Cell and Developmental Biology*, *12*(1), 463–519. https://doi.org/10.1146/annurev.cellbio.12.1.463

Calalb, M. B., Polte, T. R., & Hanks, S. K. (1995). Tyrosine phosphorylation of focal adhesion kinase at sites in the catalytic domain regulates kinase activity: a role for Src family kinases. *Molecular and Cellular Biology*, *15*(2), 954–963. https://doi.org/10.1128/MCB.15.2.954

Cammarata, G. M., Bearce, E. A., & Lowery, L. A. (2016). Cytoskeletal social networking in the growth cone: How +TIPs mediate microtubule-actin cross-linking to drive axon outgrowth and guidance. *Cytoskeleton*, *73*(9), 461–476. https://doi.org/10.1002/cm.21272

Campbell, D. S., & Holt, C. E. (2001). Chemotropic responses of retinal growth cones mediated by rapid local protein synthesis and degradation. *Neuron*, *32*(6), 1013–1026. https://doi.org/10.1016/S0896-6273(01)00551-7

Campbell, E. J. M., Agostoni, E., & Davis, J. N. (1970). *The respiratory muscles: mechanics and neural control*. WB Saunders.

Campellone, K. G., & Welch, M. D. (2010). A nucleator arms race: cellular control of actin assembly. *Nature Reviews Molecular Cell Biology*, *11*(4), 237–251. https://doi.org/10.1038/nrm2867

Chacón, M. R., Navarro, A. I., Cuesto, G., del Pino, I., Scott, R., Morales, M., & Rico, B. (2012). Focal adhesion kinase regulates actin nucleation and neuronal filopodia formation during axonal growth. *Development (Cambridge)*, *139*(17), 3200–3210. https://doi.org/10.1242/dev.080564

Chan, W. K. H., Yabe, J. T., Pimenta, A. F., Ortiz, D., & Shea, T. B. (2003). Growth cones contain a dynamic population of neurofilament subunits. *Cell Motility and the Cytoskeleton*, *54*(3), 195–207. https://doi.org/10.1002/cm.10084

Chang, L., & Goldman, R. D. (2004). Intermediate filaments mediate cytoskeletal crosstalk. *Nature Reviews Molecular Cell Biology*, *5*(8), 601–613. https://doi.org/10.1038/nrm1438

Charoy, C., Dinvaut, S., Chaix, Y., Morlé, L., Sanyas, I., Bozon, M., Kindbeiter, K., Durand, B., Skidmore, J. M., De Groef, L., Seki, M., Moons, L., Ruhrberg, C., Martin, J. F., Martin, D. M., Falk, J., & Castellani, V. (2017). Genetic specification of left–right asymmetry in the diaphragm muscles and their motor innervation. *ELife*, *6*, 1–18. https://doi.org/10.7554/elife.18481

Chen, B., Brinkmann, K., Chen, Z., Pak, C. W., Liao, Y., Shi, S., Henry, L., Grishin, N. V., Bogdan, S., & Rosen, M. K. (2014). The WAVE Regulatory Complex Links Diverse Receptors to the Actin Cytoskeleton. *Cell*, *156*(1–2), 195–207. https://doi.org/10.1016/j.cell.2013.11.048

Chen, B., Padrick, S. B., Henry, L., & Rosen, M. K. (2014). Biochemical Reconstitution of the WAVE Regulatory Complex. *Methods in Enzymology*, *540*, 55–72. https://doi.org/10.1016/B978-0-12-397924-7.00004-2

Chen, X. J., Squarr, A. J., Stephan, R., Chen, B., Higgins, T. E., Barry, D. J., Martin, M. C., Rosen, M. K., Bogdan, S., & Way, M. (2014). Ena/VASP Proteins Cooperate with the WAVE Complex to Regulate the Actin Cytoskeleton. *Developmental Cell*, *30*(5), 569–584. https://doi.org/10.1016/j.devcel.2014.08.001

Chen, Z., Borek, D., Padrick, S. B., Gomez, T. S., Metlagel, Z., Ismail, A. M., Umetani, J., Billadeau, D. D., Otwinowski, Z., & Rosen, M. K. (2010). Structure and control of the actin regulatory WAVE complex. *Nature*, *468*(7323), 533–538. https://doi.org/10.1038/nature09623

Chesarone, M. A., & Goode, B. L. (2009). Actin nucleation and elongation factors: mechanisms and interplay. *Current Opinion in Cell Biology*, *21*(1), 28–37. https://doi.org/10.1016/j.ceb.2008.12.001

Chhabra, E. S., & Higgs, H. N. (2007). The many faces of actin: Matching assembly factors with cellular structures. *Nature Cell Biology*, *9*(10), 1110–1121. https://doi.org/10.1038/ncb1007-1110

Chorev, D. S., Moscovitz, O., Geiger, B., & Sharon, M. (2014). Regulation of focal adhesion formation by a vinculin-Arp2/3 hybrid complex. *Nature Communications*, *5*(1), 3758. https://doi.org/10.1038/ncomms4758

Cingolani, L. A., & Goda, Y. (2008). Actin in action: the interplay between the actin cytoskeleton and synaptic efficacy. *Nature Reviews Neuroscience*, *9*(5), 344–356. https://doi.org/10.1038/nrn2373

Cioni, J. M., Wong, H. H. W., Bressan, D., Kodama, L., Harris, W. A., & Holt, C. E. (2018). Axon-Axon Interactions Regulate Topographic Optic Tract Sorting via CYFIP2-Dependent WAVE Complex Function. *Neuron*, *97*(5), 1078-1093.e6. https://doi.org/10.1016/j.neuron.2018.01.027

Cochard, P., & Paulin, D. (1984). Initial expression of neurofilaments and vimentin in the central and peripheral nervous system of the mouse embryo in vivo. *The Journal of Neuroscience : The Official Journal of the Society for Neuroscience*, *4*(8), 2080–2094. http://www.jneurosci.org/content/jneuro/4/8/2080.full.pdf

Coles, C. H., & Bradke, F. (2015). Coordinating Neuronal Actin–Microtubule Dynamics. *Current Biology*, *25*(15), R677–R691. https://doi.org/10.1016/J.CUB.2015.06.020

Coulombe, P. A., Bousquet, O., Ma, L., Yamada, S., & Wirtz, D. (2000). The "ins" and "outs" of intermediate filament organization. *Trends in Cell Biology*, *10*(10), 420–428. https://doi.org/10.1016/S0962-8924(00)01828-6

Courtney, K. D., Grove, M., Vandongen, H., Vandongen, A., LaMantia, A. S., & Pendergast, A. M. (2000). Localization and phosphorylation of AbI-interactor proteins, Abi-1 and Abi-2, in the developing nervous system. *Molecular and Cellular Neurosciences*, *16*(3), 244–257. https://doi.org/10.1006/mcne.2000.0865

Da Silva, J. S., Medina, M., Zuliani, C., Di Nardo, A., Witke, W., & Dotti, C. G. (2003). RhoA/ROCK regulation of neuritogenesis via profilin IIa-mediated control of actin stability. *The Journal of Cell Biology*, *162*(7), 1267–1279. https://doi.org/10.1083/jcb.200304021

Dahl, J. P., Wang-Dunlop, J., Gonzales, C., Goad, M. E. P., Mark, R. J., & Kwak, S. P. (2003). Characterization of the WAVE1 knock-out mouse: implications for CNS development. *The Journal of Neuroscience : The Official Journal of the Society for Neuroscience*, *23*(8), 3343–3352. https://doi.org/10.1523/jneurosci.23-08-03343.2003

Dale, J. M., & Garcia, M. L. (2012). Neurofilament Phosphorylation during Development and Disease: Which Came First, the Phosphorylation or the Accumulation? *Journal of Amino Acids*, *2012*, 1–10. https://doi.org/10.1155/2012/382107

Damiano-Guercio, J., Kurzawa, L., Mueller, J., Dimchev, G., Schaks, M., Nemethova, M., Pokrant, T., Brühmann, S., Linkner, J., Blanchoin, L., Sixt, M., Rottner, K., & Faix, J. (2020). Loss of Ena/VASP interferes with lamellipodium architecture, motility and integrin-dependent adhesion. *ELife*, *9*, 1–31. https://doi.org/10.7554/eLife.55351

Davenport, E. C., Szulc, B. R., Drew, J., Taylor, J., Morgan, T., Higgs, N. F., López-Doménech, G., & Kittler, J. T. (2019). Autism and Schizophrenia-Associated CYFIP1 Regulates the Balance of Synaptic Excitation and Inhibition. *Cell Reports*, *26*(8), 2037-2051.e6. https://doi.org/10.1016/j.celrep.2019.01.092

Davis-Dusenbery, B. N., Williams, L. A., Klim, J. R., & Eggan, K. (2014). How to make spinal motor neurons. *Development*, *141*(3), 491–501. https://doi.org/10.1242/dev.097410

de Castro, B. M., De Jaeger, X., Martins-Silva, C., Lima, R. D. F., Amaral, E., Menezes, C., Lima, P., Neves, C. M. L., Pires, R. G., Gould, T. W., Welch, I., Kushmerick, C., Guatimosim, C., Izquierdo, I., Cammarota, M., Rylett, R. J., Gomez, M. V, Caron, M. G., Oppenheim, R. W., … Prado, V. F. (2009). The vesicular acetylcholine transporter is required for neuromuscular development and function. *Molecular and Cellular Biology*, *29*(19), 5238–5250. https://doi.org/10.1128/MCB.00245-09

De Rubeis, S., Pasciuto, E., Li, K. W., Fernández, E., DiMarino, D., Buzzi, A., Ostroff, L. E., Klann, E., Zwartkruis, F. J. T., Komiyama, N. H., Grant, S. G. N., Poujol, C., Choquet, D., Achsel, T., Posthuma, D., Smit, A. B., & Bagni, C. (2013). CYFIP1 coordinates mRNA translation and cytoskeleton remodeling to ensure proper dendritic Spine formation. *Neuron*, *79*(6), 1169–1182. https://doi.org/10.1016/j.neuron.2013.06.039

Deakin, N. O., & Turner, C. E. (2008). Paxillin comes of age. *Journal of Cell Science*, *121*(Pt 15), 2435–2444. https://doi.org/10.1242/jcs.018044

DeChiara, T. M., Bowen, D. C., Valenzuela, D. M., Simmons, M. V, Poueymirou, W. T., Thomas, S., Kinetz, E., Compton, D. L., Rojas, E., Park, J. S., Smith, C., DiStefano, P. S., Glass, D. J., Burden, S. J., & Yancopoulos, G. D. (1996). The receptor tyrosine kinase MuSK is required for neuromuscular junction formation in vivo. *Cell*, *85*(4), 501–512. https://doi.org/10.1016/s0092-8674(00)81251-9

DeMali, K. A., Barlow, C. A., & Burridge, K. (2002). Recruitment of the Arp2/3 complex to vinculin: Coupling membrane protrusion to matrix adhesion. *Journal of Cell Biology*, *159*(5), 881–891. https://doi.org/10.1083/jcb.200206043

Denker, A., & Rizzoli, S. O. (2010). Synaptic vesicle pools: an update. *Frontiers in Synaptic Neuroscience*, *2*(OCT), 135. https://doi.org/10.3389/fnsyn.2010.00135

Dent, E. W., & Baas, P. W. (2014). Microtubules in neurons as information carriers. *Journal of Neurochemistry*, *129*(2), 235–239. https://doi.org/10.1111/jnc.12621

Dent, E. W., & Gertler, F. B. (2003). Cytoskeletal Dynamics and Transport in Growth Cone Motility and Axon Guidance. *Neuron*, *40*(2), 209–227. https://doi.org/10.1016/S0896-6273(03)00633-0

Dent, E. W., Gupton, S. L., & Gertler, F. B. (2011). The Growth Cone Cytoskeleton in Axon Outgrowth and Guidance. *Cold Spring Harbor Perspectives in Biology*, *3*(3), a001800–a001800. https://doi.org/10.1101/cshperspect.a001800

Dent, E. W., & Kalil, K. (2001). Axon Branching Requires Interactions between Dynamic Microtubules and Actin Filaments. *The Journal of Neuroscience*, *21*(24), 9757–9769. https://doi.org/10.1523/JNEUROSCI.21-24-09757.2001

Derivery, E., & Gautreau, A. (2010). Generation of branched actin networks: Assembly and regulation of the N-WASP and WAVE molecular machines. *BioEssays*, *32*(2), 119–131. https://doi.org/10.1002/bies.200900123

Derivery, E., Lombard, B., Loew, D., & Gautreau, A. (2009). The Wave complex is intrinsically inactive. *Cell Motility and the Cytoskeleton*, *66*(10), 777–790. https://doi.org/10.1002/cm.20342

Derry, J. M. J., Ochs, H. D., & Francke, U. (1994). Isolation of a novel gene mutated in Wiskott-Aldrich syndrome. *Cell*. https://doi.org/10.1016/0092-8674(94)90528-2

Desai, A., & Mitchison, T. J. (1997). MICROTUBULE POLYMERIZATION DYNAMICS. *Annual Review of Cell and Developmental Biology*, *13*(1), 83–117. https://doi.org/10.1146/annurev.cellbio.13.1.83

Desai, C. J., Sun, Q., & Zinn, K. (1997). Tyrosine phosphorylation and axon guidance: of mice and flies. *Current Opinion in Neurobiology*, *7*(1), 70–74. https://doi.org/10.1016/S0959-4388(97)80122-5

Domínguez-Iturza, N., Lo, A. C., Shah, D., Armendáriz, M., Vannelli, A., Mercaldo, V., Trusel, M., Li, K. W., Gastaldo, D., Santos, A. R., Callaerts-Vegh, Z., D'Hooge, R., Mameli, M., Van der Linden, A., Smit, A. B., Achsel, T., & Bagni, C. (2019). The autism- and schizophrenia-associated protein CYFIP1 regulates bilateral brain connectivity and behaviour. *Nature Communications*, *10*(1), 3454. https://doi.org/10.1038/s41467-019-11203-y

Dominguez, R., & Holmes, K. C. (2011). Actin Structure and Function. *Annual Review of Biophysics*, *40*(1), 169–186. https://doi.org/10.1146/annurev-biophys-042910-155359

Doornbos, M., Sikkema-Raddatz, B., Ruijvenkamp, C. A. L., Dijkhuizen, T., Bijlsma, E. K., Gijsbers, A. C. J., Hilhorst-Hofstee, Y., Hordijk, R., Verbruggen, K. T., Kerstjens-Frederikse, W. S. (Mieke), van Essen, T., Kok, K., van Silfhout, A. T., Breuning, M., & van Ravenswaaij-Arts, C. M. A. (2009). Nine patients with a microdeletion 15q11.2 between breakpoints 1 and 2 of the Prader–Willi critical region, possibly associated with behavioural disturbances. *European Journal of Medical Genetics*, *52*(2–3), 108–115. https://doi.org/10.1016/j.ejmg.2009.03.010

Döppler, H., & Storz, P. (2013). Regulation of VASP by phosphorylation. *Cell Adhesion & Migration*, *7*(6), 492–496. https://doi.org/10.4161/cam.27351

Dotti, C., Sullivan, C., & Banker, G. (1988). The establishment of polarity by hippocampal neurons in culture. *The Journal of Neuroscience*, *8*(4), 1454–1468. https://doi.org/10.1523/JNEUROSCI.08-04-01454.1988

Dubielecka, P. M., Ladwein, K. I., Xiong, X., Migeotte, I., Chorzalska, A., Anderson, K. V., Sawicki, J. A., Rottner, K., Stradal, T. E., & Kotula, L. (2011). Essential role for Abi1 in embryonic survival and WAVE2 complex integrity. *Proceedings of the National Academy of Sciences*, *108*(17), 7022–7027. https://doi.org/10.1073/pnas.1016811108

Dunaevsky, A., & Connor, E. A. (2000). F-Actin Is Concentrated in Nonrelease Domains at Frog Neuromuscular Junctions. *The Journal of Neuroscience*, *20*(16), 6007–6012. https://doi.org/10.1523/JNEUROSCI.20-16-06007.2000

Dupraz, S., Hilton, B. J., Husch, A., Santos, T. E., Coles, C. H., Stern, S., Brakebusch, C., & Bradke, F. (2019). RhoA Controls Axon Extension Independent of Specification in the Developing Brain. *Current Biology*, *29*(22), 3874-3886.e9. https://doi.org/10.1016/J.CUB.2019.09.040

Eden, S., Rohatgi, R., Podtelejnikov, A. V., Mann, M., & Kirschner, M. W. (2002). Mechanism of regulation of WAVE1-induced actin nucleation by Rac1 and Nck. *Nature*, *418*(6899), 790–793. https://doi.org/10.1038/nature00859

Erdman, N., Bell, D. C., & Reichelt, R. (2019). Scanning Electron Microscopy. In P. W. Hawkes & J. C. H. Spence (Eds.), *Springer Handbook of Microscopy* (p. 2). Springer International Publishing. https://doi.org/10.1007/978-3-030-00069-1_5

Faix, J., & Grosse, R. (2006). Staying in Shape with Formins. In *Developmental Cell* (Vol. 10, Issue 6, pp. 693–706). Cell Press. https://doi.org/10.1016/j.devcel.2006.05.001

Falet, H., Hoffmeister, K. M., Neujahr, R., Italiano, J. E., Stossel, T. P., Southwick, F. S., & Hartwig, J. H. (2002). Importance of free actin filament barbed ends for Arp2/3 complex function in platelets and fibroblasts. *Proceedings of the National Academy of Sciences of the United States of America*, *99*(26), 16782–16787. https://doi.org/10.1073/pnas.222652499

Feldman, J. L., Del Negro, C. A., & Gray, P. A. (2013). Understanding the Rhythm of Breathing: So Near, Yet So Far. *Annual Review of Physiology*, *75*(1), 423–452. https://doi.org/10.1146/annurev-physiol-040510-130049

Ferguson, S. M., Bazalakova, M., Savchenko, V., Tapia, J. C., Wright, J., & Blakely, R. D. (2004). Lethal impairment of cholinergic neurotransmission in hemicholinium-3-sensitive choline transporter knockout mice. *Proceedings of the National Academy of Sciences of the United States of America*, *101*(23), 8762–8767. https://doi.org/10.1073/pnas.0401667101

Ferguson, S. M., Savchenko, V., Apparsundaram, S., Zwick, M., Wright, J., Heilman, C. J., Yi, H., Levey, A. I., & Blakely, R. D. (2003). Vesicular Localization and Activity-Dependent Trafficking of Presynaptic Choline Transporters. *Journal of Neuroscience*, *23*(30), 9697–9709. https://doi.org/10.1523/jneurosci.23-30-09697.2003

Firat-Karalar, E. N., & Welch, M. D. (2011). New mechanisms and functions of actin nucleation. *Current Opinion in Cell Biology*, *23*(1), 4–13. https://doi.org/10.1016/j.ceb.2010.10.007

Fletcher, D. A., & Mullins, R. D. (2010). Cell mechanics and the cytoskeleton. *Nature*, *463*(7280), 485–492. https://doi.org/10.1038/nature08908

Föcking, M., Lopez, L. M., English, J. A., Dicker, P., Wolff, A., Brindley, E., Wynne, K., Cagney, G., & Cotter, D. R. (2015). Proteomic and genomic evidence implicates the postsynaptic density in schizophrenia. *Molecular Psychiatry*, *20*(4), 424–432. https://doi.org/10.1038/mp.2014.63

Forscher, P., & Smith, S. J. (1988). Actions of cytochalasins on the organization of actin filaments and microtubules in a neuronal growth cone. *The Journal of Cell Biology*, *107*(4), 1505–1516. https://doi.org/10.1083/jcb.107.4.1505

Francius, C., & Clotman, F. (2014). Generating spinal motor neuron diversity: a long quest for neuronal identity. *Cellular and Molecular Life Sciences*, *71*(5), 813–829. https://doi.org/10.1007/s00018-013-1398-x

Fricano-Kugler, C., Gordon, A., Shin, G., Gao, K., Nguyen, J., Berg, J., Starks, M., & Geschwind, D. H. (2019). CYFIP1 overexpression increases fear response in mice but does not affect social or repetitive behavioral phenotypes. *Molecular Autism*, *10*(1), 25. https://doi.org/10.1186/s13229-019-0278-0

Frisén, J., Johansson, C. B., Lothian, C., & Lendahl, U. (1998). Central nervous system stem cells in the embryo and adult. *Cellular and Molecular Life Sciences*, *54*(9), 935–945. https://doi.org/10.1007/s000180050224

Fujita, Y., & Yamashita, T. (2014). Axon growth inhibition by RhoA/ROCK in the central nervous system. *Frontiers in Neuroscience*, *8*(OCT), 338. https://doi.org/10.3389/fnins.2014.00338

Gallagher, S. R. (2006). ELECTROPHORETIC SEPARATION OF One-Dimensional SDS Gel Electrophoresis. *Current Protocols in Molecular Biology*, *Chapter 10*, Unit 10.2A. https://doi.org/10.1002/0471142727.mb1002as75

Gallo, G. (2011). The cytoskeletal and signaling mechanisms of axon collateral branching. *Developmental Neurobiology*, *71*(3), 201–220. https://doi.org/10.1002/dneu.20852

Garibyan, L., & Avashia, N. (2013). Polymerase chain reaction. *Journal of Investigative Dermatology*, *133*(3), 1–4. https://doi.org/10.1038/jid.2013.1

Gautam, M., DeChiara, T. M., Glass, D. J., Yancopoulos, G. D., & Sanes, J. R. (1999). Distinct phenotypes of mutant mice lacking agrin, MuSK, or rapsyn. *Developmental Brain Research*, *114*(2), 171–178. https://doi.org/10.1016/S0165-3806(99)00013-9

Gautam, M., Noakes, P. G., Moscoso, L., Rupp, F., Scheller, R. H., Merlie, J. P., & Sanes, J. R. (1996). Defective Neuromuscular Synaptogenesis in Agrin-Deficient Mutant Mice. *Cell*, *85*(4), 525–535. https://doi.org/10.1016/S0092-8674(00)81253-2

Gautreau, A., Ho, H. -y. H., Li, J., Steen, H., Gygi, S. P., & Kirschner, M. W. (2004). Purification and architecture of the ubiquitous Wave complex. *Proceedings of the National Academy of Sciences*, *101*(13), 4379–4383. https://doi.org/10.1073/pnas.0400628101

Gertler, F. B., Niebuhr, K., Reinhard, M., Wehland, J., & Soriano, P. (1996). Mena, a Relative of VASP and Drosophila Enabled, Is Implicated in the Control of Microfilament Dynamics. *Cell*, *87*(2), 227–239. https://doi.org/10.1016/S0092-8674(00)81341-0

Ghosh, A., Mizuno, K., Tiwari, S. S., Proitsi, P., Gomez Perez-Nievas, B., Glennon, E., Martinez-Nunez, R. T., & Giese, K. P. (2020). Alzheimer's disease-related dysregulation of mRNA translation causes key pathological features with ageing. *Translational Psychiatry*, *10*(1), 192. https://doi.org/10.1038/s41398-020-00882-7

Goldberg, D. J., & Burmeister, D. W. (1986). Stages in axon formation: Observations of growth of Aplysia axons in culture using video-enhanced contrast-differential interference contrast microscopy. *Journal of Cell Biology*, *103*(5), 1921–1931. https://doi.org/10.1083/jcb.103.5.1921

Goldberg, D. J., Foley, M. S., Tang, D., & Grabham, P. W. (2000). Recruitment of the Arp2/3 complex and mena for the stimulation of actin polymerization in growth cones by nerve growth factor. *Journal of Neuroscience Research*, *60*(4), 458–467. https://doi.org/10.1002/(SICI)1097-4547(20000515)60:4<458::AID-JNR4>3.0.CO;2-Z

Goldman, R. D., Khuon, S., Chou, Y. H., Opal, P., & Steinert, P. M. (1996). The function of intermediate filaments in cell shape and cytoskeletal integrity. *Journal of Cell Biology*, *134*(4), 971–983. https://doi.org/10.1083/jcb.134.4.971

Goley, E. D., & Welch, M. D. (2006). The ARP2/3 complex: an actin nucleator comes of age. *Nature Reviews Molecular Cell Biology*, *7*(10), 713–726. https://doi.org/10.1038/nrm2026

Gomez, T. M., & Letourneau, P. C. (2014). Actin dynamics in growth cone motility and navigation. *Journal of Neurochemistry*, *129*(2), 221–234. https://doi.org/10.1111/jnc.12506

Goshgarian, H. G., & Rafols, J. A. (1981). The phrenic nucleus of the albino rat: A correlative HRP and Golgi study. *Journal of Comparative Neurology*, *201*(3), 441–456. https://doi.org/10.1002/cne.902010309

Goulding, M. (2009). Circuits controlling vertebrate locomotion: Moving in a new direction. *Nature Reviews Neuroscience*, *10*(7), 507–518. https://doi.org/10.1038/nrn2608

Goulding, M., Lanuza, G., Sapir, T., & Narayan, S. (2002). The formation of sensorimotor circuits. *Current Opinion in Neurobiology*, *12*(5), 508–515. https://doi.org/10.1016/S0959-4388(02)00371-9

Grove, M., Demyanenko, G., Echarri, A., Zipfel, P. A., Quiroz, M. E., Rodriguiz, R. M., Playford, M., Martensen, S. A., Robinson, M. R., Wetsel, W. C., Maness, P. F., & Pendergast, A. M. (2004). ABI2-deficient mice exhibit defective cell migration, aberrant dendritic spine morphogenesis, and deficits in learning and memory. *Molecular and Cellular Biology*, *24*(24), 10905–10922. https://doi.org/10.1128/MCB.24.24.10905-10922.2004

Gupton, S. L., & Gertler, F. B. (2010). Integrin Signaling Switches the Cytoskeletal and Exocytic Machinery that Drives Neuritogenesis. *Developmental Cell*, *18*(5), 725–736. https://doi.org/10.1016/j.devcel.2010.02.017

Haarer, B. K., Petzold, A. S., Brown, S. S., Aszodi, A., Lanier, L. M., Robbens, J., Colen, I. Van, Vandekerckhove, J., Fässler, R., & Ampe, C. (1993). Mutational analysis of yeast profilin. *Molecular and Cellular Biology*, *13*(12), 7864–7873. https://doi.org/10.1128/mcb.13.12.7864

Han, J., Pluhackova, K., & Böckmann, R. A. (2017). The Multifaceted Role of SNARE Proteins in Membrane Fusion. *Frontiers in Physiology*, *8*, 5. https://doi.org/10.3389/fphys.2017.00005

Han, K., Chen, H., Gennarino, V. A., Richman, R., Lu, H.-C., & Zoghbi, H. Y. (2015). Fragile X-like behaviors and abnormal cortical dendritic spines in Cytoplasmic FMR1-interacting protein 2-mutant mice. *Human Molecular Genetics*, *24*(7), 1813–1823. https://doi.org/10.1093/hmg/ddu595

Harburger, D. S., & Calderwood, D. A. (2009). Integrin signalling at a glance. *Journal of Cell Science*, *122*(2), 159–163. https://doi.org/10.1242/jcs.018093

Havrylenko, S., Noguera, P., Abou-Ghali, M., Manzi, J., Faqir, F., Lamora, A., Guérin, C., Blanchoin, L., & Plastino, J. (2015). WAVE binds Ena/VASP for enhanced Arp2/3 complex-based actin assembly. *Molecular Biology of the Cell*, *26*(1), 55–65. https://doi.org/10.1091/mbc.E14-07-1200

Hensel, N., & Claus, P. (2018). The Actin Cytoskeleton in SMA and ALS: How Does It Contribute to Motoneuron Degeneration? *Neuroscientist*, *24*(1), 54–72. https://doi.org/10.1177/1073858417705059

Heredia, D. J., Feng, C.-Y., Agarwal, A., Nennecker, K., Hennig, G. W., & Gould, T. W. (2018). Postnatal Restriction of Activity-Induced Ca2+ Responses to Schwann Cells at the Neuromuscular Junction Are Caused by the Proximo-Distal Loss of Axonal Synaptic Vesicles during Development. *The Journal of Neuroscience : The Official Journal of the Society for Neuroscience*, *38*(40), 8650–8665. https://doi.org/10.1523/JNEUROSCI.0956-18.2018

Herman, I. M. (1993). Actin isoforms. *Current Opinion in Cell Biology*, *5*(1), 48–55. https://doi.org/10.1016/S0955-0674(05)80007-9

Hideyama, T., & Kwak, S. (2011). When Does ALS Start? ADAR2?GluA2 Hypothesis for the Etiology of Sporadic ALS. *Frontiers in Molecular Neuroscience*, *4*. https://doi.org/10.3389/fnmol.2011.00033

Hirao, N., Sato, S., Gotoh, T., Maruoka, M., Suzuki, J., Matsuda, S., Shishido, T., & Tani, K. (2006). NESH (Abi-3) is present in the Abi/WAVE complex but does not promote c-Abl-mediated phosphorylation. *FEBS Letters*, *580*(27), 6464–6470. https://doi.org/10.1016/j.febslet.2006.10.065

Hoeffer, C. A., Sanchez, E., Hagerman, R. J., Mu, Y., Nguyen, D. V., Wong, H., Whelan, A. M., Zukin, R. S., Klann, E., & Tassone, F. (2012). Altered mTOR signaling and enhanced CYFIP2 expression levels in subjects with fragile X syndrome. *Genes, Brain and Behavior*, *11*(3), 332–341. https://doi.org/10.1111/j.1601-183X.2012.00768.x

Hoffman, P N, Cleveland, D. W., Griffin, J. W., Landes, P. W., Cowan, N. J., & Price, D. L. (1987). Neurofilament gene expression: a major determinant of axonal caliber. *Proceedings of the National Academy of Sciences of the United States of America*, *84*(10), 3472–3476. https://doi.org/10.1073/pnas.84.10.3472

Hoffman, Paul N. (1995). Review : The Synthesis, Axonal Transport, and Phosphorylation of Neurofilaments Determine Axonal Caliber in Myelinated Nerve Fibers. *The Neuroscientist*, *1*(2), 76–83. https://doi.org/10.1177/107385849500100204

Hohmann, T., & Dehghani, F. (2019). The Cytoskeleton-A Complex Interacting Meshwork. *Cells*, *8*(4), 362. https://doi.org/10.3390/cells8040362

Hollenbeck, P. J., Bershadsky, A. D., Pletjushkina, O. Y., Tint, I. S., & Vasiliev, J. M. (1989). Intermediate filament collapse is an ATP-dependent and actin-dependent process. *Journal of Cell Science*, *92 (Pt 4)*, 621–631.

Holmes, K. C., Popp, D., Gebhard, W., & Kabsch, W. (1990). Atomic model of the actin filament. *Nature*, *347*(6288), 44–49. https://doi.org/10.1038/347044a0

Holt, M. R., Critchley, D. R., & Brindle, N. P. J. (1998). The focal adhesion phosphoprotein, VASP. *International Journal of Biochemistry and Cell Biology*, *30*(3), 307–311. https://doi.org/10.1016/S1357-2725(97)00101-5

Hsia, D. A., Mitra, S. K., Hauck, C. R., Streblow, D. N., Nelson, J. A., Ilic, D., Huang, S., Li, E., Nemerow, G. R., Leng, J., Spencer, K. S. R., Cheresh, D. A., & Schlaepfer, D. D. (2003). Differential regulation of cell motility and invasion by FAK. *Journal of Cell Biology*, *160*(5), 753–767. https://doi.org/10.1083/jcb.200212114

Hsiao, K., Harony-Nicolas, H., Buxbaum, J. D., Bozdagi-Gunal, O., & Benson, D. L. (2016). Cyfip1 Regulates Presynaptic Activity during Development. *The Journal of Neuroscience : The Official Journal of the Society for Neuroscience*, *36*(5), 1564–1576. https://doi.org/10.1523/JNEUROSCI.0511-15.2016

Hughes, B. W., Kusner, L. L., & Kaminski, H. J. (2006). Molecular architecture of the neuromuscular junction. *Muscle and Nerve*, *33*(4), 445–461. https://doi.org/10.1002/mus.20440

Humphries, J. D., Wang, P., Streuli, C., Geiger, B., Humphries, M. J., & Ballestrem, C. (2007). Vinculin controls focal adhesion formation by direct interactions with talin and actin. *Journal of Cell Biology*, *179*(5), 1043–1057. https://doi.org/10.1083/jcb.200703036

Hunter, D. D., Shah, V., Merlie, J. P., & Sanes, J. R. (1989). A laminin-like adhesive protein concentrated in the synaptic cleft of the neuromuscular junction. *Nature*, *338*(6212), 229–234. https://doi.org/10.1038/338229a0

Huveneers, S., & Danen, E. H. J. (2009). Adhesion signaling - crosstalk between integrins, Src and Rho. *Journal of Cell Science*, *122*(8), 1059–1069. https://doi.org/10.1242/jcs.039446

Huxley, H. E. (1963). Electron microscope studies on the structure of natural and synthetic protein filaments from striated muscle. *Journal of Molecular Biology*, *7*(3), 281-IN30. https://doi.org/10.1016/S0022-2836(63)80008-X

Hynes, R. O. (1987). Integrins: A family of cell surface receptors. In *Cell*. https://doi.org/10.1016/0092-8674(87)90233-9

Hynes, R. O. (2002). Integrins: bidirectional, allosteric signaling machines. *Cell*, *110*(6), 673–687. https://doi.org/10.1016/s0092-8674(02)00971-6

Innocenti, M., Zucconi, A., Disanza, A., Frittoli, E., Areces, L. B., Steffen, A., Stradal, T. E. B., Fiore, P. P. Di, Carlier, M.-F., & Scita, G. (2004). Abi1 is essential for the formation and activation of a WAVE2 signalling complex. *Nature Cell Biology*, *6*(4), 319–327. https://doi.org/10.1038/ncb1105

Islamov, R. R., Samigullin, D. V., Rizvanov, A. A., Bondarenko, N. I., & Nikolskiy, E. E. (2015). Synaptosome-associated protein 25 (SNAP25) synthesis in terminal buttons of mouse motor neuron. *Doklady Biochemistry and Biophysics*, *464*(1), 272–274. https://doi.org/10.1134/S1607672915050026

Ismail, A. M., Padrick, S. B., Chen, B., Umetani, J., & Rosen, M. K. (2009). The WAVE regulatory complex is inhibited. *Nature Structural & Molecular Biology*, *16*(5), 561–563. https://doi.org/10.1038/nsmb.1587

Jahn, R., & Scheller, R. H. (2006). SNAREs--engines for membrane fusion. *Nature Reviews. Molecular Cell Biology*, *7*(9), 631–643. https://doi.org/10.1038/nrm2002

Jessell, T. M. (2000). Neuronal specification in the spinal cord: inductive signals and transcriptional codes. *Nature Reviews Genetics*, *1*(1), 20–29. https://doi.org/10.1038/35049541

Jones, R. A., Harrison, C., Eaton, S. L., Llavero Hurtado, M., Graham, L. C., Alkhammash, L., Oladiran, O. A., Gale, A., Lamont, D. J., Simpson, H., Simmen, M. W., Soeller, C., Wishart, T. M., & Gillingwater, T. H. (2017). Cellular and Molecular Anatomy of the Human Neuromuscular Junction. *Cell Reports*, *21*(9), 2348–2356. https://doi.org/10.1016/J.CELREP.2017.11.008

Kabrawala, S., Zimmer, M. D., & Campellone, K. G. (2020). WHIMP links the actin nucleation machinery to Src-family kinase signaling during protrusion and motility. *PLOS Genetics*, *16*(3), e1008694. https://doi.org/10.1371/journal.pgen.1008694

Kabsch, W., & Vandekerckhove, J. (1992). Structure and function of actin. *Annual Review of Biophysics and Biomolecular Structure*, *21*(103), 49–76. https://doi.org/10.1146/annurev.bb.21.060192.000405

Kalil, K., & Dent, E. W. (2014). Branch management: mechanisms of axon branching in the developing vertebrate CNS. *Nature Reviews Neuroscience*, *15*(1), 7–18. https://doi.org/10.1038/nrn3650

Karas, M., & Hillenkamp, F. (1988). Laser Desorption Ionization of Proteins with Molecular Masses Exceeding 10 000 Daltons. *Analytical Chemistry*, *60*(20), 2299–2301. https://doi.org/10.1021/ac00171a028

Kawabata Galbraith, K., & Kengaku, M. (2019). Multiple roles of the actin and microtubule-regulating formins in the developing brain. *Neuroscience Research*, *138*, 59–69. https://doi.org/10.1016/j.neures.2018.09.008

Ketschek, A., & Gallo, G. (2010). Nerve Growth Factor Induces Axonal Filopodia through Localized Microdomains of Phosphoinositide 3-Kinase Activity That Drive the Formation of Cytoskeletal Precursors to Filopodia. *Journal of Neuroscience*, *30*(36), 12185–12197.

https://doi.org/10.1523/JNEUROSCI.1740-10.2010
Kiernan, M. C., Vucic, S., Cheah, B. C., Turner, M. R., Eisen, A., Hardiman, O., Burrell, J. R., & Zoing, M. C. (2011). Amyotrophic lateral sclerosis. *The Lancet*, *377*(9769), 942–955. https://doi.org/10.1016/S0140-6736(10)61156-7
Kirkpatrick, S. L., Goldberg, L. R., Yazdani, N., Babbs, R. K., Wu, J., Reed, E. R., Jenkins, D. F., Bolgioni, A. F., Landaverde, K. I., Luttik, K. P., Mitchell, K. S., Kumar, V., Johnson, W. E., Mulligan, M. K., Cottone, P., & Bryant, C. D. (2017). Cytoplasmic FMR1-Interacting Protein 2 Is a Major Genetic Factor Underlying Binge Eating. *Biological Psychiatry*, *81*(9), 757–769. https://doi.org/10.1016/j.biopsych.2016.10.021
Kobayashi, K., Kuroda, S., Fukata, M., Nakamura, T., Nagase, T., Nomura, N., Matsuura, Y., Yoshida-Kubomura, N., Iwamatsu, A., & Kaibuchi, K. (1998). p140Sra-1 (Specifically Rac1-associated Protein) Is a Novel Specific Target for Rac1 Small GTPase. *Journal of Biological Chemistry*, *273*(1), 291–295. https://doi.org/10.1074/jbc.273.1.291
Korobova, F., & Svitkina, T. (2008). Arp2/3 Complex Is Important for Filopodia Formation, Growth Cone Motility, and Neuritogenesis in Neuronal Cells. *Molecular Biology of the Cell*, *19*(4), 1561–1574. https://doi.org/10.1091/mbc.e07-09-0964
Kovar, D. R. (2006). Molecular details of formin-mediated actin assembly. In *Current Opinion in Cell Biology*. https://doi.org/10.1016/j.ceb.2005.12.011
Kozma, R., Sarner, S., Ahmed, S., & Lim, L. (1997). Rho family GTPases and neuronal growth cone remodelling: relationship between increased complexity induced by Cdc42Hs, Rac1, and acetylcholine and collapse induced by RhoA and lysophosphatidic acid. *Molecular and Cellular Biology*, *17*(3), 1201–1211. https://doi.org/10.1128/MCB.17.3.1201
Krause, M., Dent, E. W., Bear, J. E., Loureiro, J. J., & Gertler, F. B. (2003). Ena/VASP Proteins: Regulators of the Actin Cytoskeleton and Cell Migration. *Annual Review of Cell and Developmental Biology*, *19*(1), 541–564. https://doi.org/10.1146/annurev.cellbio.19.050103.103356
Kumar, V., Kim, K., Joseph, C., Kourrich, S., Yoo, S.-H., Huang, H. C., Vitaterna, M. H., de Villena, F. P.-M., Churchill, G., Bonci, A., & Takahashi, J. S. (2013). C57BL/6N mutation in cytoplasmic FMRP interacting protein 2 regulates cocaine response. *Science (New York, N.Y.)*, *342*(6165), 1508–1512. https://doi.org/10.1126/science.1245503
Kurisu, S., & Takenawa, T. (2009). The WASP and WAVE family proteins. *Genome Biology*, *10*(6), 226. https://doi.org/10.1186/gb-2009-10-6-226
Laemmli, U. K. (1970). Cleavage of Structural Proteins during the Assembly of the Head of Bacteriophage T4. *Nature*, *227*(5259e), 680–685. https://doi.org/10.1038/227680a0
Lanier, L. M., Gates, M. A., Witke, W., Menzies, A. S., Wehman, A. M., Macklis, J. D., Kwiatkowski, D., Soriano, P., & Gertler, F. B. (1999). Mena is required for neurulation and commissure formation. *Neuron*, *22*(2), 313–325. https://doi.org/10.1016/S0896-6273(00)81092-2
Lariviere, R. C., & Julien, J.-P. (2004). Functions of intermediate filaments in neuronal development and disease. *Journal of Neurobiology*, *58*(1), 131–148. https://doi.org/10.1002/neu.10270
Laskowski, M. B., Norton, A. S., & Berger, P. K. (1991). Branching patterns of the rat phrenic nerve during development and reinnervation. *Experimental Neurology*, *113*(2), 212–220. https://doi.org/10.1016/0014-4886(91)90177-E
Laurent, V., Loisel, T. P., Harbeck, B., Wehman, A., Gröbe, L., Jockusch, B. M., Wehland, J., Gertler, F. B., & Carlier, M. F. (1999). Role of proteins of the Ena/VASP family in actin-based motility of Listeria monocytogenes. *The Journal of Cell Biology*, *144*(6), 1245–1258. https://doi.org/10.1083/jcb.144.6.1245
Lebensohn, A. M., & Kirschner, M. W. (2009). Activation of the WAVE Complex by Coincident Signals Controls Actin Assembly. *Molecular Cell*, *36*(3), 512–524. https://doi.org/10.1016/j.molcel.2009.10.024
Lee, C. Y., Tseng, L. F., & Chiu, T. H. (1967). Influence of denervation on localization of neurotoxins from clapid venoms in rat diaphragm. *Nature*, *215*(5106), 1177–1178. https://doi.org/10.1038/2151177a0
Lee, S., Zhang, Y., Park, J., Kim, B., Kim, Y., Lee, S. H., Kim, G. H., Huh, Y. H., Lee, B., Kim, Y., Lee, Y., Kim, J. Y., Kang, H., Choi, S., Jang, S., Li, Y., Kim, S., Jin, C., Pang, K., … Han, K. (2020). Haploinsufficiency of Cyfip2 Causes Lithium-Responsive Prefrontal Dysfunction. *Annals of Neurology*, ana.25827. https://doi.org/10.1002/ana.25827

Lee, Y., Kim, D., Ryu, J. R., Zhang, Y., Kim, S., Kim, Y., Lee, B., Sun, W., & Han, K. (2017). Phosphorylation of CYFIP2, a component of the WAVE-regulatory complex, regulates dendritic spine density and neurite outgrowth in cultured hippocampal neurons potentially by affecting the complex assembly. *NeuroReport*, *28*(12), 749–754. https://doi.org/10.1097/WNR.0000000000000838

Letourneau, P. C. (1983). Differences in the organization of actin in the growth cones compared with the neurites of cultured neurons from chick embryos. *The Journal of Cell Biology*, *97*(4), 963–973. https://doi.org/10.1083/jcb.97.4.963

Letourneau, P. C. (1996). The cytoskeleton in nerve growth cone motility and axonal pathfinding. *Perspectives on Developmental Neurobiology*, *4*(2–3), 111–123. http://www.ncbi.nlm.nih.gov/pubmed/9168194

Levanon, E. Y., Eisenberg, E., Yelin, R., Nemzer, S., Hallegger, M., Shemesh, R., Fligelman, Z. Y., Shoshan, A., Pollock, S. R., Sztybel, D., Olshansky, M., Rechavi, G., & Jantsch, M. F. (2004). Systematic identification of abundant A-to-I editing sites in the human transcriptome. *Nature Biotechnology*, *22*(8), 1001–1005. https://doi.org/10.1038/nbt996

Levanon, E. Y., Hallegger, M., Kinar, Y., Shemesh, R., Djinovic-Carugo, K., Rechavi, G., Jantsch, M. F., & Eisenberg, E. (2005). Evolutionarily conserved human targets of adenosine to inosine RNA editing. *Nucleic Acids Research*, *33*(4), 1162–1168. https://doi.org/10.1093/nar/gki239

Leventhal, P. S., & Feldman, E. L. (1996). Tyrosine phosphorylation and enhanced expression of paxillin during neuronal differentiation in vitro. *Journal of Biological Chemistry*, *271*(11), 5957–5960. https://doi.org/10.1074/jbc.271.11.5957

Lewis, T. L., Courchet, J., & Polleux, F. (2013). Cellular and molecular mechanisms underlying axon formation, growth, and branching. *The Journal of Cell Biology*, *202*(6), 837–848. https://doi.org/10.1083/jcb.201305098

Lilo, E., Wald-Altman, S., Solmesky, L. J., Ben Yaakov, K., Gershoni-Emek, N., Bulvik, S., Kassis, I., Karussis, D., Perlson, E., & Weil, M. (2013). Characterization of human sporadic ALS biomarkers in the familial ALS transgenic mSOD1G93A mouse model. *Human Molecular Genetics*, *22*(23), 4720–4725. https://doi.org/10.1093/hmg/ddt325

Lin, J., Liao, S., Li, E., Liu, Z., Zheng, R., Wu, X., & Zeng, W. (2020). circCYFIP2 Acts as a Sponge of miR-1205 and Affects the Expression of Its Target Gene E2F1 to Regulate Gastric Cancer Metastasis. *Molecular Therapy - Nucleic Acids*, *21*, 121–132. https://doi.org/10.1016/j.omtn.2020.05.007

Lin, T.-Y., Huang, C.-H., Kao, H.-H., Liou, G.-G., Yeh, S.-R., Cheng, C.-M., Chen, M.-H., Pan, R.-L., & Juang, J.-L. (2009). Abi plays an opposing role to Abl in Drosophila axonogenesis and synaptogenesis. *Development (Cambridge, England)*, *136*(18), 3099–3107. https://doi.org/10.1242/dev.033324

Lin, W., Burgess, R. W., Dominguez, B., Pfaff, S. L., Sanes, J. R., & Lee, K.-F. (2001). Distinct roles of nerve and muscle in postsynaptic differentiation of the neuromuscular synapse. *Nature*, *410*(6832), 1057–1064. https://doi.org/10.1038/35074025

Liu, Y., Padgett, D., Takahashi, M., Li, H., Sayeed, A., Teichert, R. W., Olivera, B. M., McArdle, J. J., Green, W. N., & Lin, W. (2008). Essential roles of the acetylcholine receptor gamma-subunit in neuromuscular synaptic patterning. *Development (Cambridge, England)*, *135*(11), 1957–1967. https://doi.org/10.1242/dev.018119

Liu, Y., Sugiura, Y., & Lin, W. (2011). The role of Synaptobrevin1/VAMP1 in Ca2+-triggered neurotransmitter release at the mouse neuromuscular junction. *Journal of Physiology*, *589*(7), 1603–1618. https://doi.org/10.1113/jphysiol.2010.201939

Liu, Y., Sugiura, Y., Südhof, T. C., & Lin, W. (2019). Ablation of All Synaptobrevin vSNAREs Blocks Evoked But Not Spontaneous Neurotransmitter Release at Neuromuscular Synapses. *The Journal of Neuroscience*, *39*(31), 6049–6066. https://doi.org/10.1523/JNEUROSCI.0403-19.2019

López-Colomé, A. M., Lee-Rivera, I., Benavides-Hidalgo, R., & López, E. (2017). Paxillin: A crossroad in pathological cell migration. In *Journal of Hematology and Oncology* (Vol. 10, Issue 1, pp. 1–15). BioMed Central Ltd. https://doi.org/10.1186/s13045-017-0418-y

Lowery, L. A., & Vactor, D. Van. (2009). The trip of the tip: understanding the growth cone machinery. *Nature Reviews Molecular Cell Biology*, *10*(5), 332–343. https://doi.org/10.1038/nrm2679

Lu, D. C., Niu, T., & Alaynick, W. A. (2015). Molecular and cellular development of spinal cord locomotor circuitry. *Frontiers in Molecular Neuroscience*, *8*, 25. https://doi.org/10.3389/fnmol.2015.00025

Lundquist, E. A. (2003). Rac proteins and the control of axon development. In *Current Opinion in Neurobiology*. https://doi.org/10.1016/S0959-4388(03)00071-0

Luo, L. (2000). RHO GTPASES in neuronal morphogenesis. *Nature Reviews Neuroscience*, *1*(3), 173–180. https://doi.org/10.1038/35044547

Luo, L. (2002). Actin cytoskeleton regulation in neuronal morphogenesis and structural plasticity. *Annual Review of Cell and Developmental Biology*, *18*(1), 601–635. https://doi.org/10.1146/annurev.cellbio.18.031802.150501

Machesky, L M, Atkinson, S. J., Ampe, C., Vandekerckhove, J., & Pollard, T. D. (1994). Purification of a cortical complex containing two unconventional actins from Acanthamoeba by affinity chromatography on profilin-agarose. *The Journal of Cell Biology*, *127*(1), 107–115. https://doi.org/10.1083/jcb.127.1.107

Machesky, L M, Reeves, E., Wientjes, F., Mattheyse, F. J., Grogan, A., Totty, N. F., Burlingame, A. L., Hsuan, J. J., & Segal, A. W. (1997). Mammalian actin-related protein 2/3 complex localizes to regions of lamellipodial protrusion and is composed of evolutionarily conserved proteins. *The Biochemical Journal*, *328 (Pt 1*(1), 105–112. https://doi.org/10.1042/bj3280105

Machesky, Laura M., Atkinson, S. J., Ampe, C., Vandekerckhove, J., & Pollard, T. D. (1994). Purification of a cortical complex containing two unconventional actins from Acanthamoeba by affinity chromatography on profilin-agarose. *The Journal of Cell Biology*, *127*(1), 107–115. https://doi.org/10.1083/jcb.127.1.107

Machesky, Laura M., & Insall, R. H. (1998). Scar1 and the related Wiskott-Aldrich syndrome protein, WASP, regulate the actin cytoskeleton through the Arp2/3 complex. *Current Biology*, *8*(25), 1347–1356. https://doi.org/10.1016/S0960-9822(98)00015-3

Madhavan, R., Gong, Z. L., Ma, J. J., Chan, A. W. S., & Peng, H. B. (2009). The function of cortactin in the clustering of acetylcholine receptors at the vertebrate neuromuscular junction. *PloS One*, *4*(12), e8478. https://doi.org/10.1371/journal.pone.0008478

Magill-Solc, C., & McMahan, U. J. (1988). Motor neurons contain agrin-like molecules. *The Journal of Cell Biology*, *107*(5), 1825–1833. https://doi.org/10.1083/jcb.107.5.1825

Mantilla, C. B., & Sieck, G. C. (2008). Key aspects of phrenic motoneuron and diaphragm muscle development during the perinatal period. *Journal of Applied Physiology*, *104*(6), 1818–1827. https://doi.org/10.1152/japplphysiol.01192.2007

Marchand, J.-B., Kaiser, D. A., Pollard, T. D., & Higgs, H. N. (2001). Interaction of WASP/Scar proteins with actin and vertebrate Arp2/3 complex. *Nature Cell Biology*, *3*(1), 76–82. https://doi.org/10.1038/35050590

Markham, K., Bai, Y., & Schmitt-Ulms, G. (2007). Co-immunoprecipitations revisited: An update on experimental concepts and their implementation for sensitive interactome investigations of endogenous proteins. *Analytical and Bioanalytical Chemistry*, *389*(2), 461–473. https://doi.org/10.1007/s00216-007-1385-x

Marsden, K. C., Jain, R. A., Wolman, M. A., Echeverry, F. A., Nelson, J. C., Hayer, K. E., Miltenberg, B., Pereda, A. E., & Granato, M. (2018). A Cyfip2-Dependent Excitatory Interneuron Pathway Establishes the Innate Startle Threshold. *Cell Reports*, *23*(3), 878–887. https://doi.org/10.1016/J.CELREP.2018.03.095

Massimi, M. (2008). Characterization of Profilin2 Complexes in the Mouse. In *System*. Ruprecht-Karls-Universität Heidelberg.

Mayne, M., Moffatt, T., Kong, H., McLaren, P. J., Fowke, K. R., Becker, K. G., Namaka, M., Schenck, A., Bardoni, B., Bernstein, C. N., & Melanson, M. (2004). CYFIP2 is highly abundant in CD4+ cells from multiple sclerosis patients and is involved in T cell adhesion. *European Journal of Immunology*, *34*(4), 1217–1227. https://doi.org/10.1002/eji.200324726

McCormick, L. E., & Gupton, S. L. (2020). Mechanistic advances in axon pathfinding. *Current Opinion in Cell Biology*, *63*, 11–19. https://doi.org/10.1016/j.ceb.2019.12.003

McGovern, V. L., Gavrilina, T. O., Beattie, C. E., & Burghes, A. H. M. (2008). Embryonic motor axon development in the severe SMA mouse. *Human Molecular Genetics*, *17*(18), 2900–2909. https://doi.org/10.1093/hmg/ddn189

McRobbie, S. J., & Newell, P. C. (1983). Changes in actin associated with the cytoskeleton following chemotactic stimulation of Dictyostelium discoideum. *Biochemical and Biophysical Research Communications*, *115*(1), 351–359. https://doi.org/10.1016/0006-291X(83)91011-2

Medeiros, N. A., Burnette, D. T., & Forscher, P. (2006). Myosin II functions in actin-bundle turnover in neuronal growth cones. *Nature Cell Biology*, *8*(3), 216–226. https://doi.org/10.1038/ncb1367

Merrell, A. J., Ellis, B. J., Fox, Z. D., Lawson, J. A., Weiss, J. A., & Kardon, G. (2015). Muscle connective tissue controls development of the diaphragm and is a source of congenital diaphragmatic hernias. *Nature Genetics*, *47*(5), 496–504. https://doi.org/10.1038/ng.3250

Merrell, A. J., & Kardon, G. (2013). Development of the diaphragm - a skeletal muscle essential for mammalian respiration. *FEBS Journal*, *280*(17), 4026–4035. https://doi.org/10.1111/febs.12274

Meyer, G., & Feldman, E. L. (2002). Signaling mechanisms that regulate actin-based motility processes in the nervous system. *Journal of Neurochemistry*, *83*(3), 490–503. https://doi.org/10.1046/j.1471-4159.2002.01185.x

Mi, H., Muruganujan, A., Ebert, D., Huang, X., & Thomas, P. D. (2019). PANTHER version 14: More genomes, a new PANTHER GO-slim and improvements in enrichment analysis tools. *Nucleic Acids Research*, *47*(D1), D419–D426. https://doi.org/10.1093/nar/gky1038

Miki, H., Sasaki, T., Takai, Y., & Takenawa, T. (1998). Induction of filopodium formation by a WASP-related actin- depolymerizing protein N-WASP. *Nature*, *391*(6662), 93–96. https://doi.org/10.1038/34208

Miki, H., Suetsugu, S., & Takenawa, T. (1998). WAVE, a novel WASP-family protein involved in actin reorganization induced by Rac. *The EMBO Journal*, *17*(23), 6932–6941. https://doi.org/10.1093/emboj/17.23.6932

Miller, C. C. J., Ackerley, S., Brownlees, J., Grierson, A. J., Jacobsen, N. J. O., & Thornhill, P. (2002). Axonal transport of neurofilaments in normal and disease states. *Cellular and Molecular Life Sciences CMLS*, *59*(2), 323–330. https://doi.org/10.1007/s00018-002-8425-7

Misgeld, T., Burgess, R. W., Lewis, R. M., Cunningham, J. M., Lichtman, J. W., & Sanes, J. R. (2002). Roles of Neurotransmitter in Synapse Formation. *Neuron*, *36*(4), 635–648. https://doi.org/10.1016/S0896-6273(02)01020-6

Mishina, M., Takai, T., Imoto, K., Noda, M., Takahashi, T., Numa, S., Methfessel, C., & Sakmann, B. (1986). Molecular distinction between fetal and adult forms of muscle acetylcholine receptor. *Nature*, *321*(6068), 406–411. https://doi.org/10.1038/321406a0

Mitchison, T., & Kirschner, M. (1988). Cytoskeletal dynamics and nerve growth. *Neuron*, *1*(9), 761–772. https://doi.org/10.1016/0896-6273(88)90124-9

Mitra, S. K., Hanson, D. A., & Schlaepfer, D. D. (2005). Focal adhesion kinase: in command and control of cell motility. *Nature Reviews Molecular Cell Biology*, *6*(1), 56–68. https://doi.org/10.1038/nrm1549

Moloney, E. B., de Winter, F., & Verhaagen, J. (2014). ALS as a distal axonopathy: Molecular mechanisms affecting neuromuscular junction stability in the presymptomatic stages of the disease. *Frontiers in Neuroscience*, *8*(8 JUL), 1–18. https://doi.org/10.3389/fnins.2014.00252

Morihara, T., Mizoguchi, A., Takahashi, M., Kozaki, S., Tsujihara, T., Kawano, S., Shirasu, M., Ohmukai, T., Kitada, M., Kimura, K., Okajima, S., Tamai, K., Hirasawa, Y., & Ide, C. (1999). Distribution of synaptosomal-associated protein 25 in nerve growth cones and reduction of neurite outgrowth by botulinum neurotoxin a without altering growth cone morphology in dorsal root ganglion neurons and PC-12 cells. *Neuroscience*, *91*(2), 695–706. https://doi.org/10.1016/s0306-4522(98)00671-x

Mullins, R. D., Heuser, J. A., & Pollard, T. D. (1998). The interaction of Arp2/3 complex with actin: Nucleation, high affinity pointed end capping, and formation of branching networks of filaments. *Proceedings of the National Academy of Sciences*, *95*(11), 6181–6186. https://doi.org/10.1073/pnas.95.11.6181

Myers, J. P., Santiago-Medina, M., & Gomez, T. M. (2011). Regulation of axonal outgrowth and pathfinding by integrin-ecm interactions. *Developmental Neurobiology*, *71*(11), 901–923. https://doi.org/10.1002/dneu.20931

Nachmany, H., Wald, S., Abekasis, M., Bulvik, S., & Weil, M. (2012). Two potential biomarkers identified in mesenchymal stem cells and leukocytes of patients with sporadic amyotrophic lateral sclerosis. *Disease Markers*, *32*(4), 211–220. https://doi.org/10.3233/DMA-2011-0885

Nakamoto, T., Kain, K. H., & Ginsberg, M. H. (2004). Neurobiology: New Connections between Integrins and Axon Guidance. *Current Biology*, *14*(3), R121–R123. https://doi.org/10.1016/j.cub.2004.01.020

Nakashima, M., Kato, M., Aoto, K., Shiina, M., Belal, H., Mukaida, S., Kumada, S., Sato, A., Zerem, A., Lerman-Sagie, T., Lev, D., Leong, H. Y., Tsurusaki, Y., Mizuguchi, T., Miyatake, S., Miyake, N., Ogata, K., Saitsu, H., & Matsumoto, N. (2018). De novo hotspot variants in CYFIP2 cause early-onset epileptic encephalopathy. *Annals of Neurology*, *83*(4), 794–806. https://doi.org/10.1002/ana.25208

Napoli, I., Mercaldo, V., Boyl, P. P., Eleuteri, B., Zalfa, F., De Rubeis, S., Di Marino, D., Mohr, E., Massimi, M., Falconi, M., Witke, W., Costa-Mattioli, M., Sonenberg, N., Achsel, T., & Bagni, C. (2008). The Fragile X Syndrome Protein Represses Activity-Dependent Translation through CYFIP1, a New 4E-BP. *Cell*, *134*(6), 1042–1054. https://doi.org/10.1016/j.cell.2008.07.031

Navarro, A. I., & Rico, B. (2014). Focal adhesion kinase function in neuronal development. *Current Opinion in Neurobiology*, *27*, 89–95. https://doi.org/10.1016/j.conb.2014.03.002

Ng, J., & Luo, L. (2004). Rho GTPases Regulate Axon Growth through Convergent and Divergent Signaling Pathways. *Neuron*, *44*(5), 779–793. https://doi.org/10.1016/j.neuron.2004.11.014

Nichol, R. H., Hagen, K. M., Lumbard, D. C., Dent, E. W., & Gómez, T. M. (2016). Guidance of axons by local coupling of retrograde flow to point contact adhesions. *Journal of Neuroscience*, *36*(7), 2267–2282. https://doi.org/10.1523/JNEUROSCI.2645-15.2016

Nishimoto, Y., Yamashita, T., Hideyama, T., Tsuji, S., Suzuki, N., & Kwak, S. (2008). Determination of editors at the novel A-to-I editing positions. *Neuroscience Research*, *61*(2), 201–206. https://doi.org/10.1016/j.neures.2008.02.009

Nishimura, Y., Martin, C. L., Vazquez-Lopez, A., Spence, S. J., Alvarez-Retuerto, A. I., Sigman, M., Steindler, C., Pellegrini, S., Schanen, N. C., Warren, S. T., & Geschwind, D. H. (2007). Genome-wide expression profiling of lymphoblastoid cell lines distinguishes different forms of autism and reveals shared pathways. *Human Molecular Genetics*, *16*(14), 1682–1698. https://doi.org/10.1093/hmg/ddm116

Noroozi, R., Omrani, M. D., Sayad, A., Taheri, M., & Ghafouri-Fard, S. (2018). Cytoplasmic FMRP interacting protein 1/2 (CYFIP1/2) expression analysis in autism. *Metabolic Brain Disease*, *2*, 1–6. https://doi.org/10.1007/s11011-018-0249-8

Norris, A. D., Dyer, J. O., & Lundquist, E. A. (2009). The Arp2/3 complex, UNC-115/abLIM, and UNC-34/Enabled regulate axon guidance and growth cone filopodia formation in Caenorhabditis elegans. *Neural Development*, *4*(1), 38. https://doi.org/10.1186/1749-8104-4-38

Nozumi, M., Nakagawa, H., Miki, H., Takenawa, T., & Miyamoto, S. (2003). Differential localization of WAVE isoforms in filopodia and lamellipodia of the neuronal growth cone. *Journal of Cell Science*, *116*(Pt 2), 239–246. https://doi.org/10.1242/jcs.00233

Osen-Sand, A., Catsicas, M., Staple, J. K., Jones, K. A., Ayala, G., Knowles, J., Grenningloh, G., & Catsicas, S. (1993). Inhibition of axonal growth by SNAP-25 antisense oligonucleotides in vitro and in vivo. *Nature*, *364*(6436), 445–448. https://doi.org/10.1038/364445a0

Osen-Sand, A., Staple, J. K., Naldi, E., Schiavo, G., Rossetto, O., Petitpierre, S., Malgaroli, A., Montecucco, C., & Catsicas, S. (1996). Common and distinct fusion proteins in axonal growth and transmitter release. *The Journal of Comparative Neurology*, *367*(2), 222–234. https://doi.org/10.1002/(SICI)1096-9861(19960401)367:2<222::AID-CNE5>3.0.CO;2-7

Özer, I. (2019). *Analyzing the Role of CyFIP2 in the Mouse Brain*. University of Bonn.

Padrick, S. B., Cheng, H. C., Ismail, A. M., Panchal, S. C., Doolittle, L. K., Kim, S., Skehan, B. M., Umetani, J., Brautigam, C. A., Leong, J. M., & Rosen, M. K. (2008). Hierarchical Regulation of WASP/WAVE Proteins. *Molecular Cell*, *32*(3), 426–438. https://doi.org/10.1016/j.molcel.2008.10.012

Parsons, J. T. (2003). Focal adhesion kinase: the first ten years. *Journal of Cell Science*, *116*(8), 1409–1416. https://doi.org/10.1242/jcs.00373

Parsons, J. T., Horwitz, A. R., & Schwartz, M. A. (2010). Cell adhesion: integrating cytoskeletal dynamics and cellular tension. *Nature Reviews. Molecular Cell Biology*, *11*(9), 633–643. https://doi.org/10.1038/nrm2957

Pathania, M., Davenport, E. C., Muir, J., Sheehan, D. F., López-Doménech, G., & Kittler, J. T. (2014). The autism and schizophrenia associated gene CYFIP1 is critical for the maintenance of dendritic complexity and the stabilization of mature spines. *Translational Psychiatry*, *4*(3), e374–e374.

https://doi.org/10.1038/tp.2014.16
Perrin, B. J., & Ervasti, J. M. (2010). The actin gene family: Function follows isoform. *Cytoskeleton*, *67*(10), 630–634. https://doi.org/10.1002/cm.20475
Perrot, R., & Eyer, J. (2009). Neuronal intermediate filaments and neurodegenerative disorders. *Brain Research Bulletin*, *80*(4–5), 282–295. https://doi.org/10.1016/j.brainresbull.2009.06.004
Perry, S. F., Similowski, T., Klein, W., & Codd, J. R. (2010). The evolutionary origin of the mammalian diaphragm. *Respiratory Physiology and Neurobiology*, *171*(1), 1–16. https://doi.org/10.1016/j.resp.2010.01.004
Pilo Boyl, P., Di Nardo, A., Mulle, C., Sassoè-Pognetto, M., Panzanelli, P., Mele, A., Kneussel, M., Costantini, V., Perlas, E., Massimi, M., Vara, H., Giustetto, M., & Witke, W. (2007). Profilin2 contributes to synaptic vesicle exocytosis, neuronal excitability, and novelty-seeking behavior. *The EMBO Journal*, *26*(12), 2991–3002. https://doi.org/10.1038/sj.emboj.7601737
Pinyol, R., Haeckel, A., Ritter, A., Qualmann, B., & Kessels, M. M. (2007). Regulation of N-WASP and the Arp2/3 Complex by Abp1 Controls Neuronal Morphology. *PLoS ONE*, *2*(5), e400. https://doi.org/10.1371/journal.pone.0000400
Pittman, A. J., Gaynes, J. A., & Chien, C.-B. (2010). nev (cyfip2) is required for retinal lamination and axon guidance in the zebrafish retinotectal system. *Developmental Biology*, *344*(2), 784–794. https://doi.org/10.1016/j.ydbio.2010.05.512
Playford, M. P., & Schaller, M. D. (2004). The interplay between Src and integrins in normal and tumor biology. *Oncogene*, *23*(48), 7928–7946. https://doi.org/10.1038/sj.onc.1208080
Pollard, T. D. (1986). Rate constants for the reactions of ATP- and ADP-actin with the ends of actin filaments. *Journal of Cell Biology*, *103*(6), 2747–2754. https://doi.org/10.1083/jcb.103.6.2747
Pollard, T. D. (2016). Actin and Actin-Binding Proteins. *Cold Spring Harbor Perspectives in Biology*, *8*(8), a018226. https://doi.org/10.1101/cshperspect.a018226
Pollard, T. D., Blanchoin, L., & Mullins, R. D. (2000). MOLECULAR MECHANISMS CONTROLLING ACTIN FILAMENT DYNAMICS IN NONMUSCLE CELLS. *Annual Review of Biophysics and Biomolecular Structure*, *29*(1), 545–576. https://doi.org/10.1146/annurev.biophys.29.1.545
Pollard, T. D., & Borisy, G. G. (2003). Cellular Motility Driven by Assembly and Disassembly of Actin Filaments. *Cell*, *112*(4), 453–465. https://doi.org/10.1016/S0092-8674(03)00120-X
Pollard, T. D., & Cooper, J. A. (2009). Actin, a Central Player in Cell Shape and Movement. *Science*, *326*(5957), 1208–1212. https://doi.org/10.1126/science.1175862
Pollard, T. D., & Craig, S. W. (1982). Mechanism of actin polymerization. *Trends in Biochemical Sciences*, *7*(2), 55–58. https://doi.org/10.1016/0968-0004(82)90076-7
Pollard, T. D., Earnshaw, W. C., Lippincott-Schwartz, J., & Johnson, G. T. (2017). Actin and Actin-Binding Proteins. In T. D. Pollard, W. C. Earnshaw, J. Lippincott-Schwartz, & G. T. Johnson (Eds.), *Cell Biology* (Third Edit, pp. 575–591). Elsevier. https://doi.org/10.1016/B978-0-323-34126-4.00033-5
Purves, D., Augustine, G. J., Fitzpatrick, D., Hall, W. C., LaMAntia, A.-S., Mooney, R. D., Platt, M. L., & White, L. E. (2018). *Neuroscience* (Sixth Edit). Oxford University Press.
Qualmann, B., & Kessels, M. M. (2009). New players in actin polymerization - WH2-domain-containing actin nucleators. In *Trends in Cell Biology*. https://doi.org/10.1016/j.tcb.2009.03.004
Qurashi, A., Sahin, H. B., Carrera, P., Gautreau, A., Schenck, A., & Giangrande, A. (2007). HSPC300 and its role in neuronal connectivity. *Neural Development*, *2*(1), 18. https://doi.org/10.1186/1749-8104-2-18
Rakeman, A. S., & Anderson, K. V. (2006). Axis specification and morphogenesis in the mouse embryo require Nap1, a regulator of WAVE-mediated actin branching. *Development (Cambridge, England)*, *133*(16), 3075–3083. https://doi.org/10.1242/dev.02473
Reinhard, M., Halbrugge, M., Scheer, U., Wiegand, C., Jockusch, B. M., & Walter, U. (1992). The 46/50 kDa phosphoprotein VASP purified from human platelets is a novel protein associated with actin filaments and focal contacts. *EMBO Journal*, *11*(6), 2063–2070. https://doi.org/10.1002/j.1460-2075.1992.tb05264.x
Reinhard, M., Halbrügge, M., Scheer, U., Wiegand, C., Jockusch, B. M., & Walter, U. (1992). The 46/50 kDa phosphoprotein VASP purified from human platelets is a novel protein associated with actin filaments and focal contacts. *The EMBO Journal*, *11*(6), 2063–2070. https://doi.org/10.1002/j.1460-2075.1992.tb05264.x

Reinhard, Matthias, Rüdiger, M., Jockusch, B. M., & Walter, U. (1996). VASP interaction with vinculin: a recurring theme of interactions with proline-rich motifs. *FEBS Letters*, *399*(1–2), 103–107. https://doi.org/10.1016/s0014-5793(96)01295-1

Ren, X. R., Ming, G. L., Xie, Y., Hong, Y., Sun, D. M., Zhao, Z. Q., Feng, Z., Wang, Q., Shim, S., Chen, Z. F., Song, H. J., Mei, L., & Xiong, W. C. (2004). Focal adhesion kinase in netrin-1 signaling. *Nature Neuroscience*, *7*(11), 1204–1212. https://doi.org/10.1038/nn1330

Renaudin, A., Lehmann, M., Girault, J.-A. A., & McKerracher, L. (1999). Organization of point contacts in neuronal growth cones. *Journal of Neuroscience Research*, *55*(4), 458–471. https://doi.org/10.1002/(SICI)1097-4547(19990215)55:4<458::AID-JNR6>3.0.CO;2-D

Richards, D. A., Rizzoli, S. O., & Betz, W. J. (2004). Effects of wortmannin and latrunculin A on slow endocytosis at the frog neuromuscular junction. *The Journal of Physiology*, *557*(Pt 1), 77–91. https://doi.org/10.1113/jphysiol.2004.062158

Ridley, A. J. (2006). Rho GTPases and actin dynamics in membrane protrusions and vesicle trafficking. *Trends in Cell Biology*, *16*(10), 522–529. https://doi.org/10.1016/j.tcb.2006.08.006

Riedmann, E. M., Schopoff, S., Hartner, J. C., & Jantsch, M. F. (2008). Specificity of ADAR-mediated RNA editing in newly identified targets. *RNA (New York, N.Y.)*, *14*(6), 1110–1118. https://doi.org/10.1261/rna.923308

Rizzoli, S. O., & Betz, W. J. (2005). Synaptic vesicle pools. *Nature Reviews. Neuroscience*, *6*(1), 57–69. https://doi.org/10.1038/nrn1583

Robinson, R. C., Turbedsky, K., Kaiser, D. A., Marchand, J. B., Higgs, H. N., Choe, S., & Pollard, T. D. (2001). Crystal structure of Arp2/3 complex. *Science*, *294*(5547), 1679–1684. https://doi.org/10.1126/science.1066333

Robles, E., Woo, S., & Gomez, T. (2005). Src-Dependent Tyrosine Phosphorylation at the Tips of Growth Cone Filopodia Promotes Extension. *Journal of Neuroscience*, *25*(33), 7669–7681. https://doi.org/10.1523/JNEUROSCI.2680-05.2005

Rogers, R. S., & Nishimune, H. (2017). The role of laminins in the organization and function of neuromuscular junctions. *Matrix Biology*, *57–58*, 86–105. https://doi.org/10.1016/j.matbio.2016.08.008

Rottner, K., Behrendt, B., Small, J. V., & Wehland, J. (1999). VASP dynamics during lamellipodia protrusion. *Nature Cell Biology*, *1*(5), 321–322. https://doi.org/10.1038/13040

Rottner, K., Hänisch, J., & Campellone, K. G. (2010). WASH, WHAMM and JMY: regulation of Arp2/3 complex and beyond. *Trends in Cell Biology*, *20*(11), 650–661. https://doi.org/10.1016/J.TCB.2010.08.014

Rotty, J. D., Wu, C., & Bear, J. E. (2013). New insights into the regulation and cellular functions of the ARP2/3 complex. *Nature Reviews Molecular Cell Biology*, *14*(1), 7–12. https://doi.org/10.1038/nrm3492

Rouiller, I., Xu, X.-P., Amann, K. J., Egile, C., Nickell, S., Nicastro, D., Li, R., Pollard, T. D., Volkmann, N., & Hanein, D. (2008). The structural basis of actin filament branching by the Arp2/3 complex. *Journal of Cell Biology*, *180*(5), 887–895. https://doi.org/10.1083/jcb.200709092

Saller, E., Tom, E., Brunori, M., Otter, M., Estreicher, A., Mack, D. H., & Iggo, R. (1999). Increased apoptosis induction by 121F mutant p53. *The EMBO Journal*, *18*(16), 4424–4437. https://doi.org/10.1093/emboj/18.16.4424

Samuel, M. A., Valdez, G., Tapia, J. C., Lichtman, J. W., & Sanes, J. R. (2012). Agrin and Synaptic Laminin Are Required to Maintain Adult Neuromuscular Junctions. *PLoS ONE*, *7*(10), e46663. https://doi.org/10.1371/journal.pone.0046663

San Ruiz-Miguel, J. E., & Letourneau, P. C. (2014). The role of Arp2/3 in growth cone actin dynamics and guidance is substrate dependent. *Journal of Neuroscience*, *34*(17), 5895–5908. https://doi.org/10.1523/JNEUROSCI.0672-14.2014

Sanes, J. R., & Lichtman, J. W. (1999). DEVELOPMENT OF THE VERTEBRATE NEUROMUSCULAR JUNCTION. *Annual Review of Neuroscience*, *22*(1), 389–442. https://doi.org/10.1146/annurev.neuro.22.1.389

Sanes, J. R., & Lichtman, J. W. (2001). Induction, assembly, maturation and maintenance of a postsynaptic apparatus. *Nature Reviews Neuroscience*, *2*(11), 791–805. https://doi.org/10.1038/35097557

Santos, T. E., Schaffran, B., Broguière, N., Meyn, L., Zenobi-Wong, M., & Bradke, F. (2020). Axon Growth of CNS Neurons in Three Dimensions Is Amoeboid and Independent of Adhesions. *Cell Reports*, *32*(3), 107907. https://doi.org/10.1016/j.celrep.2020.107907

Schaks, M., Reinke, M., Witke, W., & Rottner, K. (2020). Molecular Dissection of Neurodevelopmental Disorder-Causing Mutations in CYFIP2. *Cells*, *9*(6), 1355. https://doi.org/10.3390/cells9061355

Schaks, M., Singh, S. P., Kage, F., Thomason, P., Klünemann, T., Steffen, A., Blankenfeldt, W., Stradal, T. E., Insall, R. H., & Rottner, K. (2018). Distinct Interaction Sites of Rac GTPase with WAVE Regulatory Complex Have Non-redundant Functions in Vivo. *Current Biology*, *28*(22), 3674-3684.e6. https://doi.org/10.1016/j.cub.2018.10.002

Schenck, A., Bardoni, B., Langmann, C., Harden, N., Mandel, J.-L., & Giangrande, A. (2003). CYFIP/Sra-1 Controls Neuronal Connectivity in Drosophila and Links the Rac1 GTPase Pathway to the Fragile X Protein. *Neuron*, *38*(6), 887–898. https://doi.org/10.1016/S0896-6273(03)00354-4

Schenck, A., Bardoni, B., Moro, A., Bagni, C., & Mandel, J.-L. (2001). A highly conserved protein family interacting with the fragile X mental retardation protein (FMRP) and displaying selective interactions with FMRP-related proteins FXR1P and FXR2P. *Proceedings of the National Academy of Sciences*, *98*(15), 8844–8849. https://doi.org/10.1073/pnas.151231598

Schenck, A., Qurashi, A., Carrera, P., Bardoni, B., Diebold, C., Schejter, E., Mandel, J.-L., & Giangrande, A. (2004). WAVE/SCAR, a multifunctional complex coordinating different aspects of neuronal connectivity. *Developmental Biology*, *274*(2), 260–270. https://doi.org/10.1016/j.ydbio.2004.07.009

Sefton, E. M., Gallardo, M., & Kardon, G. (2018). Developmental origin and morphogenesis of the diaphragm, an essential mammalian muscle. *Developmental Biology*, *440*(2), 64–73. https://doi.org/10.1016/j.ydbio.2018.04.010

Sengul, G., & Watson, C. (2012). Spinal Cord. In *The Mouse Nervous System* (pp. 424–458). Elsevier. https://doi.org/10.1016/B978-0-12-369497-3.10013-5

Shakir, M. A., Jiang, K., Struckhoff, E. C., Demarco, R. S., Patel, F. B., Soto, M. C., & Lundquist, E. A. (2008). The Arp2/3 Activators WAVE and WASP Have Distinct Genetic Interactions With Rac GTPases in Caenorhabditis elegans Axon Guidance. *Genetics*, *179*(4), 1957–1971. https://doi.org/10.1534/genetics.108.088963

Shevchenko, A., Tomas, H., Havliš, J., Olsen, J. V., & Mann, M. (2007). In-gel digestion for mass spectrometric characterization of proteins and proteomes. *Nature Protocols*, *1*(6), 2856–2860. https://doi.org/10.1038/nprot.2006.468

Shi, L., Fu, A. K. Y., & Ip, N. Y. (2012). Molecular mechanisms underlying maturation and maintenance of the vertebrate neuromuscular junction. *Trends in Neurosciences*, *35*(7), 441–453. https://doi.org/10.1016/j.tins.2012.04.005

Shirasaki, R., & Pfaff, S. L. (2002). Transcriptional Codes and the Control of Neuronal Identity. *Annual Review of Neuroscience*, *25*(1), 251–281. https://doi.org/10.1146/annurev.neuro.25.112701.142916

Shirasu, M., Kimura, K., Kataoka, M., Takahashi, M., Okajima, S., Kawaguchi, S., Hirasawa, Y., Ide, C., & Mizoguchi, A. (2000). VAMP-2 promotes neurite elongation and SNAP-25A increases neurite sprouting in PC12 cells. *Neuroscience Research*, *37*(4), 265–275. https://doi.org/10.1016/S0168-0102(00)00125-5

Short, C. A., Suarez-Zayas, E. A., & Gomez, T. M. (2016). Cell adhesion and invasion mechanisms that guide developing axons. *Current Opinion in Neurobiology*, *39*, 77–85. https://doi.org/10.1016/j.conb.2016.04.012

Shtrichman, R., Germanguz, I., Mandel, R., Ziskind, A., Nahor, I., Safran, M., Osenberg, S., Sherf, O., Rechavi, G., & Itskovitz-Eldor, J. (2012). Altered A-to-I RNA Editing in Human Embryogenesis. *PLoS ONE*, *7*(7), e41576. https://doi.org/10.1371/journal.pone.0041576

Silva, A. I., Haddon, J. E., Ahmed Syed, Y., Trent, S., Lin, T.-C. E., Patel, Y., Carter, J., Haan, N., Honey, R. C., Humby, T., Assaf, Y., Owen, M. J., Linden, D. E. J., Hall, J., & Wilkinson, L. S. (2019). Cyfip1 haploinsufficient rats show white matter changes, myelin thinning, abnormal oligodendrocytes and behavioural inflexibility. *Nature Communications*, *10*(1), 3455. https://doi.org/10.1038/s41467-019-11119-7

Singhal, N., & Martin, P. T. (2011). Role of extracellular matrix proteins and their receptors in the development of the vertebrate neuromuscular junction. *Developmental Neurobiology*, *71*(11), 982–1005. https://doi.org/10.1002/dneu.20953

Smith, J. C., Abdala, A. P. L., Borgmann, A., Rybak, I. A., & Paton, J. F. R. (2013). Brainstem respiratory networks: Building blocks and microcircuits. *Trends in Neurosciences*, *36*(3), 152–162. https://doi.org/10.1016/j.tins.2012.11.004

Smith, J., Ellenberger, H., Ballanyi, K., Richter, D., & Feldman, J. (1991). Pre-Botzinger complex: a brainstem region that may generate respiratory rhythm in mammals. *Science*, *254*(5032), 726–729. https://doi.org/10.1126/science.1683005

Spillane, M., & Gallo, G. (2014). Involvement of Rho-family GTPases in axon branching. *Small GTPases*, *5*(MAR). https://doi.org/10.4161/sgtp.27974

Spillane, M., Ketschek, A., Donnelly, C. J., Pacheco, A., Twiss, J. L., & Gallo, G. (2012). Nerve Growth Factor-Induced Formation of Axonal Filopodia and Collateral Branches Involves the Intra-Axonal Synthesis of Regulators of the Actin-Nucleating Arp2/3 Complex. *Journal of Neuroscience*, *32*(49), 17671–17689. https://doi.org/10.1523/JNEUROSCI.1079-12.2012

Spillane, M., Ketschek, A., Jones, S. L., Korobova, F., Marsick, B., Lanier, L., Svitkina, T., & Gallo, G. (2011). The actin nucleating Arp2/3 complex contributes to the formation of axonal filopodia and branches through the regulation of actin patch precursors to filopodia. *Developmental Neurobiology*, *71*(9), 747–758. https://doi.org/10.1002/dneu.20907

Steffen, A., Rottner, K., Ehinger, J., Innocenti, M., Scita, G., Wehland, J., & Stradal, T. E. B. B. (2004). Sra-1 and Nap1 link Rac to actin assembly driving lamellipodia formation. *EMBO Journal*, *23*(4), 749–759. https://doi.org/10.1038/sj.emboj.7600084

Stiess, M., & Bradke, F. (2011). Neuronal polarization: The cytoskeleton leads the way. *Developmental Neurobiology*, *71*(6), 430–444. https://doi.org/10.1002/dneu.20849

Stifani, N. (2014). Motor neurons and the generation of spinal motor neuron diversity. *Frontiers in Cellular Neuroscience*, *8*(October), 1–22. https://doi.org/10.3389/fncel.2014.00293

Stöcker, S. (2015). *Function of the Cytoplasmic FMRP Interacting Protein 1 (CyFIP1) in mouse embryonic development* (Vol. 1, Issue August). Rheinischen-Friedrich-Wilhelms-Universität Bonn.

Stradal, T. E. B., Rottner, K., Disanza, A., Confalonieri, S., Innocenti, M., & Scita, G. (2004). Regulation of actin dynamics by WASP and WAVE family proteins. *Trends in Cell Biology*, *14*(6), 303–311. https://doi.org/10.1016/j.tcb.2004.04.007

Strasser, G. A., Rahim, N. A., VanderWaal, K. E., Gertler, F. B., & Lanier, L. M. (2004). Arp2/3 is a negative regulator of growth cone translocation. *Neuron*, *43*(1), 81–94. https://doi.org/10.1016/j.neuron.2004.05.015

Sturner, T., Tatarnikova, A., Mueller, J., Schaffran, B., Cuntz, H., Zhang, Y., Nemethova, M., Bogdan, S., Small, V., Tavosanis, G., Stürner, T., Tatarnikova, A., Mueller, J., Schaffran, B., Cuntz, H., Zhang, Y., Nemethova, M., Bogdan, S., Small, V., & Tavosanis, G. (2019). Transient localization of the arp2/3 complex initiates neuronal dendrite branching in vivo. *Development (Cambridge)*, *146*(7). https://doi.org/10.1242/dev.171397

Südhof, T. C. (2012). The Presynaptic Active Zone. *Neuron*, *75*(1), 11–25. https://doi.org/10.1016/j.neuron.2012.06.012

Suetsugu, S., Miki, H., & Takenawa, T. (1999). Identification of Two Human WAVE/SCAR Homologues as General Actin Regulatory Molecules Which Associate with the Arp2/3 Complex. *Biochemical and Biophysical Research Communications*, *260*(1), 296–302. https://doi.org/10.1006/bbrc.1999.0894

Suter, D. M., & Miller, K. E. (2011). The emerging role of forces in axonal elongation. *Progress in Neurobiology*, *94*(2), 91–101. https://doi.org/10.1016/j.pneurobio.2011.04.002

Svitkina, T. M., & Borisy, G. G. (1999). Arp2/3 Complex and Actin Depolymerizing Factor/Cofilin in Dendritic Organization and Treadmilling of Actin Filament Array in Lamellipodia. *Journal of Cell Biology*, *145*(5), 1009–1026. https://doi.org/10.1083/jcb.145.5.1009

Svitkina, T. M., Bulanova, E. A., Chaga, O. Y., Vignjevic, D. M., Kojima, S., Vasiliev, J. M., & Borisy, G. G. (2003). Mechanism of filopodia initiation by reorganization of a dendritic network. *The Journal of Cell Biology*, *160*(3), 409–421. https://doi.org/10.1083/jcb.200210174

Svitkina, T. M., Verkhovsky, A. B., & Borisy, G. G. (1996). Plectin sidearms mediate interaction of intermediate filaments with microtubules and other components of the cytoskeleton. *Journal of Cell Biology*, *135*(4), 991–1007. https://doi.org/10.1083/jcb.135.4.991

Swaminathan, V., Fischer, R. S., & Waterman, C. M. (2016). The FAK–Arp2/3 interaction promotes leading edge advance and haptosensing by coupling nascent adhesions to lamellipodia actin. *Molecular Biology of the Cell*, *27*(7), 1085–1100. https://doi.org/10.1091/mbc.E15-08-0590

Szaro, B. G., & Strong, M. J. (2010). Post-transcriptional control of neurofilaments: New roles in development, regeneration and neurodegenerative disease. In *Trends in Neurosciences*. https://doi.org/10.1016/j.tins.2009.10.002

Tahirovic, S., Hellal, F., Neukirchen, D., Hindges, R., Garvalov, B. K., Flynn, K. C., Stradal, T. E., Chrostek-Grashoff, A., Brakebusch, C., & Bradke, F. (2010). Rac1 regulates neuronal polarization through the WAVE complex. *Journal of Neuroscience*, *30*(20), 6930–6943. https://doi.org/10.1523/JNEUROSCI.5395-09.2010

Takenawa, T., & Suetsugu, S. (2007). The WASP–WAVE protein network: connecting the membrane to the cytoskeleton. *Nature Reviews Molecular Cell Biology*, *8*(1), 37–48. https://doi.org/10.1038/nrm2069

Tanaka, E., Ho, T., & Kirschner, M. W. (1995). The role of microtubule dynamics in growth cone motility and axonal growth. *Journal of Cell Biology*, *128*(1), 139–155. https://doi.org/10.1083/jcb.128.1.139

Tanaka, E. M., & Kirschner, M. W. (1991). Microtubule behavior in the growth cones of living neurons during axon elongation. *Journal of Cell Biology*, *115*(2), 345–363. https://doi.org/10.1083/jcb.115.2.345

Tanaka, K., Waki, H., Ido, Y., Akita, S., Yoshida, Y., Yoshida, T., & Matsuo, T. (1988). Protein and polymer analyses up tom/z 100 000 by laser ionization time-of-flight mass spectrometry. *Rapid Communications in Mass Spectrometry*, *2*(8), 151–153. https://doi.org/10.1002/rcm.1290020802

Tang, H., Li, A., Bi, J., Veltman, D. M., Zech, T., Spence, H. J., Yu, X., Timpson, P., Insall, R. H., Frame, M. C., & MacHesky, L. M. (2013). Loss of scar/WAVE complex promotes N-WASP- and FAK-dependent invasion. *Current Biology*, *23*(2), 107–117. https://doi.org/10.1016/j.cub.2012.11.059

Tessier-Lavigne, M., & Goodman, C. S. (1996). The molecular biology of axon guidance. *Science (New York, N.Y.)*, *274*(5290), 1123–1133. https://doi.org/10.1126/science.274.5290.1123

Theriot, J. A., & Mitchison, T. J. (1991). Actin microfilament dynamics in locomoting cells. *Nature*, *352*(6331), 126–131. https://doi.org/10.1038/352126a0

Tintignac, L. A., Brenner, H.-R., & Rüegg, M. A. (2015). Mechanisms Regulating Neuromuscular Junction Development and Function and Causes of Muscle Wasting. *Physiological Reviews*, *95*(3), 809–852. https://doi.org/10.1152/physrev.00033.2014

Tiwari, S. S., Mizuno, K., Ghosh, A., Aziz, W., Troakes, C., Daoud, J., Golash, V., Noble, W., Hortobágyi, T., & Giese, K. P. (2016). Alzheimer-related decrease in CYFIP2 links amyloid production to tau hyperphosphorylation and memory loss. *Brain*, *139*(10), 2751–2765. https://doi.org/10.1093/brain/aww205

Tojima, T., & Kamiguchi, H. (2015). Exocytic and endocytic membrane trafficking in axon development. *Development, Growth & Differentiation*, *57*(4), 291–304. https://doi.org/10.1111/dgd.12218

Turgeon, B., & Meloche, S. (2009). Interpreting Neonatal Lethal Phenotypes in Mouse Mutants: Insights Into Gene Function and Human Diseases. *Physiological Reviews*, *89*(1), 1–26. https://doi.org/10.1152/physrev.00040.2007

Turner, C. E. (2000). Paxillin and focal adhesion signalling. *Nature Cell Biology*, *2*(12), E231–E236. https://doi.org/10.1038/35046659

van der Zwaag, B., Staal, W. G., Hochstenbach, R., Poot, M., Spierenburg, H. A., de Jonge, M. V., Verbeek, N. E., van 't Slot, R., van Es, M. A., Staal, F. J., Freitag, C. M., Buizer-Voskamp, J. E., Nelen, M. R., van den Berg, L. H., van Amstel, H. K. P., van Engeland, H., & Burbach, J. P. H. (2009). A co-segregating microduplication of chromosome 15q11.2 pinpoints two risk genes for autism spectrum disorder. *American Journal of Medical Genetics Part B: Neuropsychiatric Genetics*, *9999B*(4), n/a-n/a. https://doi.org/10.1002/ajmg.b.31055

Varnum-Finney, B., & Reichardt, L. F. (1994). Vinculin-deficient PC12 cell lines extend unstable lamellipodia and filopodia and have a reduced rate of neurite outgrowth. *Journal of Cell Biology*,

127(4), 1071–1084. https://doi.org/10.1083/jcb.127.4.1071

Vicente-Manzanares, M., Choi, C. K., & Horwitz, A. R. (2009). Integrins in cell migration - the actin connection. *Journal of Cell Science*, *122*(2), 199–206. https://doi.org/10.1242/jcs.018564

Vicente-Manzanares, M., Ma, X., Adelstein, R. S., & Horwitz, A. R. (2009). Non-muscle myosin II takes centre stage in cell adhesion and migration. *Nature Reviews Molecular Cell Biology*, *10*(11), 778–790. https://doi.org/10.1038/nrm2786

Vignjevic, D., Yarar, D., Welch, M. D., Peloquin, J., Svitkina, T., & Borisy, G. G. (2003). Formation of filopodia-like bundles in vitro from a dendritic network. *Journal of Cell Biology*, *160*(6), 951–962. https://doi.org/10.1083/jcb.200208059

Vinzenz, M., Nemethova, M., Schur, F., Mueller, J., Narita, A., Urban, E., Winkler, C., Schmeiser, C., Koestler, S. A., Rottner, K., Resch, G. P., Maeda, Y., & Small, J. V. (2012). Actin branching in the initiation and maintenance of lamellipodia. *Journal of Cell Science*, *125*(11), 2775–2785. https://doi.org/10.1242/jcs.107623

Vitriol, E. A., & Zheng, J. Q. (2012). Growth Cone Travel in Space and Time: the Cellular Ensemble of Cytoskeleton, Adhesion, and Membrane. *Neuron*, *73*(6), 1068–1081. https://doi.org/10.1016/J.NEURON.2012.03.005

Wahlstedt, H., Daniel, C., Enstero, M., & Ohman, M. (2009). Large-scale mRNA sequencing determines global regulation of RNA editing during brain development. *Genome Research*, *19*(6), 978–986. https://doi.org/10.1101/gr.089409.108

Wang, Y., Shan, Q., Pan, J., & Yi, S. (2018). Actin Cytoskeleton Affects Schwann Cell Migration and Peripheral Nerve Regeneration. *Frontiers in Physiology*, *9*(JAN), 23. https://doi.org/10.3389/fphys.2018.00023

Washbourne, P., Thompson, P. M., Carta, M., Costa, E. T., Mathews, J. R., Lopez-Benditó, G., Molnár, Z., Becher, M. W., Valenzuela, C. F., Partridge, L. D., & Wilson, M. C. (2002). Genetic ablation of the t-SNARE SNAP-25 distinguishes mechanisms of neuroexocytosis. *Nature Neuroscience*, *5*(1), 19–26. https://doi.org/10.1038/nn783

Wear, M. A., Schafer, D. A., & Cooper, J. A. (2000). Actin dynamics: Assembly and disassembly of actin networks. *Current Biology*, *10*(24), R891–R895. https://doi.org/10.1016/S0960-9822(00)00845-9

Weston, C. A., Teressa, G., Weeks, B. S., & Prives, J. (2007). Agrin and laminin induce acetylcholine receptor clustering by convergent, Rho GTPase-dependent signaling pathways. *Journal of Cell Science*, *120*(Pt 5), 868–875. https://doi.org/10.1242/jcs.03367

Weston, C., Yee, B., Hod, E., & Prives, J. (2000). Agrin-Induced Acetylcholine Receptor Clustering Is Mediated by the Small Guanosine Triphosphatases Rac and Cdc42. *Journal of Cell Biology*, *150*(1), 205–212. https://doi.org/10.1083/jcb.150.1.205

Winder, S. J., & Ayscough, K. R. (2005). Actin-binding proteins. *Journal of Cell Science*, *118*(4), 651–654. https://doi.org/10.1242/jcs.01670

Witke, W., Podtelejnikov, A. V, Di Nardo, A., Sutherland, J. D., Gurniak, C. B., Dotti, C., & Mann, M. (1998). In mouse brain profilin I and profilin II associate with regulators of the endocytic pathway and actin assembly. *The EMBO Journal*, *17*(4), 967–976. https://doi.org/10.1093/emboj/17.4.967

Witzemann, V. (2006). Development of the neuromuscular junction. *Cell and Tissue Research*, *326*(2), 263–271. https://doi.org/10.1007/s00441-006-0237-x

Wu, C., Asokan, S. B., Berginski, M. E., Haynes, E. M., Sharpless, N. E., Griffith, J. D., Gomez, S. M., & Bear, J. E. (2012). Arp2/3 Is Critical for Lamellipodia and Response to Extracellular Matrix Cues but Is Dispensable for Chemotaxis. *Cell*, *148*(5), 973–987. https://doi.org/10.1016/j.cell.2011.12.034

Wu, X., & Reddy, D. S. (2012). Integrins as receptor targets for neurological disorders. *Pharmacology and Therapeutics*, *134*(1), 68–81. https://doi.org/10.1016/j.pharmthera.2011.12.008

Xu, K., Zhong, G., & Zhuang, X. (2013). Actin, spectrin, and associated proteins form a periodic cytoskeletal structure in axons. *Science*, *339*(6118), 452–456. https://doi.org/10.1126/science.1232251

Yagi, T. (1994). Src Family Kinases Control Neural Development and Function: gene targeting/tyrosine kinase/Fyn/behavior/learning/emotion. *Development, Growth & Differentiation*, *36*(6), 543–550. https://doi.org/10.1111/j.1440-169X.1994.00543.x

Yamada, K. M., Spooner, B. S., & Wessells, N. K. (1970). Axon growth: roles of microfilaments and microtubules. *Proceedings of the National Academy of Sciences of the United States of America*, *66*(4), 1206–1212. https://doi.org/10.1073/pnas.66.4.1206

Yan, C., Martinez-Quiles, N., Eden, S., Shibata, T., Takeshima, F., Shinkura, R., Fujiwara, Y., Bronson, R., Snapper, S. B., Kirschner, M. W., Geha, R., Rosen, F. S., & Alt, F. W. (2003). WAVE2 deficiency reveals distinct roles in embryogenesis and Rac-mediated actin-based motility. *The EMBO Journal*, *22*(14), 3602–3612. https://doi.org/10.1093/emboj/cdg350

Yang, X., Arber, S., William, C., Li, L., Tanabe, Y., Jessell, T. M., Birchmeier, C., & Burden, S. J. (2001). Patterning of Muscle Acetylcholine Receptor Gene Expression in the Absence of Motor Innervation. *Neuron*, *30*(2), 399–410. https://doi.org/10.1016/S0896-6273(01)00287-2

Yogev, S., & Shen, K. (2017). Establishing Neuronal Polarity with Environmental and Intrinsic Mechanisms. *Neuron*, *96*(3), 638–650. https://doi.org/10.1016/j.neuron.2017.10.021

Yokota, Y., Ring, C., Cheung, R., Pevny, L., & Anton, E. S. (2007). Nap1-Regulated Neuronal Cytoskeletal Dynamics Is Essential for the Final Differentiation of Neurons in Cerebral Cortex. *Neuron*, *54*(3), 429–445. https://doi.org/10.1016/j.neuron.2007.04.016

Yoon, T.-Y., & Munson, M. (2018). SNARE complex assembly and disassembly. *Current Biology*, *28*(8), R397–R401. https://doi.org/10.1016/j.cub.2018.01.005

Yuan, A., Rao, M. V., Veeranna, & Nixon, R. A. (2012). Neurofilaments at a glance. *Journal of Cell Science*, *125*(14), 3257–3263. https://doi.org/10.1242/jcs.104729

Zallen, J. A., Cohen, Y., Hudson, A. M., Cooley, L., Wieschaus, E., & Schejter, E. D. (2002). SCAR is a primary regulator of Arp2/3-dependent morphological events in Drosophila. *Journal of Cell Biology*, *156*(4), 689–701. https://doi.org/10.1083/jcb.200109057

Zhang, Y., Kang, H., Lee, Y., Kim, Y., Lee, B., Kim, J. Y., Jin, C., Kim, S., Kim, H., & Han, K. (2019). Smaller Body Size, Early Postnatal Lethality, and Cortical Extracellular Matrix-Related Gene Expression Changes of Cyfip2-Null Embryonic Mice. *Frontiers in Molecular Neuroscience*, *11*, 482. https://doi.org/10.3389/fnmol.2018.00482

Zhang, Y., Kang, H. R., & Han, K. (2019). Differential cell-type-expression of CYFIP1 and CYFIP2 in the adult mouse hippocampus. *Animal Cells and Systems*, *23*(6), 380–383. https://doi.org/10.1080/19768354.2019.1696406

Zhang, Y., Kang Hyae, R., Lee, S.-H., Kim, Y., Ma, R., Jin, C., Lim, J.-E., Kim, S., Kang, Y., Kang, H., Kim, S. Y., Kwon, S.-K., Choi, S.-Y., & Han, K. (2020). Enhanced Prefrontal Neuronal Activity and Social Dominance Behavior in Postnatal Forebrain Excitatory Neuron-Specific Cyfip2 Knock-Out Mice. *Frontiers in Molecular Neuroscience*, *13*, 574947. https://doi.org/10.3389/fnmol.2020.574947

Zhao, L., Wang, D., Wang, Q., Rodal, A. A., & Zhang, Y. Q. (2013). Drosophila cyfip regulates synaptic development and endocytosis by suppressing filamentous actin assembly. *PLoS Genetics*, *9*(4), e1003450. https://doi.org/10.1371/journal.pgen.1003450

Ziegler, W. H., Liddington, R. C., & Critchley, D. R. (2006). The structure and regulation of vinculin. *Trends in Cell Biology*, *16*(9), 453–460. https://doi.org/10.1016/j.tcb.2006.07.004

Zweier, M., Begemann, A., McWalter, K., Cho, M. T., Abela, L., Banka, S., Behring, B., Berger, A., Brown, C. W., Carneiro, M., Chen, J., Cooper, G. M., Finnila, C. R., Guillen Sacoto, M. J., Henderson, A., Hüffmeier, U., Joset, P., Kerr, B., Lesca, G., … Rauch, A. (2019). Spatially clustering de novo variants in CYFIP2, encoding the cytoplasmic FMRP interacting protein 2, cause intellectual disability and seizures. *European Journal of Human Genetics*, *27*(5), 747–759. https://doi.org/10.1038/s41431-018-0331-z

8. Appendix

8.1 Supplementary Figures

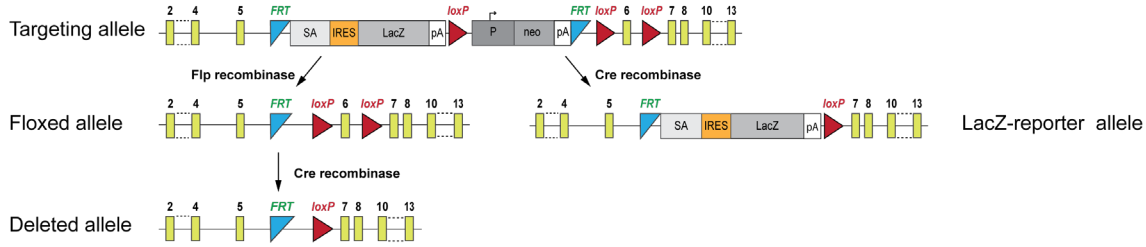

Supplementary Figure. 8.1 Organization of the *Cyfip2* locus to produce *LacZ* reporter and conditional mouse lines.
The targeted allele before recombination with splice acceptor site (SA), internal ribosomal entry site (IRES), *LacZ* gene and polyA signal (pA), β-actin promoter (P), neomycin resistance (*Neo*) with the pA signal. Breeding of mice with a Flp recombinase mouse line removes the *LacZ* and *Neo* cassette between the FRT sites, leaving exon 6 flanked by loxP sites. The mice carrying the floxed allele (middle left) can be bred with Cre-recombinase mice to generate heterozygous *Cyfip2* (*Cyfip2*$^{+/-}$) animals. The generation of homozygous *Cyfip2* (*Cyfip2*$^{-/-}$) mice was obtained by breeding heterozygous *Cyfip2*$^{+/-}$ animals. The generation of the *Cyfip2-LacZ* reporter mouse (right) was done by breeding the mice with the targeted allele with Cre-recombinase mice to remove both the *Neo* cassette and the flanked exon 6. This generates a reporter-tagged deleted allele.

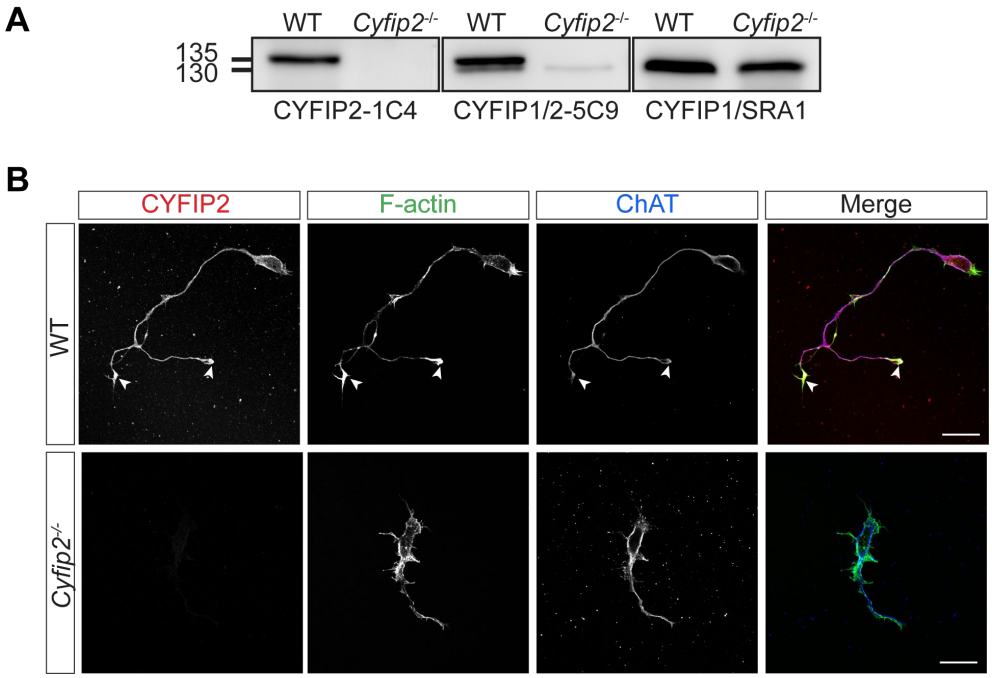

Supplementary Figure. 8.2. Validation of monoclonal mouse anti-CYFIP2-1C4 antibody
(**A**) Western blot shows the reactivity of anti-CYFIP2-1C4 antibody that detects CYFIP2 at 135 kDa when tested on E18.5 WT and *Cyfip2*$^{-/-}$ total brain lysates. CYFIP1/2-5C9 detects both CYFIP2 and CYFIP1 at 135kDa and 130 kDa, respectively. CYFIP1/SRA1 antibody detects CYFIP1 in both WT and *Cyfip2*$^{-/-}$ total brain lysates at 130 kDa. (**B**) DIV 3 WT and *Cyfip2*$^{-/-}$ MNs immunolabeled with CYFIP2-1C4 (red), F-actin (green) and ChAT (blue). CYFIP2 is expressed in the cytoplasm, the axon and in growth cones (arrowhead). CYFIP2 is expressed is ChAT+ MNs and colocalizes with F-actin in the growth cones. Scale bar: 20 µm.

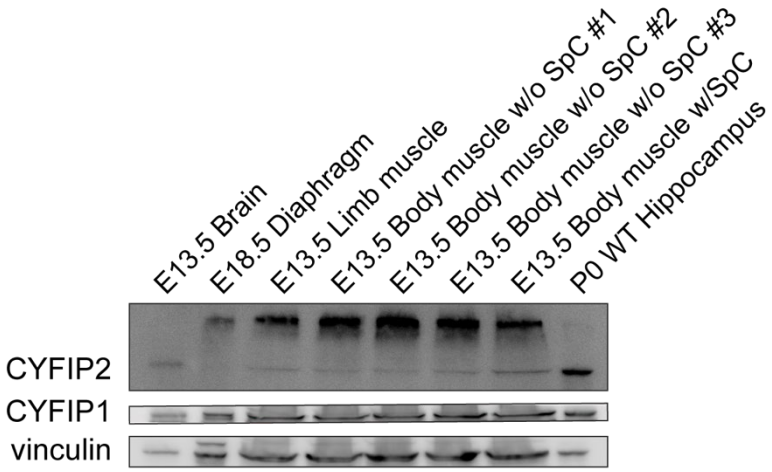

Supplementary Figure. 8.3 CYFIP2 expression in peripheral tissue during mouse embryonic development.
Western blots show low CYFIP2 protein expression in peripheral tissues. CYFIP1 ubiquitously expressed in non-CNS tissue. Vinculin is highly expressed in the peripheral tissue compared to brain tissue. SpC: spinal cord.

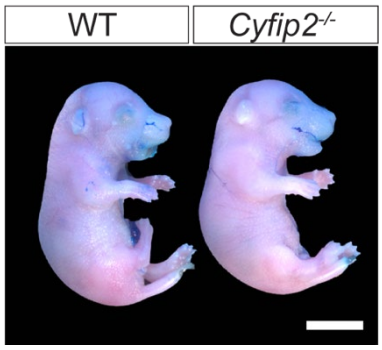

Supplementary Figure 8.4. CYFIP2 deletion does not affect skin permeability.
Immersion of E18.5 embryos in Toluidine blue solution shows intact skin barrier properties in *Cyfip2*$^{-/-}$ (right) compared to WT (left) animals. Scale bar: 5 mm.

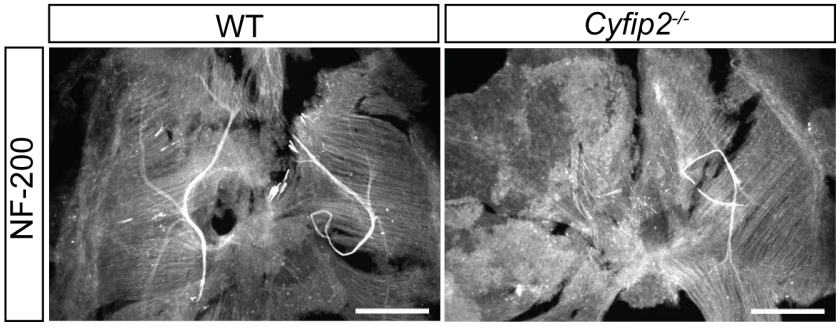

Supplementary Figure 8.5. Loss of phrenic nerve trifurcation in *Cyfip2*$^{-/-}$ diaphragms.
E13.5 diaphragms immunolabelled with anti-neurofilament-200 (NF-200) Ab shows lack of phrenic nerve trifurcation (indicated with white arrowhead) in *Cyfip2*$^{-/-}$ compared to WT tissue. Scale bar: 500 μm. D: dorsal, v: ventral.

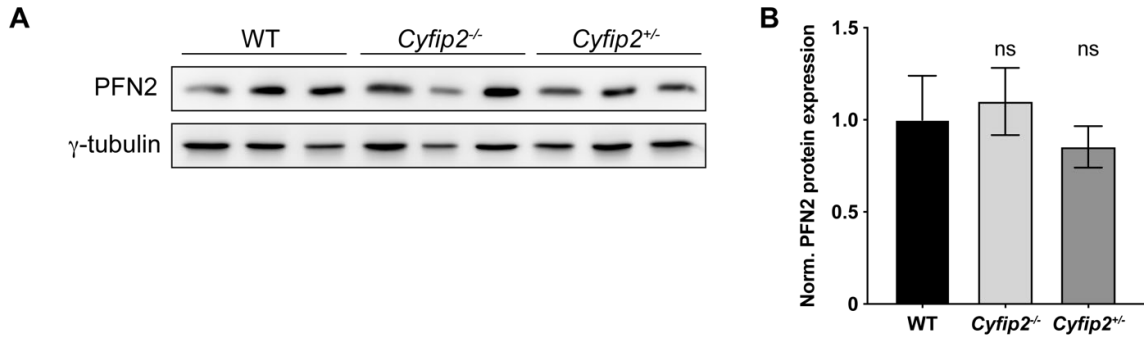

Supplementary Figure. 8.6. Profilin 2 levels are not altered by loss of CYFIP2 in the spinal cord. (**A**) Western blot and (**B**) quantification shows profilin 2 (PFN2) levels are not altered in *Cyfip2*$^{-/-}$ and *Cyfip2*$^{+/-}$ total spinal cord lysates compared to controls. γ-tubulin was used as a loading control.

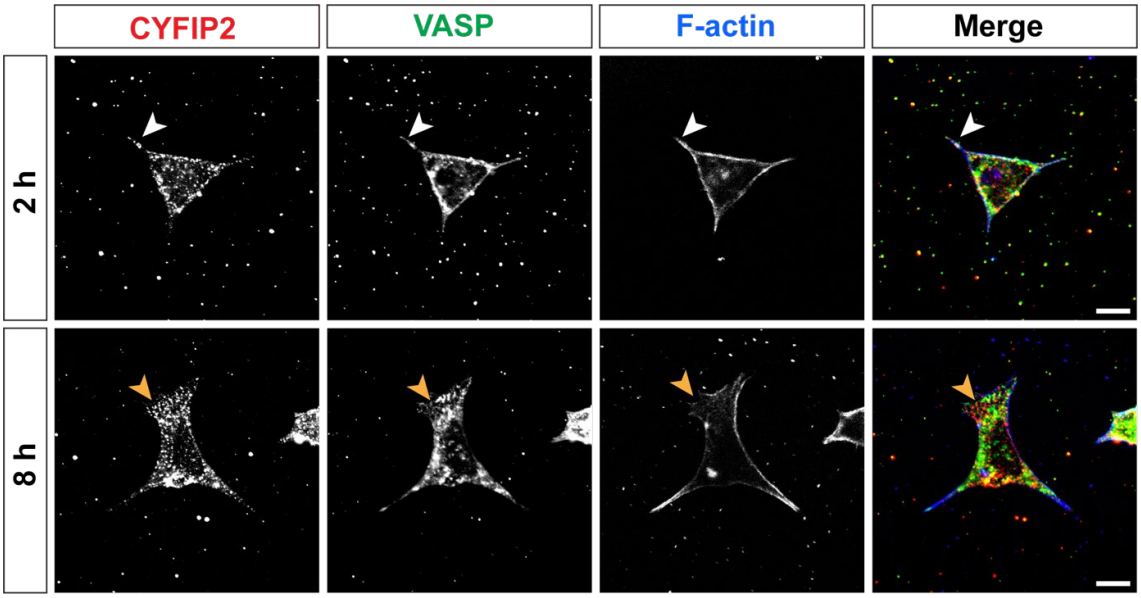

Supplementary Figure. 8.7. Localization of CYFIP2 in HEK293 cells during early adhesion phase.
Immunolabelled HEK293 cells with anti-CYFIP2 Ab (red), anti-VASP Abs (green) and phalloidin (blue) after 2 h (top panel) and 8 h (bottom panel) adhesion time. In early contact sites (2 h) CYFIP2 is found in the cytoplasm and filopodia tips (white arrowhead). After 8 h CYFIP2 localizes mainly in lamellipodia-like structures (orange arrowhead). CYFIP2 colocalizes with VASP and F-actin in regions of cortical actin along the cell membrane. Scale bar: 10 μm.

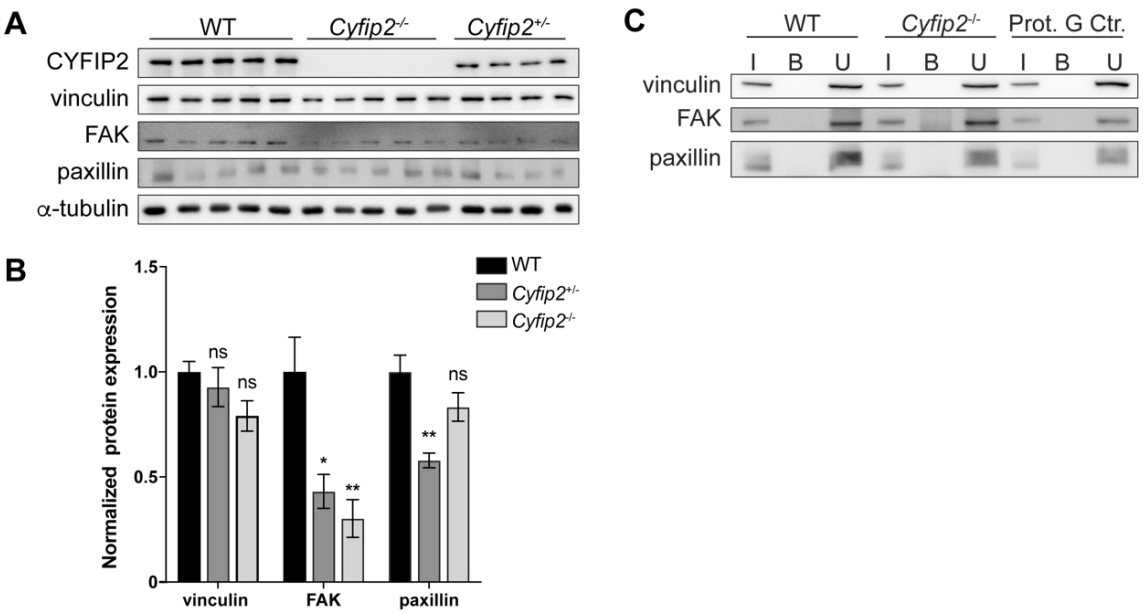

Supplementary Figure. 8.8. CYFIP2 depletion causes loss of certain adhesion markers and CYFIP2 does not interact with them.

(**A**) Western blot and (**B**) quantification of vinculin ($F(2,11) = 2.44$, p= 0.13. WT: *Cyfip2*$^{+/-}$ p = 0.76; WT:*Cyfip2*$^{-/-}$ p = 0.12), FAK ($F(2,11) = 9.554$, p = 0.004. WT: *Cyfip2*$^{+/-}$ p = 0.022; WT:*Cyfip2*$^{-/-}$ p = 0.004) and paxillin ($F(2,11) = 9.36$, p = 0.004. WT:*Cyfip2* $^{+/-}$ p = 0.003; WT:*Cyfip2*$^{-/-}$ p = 0.208) in E18.5 spinal cord lysates (WT: n = 5, *Cyfip2* $^{+/-}$: n = 4, *Cyfip2*$^{-/-}$: n = 5). One-way ANOVA with Tukey's post-hoc test. ns: not significant, * $p < 0.05$, **$p < 0.01$. Data are mean ± SEM. (**C**) Co-IP with E18.5 brain lysates shows neither vinculin, nor FAK, nor paxillin interact with CYFIP2. *Cyfip2*$^{-/-}$ lysate and Protein G beads were used as controls. B: bound fraction, I: input fraction, U: unbound fraction.

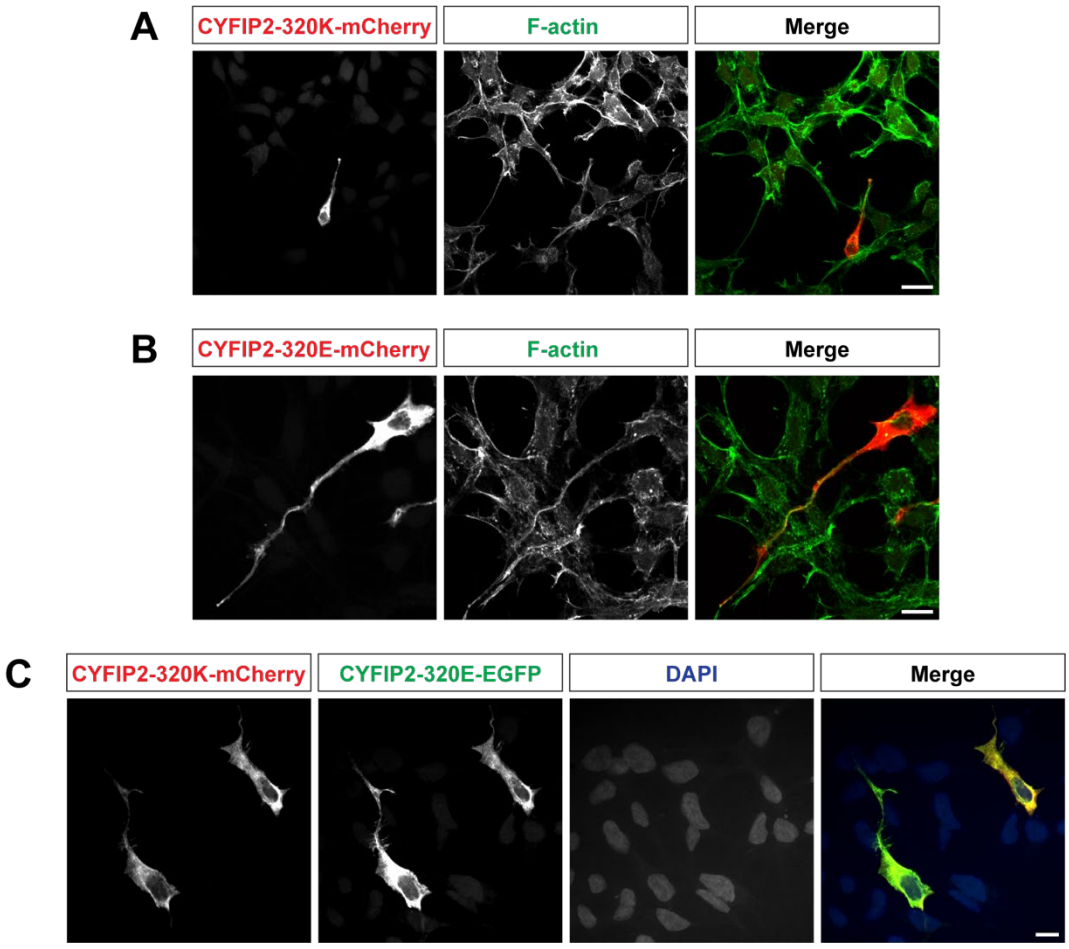

Supplementary Figure. 8.9. Fluorescently tagged CYFIP2-320K and 320E localization in transfected HEK293 cells.
(**A**) Sample images of HEK293 cells expressing CYFIP2-320K-mCherry (red) and stained for F-actin (phalloidin, green) show CYFIP2-320K localization in the cytoplasm and in protrusions. (**B**) Sample images of HEK293 cells expressing CYFIP2-320E-mCherry (red) and stained for F-actin (phalloidin, green) shows CYFIP2-320E localization in the cytoplasm and in protrusions. The neuronal isoform CYFIP2-320E-mCherry appears to induce longer protrusions than CYFIP2-320K-mCherry. (**C**) Co-transfected CYFIP2-320K-mCherry and CYFIP2-320E-EGFP have similar subcellular localization pattern in the cytoplasm and in protrusions. Scale bar: 10 µm.

8.2 Supplementary Tables

Supplementary Table 8.1. WRC proteins that interact with CYFIP2

Protein name	Gene	UniProt ID	A_nCYFIP2 (%)
CYFIP2	*Cyfip2*	Q5SQX6	100
NAP1 (isoform 2)	*Nckap1*	P28660	148.5
NAP1-like	*Nckap1l*	Q8K1X4	12.6
WAVE1	*Wasf1*	Q8R5H6	70.1
WAVE2	*Wasf2*	Q8BH43	0.5
WAVE3	*Wasf3*	Q8VHI6	19.0
ABI1	*Abi1*	Q8CBW3	41.1
ABI2	*Abi2*	P62484	39.0
BRICK1	*Brk1*	Q91VR8	1.8

Supplementary Table 8.2. Adhesion proteins that interact with CYFIP2

Protein name	Gene	UniProt ID	A_nCYFIP2 (%)
Ankyrin-2 (isoforms 2 & 5)	*Ank2*	Q8C8R3	0.2
Catenin alpha-2	*Ctnna2*	Q61301	0.1
Contactin-1	*Ctn1*	P12960	0.2
Neural cell adhesion molecule 1 (isoforms 2, 3 & 4)	*Ncam1*	P13595	0.6

Supplementary Table 8.3. Neurite extension and growth cone proteins that interact with CYFIP2

Protein name	Gene	UniProt ID	A_nCYFIP2 (%)
Brain acid soluble protein 1	*Basp1*	Q91XV3	0.8
SLIT-ROBO Rho GTPase activating protein 3	*Srgap3*	Q812A2	1.8
Neurochondrin (isoform 2)	*Nptn*	Q9Z0E0	0.5
Tenascin-R	*Tne*	Q8BYI9	0.4
Neuroplastin (isoform 3	*Nptn*	P97300	0.2
Protein RUFY3 (isoform 2, 3 & 4)	*Rufy3*	Q9D394	0.2
Protein Rogdi homolog (isoform 2 & 3)	*Rogdi*	Q3TDK6	9.5
Protein NDRG2 (isoform 2)	*Ndrg2*	Q9QYG0	0.3
Neuronal membrane glycoprotein M6-a	*Gpm6a*	P35802	0.7

Proteins listed are represented as normalized protein abundance (A_n) specific to CYFIP2.

Supplementary Table 8.4. Presynaptic and neurotransmitter vesicles proteins that interact with CYFIP2

Protein name	Gene	UniProt ID	A_nCYFIP2 (%)
Alpha-synuclein (isoform 2)	*Snca*	O55042	0.3
Beta-synuclein	*Sncb*	Q91ZZ3	0.4
Amphiphysin	*Amph*	Q7TQF7	0.1
Synaptojanin-1	*Synj1*	Q8CHC4	0.3
Synaptotagmin-1	*Syt1*	P46096	0.9
Syntaxin-1B	*Stx1b*	P61264	0.8
Syntaxin binding protein 1	*Stxbp1*	O085599	4.0
Synaptogyrin-1 (isoform 1b)	*Syngr1*	O55100	0.6
Complexin-1	*Cplx1*	P63040	0.1
Proline-rich transmembrane protein 2	*Prrt2*	E9PUL5	0.1
AP2 complex subunit alpha-2	*Ap2a2*	P17427	0.1
AP2-associated protein kinase 1 (isoform 2)	*Aak1*	Q3UHJ0	0.1
Dynamin-like 120kDa protein, mitochondrial	*Opa1*	P58281	0.3
Endophilin-A1	*Sh3gl2*	Q62420	0.4
Caskin1 (isoform 2 & 4)	*Caskin1*	Q6P9K8	3.8
Caskin1 (isoform 2 & 4)	*Caskin1*	Q6P9K8	3.8
Caskin1 (isoform 2 & 4)	*Caskin1*	Q6P9K8	3.8

Proteins listed are represented as normalized protein abundance (A_n) specific to CYFIP2.

8.3 Acknowledgements

I would like to thank my supervisor Prof. Dr. Walter Witke for given me the opportunity to work on this project. I am forever grateful for all his support and mentorship over the years. I truly appreciate the countless constructive discussions, great work environment, encouragement, and motivation. I also want to thank my thesis committee Prof. Dr. Fürst, Prof. Dr. Bradke and Prof. Dr. Conti for agreeing to be part of my thesis committee.

I want to thank Dr. Pietro Pilo Boyl for his supervision throughout my project and for his suggestions for this thesis. I am grateful for all his assistance and discussions that enabled this project to happen. I also want to thank Dr. Stefanie Stöcker for all the initial help with the *Cyfip2* animal models that paved the way for this work.

I would also like to thank all the members of the Witke lab: Marina Di Domenico, Michael Reinke, Carina Beuck, Dr. Christine Witke, Gerda Hertig, Melli Jokwitz, Gabi Matern, Gertrud Dienst, Simone Christian and Stefan Klein. Thank you for the great work environment, your help and all the memorable lab experiences! I also want to acknowledge Zerlina Wuisan and Teresa Steffen for their contributions to this project. Furthermore, I want to thank Juan-Edo Rodriguez Gatica, Dr. Jan-Peter Siebrasse, Dr. Gregor Kirfel, Dr. Andreas Schoofs and Liane Meyn for the tremendous technical support with optimizing protocols, microscope setups and much more.

I want to give a special thanks Tessy, George, Badou, Abiola, Jenn, Shanelle, Rakeda, Tomke, Gio, Telma, Nora, Babbi, Gigi and Moni. Your friendship and moral support (from all around the world) kept me motivated all these years. Finally, special thanks to family, especially my mother, my father and my brother, Oliver, for their moral support, love, and encouragement in all my endeavors over the years. Thank you!! Danke! Merci!

.